

# IDEALISED HYDRODYNAMIC AND LAGRANGIAN MODELLING OF FLOW PAST THE BREMER CANYON SYSTEM: IMPLICATIONS FOR UPWELLING



Two orcas playing in the western Great Australian Bight. Photo taken by Jochen Kämpf and was reproduced with permission.

By

Nathan Teder

*Thesis*

*Submitted to Flinders University*

*for the degree of*

Master of Science by Research

College of Science and Engineering

27/08/2020

# CONTENTS

<b>CONTENTS</b> .....	<b>I</b>
<b>LIST OF FIGURES</b> .....	<b>III</b>
<b>LIST OF TABLES</b> .....	<b>VI</b>
<b>SUMMARY</b> .....	<b>IX</b>
<b>DECLARATION</b> .....	<b>X</b>
<b>ACKNOWLEDGEMENTS</b> .....	<b>XI</b>
<b>CHAPTER 1 BACKGROUND</b> .....	<b>1</b>
1.1 Western Great Australian Bight .....	1
1.1.1 Ocean Circulation .....	1
1.1.2 Topography and Hydrodynamics .....	3
1.1.3 Orcas .....	6
1.2 Upwelling.....	7
1.2.1 Shelf Break Canyon Upwelling.....	7
1.2.2. Deeper Upwelling.....	9
1.3 Experimental Methods for Canyon Based Upwelling .....	11
1.4 Objectives of this Study .....	12
<b>CHAPTER 2 METHODS</b> .....	<b>13</b>
2.1 Bathymetry .....	13
2.2 Canyons .....	15
2.3 Altimetry .....	18
2.4 Experiment Design .....	20
2.4.1 Shelf Break Experiments.....	20
2.4.2 Deep Canyons Experiments.....	23
2.4.3 Hydrodynamic Model .....	28
2.5 Temperature and Salinity Profiles.....	31
<b>CHAPTER 3 SHELF BREAK EXPERIMENTS</b> .....	<b>34</b>
3.1 Coastal Current .....	34
3.2 Experiment SB1 .....	42
3.2.1 Sea Level Elevation and Velocity Fields.....	42
3.2.2 Lagrangian Particle Tracker .....	45
3.3 Experiment SB2 .....	47
3.3.1 Sea Level Elevation and Velocity Fields.....	47
3.4.2 Lagrangian Particle Tracker .....	50
3.5 Experiment SB3 .....	52
3.5.1 Sea Level Elevation and Velocity Fields.....	52
3.5.2 Lagrangian Particle Tracker .....	55
3.6 Experiment SB4 .....	57
3.6.1 Sea Level Elevation and Velocity Fields.....	57

3.6.2 Lagrangian Particle Tracker .....	60
3.7 Experiment SB5 .....	62
3.7.1 Sea Level Elevation and Velocity Fields.....	62
3.7.2 Lagrangian Particle Tracker .....	65
3.8 Experiment SB6 .....	67
3.8.1 Sea Level Elevation and Velocity Fields.....	67
3.8.2 Lagrangian Particle Tracker .....	70
3.9: Temperature and Salinity Profiles.....	72
<b>CHAPTER 4 DEEP CANYON EXPERIMENTS .....</b>	<b>76</b>
4.1 Experiment DC1 .....	76
4.1.1 Sea Level Elevation and Velocity Fields.....	76
4.1.2 Lagrangian Particle Tracker Results .....	79
4.2 Experiment DC2 .....	82
4.2.1 Sea Level Elevation and Velocity Fields.....	82
4.2.2 Lagrangian Particle Tracker Results .....	85
4.3 Experiment DC3 .....	88
4.3.1 Sea Level Elevation and Velocity Fields.....	88
4.3.2 Lagrangian Particle Tracker .....	91
4.4 Experiment DC4 .....	94
4.4.1 Sea Level Elevation and Velocity Fields.....	94
4.4.2 Lagrangian Particle Tracker .....	97
4.5 Experiment DC5 .....	99
4.5.1 Sea Level Elevation and Velocity Fields.....	99
4.5.2 Lagrangian Particle Tracker Results .....	102
4.6 Experiment DC6 .....	105
4.6.1 Sea Level Elevation and Velocity Fields.....	105
4.6.2 Lagrangian Particle Tracker .....	108
4.7 Glider Temperature and Salinity Data.....	110
<b>CHAPTER 5 DISCUSSION .....</b>	<b>113</b>
5.1 Shelf Break Experiments .....	113
5.2 Deep Upwelling Experiments.....	116
5.3 Improvements/Justification .....	118
<b>CHAPTER 6 CONCLUSION.....</b>	<b>121</b>
<b>BIBLIOGRAPHY .....</b>	<b>123</b>
<b>APPENDICES .....</b>	<b>139</b>

## LIST OF FIGURES

Figure 1.1: The study area for this thesis. ....	1
Figure 1.2: The subsection of the Albany Canyon group within the study area, and orca sightings .....	4
Figure 1.3: The survey data taken from the RV Investigator after the CAPSTAN 2017 cruise .....	5
Figure 1.4: Monthly temperature and salinity data from the Great Australian Bight from 1989 to 2002 .....	6
Figure 1.5: Track path of “Lucy”, a tagged orca between 10 <sup>th</sup> to 15 <sup>th</sup> of March 2014 .....	7
Figure 1.6: Surface temperature from the Southern Surveyor April 2006 voyage .....	8
Figure 1.7: Schematic for how a topographic Rossby wave works .....	10
Figure 1.8: Diagram of how flows interact with a canyon in upwelling conducive conditions in the Southern Hemisphere .....	11
Figure 2.1: Bathymetry from the western Great Australian Bight from GEBCO 2012, CAPSTAN 2017 and the resulting combined bathymetry from CAPSTAN 2017, and GEBCO 2012 .....	14
Figure 2.2: The slope of the Bremer Canyon .....	16
Figure 2.3: The slope of the Whale Canyon .....	17
Figure 2.4: The slope of the Hood Canyon .....	18
Figure 2.5: Locations of stations used for altimetry data .....	20
Figure 2.6: The domain and the locations of interest for the shelf break upwelling model .....	22
Figure 2.7: The domain and the locations of interest for the deeper upwelling model .....	26
Figure 2.8: Grid spacing for the heat map in the shelf break upwelling model .....	30
Figure 2.9: Grid spacing for the heat map in the deeper upwelling model .....	30
Figure 2.10: The location for stations where the SonTek CastAway CTD was used .....	32
Figure 2.11: Glider path from the 2013, and 2017 Bremer Bay deployment .....	33
Figure 3.1: Climatological current velocity for off the Bremer Bay coastline .....	34
Figure 3.2: Time series of current velocity for off the Bremer Bay coastline .....	34
<b>Error!</b>	
<b>Bookmark</b>	<b>not</b>
	<b>defined.</b>
Figure 3.3: Climatological current velocity for off the Esperance coastline .....	37
Figure 3.4: Time series of current velocity for off the Esperance coastline .....	38
Figure 3.5: Climatological current velocity for off the Albany coastline .....	40
Figure 3.6: Time series of current velocity for off the Albany coastline .....	41
Figure 3.7: The sea level elevation for experiment SB1 .....	43
Figure 3.8: The zonal Eulerian velocity for experiment SB1 .....	44
Figure 3.9: The meridional Eulerian velocity for experiment SB1 .....	44
Figure 3.10: The trajectory of released particles for experiment SB1 .....	46
Figure 3.11: The heat-map of released particles for experiment SB1 .....	46
Figure 3.12: The sea level elevation for experiment SB2 .....	48

Figure 3.13: The zonal Eulerian velocity for experiment SB2 .....	49
Figure 3.14: The meridional Eulerian velocity for experiment SB2 .....	49
Figure 3.15: The trajectory of released particles for experiment SB2 .....	51
Figure 3.16: The heat-map of released particles for experiment SB2 .....	51
Figure 3.17: The sea level elevation for experiment SB3 .....	53
Figure 3.18: The zonal Eulerian velocity for experiment SB3 .....	54
Figure 3.19: The meridional Eulerian velocity for experiment SB3 .....	54
Figure 3.20: The trajectory of released particles for experiment SB3 .....	56
Figure 3.21: The heat-map of released particles for experiment SB3 .....	56
Figure 3.22: The sea level elevation for experiment SB4 .....	58
Figure 3.23: The zonal Eulerian velocity for experiment SB4 .....	59
Figure 3.24: The meridional Eulerian velocity for experiment SB4 .....	59
Figure 3.25: The trajectory of released particles for experiment SB4 .....	61
Figure 3.26: The heat-map of released particles for experiment SB4 .....	61
Figure 3.27: The sea level elevation for experiment SB5 .....	63
Figure 3.28: The zonal Eulerian velocity for experiment SB5 .....	64
Figure 3.29: The meridional Eulerian velocity for experiment SB5 .....	64
Figure 3.30: The trajectory of released particles for experiment SB5 .....	66
Figure 3.31: The heat-map of released particles for experiment SB5 .....	66
Figure 3.32: The sea level elevation for experiment SB6 .....	68
Figure 3.33: The zonal Eulerian velocity for experiment SB6 .....	69
Figure 3.34: The meridional Eulerian velocity for experiment SB6 .....	69
Figure 3.35: The trajectory of released particles for experiment SB6 .....	73
Figure 3.36: The heat-map of released particles for experiment SB6 .....	71
Figure 3.37: Temperature against depth for all stations used on the Bremer Bay coastline .....	76
Figure 3.38: Salinity against depth all stations used on the Bremer Bay coastline .....	77
Figure 4.1: The sea level elevation for experiment DC1 .....	77
Figure 4.2: The zonal Eulerian velocity for experiment DC1 .....	77
Figure 4.3: The meridional Eulerian velocity for experiment DC1 .....	78
Figure 4.4: The trajectory of released particles for experiment DC1 .....	80
Figure 4.5: The heat-map of released particles for experiment DC1 .....	81
Figure 4.6: The pathways for particles released in each 600 m block for experiment DC1 .....	81
Figure 4.7: The sea level elevation for experiment DC2 .....	84
Figure 4.8: The zonal Eulerian velocity for experiment DC2 .....	84
Figure 4.9: The meridional Eulerian velocity for experiment DC2 .....	84
Figure 4.10: The trajectory of released particles for experiment DC2 .....	86
Figure 4.11: The heat-map of released particles for experiment DC2 .....	87
Figure 4.12: The pathways for particles released in each 600 m block for experiment DC2 .....	87

Figure 4.13: The sea level elevation for experiment DC3 .....	89
Figure 4.14: The zonal Eulerian velocity for experiment DC3 .....	90
Figure 4.15: The meridional Eulerian velocity for experiment DC3 .....	90
Figure 4.16: The trajectory of released particles for experiment DC3 .....	92
Figure 4.17: The heat-map of released particles for experiment DC3 .....	93
Figure 4.18: The sea level elevation for experiment DC4 .....	95
Figure 4.19: The zonal Eulerian velocity for experiment DC4 .....	95
Figure 4.20: The meridional Eulerian velocity for experiment DC4 .....	96
Figure 4.21: The trajectory of released particles for experiment DC4 .....	98
Figure 4.22: The heat-map of released particles for experiment DC4 .....	98
Figure 4.23: The sea level elevation for experiment DC5 .....	100
Figure 4.24: The zonal Eulerian velocity for experiment DC5 .....	101
Figure 4.25: The meridional Eulerian velocity for experiment DC5 .....	101
Figure 4.26: The trajectory of released particles for experiment DC5 .....	103
Figure 4.27: The heat-map of released particles for experiment DC5 .....	104
Figure 4.28: The pathways for particles released in each 600 m block for DC5 .....	104
Figure 4.29: The sea level elevation for experiment DC6 .....	106
Figure 4.30: The zonal Eulerian velocity for experiment DC6 .....	107
Figure 4.31: The meridional Eulerian velocity for experiment DC6 .....	107
Figure 4.32: The trajectory of released particles for experiment DC6 .....	109
Figure 4.33: The heat-map of released particles for experiment DC6 .....	109
Figure 4.34: Comparison of temperature verse depth for the hotspot, Hood Canyon outlet and reference area using the 2013 glider deployment in Bremer Bay .....	110
Figure 4.35: Comparison of salinity verse depth for the hotspot, Hood Canyon outlet and the reference area from the 2013 glider deployment in Bremer Bay .....	110

## LIST OF TABLES

Table 2.1: List of shelf break experiments .....	21
Table 2.2: The locations of interest within the shelf break model .....	23
Table 2.3: List of deep canyon experiments .....	25
Table 2.4: The locations of interest within the deep canyon model .....	27
Table 2.5: The stations where the CastAway CTD was launched. ....	32
Table 3.1: Event analysis for altimetry data taken from the Bremer Bay region in between 1993-2014 .....	38
Table 3.2: Event analysis for altimetry data taken from the Esperance region in between 1993-2014 .....	41
Table 3.3: Event analysis for altimetry data taken from the Albany region in between 1993-2014 .....	44
Table 3.4: The average sea level elevation, zonal Eulerian velocity, and meridional Eulerian velocity for areas of interest within experiment SB1 model domain .....	45
Table 3.5: Percentage of particles passing through each area of interest, and the breakdown for each depth range where particles were released in the SB1 model domain. ....	47
Table 3.6: Time and the range of velocities for particles travelling through the SB1 model domain and for each depth range that particles were released in. ....	47
Table 3.7: The average sea level elevation, zonal Eulerian velocity, and meridional Eulerian velocity for areas of interest within experiment SB2 model domain. ....	50
Table 3.8: Percentage of particles passing through each area of interest, and the breakdown for each depth range where particles were released in the SB2 model domain. ....	54
Table 3.9: Time and the range of velocities for particles travelling through the SB2 model domain and for each depth range that particles were released in. ....	52
Table 3.10: The average sea level elevation, zonal Eulerian velocity, and meridional Eulerian velocity for areas of interest within experiment SB3 model domain. ....	55
Table 3.11: Percentage of particles passing through each area of interest, and the breakdown for each depth range where particles were released in the SB3 model domain. ....	57
Table 3.12: Time and the range of velocities for particles travelling through the SB3 model domain and for each depth range that particles were released in. ....	57
Table 3.13: The average sea level elevation, zonal Eulerian velocity, and meridional Eulerian velocity for areas of interest within experiment SB4 model domain. ....	59
Table 3.14: Percentage of particles passing through each area of interest, and the breakdown for each depth range where particles were released in the SB4 model domain. ....	61

Table 3.15: Time and the range of velocities for particles travelling through the SB4 model domain and for each depth range that particles were released in. ....	62
Table 3.16: The average sea level elevation, zonal Eulerian velocity, and meridional Eulerian velocity for areas of interest within experiment SB5 model domain .....	65
Table 3.17: Percentage of particles passing through each area of interest, and the breakdown for each depth range where particles were released in the SB5 model domain. ....	67
Table 3.18: Time and the range of velocities for particles travelling through the SB5 model domain and for each depth range that particles were released in. ....	67
Table 3.19: The average sea level elevation, zonal Eulerian velocity, and meridional Eulerian velocity for areas of interest within experiment SB6 model domain .....	70
Table 3.20: Percentage of particles passing through each area of interest, and the breakdown for each depth range where particles were released in the SB6 model domain. ....	72
Table 3.21: Time and the range of velocities for particles travelling through the SB6 model domain, and for each depths that particles were released in. ....	72
Table 4.1: The average sea level elevation, zonal Eulerian velocity, and meridional Eulerian velocity for areas of interest within experiment DC1 model domain .....	78
Table 4.2: Percentage of particles passing through each area of interest, and the breakdown for each depth range where particles were released in the DC1 model domain. ....	81
Table 4.3: Time and the range of velocities for particles travelling through the DC1 model domain, and for each depths that particles were released in. ....	82
Table 4.4: The average sea level elevation, zonal Eulerian velocity, and meridional Eulerian velocity for areas of interest within experiment DC2 model domain .....	85
Table 4.5: Percentage of particles passing through each area of interest, and the breakdown for each depth range where particles were released in the DC2 model domain. ....	88
Table 4.6: Time and the range of velocities for particles travelling through the DC2 model domain, and for each depths that particles were released in. ....	88
Table 4.7: The average sea level elevation, zonal Eulerian velocity, and meridional Eulerian velocity for areas of interest within experiment DC3 model domain .....	91
Table 4.8: Percentage of particles passing through each area of interest, and the breakdown for each depth range where particles were released in the DC3 model domain. ....	93
Table 4.9: Time and the range of velocities for particles travelling through the DC3 model domain, and for each depths that particles were released in .....	93
Table 4.10: The average sea level elevation, zonal Eulerian velocity, and meridional Eulerian velocity for areas of interest within experiment DC4 model domain .....	96
Table 4.11 Percentage of particles passing through each area of interest, and the breakdown for each depth range where particles were released in the DC4 model domain. ....	99
Table 4.12: Time and the range of velocities for particles travelling through the DC4 model domain, and for each depths that particles were released in. ....	99

Table 4.13: The average sea level elevation, zonal Eulerian velocity, and meridional Eulerian velocity for areas of interest within experiment DC5 model domain. ....	102
Table 4.14: Percentage of particles passing through each area of interest, and the breakdown for each depth range where particles were released in the DC5 model domain. ....	104
Table 4.15: Time and the range of velocities for particles travelling through the DC5 model domain, and for each depths that particles were released in. ....	105
Table 4.16: The average sea level elevation, zonal Eulerian velocity, and meridional Eulerian velocity for areas of interest within experiment DC6 model domain. ....	108
Table 4.17: Percentage of particles passing through each area of interest, and the breakdown for each depth range where particles were released in the DC6 model domain. ....	110
Table 4.18: Time and the range of velocities for particles travelling through the DC6 model domain, and for each depth range that particles were released in. ....	110

## SUMMARY

The western Great Australian Bight is home to a seasonal hotspot for orca aggregation (*Orcinus orca*, also known as killer whales), which occurs from November to March. The current reason why this aggregation occurs is unknown, however, Pattiaratchi (2007) linked this to a possible subsurface upwelling event. A potential cause of subsurface upwelling is through a submarine canyon being able to drive an upwelling conducive flow upwards, propelling either a source of nutrient rich water into the euphotic zone, or creating a pathway for marine organisms to congregate higher up in the water column. This research is focused around the Bremer, Hood and Whale Canyon due to the proximity to where orcas are aggregating, as well as the Bremer and Whale Canyon existing on the edge of the continental shelf.

To test if either the Hood, Bremer or Whale Canyon can support an upwelling event capable of sustaining an orca aggregation, a single layer hydrodynamic model based on the shallow-water equations was used. This model predicted flow velocity from a barotropic pressure gradient due to a sloping sea surface, and ignored wind, tidal forcing, and density stratification. The single-layer model was set to adjust to a forced change on the northern boundary to create that barotropic pressure gradient for six days before being treated as a constant. Neutrally buoyant particles were released into the model on the fifth day and allowed to run until the sixtieth day. Temperature and salinity data from either a CTD device, or ocean-gliders was used to test if the results from these models could realistically happen.

When the single-layer model was used to test if the formation of a topographic Rossby wave was possible, 71.76% of particles released were upwelled onto the continental shelf from the Whale Canyon, and 83.58% of particles were upwelled from the Bremer Canyon. This showed that both canyons were capable of supporting upwelling via a topographic Rossby wave and temperature and salinity profiles taken in the region during February 2019 showed a  $>2^{\circ}\text{C}$  change of temperature in a 10 m band between a depth of 30 m to 70 m. This rapid decrease occurred regardless where the measurement was taken, it ruled out that upwelling was occurring in the upper 100 m during February 2019.

Using a single-layer model to test if a deeper upwelling was occurring, the results showed that 89.1% of particles were entering the area where orcas were aggregating (“hotspot”). This indicated that when deep flow interacted with the Hood and Bremer Canyon, it was able to upwell and provide a pathway for marine organisms to end up in the hotspot and support orca

aggregation. This was supported by temperature and salinity profiles which showed similar conditions in the hotspot and the head of the Hood Canyon.

## **DECLARATION**

I certify that this thesis does not incorporate without acknowledgment any material previously submitted for a degree or diploma in any university; and that to the best of my knowledge and belief it does not contain any material previously published or written by another person except where due reference is made in the text.

Signed: Nathan Teder

Date: 30/01/2020

## ACKNOWLEDGEMENTS

I wish to express my deepest gratitude to Associate Professor Jochen Kämpf for being my supervisor, and mentor for the past three years. Through Associate Professor Kämpf guidance I have gained confidence, encouragement, knowledge, and experience in researching oceanography. I would also like to thank Dr Graziela Miot Da Silva for being my co-supervisor and giving me constructive feedback regarding both oral and written presentation during this project.

A big thank you to Mr. Paul Cross of Naturaliste Charters and his crew for giving Jochen and I the opportunity in early February 2019 to collect temperature and salinity data onboard his vessel and for providing us with the locations of orca sightings in the area. This data ended up being a key part of this project.

I would like to thank Professor Leah Moore, Dr. James Daniell and the trainers and students who were aboard the 2<sup>nd</sup> CAPSTAN voyage for giving the opportunity to developing new skills and confidence in oceanography.

I would like to acknowledge CSIRO MNF, IMOS and AVISO for making bathymetry, ocean glider and satellite altimetry data freely available. I would also like to acknowledge AMOS and GESS-SA for giving me the opportunity to present my work in this project to the wider community.

I would like to acknowledge and thank Flinders University for providing travel grants, funding they set aside for the project, and maintaining the licence for ArcGIS.

I would like to acknowledge and thank my family and friends who have supported me throughout this degree.

# CHAPTER 1 BACKGROUND

The western Great Australian Bight is home to a seasonal hotspot for orca aggregation (*Orcinus orca*, also known as killer whales), which occurs from November to March (Wellard et al., 2016, Meeuwig et al., 2016, Figure 1.1). Currently it is unknown why this aggregation occurs. A potential cause for this aggregation could be from a subsurface upwelling event, where a current interacts with a canyon to push nutrients up the water column. A subsurface upwelling event could also create a pathway for marine creatures deeper in the water column to congregate near the continental shelf. To date there has been no substantial research undertaken in the western Great Australian Bight to investigate whether canyons in that area cause subsurface upwelling events.

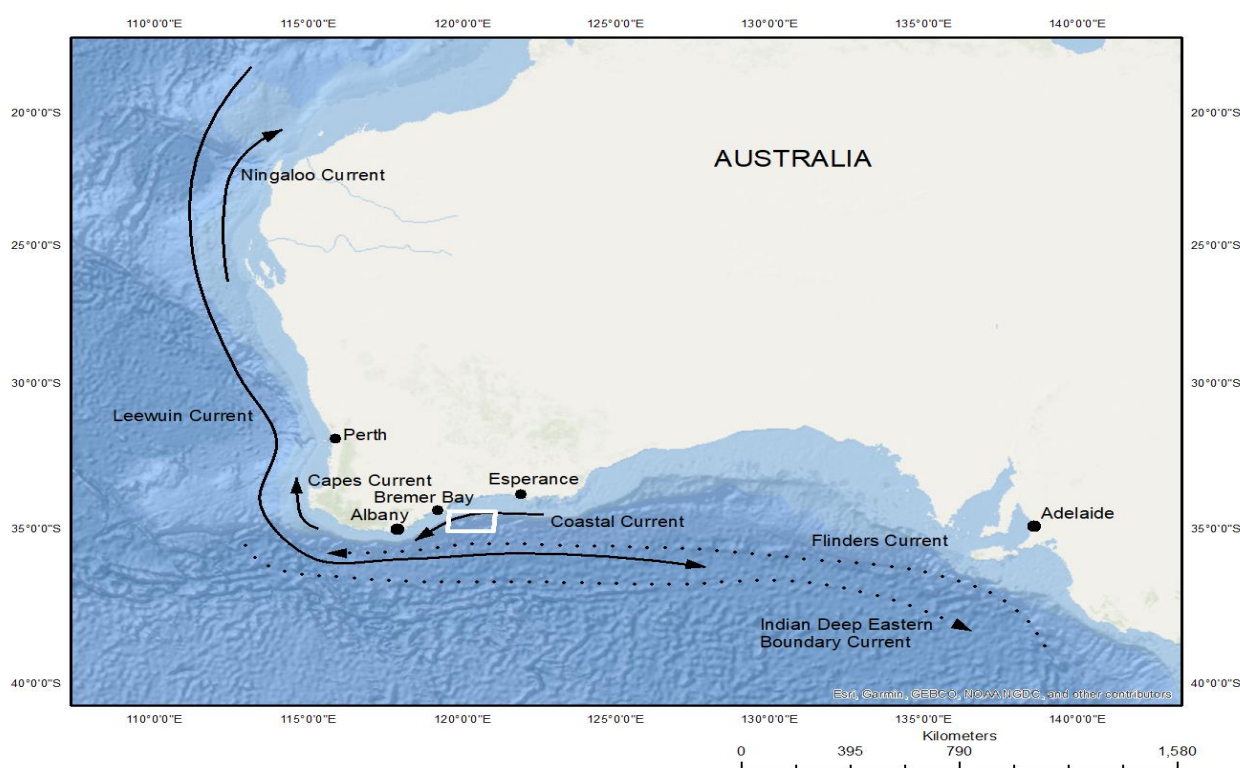


Figure 1.1: Location of where this research is focused. The white square is where the locations that Naturaliste Charters had recorded orca sightings and is the study area for this project

## 1.1 Western Great Australian Bight

### 1.1.1 Ocean Circulation

The oceanic circulation in the western Great Australian Bight varies with depth (Figure 1.1), with the eastwards flowing Leewuin Current being the dominant flow in the upper 300 m (Cresswell and Golding, 1980, Legeckis and Cresswell, 1981, Herzfeld, 1997). Below 300 m, the Leewuin Current is superseded by the westwards flowing Flinders Current, which continues down to 1500 m (Bye, 1983, Middleton and Cirano, 2002, Woo, 2005, Ridgway and Dunn, 2007). After 1500 m,

the Indian Deep Eastern Boundary Current forms which drives an eastwards flow (Tamsitt et al., 2019).

The Leeuwin Current is a poleward current off the Western Australian coastline until Cape Leeuwin and then turns into an eastward current as the coastline changes orientation (Cresswell and Golding, 1980, Legeckis and Cresswell, 1981, Herzfeld and Tomczak, 1997, Ridgway and Condie, 2004, Cresswell and Domingues, 2009). The Leeuwin Current is a narrow current ( $\leq 100$  km wide) that transports warm, low salinity and oligotrophic water, which makes it a downwelling current (Rochford, 1986, Church et al., 1989, Johannes et al., 1994, Hanson et al., 2005). The average velocity for the Leeuwin Current has been measured at  $0.5 \text{ ms}^{-1}$  via drifters by Smith et al. (1991). The maximum observed velocity with drifters was  $1.7 \text{ ms}^{-1}$  by Cresswell and Golding (1980) in May 1976, whereas Weller et. al., (2011) measured the velocity peak of the Leeuwin Current at its strongest at  $1 \text{ ms}^{-1}$ . The flow velocity is periodic, strengthening in late autumn-winter and weakening in late spring-summer (Rochford, 1986, Feng et al., 2003, Ridgway and Condie, 2004, Koslow et al., 2008). This variability affects coastal sea level height, with elevations rising by  $\sim 15$  cm in late autumn-winter and lowering by  $\sim 15$  cm in late spring-summer (Ridgway and Condie, 2004). This variability in the Leeuwin current is attributed to the halting of equatorial wind stress during the winter which allows the Leeuwin Current to flow unimpeded (McCreary et al., 1986, Smith et al., 1991, Koslow et al., 2008). Nonetheless, Morrow and Birol (1998) stated that a strengthening of a southern pressure gradient is the cause of this variability. Another driver of the Leeuwin current variability is the El Nino Southern Oscillation (ENSO), with La Nina years tending to record a stronger Leeuwin Current presence (Pariwono et al., 1986, Pearce and Phillips, 1988, Feng et al., 2003, Pattiaratchi and Woo, 2009).

As the Leeuwin Current weakens in the late spring/summer, it can be overpowered by a coastal current (Ridgway and Condie, 2004, Pattiaratchi, 2007, Cresswell and Domingues, 2009, Mondello, 2017, Wijeratne, et. al., 2018). This reversal of flow has been considered to be a surface expression of the Flinders Current (Bye, 1986, James et al., 2001, Middleton and Cirano, 2002, Ridgway and Condie, 2004, Middleton and Bye, 2007) or a separate wind-driven current known as the Coastal Current, or Cresswell Current (Pattiaratchi, 2007, Cresswell and Domingues, 2009, Mondello, 2017). Using a wind event in November 2001, Cresswell and Domingues (2009), determined that the peak velocity of this coastal current was  $25 \text{ cms}^{-1}$ , which lasted for two days. The width of the coastal current was measured to be in between 150 km to 200 km (Ridgway and Condie, 2004). The development of this coastal current should create favourable conditions for upwelling; however, research is lacking to support this. Elsewhere on the Western Australian Coastline there are two more broadly studied wind-driven counter currents which periodically appear in summer. The Capes Current, which is off the Cape Leeuwin and Cape Naturaliste coastlines (Gersbach et al., 1999, Pearce and Pattiaratchi, 1999, Woo and Pattiaratchi, 2010), and the Ningaloo Current which occurs around the Ningaloo reef (Taylor and

Pearce, 1999, Pattiaratchi, 2006, Woo et al., 2006). Both the Capes Current and the Ningaloo Current support small wind-driven upwelling centres when they do become the dominant current in the region (Gersbach et al., 1999, Woo et al., 2006).

The Flinders Current transports colder and more saline water within the Great Australian Bight before feeding into the Leeuwin Undercurrent (Middleton and Cirano, 2002, Ridgway and Condie, 2004, Ridgway and Dunn, 2007, Tamsitt et al., 2019). Due to this transport, the Flinders Current can precondition an area for upwelling (Middleton and Cirano, 2002, Middleton and Platov, 2003, Nieblas et al., 2009). The Flinders Current is a seasonal current with its flow tending to peak in the late spring and early summer (Arthur, 2006). It can be inferred that this peak is related to the weakening of the Leeuwin Current (Middleton and Cirano, 2002, Ridgway and Condie, 2004). Numerical modelling showed that the current speeds peaked at a depth of 600 m, with the maximum current speed being calculated at  $20 \text{ cms}^{-1}$ , and an average shelf-slope speed of  $10 \text{ cms}^{-1}$  (Arthur, 2006, Middleton and Bye, 2007, Seuront, et. al., 2010). Influence from the Flinders Current disappears around the 1500 m isobath, where it is superseded by the Indian Deep Eastern Boundary Current (Tamsitt et al., 2019).

The Indian Deep Eastern Boundary Current is an eastwards current that transports Indian Ocean deep water through the Great Australian Bight and into the Antarctic Circumpolar Current (McCartney and Donohue, 2007, Tamsitt et al., 2019). The Indian deep-water has a large nutrient concentration, especially silicate ( $>100 \mu\text{molkg}^{-1}$ ), and a relatively high salinity compared to other deep waters, being in a density band of  $27.70 \text{ kgm}^{-3}$  to  $28.11 \text{ kgm}^{-3}$  (McDonagh et al., 2008, Tamsitt et al., 2019). Whilst McCartney and Donohue (2007) did note that there was an eastwards flow present at a depth below 1500 m in the Great Australian Bight, it was only recently linked as being an extension to the Indian Deep Eastern Boundary Current (Tamsitt et al., 2019).

### 1.1.2 Topography and Hydrodynamics

The area of interest is a subsection in the western Great Australian Bight off the Bremer Bay coastline ( $115^\circ\text{E}$  to  $124^\circ\text{E}$ , Figure 1.1), which has also been called the Bremer Sub-Basin (Bradshaw, 2003, Exon et al., 2005, Wellard et al., 2016). The width of the continental shelf in this area is around 50-100 km (Ridgway and Condie, 2004, Exon et al., 2005) with a depth of  $< 100 \text{ m}$ . On the continental slope the depth increases from 100 m to 4500 m (Bradshaw, 2003, Blevin, 2005). The main surface current in the area is the Leeuwin current, with the Flinders current existing below 300 m.

The study area is home to a subsection of the Albany Canyon group, which contains 4 submarine canyons. These are the Henry, Hood, Bremer, and Whale Canyon (Figure 1.2) (Von der Borch, 1968, Exon et al., 2005, Pattiaratchi, 2007). Pattiaratchi (2007) stated that whilst all the canyons have a presence on the continental slope, none of those canyons cut into the continental shelf.

When Huang et al. (2014) surveyed the area, it was found that the Bremer Canyon did cut into the edge of the shelf. This shelf break location of the Bremer Canyon was supported by a recent survey by CAPSTAN (Collaborative Australian Postgraduate Sea Training Alliance Network) (Figure 1.3) and showed that the Whale Canyon is also on the edge of the shelf break.

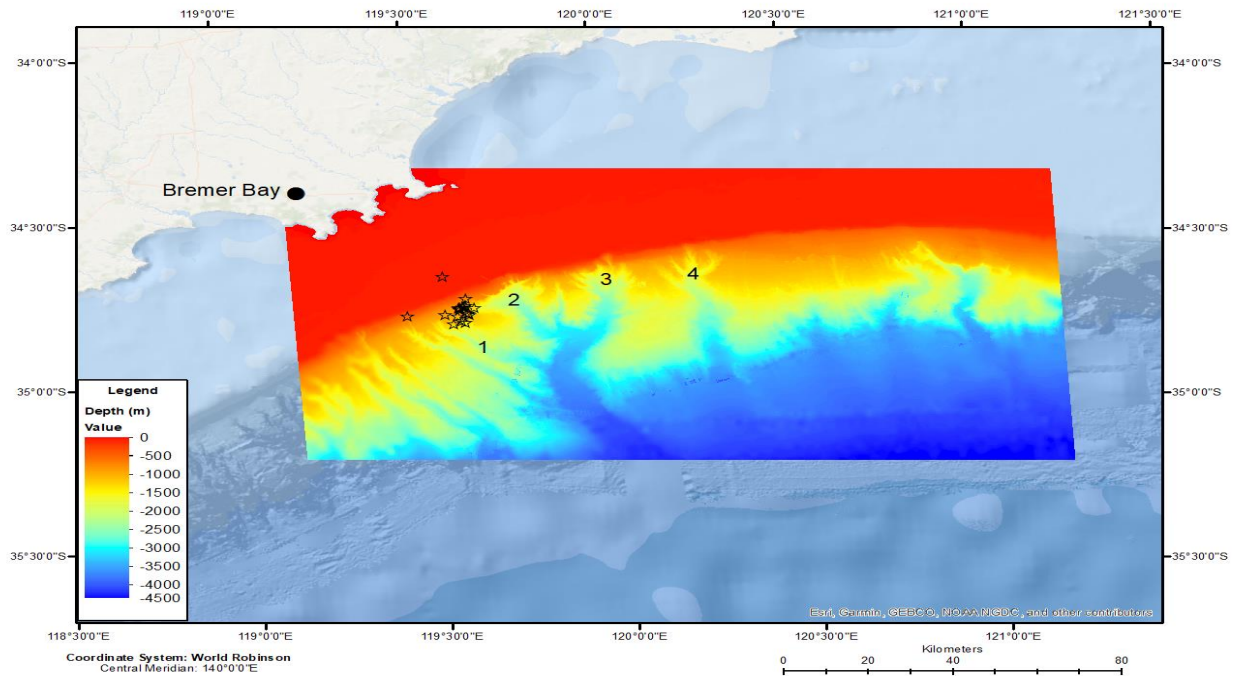


Figure 1.2: The subsection of the Albany Canyon Group within the study area. The numbered canyons are (1) Henry Canyon, (2) Hood Canyon, (3) Bremer Canyon, and (4) Whale Canyon. Stars show the location of orca sightings made by Naturaliste Charters during January-February 2019.

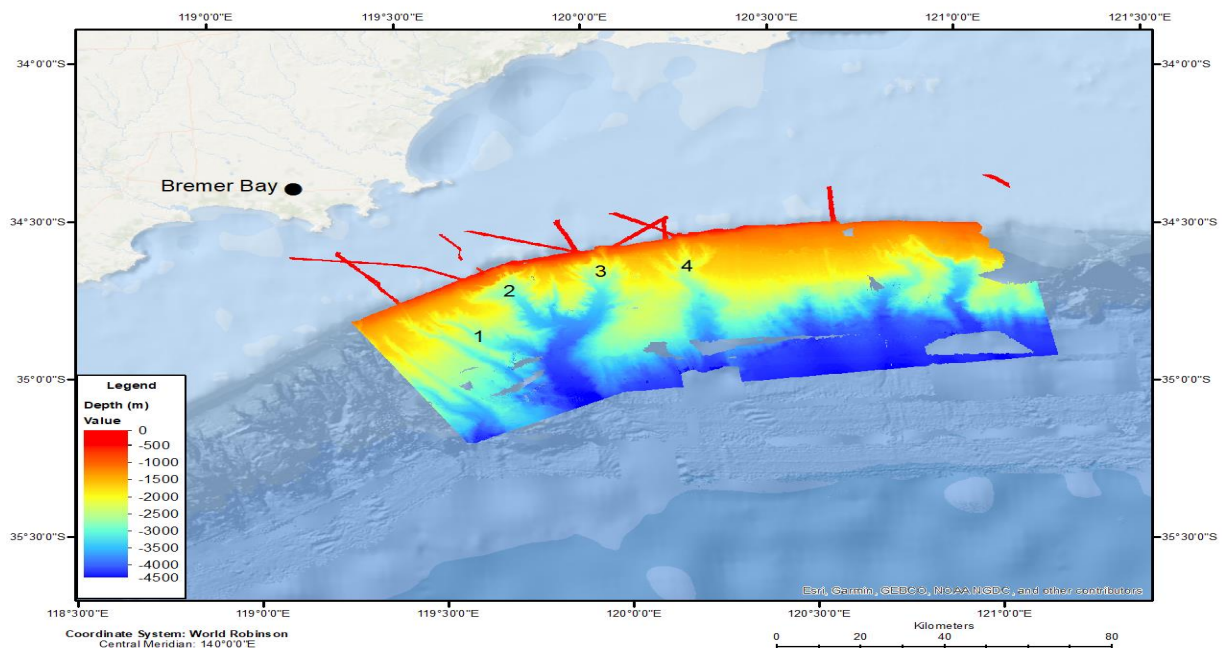


Figure 1.3: The survey data from CAPSTAN 2017 cruise between 119.15° E to 121.20° E and 34.32° S to 35.21° S. The minimum depth for the data available is 61.07 m and the maximum depth is 4391.06 m.

Temperature and salinity data in the western Great Australian Bight showed that the ocean had an average temperature of 17-18°C in summer, and ~ 20°C in winter. The average salinity varies from 35.8-35.9 PSU in summer and 35.7-35.8 PSU in winter (Figure 1.4) (Ridgway and Condie, 2004). The finding of a  $\geq 2^{\circ}\text{C}$  increase in temperature in winter and a decrease in salinity is caused by the Leeuwin Current, due to it transporting warm and low saline water into the bight, and its transport peaking in winter (Rochford, 1986, Church et al., 1989, Feng et. al., 2003, Koslow et al., 2008). Another potential factor to the relatively large temperature decrease is that due to the Leeuwin Current weakening in summer, a localised pulse of eastwards colder water can overpower the Leeuwin Current, and can be periodically cooling surface temperature in summer (Ridgway and Condie, 2004).

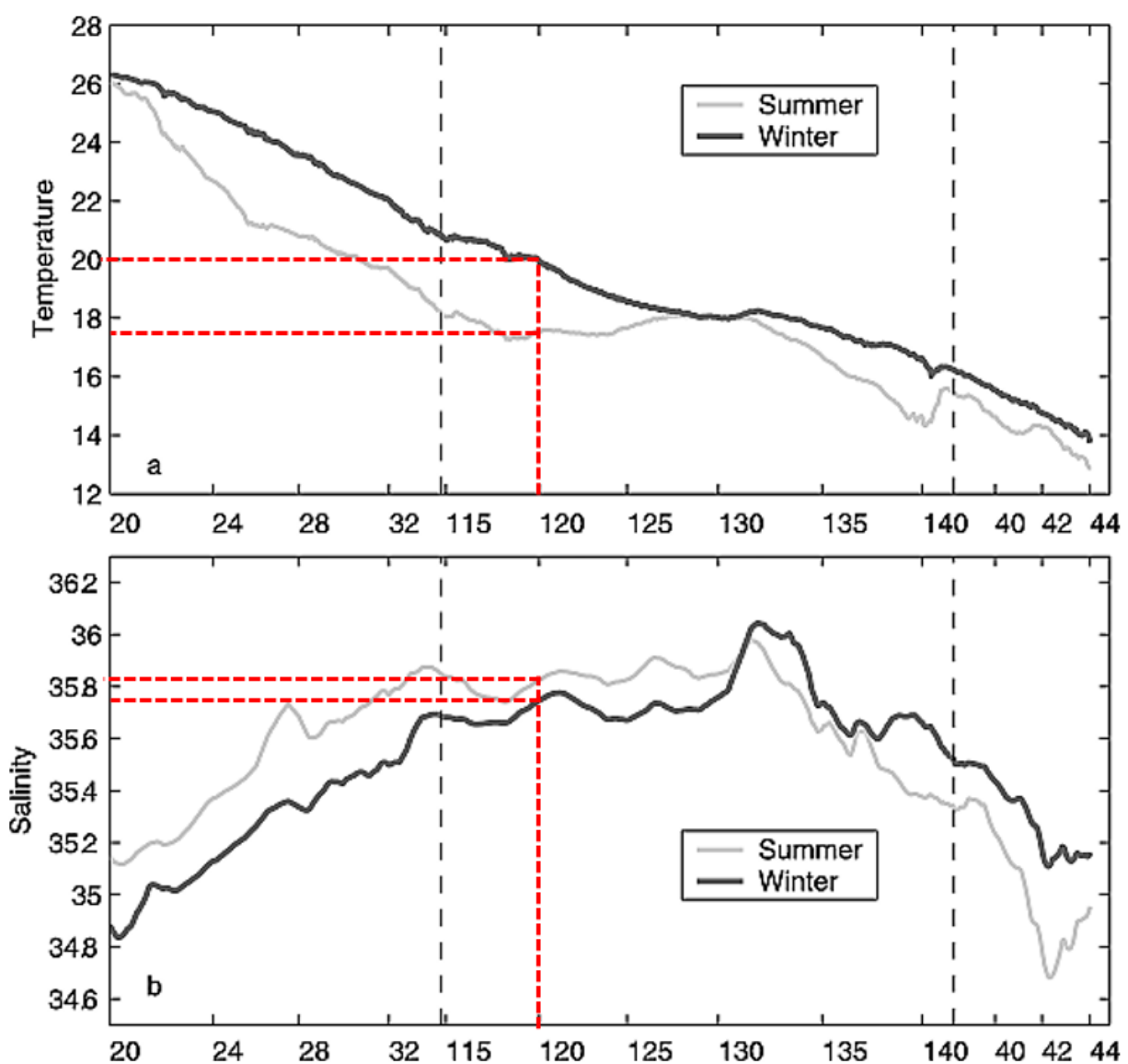


Figure 1.4: Monthly temperature and salinity data for the Great Australian Bight from 1989 to 2002. This data is from the advanced very high-resolution radiometers (AVHRR) aboard the polar orbiting NOAA satellites and has been corrected for cloud cover and a regional temperature anomaly. The red dotted line indicating what the temperature and salinity is at ~ 120°E which is the area focused on in this study. Figure is from Ridgway and Condie (2004) and was reproduced with permission.

### 1.1.3 Orcas

Most orca sightings in the western Great Australian Bight have been around the head of the Hood and Henry Canyons (Totterdell, 2014, Meeuwig et al., 2016, Meeuwig and Turner, 2017, Figure 1.2, 1.4). A recent well documented source of sightings was from Wellard et al. (2016) which detailed four predation events on beaked whales between 2014 to 2016. All four of these events involved a group of ~ 20 orcas attacking a lone beaked whale, with a smaller group of adult males trailing behind, resulting in a likely kill. Wellard et al. (2016) noted that there have been some observations of orcas predated on sunfish, as well as Meeuwig and Turner (2017) documenting that they have predated on giant squid. This orca aggregation is based on the availability of food, which is consistent with other orca aggregations in Australia, and worldwide (Nichol and Shackleton, 1996, Morrice, 2004, Barrett-Lennard and Heise, 2006, Wellard et al., 2016). Due to beaked whales' preference for deep-sea squid and benthic fish, their presence is indicative that this region food-chain is not based on plankton or krill (MacLeod et al., 2003).

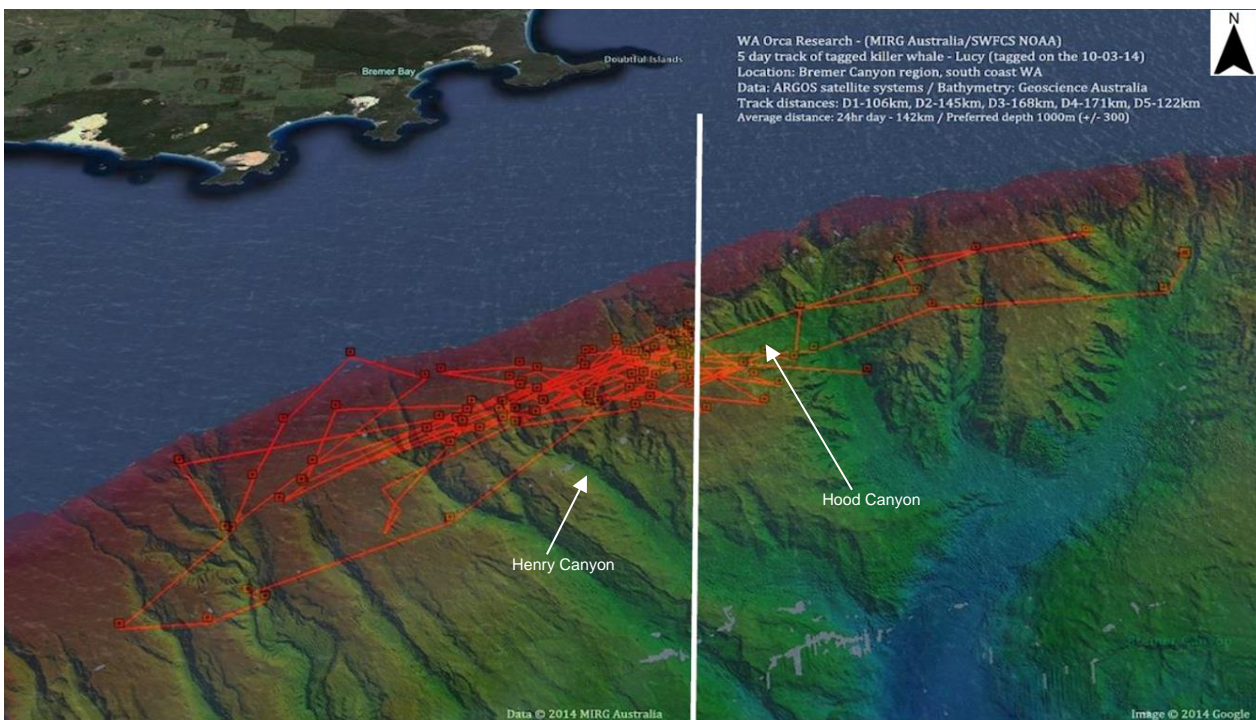


Figure 1.5: Satellite track of a tagged orca named “Lucy” which was observed between the 10<sup>th</sup> of March to the 15<sup>th</sup> of March 2014 (Totterdell, 2014). The area in which Lucy spent the highest proportion of time is the same area that 2019 sightings occurred (Figure 1.2). The white line is the western boundary to the Commonwealth Marine Park (Meeuwig et al., 2016) and was reproduced with permission.

Previous research into orca aggregations in the western Great Australian Bight has indicated that wind-driven upwelling events do not occur, despite the austral summer triggering upwelling events elsewhere in the Great Australian Bight (Kämpf et al., 2004, Mondello, 2017, Kämpf and Kavi, 2017). Nutrient studies undertaken in the region from 1995 to 2003 indicated that the western Great Australian Bight had a chlorophyll-a average between 0.10 mgm<sup>-3</sup> to 0.35 mgm<sup>-3</sup>, which indicates that if phytoplankton concentration are supporting any upwelling, it is done in events (Cetina-Heredia et. al, 2017). The Southern Surveyor voyage in April 2006 supported the

potential of a canyon based upwelling event due to observing a decrease of sea surface temperature around the Bremer Canyon (Pattiaratchi, 2007, Meeuwig et al., 2016, Figure 1.5). There has been a limited amount of research into testing if there is a canyon in the Albany canyon group which could be suitable for triggering a canyon based upwelling event. A subsurface upwelling mechanism has been proposed by Hovland and Riggs (2012) with hydrocarbon seeps pumping up methane as a potential cause for upwelling. Measurements from a recent glider deployment by Pattiaratchi (2017) were unable to link this mechanism to the aggregation of orcas (Meeuwig and Turner, 2017).

[Figure 1.6 has been removed due to copywrite restriction. The image is available online from Pattiaratchi (2007). URL: <https://parksaustralia.gov.au/marine/pub/scientific-publications/archive/sw-high-productivity.pdf>]

Figure 1.6: Sea surface temperature taken from the southern surveyor voyage in April 2006 which shows a localised patch of colder water around the Bremer Canyon. Image from Pattiaratchi (2007).

## 1.2 Upwelling

The availability of primary producers (i.e. phytoplankton) in the ocean is limited by the availability of light and nutrients, with the euphotic zone being light rich, but nutrient poor, whereas the disphotic and aphotic zones are light poor, but nutrient rich (Dugdale, 1972, Eppley and Peterson, 1979, Martin et al., 1987, Cullen et al., 1992, Legendre and Rivkin, 2002, Kämpf and Chapman, 2016). To overcome this limitation and due to seawater incompressibility, water must be laterally transported away from a region to trigger the vertical movement of deeper water to replace it (Currie, 1953, Hill and Johnson, 1974, Huthnance, 1981). This vertical movement of water from the disphotic zone for a prolonged period (few days to a few weeks), which is known as upwelling (Kämpf and Chapman, 2016), brings nutrients into the euphotic zone, creating conditions that are ideal for photosynthesis, as well as providing more food for heterotrophs through the increased phytoplankton biomass (Kämpf and Chapman, 2016). Until the excess of phytoplankton is exhausted by either grazing (Parsons et al., 1981, Frost, 1987), or the removal of nutrients by conditions returning to equilibrium (Cullen et al., 1992, De Baar, 1994), a region experiencing upwelling will have a higher amount of biological productivity compared to normal conditions (Bakun, 1990, Nieblas et al., 2009, Hales et al., 2006). These upwelling events typically last for 5-13 days but can last for 30 days depending on the quantity of nutrients that were upwelled by an event, as well as how the bottom water is upwelled into the euphotic zone (MacIsaac et al., 1985, Bakun, 1990, Wilkerson et al., 2006, Nieblas et al., 2009, Kämpf, 2012, Kämpf and Chapman, 2016).

### 1.2.1 Shelf Break Canyon Upwelling

Shelf break canyons are canyons which cut into the continental shelf. Like all submarine canyons, they tend to act to transport sediment from the surface to the abyssal plain (Paull et al.,

2005, Fildani, 2017). However, it is also possible to have the opposite flow present, causing nutrient-rich deep water to flow onto the continental shelf if certain conditions are met (Hickey, 1997, Allen et al., 2001, Kämpf, 2009). To allow upwelling to occur, a shelf break canyon needs to have a deep, steep, and narrow formation, as well as not being too close to the coastline (Allen and Durrieu de Madron, 2009, Allen and Hickey, 2010). It also requires a uniform oceanic flow that has the coastline on the right (left) of it in the southern (northern) hemisphere (Klinck, 1996, Hickey, 1997, Allen and Durrieu de Madron, 2009, Kämpf and Chapman, 2016). If the flow has the coastline on the left of the canyon in the southern hemisphere it can induce downwelling, however for an equivalent flow speed, the resulting downwelling would be weaker than upwelling (Boyer et al., 2004, Spurgin and Allen, 2014).

Should the change of depth between the canyon and the shelf be large enough, the cross-shelf flow interacting with the canyon can form a topographic Rossby wave. A topographic Rossby wave is an inertial wave which travels downstream and near parallel to a vertical structure (Rossby, 1939, Martell and Allen, 1979, Pond and Pickard, 1983, Kinsella et al., 1987, Pedlosky, 2013). As a current flow crosses the rim of the canyon, it gets stretched by the ocean suddenly becoming deeper (Hickey, 1997, Allen et al., 2001, Boyer et al., 2006, Allen and Durrieu de Madron, 2009, Dawe and Allen, 2010). Due to this stretching, the current can gain enough vorticity required for it to flow up the downstream rim and once it does that the current is squashed back into the shape it was prior to entering the canyon (the 'launch zone' in Figure 1.7). Depending on the amount of force is present in the current, as well as if there is a flow present in the opposite direction to the exiting flow, it will create a standing wave which will cause an increased amount of nutrients in and along the canyon rim (Kämpf, 2012, Kämpf and Chapman, 2016). If there is no opposing ambient current and enough force generated from the launch zone, a topographic Rossby wave will form. A result of this formation is that upwelling could occur anywhere from 20-100 km downstream of the canyon due to the heightened nutrient transport from mixing in the canyon (Kämpf, 2012, Kämpf and Chapman, 2016). A topographic Rossby wave could also result in a "breaking wave" forming as it leaves the canyon, which could steer the flow back towards the canyon Kämpf (2018).

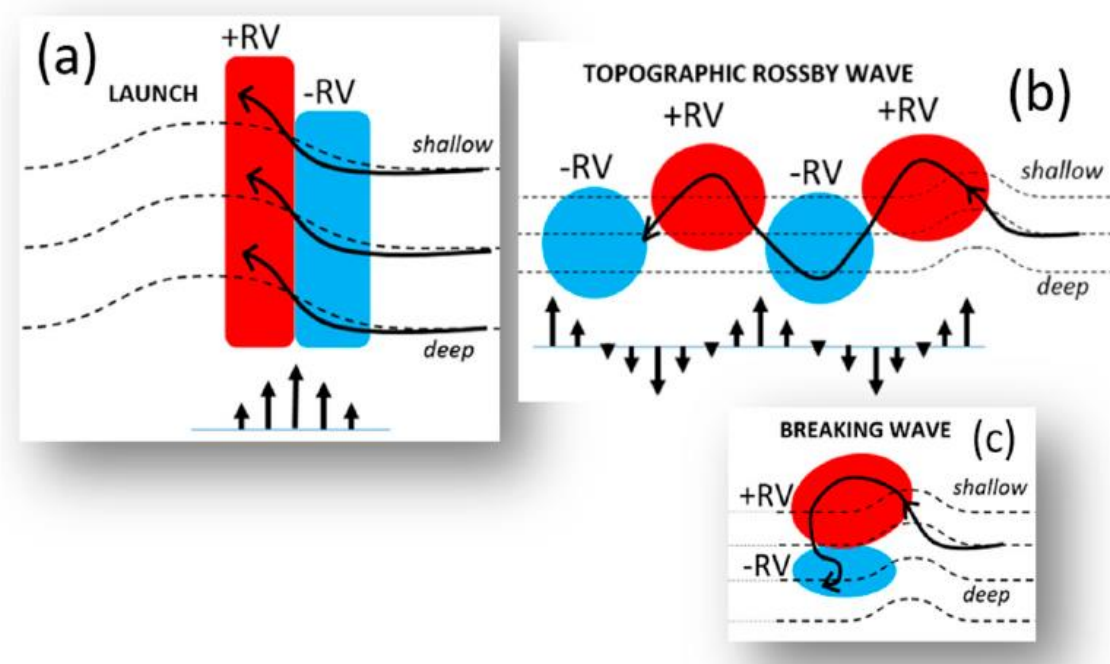


Figure 1.7: The schematic for how a topographic Rossby wave form. A) is the 'launch phase', B) the initiation phase and c) how breaking waves can form. Dashed lines are bathymetric contours, long arrows are flow trajectories, small arrows are the cross-shelf flow-direction and coloured regions notate areas of positive or negative vorticity (RV). Image is from Kämpf (2018) and was reproduced with permission.

Examples of shelf break upwelling occurring in Australia are the formation of the Kangaroo Island pool (McClatchie et al., 2006, Kämpf, 2007, Middleton and Bye, 2007, Kämpf, 2010, Kämpf, 2012) and a subsurface upwelling system that is caused by the Perth Canyons (Rennie et al., 2007, Rennie et al., 2009a, Rennie et al., 2009b). The Perth Canyon combined with a weakening Leeuwin Current and southerly winds forms an upwelling event at the head of the canyon (Pattiaratchi and Woo, 2009, Rennie et al., 2009b).

### 1.2.2. Deeper Upwelling.

Vertically migrating species such as zooplankton, some squid species and copepods have long been considered to aggregate around submarine canyons. (Olesiuk et al., 1990, Macquart-Moulin and Patriiti, 1996, Allen et al., 2001, Moors-Murphy, 2014, Rennie et al., 2009). The attraction for these species is that it allows them to reliably descend to a preferred daytime depth, as well as ascend to the surface during night-time. (Koslow and Ota, 1981). Lampert (1989) review on why zooplankton opted for a diurnal vertical migration supported the hypothesis that this was driven by avoiding predators instead of offering any tangible benefit to the zooplankton; undertaking a mantra of "better hungry than dead" (Zaret and Suffern, 1976, Kremer and Kremer, 1988). Unlike zooplankton, squid species migrate vertically due to its preferred prey also being vertical migrators (Bazzino et al., 2010). This contrasts with Gilly et al. (2006) findings that this vertical migration is primarily due to seawater temperature, as warmer conditions can cause physiological stress on squid. It is likely that both reasons play a role in migration seeing that different locations and squid species were used.

It had been proposed by Koslow and Ota (1981) and expanded on by Greene et al. (1988) that due to a canyon topography, there is the potential that a downwards flow could be forming which is both funnelling and trapping zooplankton into the canyon. This idea of flows pushing fauna downwards has not gained much traction, with Genin (2004) noting that neither Koslow and Ota (1981), or Greene et al. (1988) had supplied evidence behind their proposal. The current consensus why there is an increased amount of life within a canyon is due to a downwards flow transporting detritus deeper into the canyon, which acts as a reliable food source (Stefanescu et al., 1994, Cartes et al., 1994, Vetter and Dayton, 1998, Vetter and Dayton, 1999, Moors-Murphy, 2014). It has been noted by Stefanescu et al. (1994) that there is the potential that small fish use canyons as a place to breed and give shelter to their young.

Allen et al. (2001) found the opposite of what Greene et al. (1988) proposed, with a funnel-like effect assisting to push fauna out of the canyon. This was shown when deep water copepods such as *neocalanus plumchrus* found at depths < 150 m near the mouth of the Barkley Canyon. The reason a vertically migrating species exit the canyon in upwelling conducive conditions is a result of a canyon forming an upwards flow, which pushes them out of the canyon, or prevents a vertical migrator from descending (Macquart-Moulin and Patriiti, 1996, Hickey, 1997, Allen et al., 2001, Genin, 2004, Figure 1.8). This could potentially be a mechanism for canyons that do not cut into the shelf break to be productive, however, there has been an insufficient amount of research to evaluate whether this would cause a biological response.

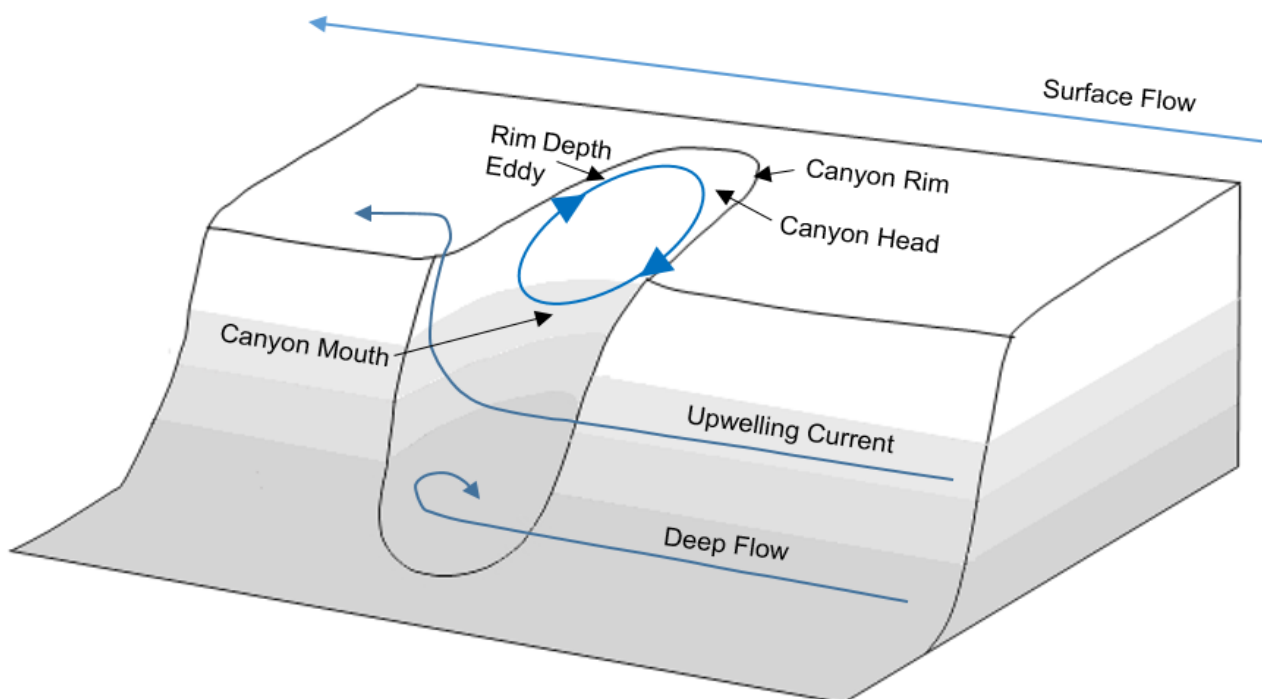


Figure 1.8: Sketch of how flows at varying depths will interact with a canyon when upwelling conducive conditions are present in the Southern Hemisphere. Based on the Northern Hemisphere equivalent by Allen and Hickey (2010).

### 1.3 Experimental Methods for Canyon Based Upwelling

Over the past forty years there have been numerous works on solving what is the dynamics of canyon based upwelling events, including observations (Hickey et al., 1986, Hickey, 1997, Allen et al., 2001, Flexas et al., 2008), laboratory experiments (Pérenne et al., 2001, Allen et al., 2003, Mirshak and Allen, 2005, Boyer et al., 2006) and hydrodynamic models (Klinck, 1988, Klinck, 1996, Allen et al., 2003, Lett et al., 2006, Kämpf, 2007, Rennie et al., 2007, Mason et al., 2012, Connolly and Hickey, 2014, Saldias and Allen, 2020). When comparing laboratory experiments with hydrodynamic models, Dawe and Allen (2010) noted that results tended to be replicable for canyons with shallow slopes, and not with steep slopes. Most hydrodynamic models based around canyons are in three-dimensions (Klinck, 1996, Allen et al., 2003, Kämpf, 2007, Rennie et al., 2007, Kämpf, 2018, Saldias and Allen, 2020), however, two-dimensional (“idealised”) models have also been used to resolve upwelling in canyons (Kämpf, 2005), jet formations due to wind driven upwelling (Castelao and Luo, 2018), and physical characteristics of an upwelling flow (Allen et al., 1995, Chapman and Lentz, 2005, Estrade et al., 2008).

One hydrodynamical model that has been used for canyon based upwelling is the Coupled Hydrodynamical-Ecological Model for Regional Shelf Seas (COHERENS) model, which is an open source model program released in 1999 and coded with Fortran 90/95 (Luyten et al. 1999). The COHERENS model has been used in both theoretical canyon-based upwelling projects, as well as case studies within the Great Australian Bight (Kämpf, 2007, Kämpf, 2009, Kämpf, 2012, Kämpf, 2018). An alternative model for canyon-based upwelling is the Regional Ocean Modelling System, which is open source model using Fortran 95 as its base language. This has also been used in theoretical studies involving canyon-based upwelling (She and Klink, 2000, Chen et al., 2014, Connolly and Hickey, 2014, Saldias and Allen, 2020) and case studies focused on the Perth Canyons (Rennie et al., 2007, Rennie et al., 2009a). Whilst there is no direct comparison between the two products in the literature, there is an indirect comparison as whilst both COHERENS and ROMS are primarily driven by a  $\sigma$  (terrain) co-ordinate model in the vertical grid, ROMS does hybridise with both z and density co-ordinate systems, whereas COHERENS is just a  $\sigma$  co-ordinate model (Luyten, 1999, Shchepetkin and McWilliams, 2005). This does have a trade off as the  $\sigma$  co-ordinate model has the possibility of generating geostrophic flow off truncation errors occurring when steep slopes are present (Haney, 1991, Auclair et al., 2000, Khorrami and Banihashemi, 2019), however a hybrid model does end up utilising more computational power to calculate a result by virtue of being more of a hybrid model, which could lead to sacrifices elsewhere in the model.

A method to both visualise the results of a hydrodynamic model and to test what would occur with the resultant flow paths is to use a Lagrangian particle tracker. This simulates what would occur to neutrally buoyant, passive floats in the water column at a predefined depth and can be used as a proxy for water particles (Kämpf 2010, Rivas and Samelson, 2011, Mason et al., 2012,

Connolly and Hickey, 2014), marine organisms (Lett et al., 2006, Clavel-Henry et. al., 2019) and nutrients (Cetina-Heredia et. al, 2017). This gives the advantage of being able to show the flow path of a particle interacting with a topographic feature. (Kämpf, 2006, Connolly and Hickey, 2014, Ahumada-Sempoal et al., 2015). This has led to Lagrangian particles to being used in theoretical studies of canyon upwelling (Jordi et. al., 2005, Kämpf, 2006, Kämpf, 2018) and case studies (Ardhuin et. al., 1999, Allen et al., 2001, D'Asaro 2004, Kämpf 2010, Connolly and Hickey, 2014, Clavel-Henry et. al., 2019). Lagrangian particle trackers are built into COHERENS and ROM models (Luyten, 1999, Shchepetkin and McWilliams, 2005).

A substantial decrease in temperature in the water column is one indicator of a canyon based upwelling event, as deep water is pushed upwards (Allen et al., 2001, Rennie et al., 2007, Connolly and Hickey, 2014). Should that deeper water be upwelled into the euphotic zone, the concentration of chlorophyll or nutrients can also be used as an indicator of upwelling (Macquart-Moulin and Patriiti, 1996, Genin, 2004). Alternatively, as a biological response is expected for upwelling, an increased concentration of marine life in a region can also indicate that upwelling is occurring in the shelf break (Moulins et al., 2007, Moors-Murphy, 2014).

#### 1.4 Objectives of this Study

This thesis is focused on two hypotheses for how the western Great Australian Bight can support an orca aggregation via an upwelling event involving the Bremer, Hood and Whale canyons. The first hypothesis is that a topography Rossby wave could form to drive upwelling at the shelf break. The second hypothesis is that an interaction between the Flinders current and canyons which may drive a subsurface upwelling event through the canyon at depth, which would allow a pathway to form for marine organisms to travel through the canyon and enter the area where orcas are predating.

To test these hypotheses, a hydrodynamic model of the western Great Australian Bight was used with bathymetry obtained during a CAPSTAN cruise To test for a topographic Rossby wave, the model was based on velocity fields which were obtained from satellite derived altimetry (Ridgway and Condie, 2004). For the Flinders Current using the canyons as a pathway for deeper water to end up in the upper continental slope, velocity fields were estimated from the modelling work of Arthur (2006) resembling the average flow of the Flinders Current at 600 m. Any hydrodynamic modelling results obtained were compared to temperature and salinity data from the western Great Australian Bight to test the likelihood of any modelling result occurring. This research can help further the understanding the relationship that currents have with canyons.

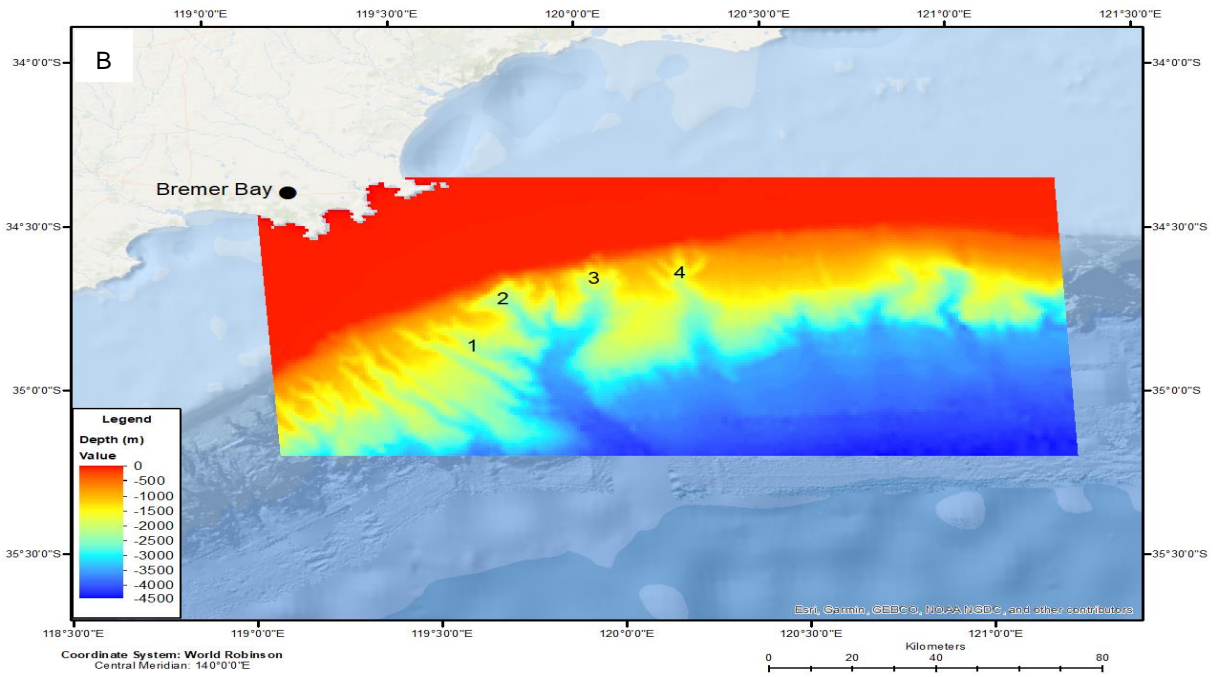
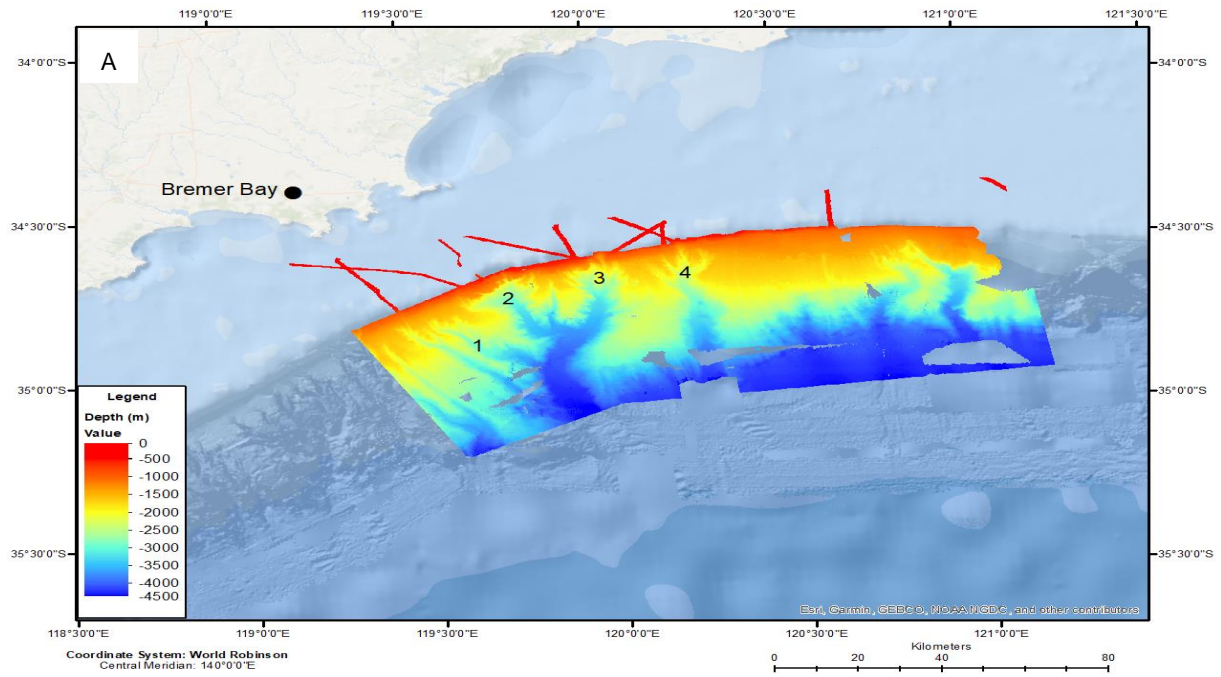
## CHAPTER 2 METHODS

### 2.1 Bathymetry

The area of focus for this research is a 103.2 km by 97.2 km section of ocean off the Bremer Bay coastline (Figure 1.1). For the research to show that a canyon has the necessary structure for an upwards flow, bathymetry data for the area was needed. For this, CAPSTAN (Collaborative Australian Postgraduate Sea Training Alliance Network) 2017 cruise obtained bathymetric multibeam data from a section of the western Great Australian Bight in between 119.15°E to 121.20°E, and 34.32°S to 35.21°S, with the use of a multi-beam echo sounder. This allowed a resolution of  $4.51 \times 10^{-4}$  degrees by  $4.51 \times 10^{-4}$  degrees per measurement (Figure 1.3, 2.1A), which equals to 0.0413 km per measurement horizontally, and 0.0503 km per measurement vertically. This bathymetry showed that both Bremer and Whale Canyon are on the edge of the shelf break, and that the Hood Canyon structure showed a potential funnel shape on the western arm of the canyon.

After the CAPSTAN 2017 cruise, there was 57.18% of the area which did not have bathymetric data at a resolution of 0.0413 km by 0.0503 km (Figure 1.3, 2.1A). Due to this missing data, a composite bathymetry was created using the GEBCO (General Bathymetric Chart of the Oceans) 2014 dataset to fill in gaps. This GEBCO 2014 grid was measured using a combination of ship sounding, and satellite measurements which was used to interpolate any gaps in the ship sounding measurements. The GEBCO 2014 grid was measured at a resolution of 0.94 km by 0.795 km per pixel, however, due to that interpolation it is not missing any data in the southwestern section of Australia (Figure 2.1B).

To merge the CAPSTAN and GEBCO bathymetry data together for a composite bathymetry of the region, the GEBCO data was converted to a resolution of 0.0503 km by 0.0413 km per pixel. This conversion added ~18.48 cells for each cell of GEBCO data to make it the same resolution as the CAPSTAN data. This conversion was done as a cubic convolution through ArcGIS, which also smoothed the added GEBCO cells by taking the weighted average of the 16 closest cells for each created cell. Once that was completed and the locations for both bathymetry sources locations were lined up perfectly, they were merged together using ArcGIS keeping the CAPSTAN data untouched, and the GEBCO data filling in the spaces with no data (Figure 2.1C). This created a dataset that was 4545 by 1968 cells for the composite bathymetry. No smoothing was done to the composite bathymetry once that occurred as both data sets melded together with no significant depth changes occurring at the edge of the CAPSTAN data.



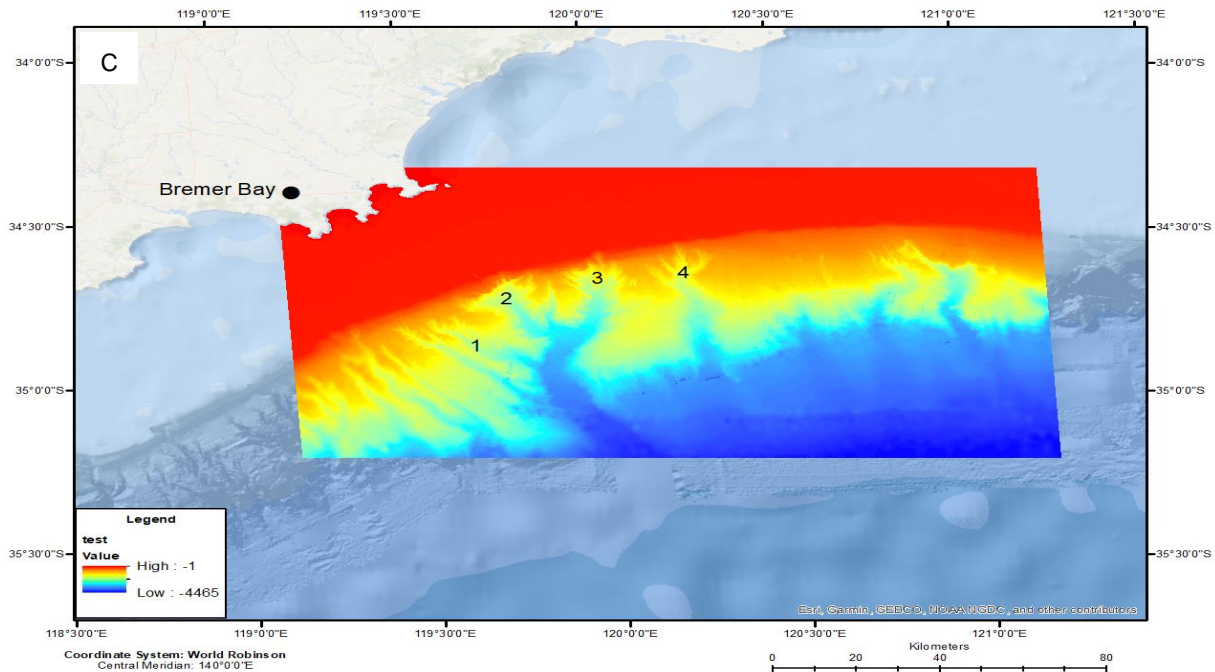


Figure 2.1: The GEBCO bathymetry (A), The CAPSTAN bathymetry (B), and the resulting bathymetry (C) after combining the GEBCO data with the multibeam echo data from CAPSTAN for the Western Great Australian Bight. As a result, the fidelity of the canyons has increased, as well as the voids in the CAPSTAN bathymetry filled out by the GEBCO dataset.

## 2.2 Canyons

Using the composite bathymetry, the depth of the Bremer Canyon ranged from ~ 145 m to 4264 m. The length of the Bremer Canyon varied from ~ 2.5 km to ~ 9 km, and there was an average horizontal difference in depth from outside of the canyon to the bottom of the canyon of ~ 1200 m to ~ 1600 m for north of where the Hood Canyon forms, with a minimum difference of ~300 m at the uppermost north point. Slope was calculated using a z-factor of  $1.11 \times 10^{-5}$ , which was approximately the equivalent of 40 degrees of latitude. For areas north of where the Hood tributary canyon forms, the Bremer Canyon formed an average slope on its northern wall at  $23^\circ$ , the eastern wall at  $22.68^\circ$  and the western wall at  $28.95^\circ$ . The plateau had an average slope to enter or exit the canyon of  $18.96^\circ$ , and the western canyon wall next to the plateau had a slope of  $23.05^\circ$  (Figure 2.2). The depth difference between the plateau and the canyon was ~ 1000 m to ~ 1200 m horizontally compared to the Bremer Canyon.

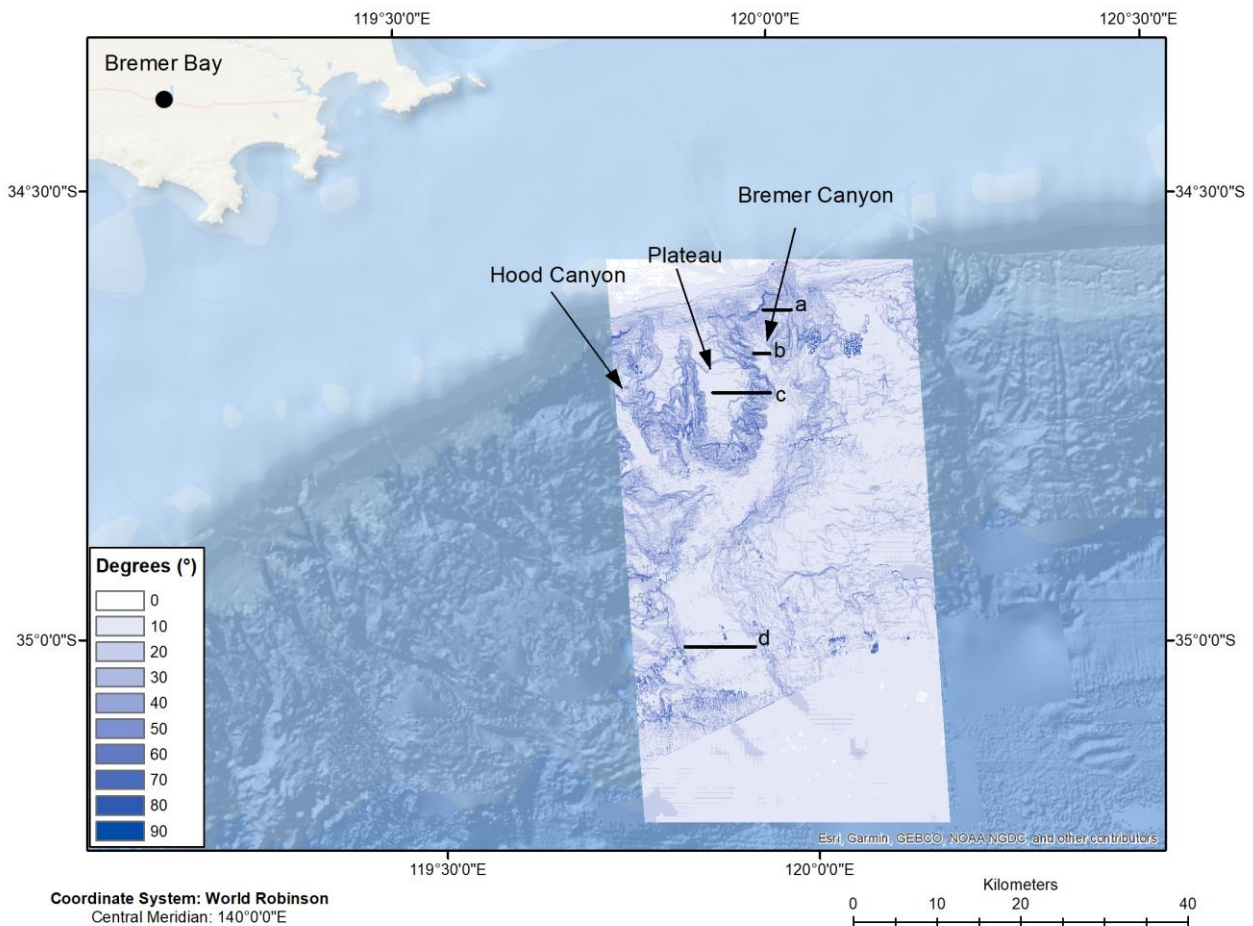


Figure 2.2: The slope of the Bremer Canyon (119.86°E to 120.13°, and 34.57°S to 34.71°S), with a red to blue colouring to indicate the amount of slope encountered in each cell. The maximum slope present in the canyon is 74°, which is located on the northern canyon wall, and the minimum slope present is 0°, which represents 1.41% of the area used for the Bremer Canyon and is primarily located on the continental shelf. a) has a width of 4 km with a  $\Delta$ depth (how deeper it is compared to the depth outside of the canyon) of 300 m, b) has a width of 2.5 km with a  $\Delta$ depth of 1000m, c) has a  $\Delta$ depth of 1200 m and d) has a width of 9 km with a  $\Delta$ depth of 1200 m to 1600m.

The depth of the Whale Canyon ranged from ~ 174 m to 4391.06 m. The length of the Whale Canyon ranged from ~ 3 km to ~ 7 km south of where it branches off into three arms and ranged from ~ 0.8 km to ~ 3 km once it has branched off. Depth wise, the difference between the bottom of the canyon and outside of the canyon ranged from ~ 300 m at the most northern extent of the canyon, to ~ 600 m around the canyon arms and ~ 900 m south of those arms. The mid-arm of the canyon had an average slope of 24.88°, the eastern arm had an average slope of 21.99°, and the western arm was 27.88° (Figure 2.3).

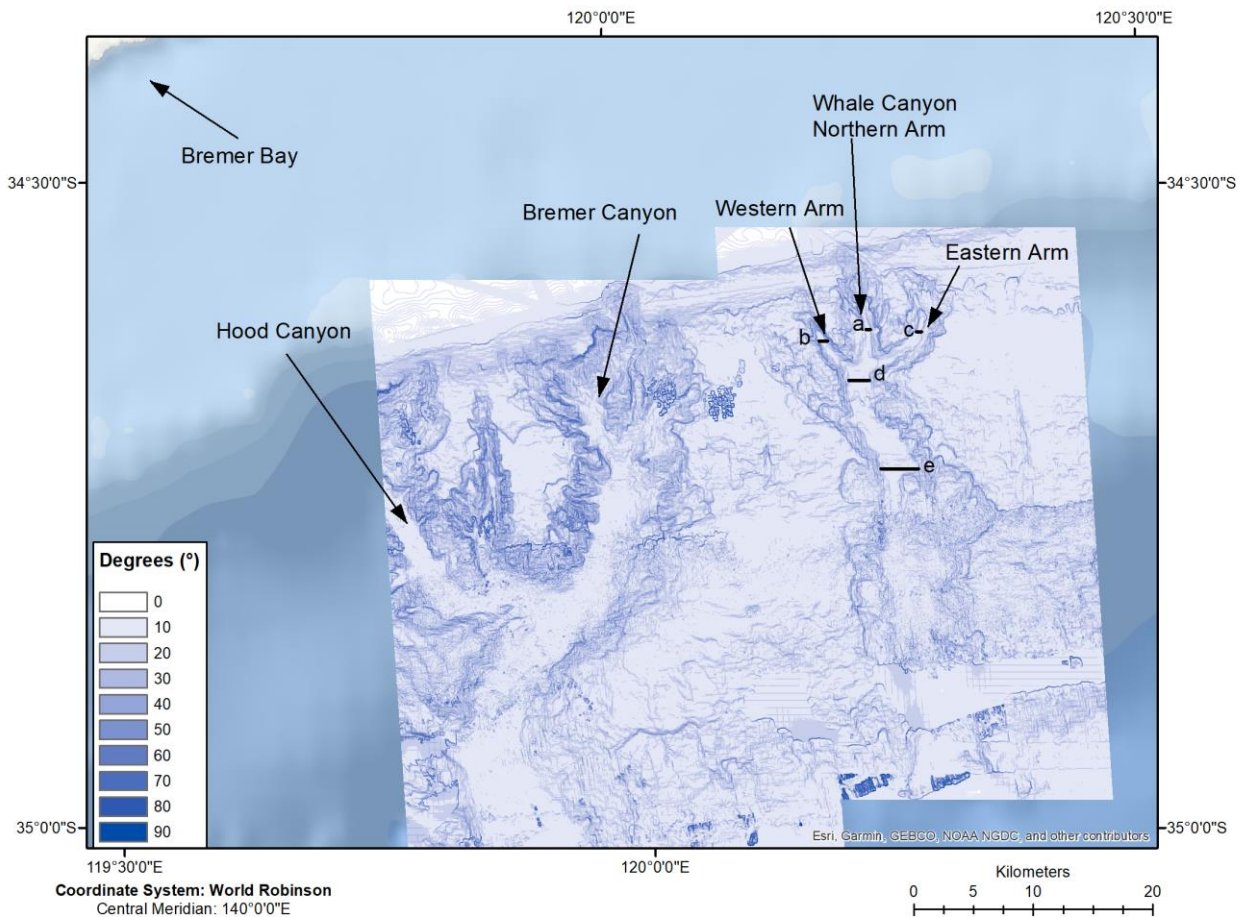


Figure 2.3: The slope of the Whale Canyon (120.11°E to 120.36°E, and 34.54°S to 34.98°S). The maximum slope is 67.35° in the northern arm of the canyon, and the minimum slope of 0°, which accounts for 0.50% of the area used to represent the Whale Canyon. A) has a width of 0.8 km and a  $\Delta$ depth of 300 m, b) has a width of 0.6 km and a  $\Delta$ depth of 600 m, c) has a width of 0.3 km and a  $\Delta$ depth of 600 m, d) has a width of 1.5 km and a  $\Delta$ depth of 900 m and e) has a width of 3.0 km and a  $\Delta$ depth of 900 m.

The depth of the Hood Canyon ranged from ~178 m to 2934.84 m. The length of the Hood Canyon varies from ~ 2 km to ~ 6 km horizontally, and a maximum of ~ 3.5 km vertically in the outlet. The difference in depth between the bottom of the Hood Canyon and the external seafloor is ~ 1200 to 1500 m horizontally. The average slope of the outlet on the western side of the canyon was 22.55°, which was a 6.88° decrease in slope from the canyon wall on the western side to the south of it, at 29.23°. The northern canyon wall had an average slope of 27.22°, and the eastern canyon wall, which had a slope of 26.79° (Figure 2.4). Due to a ~5-7° difference between the hypothesised outlet point, and the rest of the Hood Canyon, this supported the idea that it could support a pathway between the area where orcas are sighted and the deeper sections of the continental slope.

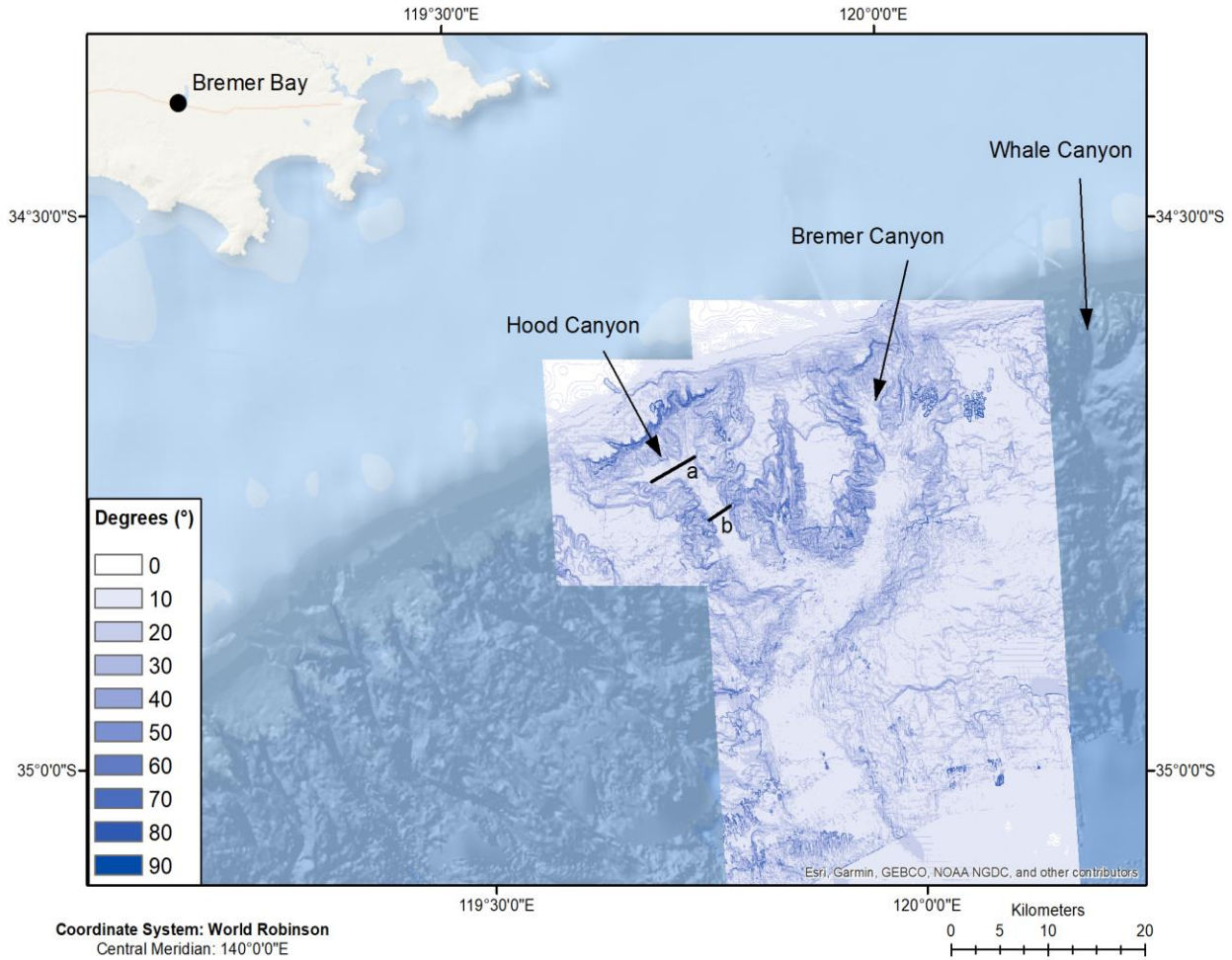


Figure 2.4: The slope of the Hood Canyon (119.59°E to 119.90°E, and 34.63°S to 34.83°S). The maximum slope is 82°, which is located on the northern wall, and the minimum slope of 0°, which accounts for 4.75% of the Hood Canyon domain. A) has a width of 6 km and a  $\Delta$ depth of 1200 m and b) has a width of 2 km and a  $\Delta$ depth of 1500 m.

## 2.3 Altimetry

To test whether the Whale or Bremer Canyons can upwell water via a topographical Rossby wave, the geostrophic flow for the region was needed. Geostrophic flow is the result of the Coriolis force balancing out any water movement which is caused by a pressure gradient causing the direction of the flow to pivot 90° to the left of where the high pressure originates in the southern hemisphere (and to the right in the northern hemisphere). The equation to calculate geostrophic flow at the surface is from Pond and Pickard (1983) (2):

$$v = \frac{g}{f} * \frac{\delta\zeta}{\delta x} \quad (2)$$

where  $v$  is the velocity ( $\text{ms}^{-1}$ ),  $g$  is gravity ( $9.8 \text{ ms}^{-2}$ ),  $f$  is the Coriolis force ( $10^{-4} \text{ s}^{-1}$ ),  $\zeta$  is the sea level height (m), and  $x$  is the length between the two stations used (m). Sea level height is used as changes in sea level height directly proportional to changes in pressure. This allows satellite-

based sea surface height data to be used to estimate the geostrophic velocity at the surface (Ducet et al., 2000, Scharffenberg and Stammer, 2010).

Altimetry (also known as sea surface height) data from Archiving Validation and Interpretation of Satellite Oceanographic data (AVISO) was obtained to measure the change in sea level elevation between two points (<https://las.aviso.altimetry.fr/las/UI.vm>). This data used a combination of measurements from the JASON-1, JASON-2/OSTM, and TOPEX/POSEIDON satellites, which had operated from 04/01/1993 to 31/05/2017. These satellites had a resolution of 0.25 degrees by 0.25 degrees per measurement, and had no missing data due to cloud cover, with measurements taken weekly. This conglomeration of satellites was preferred for this study over the new generation due to the number of years of available data, as the new generation of satellites came into operation during 2017. AVISO has two ways to show altimetry measurements, absolute dynamic topography, and sea surface anomaly (Pujol et al., 2016, Pujol, 2017). Absolute dynamic topography is a measure of the sea surface height relative to the geoid height in the measured location. Sea level anomaly is similar, except that the measured sea surface height is subtracted by the overall average of altimetry data in the area (Dibarboure et al., 2011, Pujol et al., 2016, Pujol, 2017).

For this project, altimetry data was used to calculate surface current velocity, with absolute dynamic topography being preferred to minimise potential errors with averaging (equation 2). For measuring the sea height gradient, the stations used were the ones closest to the coastline and one ~ 150-200 km to the south of the first measurement. This method was consistent with the method Ridgway and Condie (2004) used to calculate the change in altimetry. Stations used were “Albany” (118°E, 34.9°S to 36.6°S), “Bremer Bay” (119.7° E, 34.1° S to 35.6° E), and “Esperance” (121.9°E, 33.9°S to 35.4°S), using local towns as landmarks to place these measurements (Figure 2.5). The eastwards flow is the Leeuwin Current, a seasonal current which flow speed peaks during the Austral wintertime, and a westwards flow indicates the formation of a periodic coastal current (Cresswell and Golding, 1980, Herzfeld and Tomczak, 1997, Ridgway and Condie, 2004, Cresswell and Domingues, 2009). To show when a coastal current had formed, “events” where a westwards current had formed with a current velocity of  $2.5 \text{ cms}^{-1}$  for at least three weeks was used. The total time each November to March each year that was under event condition, alongside the longest event each year, the average weekly velocity for an event and the maximum weekly velocity was taken and used to pair with modelling results.

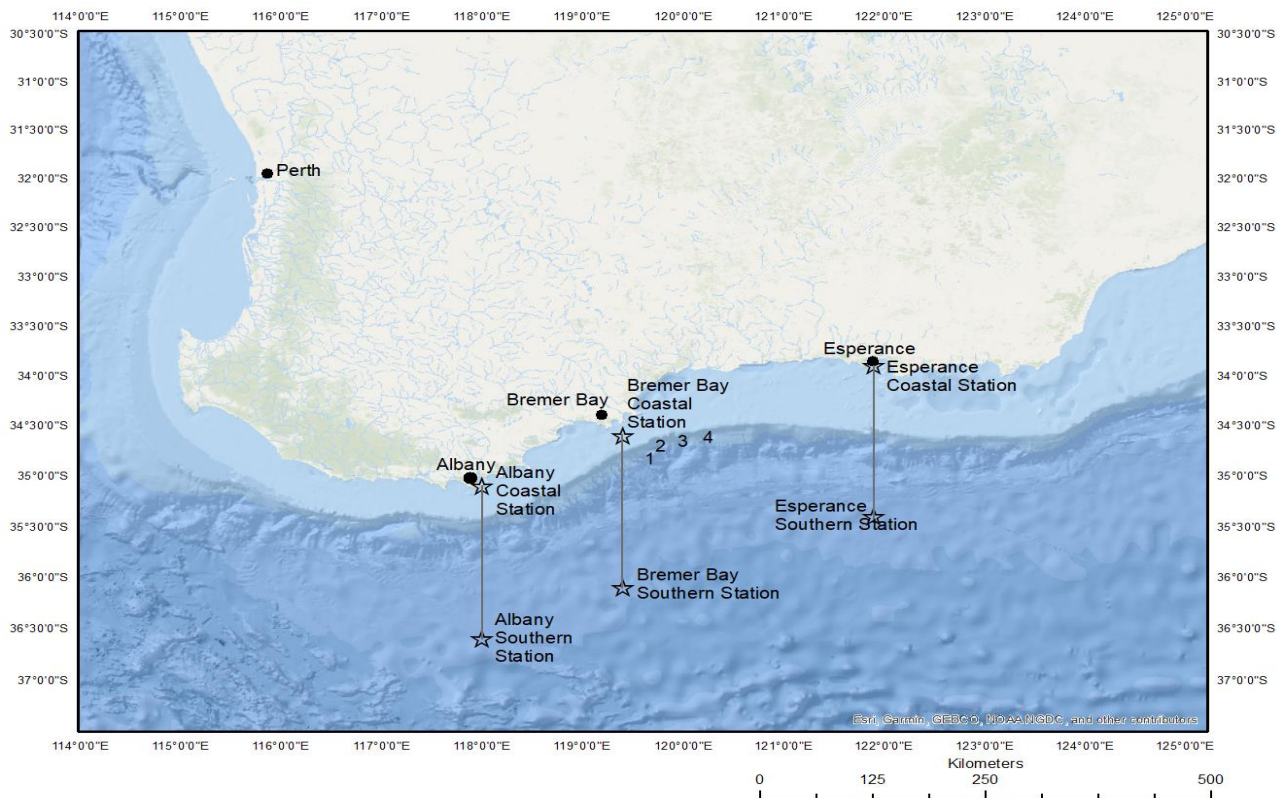


Figure 2.5: Location of the areas used for altimetry data, with one station as close to the coastline as possible, and the other station around ~ 150-200 km away. The shelf break is around the middle of these stations, which is the area of interest for flow.

## 2.4 Experiment Design

### 2.4.1 Shelf Break Experiments

The model domain for the shelf break experiments is shown in Figure 2.6. The grid is a 1800 by 500 grid which had the south-western corner at 0,0. This covered a 48 km by 20 km section of the western Great Australian Bight with resulting grid spacing of  $\Delta x = 0.32$  km and  $\Delta y = 0.4$  km. The domain was rotated by  $15^\circ$  in a clockwise direction to get the shelf break as horizontal as possible, as the continental shelf has a southwest orientation (Figure 1.1), which is to resolve the canyons interaction with the horizontal flow. This domain had a minimum depth of 0 m and had its maximum depth capped at 1000 m to save on computational power. Six days of run time for the sea height change and three-hour timesteps were chosen by trial and error as it offered a balance between model stability and accuracy. The model domain was made up of 65.93% of cells within the continental shelf ( $< 100$  m), and 34.07% in the continental slope ( $> 100$  m). The eastern boundary for this model was set to 47.04 km to 48 km, and the western boundary was set to 0 to 0.96 km. For the shelf break experiments, the change in sea height was set to occur on the northern boundary, and the simulation was given six days to adjust to this change, with a timestep of three hours per calculation. The northern and southern boundary was set to prevent particles from leaving the model domain, whereas the eastern and western allowed particles to

leave the model domain. This should prevent any influence the southern boundary could have on the canyons nearby.

On the fifth day of model run time, 5000 particles were immediately released in the confines of either the eastern or western boundary, being dependant on the direction of flow. If these particles were released on the western boundary, it was confined to 0 to 0.96 km in the x direction and 0.8 to 6.4 km in the y direction. For the eastern boundary, they were released between 46 km to 48 km in the x direction and 0.8 to 6.4 km in the y direction. These particles were split into five groups of 1000, and a set was released between 100 m to 200 m (dubbed PG1), 200 m to 300 m (PG2), 300 m to 400 m (PG3), 400 m to 500 m (PG4) and > 500 m (PG5). Particles are not consigned to the range of depths they were released in as they travel through the model. The location of these particles was calculated for fifty-five days after they were released, with a three-hour timestep for each calculation.

Six experiments were planned for the shelf break model (Table 2.1). SB1 was designed with the formation of a westerly flow in the western Great Australian Bight, with an average velocity calculated from altimetry in the region. SB2 represents when an easterly flow which was based off the Leeuwin current is present in the western Great Australian Bight. SB3 and SB4 were designed to simulate SB1 and SB2 in the northern hemisphere. This will act to test if the model works properly and if the canyon structure is capable of supporting upwelling regardless of flow direction. SB5 and SB6 were designed to test how an upwelling event could change by varying the flow velocity. The data that was extracted from these experiments was the sea level elevation, the zonal and meridional Eulerian velocity for the entire domain, as well as at specific locations after the model has reached its final state (Figure 2.6, Table 2.2). After particles have passed through the model the percentage of particles entering areas of interest and the velocity of particles travelling through the model domain was taken.

Table 2.1: List of shelf break experiments, as well as the hemisphere the experiment is set in, and the change of sea level elevation from a mean of 0.

Experiment Number	Experiment
SB1	Southern hemisphere with a 2 cm decrease in sea level elevation at the northern boundary.
SB2	Southern hemisphere with a 2 cm increase in sea level elevation at the northern boundary.
SB3	Northern hemisphere with a 2 cm decrease in sea level elevation at the northern boundary.
SB4	Northern hemisphere with a 2 cm increase in sea level elevation at the northern boundary.
SB5	Southern hemisphere with a 4 cm decrease in sea level elevation at the northern boundary.

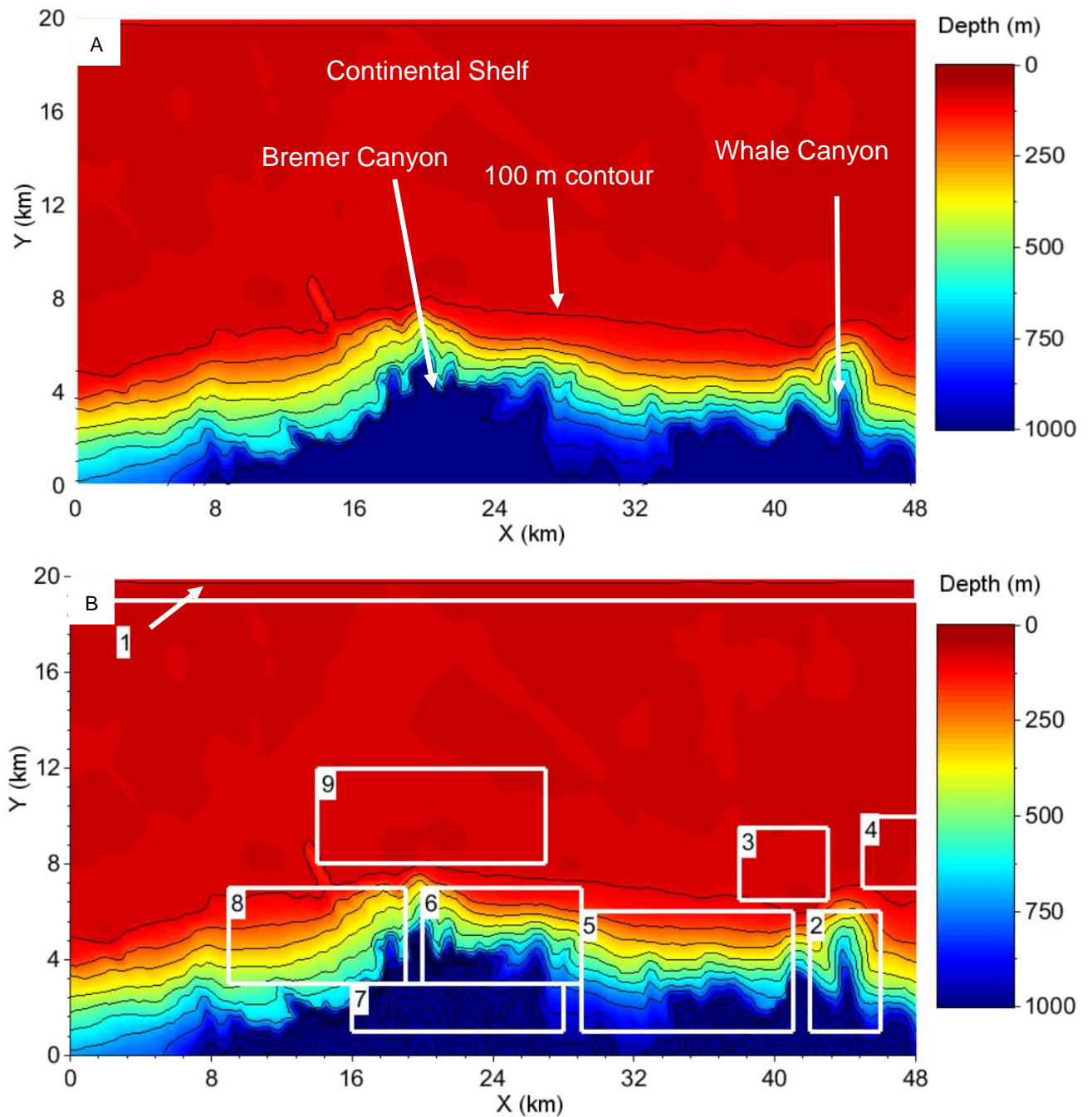


Figure 2.6: The domain for the shelf break upwelling model (A), and the locations of interest within the shelf break experiments (B), overlain by 100 m contours (black). The location of the Whale Canyon is at ~ 43 km to ~ 45 km horizontally, and 0 to 7 km vertically, and the Bremer Canyon is at ~ 18 km to ~ 27 km horizontally, and 0 to 7 km vertically.

Table 2.2: The locations of interest within the shelf break model domain (Figure 2.6B).

Square	Location	Reason
1	Northern boundary	Test if the model is working as designed as the northern boundary is where the sea level elevation is set to change in.
2	Whale Canyon	One of the canyons which could form a topographic Rossby wave
3	Continental shelf to the northeast of the Whale Canyon	Particles should upwell from the Whale Canyon into this location with a westwards flow.
4	Continental shelf to the northwest of the Whale Canyon	Particles should upwell from the Whale Canyon into this location with an eastwards flow.
5	Between the Whale and Bremer Canyon	To show how many particles are approaching either the Bremer Canyon or Whale Canyon which are within the continental slope.
6	The eastern Bremer Canyon perimeter	The entry point for particles that could upwell out of the Bremer Canyon with a westward flow.
7	The head of the Bremer Canyon	The area that would show if downwelling occurs in the Bremer Canyon.
8	The western Bremer Canyon perimeter	The entry point for particles that could upwell out of the Bremer Canyon with an eastward flow.
9	Continental shelf north of the Bremer Canyon	The first location that particles which upwell from the Bremer Canyon will land into.

#### 2.4.2 Deep Canyons Experiments

For each deep canyon experiment (notated DC1-6, Table 2.2), a 2000 by 1200 cell grid was taken from the composite bathymetry between 1 to 2000 in the x-direction, and 600 to 1800 in the y-direction. This was condensed into a 100 x 60 grid (Figure 2.7) by using the weighted average

of cells around it. This gave an 80 km by 60 km domain of the western Great Australian Bight, with a grid spacing of  $\Delta x = 0.8$  km and  $\Delta y = 1$  km, and the 0,0 point in the south-western corner. To make the shelf as straight as possible the domain was rotated clockwise by  $15^\circ$ , due to the south-westward slope of the continental shelf. The idea behind this experiment was to test that when the westward Flinders current hits the Bremer Canyon, it will flow northwards and end up outflowing via the westward arm of the Hood Canyon. If so, this offers an easy and predictable path for squid to exit the canyon, and from that, offered a potential hunting ground for orcas, as well as other cetaceans. The minimum depth for this experiment was 60 m, and the maximum depth was set to 3500 m, which only affects a small amount of the model domain, which is mostly in the Bremer Canyon. Of this, 16.52% of the model domain was located within the continental shelf, and 83.48% is located within the continental slope. The eastern boundary for the deep canyon experiments was set between 76 km and 80 km, the western boundary was set between 0 km and 4 km. The boundary conditions that were used in SB 1-6 were also used in DC 1-6. Like SB 1-6, the change in sea height was set to occur on the northern boundary, and the simulation was given six days to adjust to this change, with a timestep of 3 hours per calculation.

After five days of model runtime, 4000 particles were instantaneously released into the model domain from either the eastern or western boundary, with a timestep of three hours per calculation and an overall run time for particles of fifty-five days. These particles were released between 0 to 4 km in the x direction and 14 km to 44.5 km in the y direction on the western boundary. When released on the eastern boundary, the x direction shifts to between 76 km to 80 km, whilst the y-direction remains constant. These 4000 particles were released in four groups of 1000, which were set to be in between 600 m to 1200 m (dubbed PG1), 1200 m to 1800 m (PG2), 1800 m to 2400 m (PG3) and 2400 m to 3000 m (PG4). Particles are not consigned to the range of depths they were released in as they travel through the model.

Like the shelf break experiments, six experiments were planned for the deep canyon model. (Table 2.3), and they follow a similar design principle. DC1 was focused around the average Flinders Current velocity in the western Great Australian Bight, and DC2 was if the eastward flow formed in the area with a reversed sea level gradient to DC1. DC3 and DC4 were focused on creating an eastward and westward flow in the northern hemisphere. DC5 and DC6 were focused on how different flow velocities impacted upwelling. The data that was extracted from these experiments was the sea level elevation, the zonal and meridional Eulerian velocity for the entire domain, as well as at specific locations after the model has reached its final state for sea level elevation (Figure 2.7, Table 2.4). After particles has passed through the model the percentage of particles entering areas of interest and the velocity of particles travelling through the model domain was taken.

Table 2.3: List of deep canyon experiments, as well as the hemisphere the experiment is set in, and the change of sea level elevation from a mean of 0.

Experiment Number	Experiment
DC1	Southern hemisphere with a 5 cm decrease in sea level elevation on the northern boundary.
DC2	Southern hemisphere with a 5 cm increase in sea level elevation on the northern boundary.
DC3	Northern hemisphere with a 5 cm decrease in sea level elevation on the northern boundary.
DC4	Northern hemisphere with a 5 cm increase in sea level elevation on the northern boundary.
DC5	Southern hemisphere with a 10 cm decrease in sea level elevation on the northern boundary.
DC6	Southern hemisphere with a 2.5 cm decrease in sea level elevation on the northern boundary.

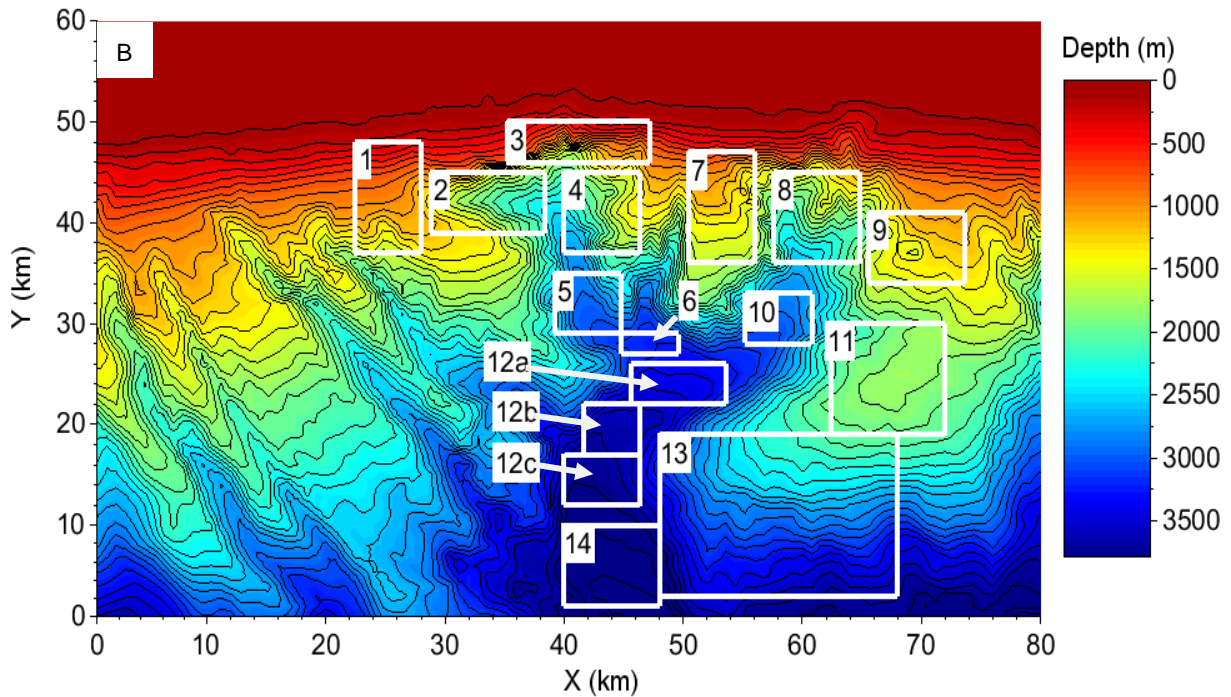
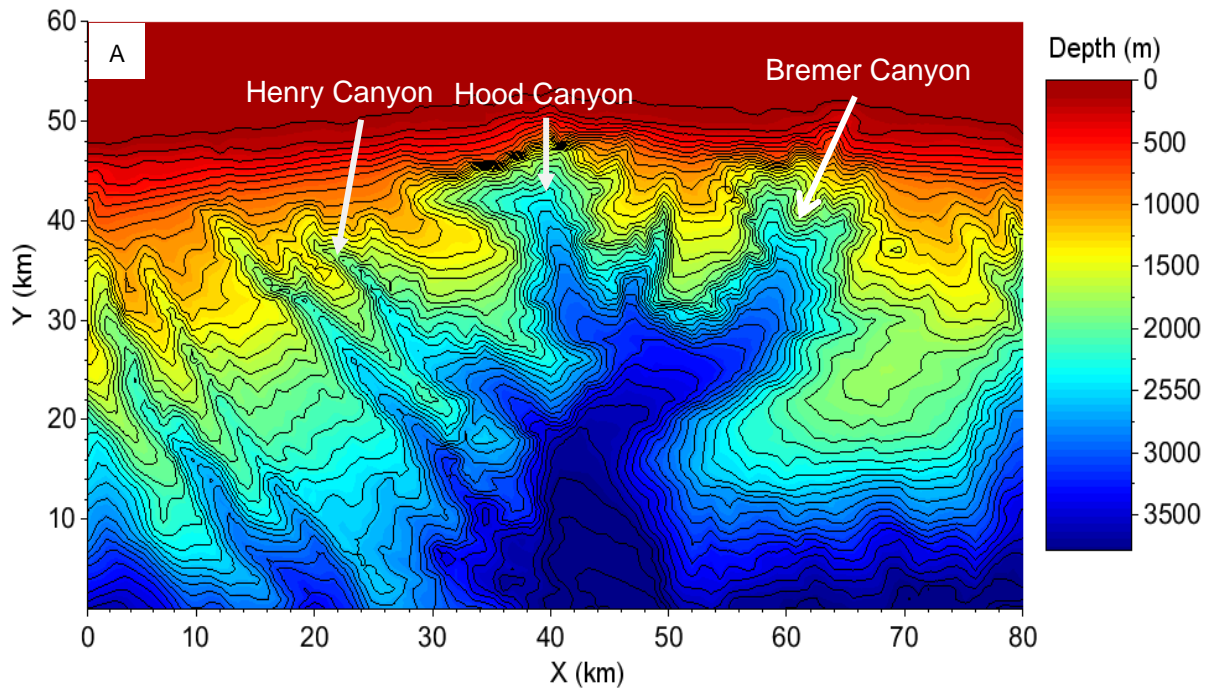


Figure 2.7: The domain for the deeper upwelling model (A), and the locations of interest (B) which is overlain with 100 m, contours (black lines). The minimum depth of this domain is 60 m, and maximum is 3785 m. The location of the Hood canyon is ~28 km to ~46 km horizontally, and ~28 km to 48 km vertically.

Table 2.4: The areas of interest within the deep canyon experiments.

Square	Location	Reason
1	Hotspot	Location where the orcas are aggregating in.
2	Hood Canyon outlet	The area in the Hood Canyon where flow was expected to exit the canyon and enter the hotspot
3	Northern wall of the Hood Canyon	An area where particles could outflow into when in the head of the Hood Canyon.
4	Eastern wall of the Hood Canyon	An area where particles could outflow into when in the head of the Hood Canyon with an eastward flow. Also, a location where a westward flow can enter the Hood Canyon.
5	The mid-slope of the Hood Canyon	The section of the Hood Canyon in between the head of the Hood Canyon, and the area the Hood Canyon forms.
6	The lower slope of the Hood Canyon	The section of the Hood Canyon where it forms from the Bremer Canyon.
7	Headland	The continental slope between the heads of the Bremer and Hood Canyon.
8	The head of the Bremer Canyon	The section of the canyon that particles are expected to pass through if any upwelling occurs.
9	Eastern hotspot	The expected outflow from the head of the Bremer Canyon with an eastward flow.
10	The mid-slope of the Bremer Canyon	The area in between the head and the lower slope of the Bremer Canyon.
11	Area to the west of the mid-slope	Potential inflow, or outflow to the mid-slope of the Bremer Canyon.
12a, 12b, 12c	The lower slope of the Bremer Canyon	The section of the Bremer Canyon which is in between the formation of the Hood Canyon and the plateau.

13	Plateau	The area to the east of the lower slope of the Bremer Canyon, which should inflow into the canyon with a westwards flow.
14	Bottom of the Bremer Canyon	The area of the Bremer Canyon which is to the south of where the plateau would flow into.

### 2.4.3 Hydrodynamic Model

All experiments used a single layer version of the Coupled Hydrodynamical-Ecological Model for Regional Shelf Seas (COHERENS) model (Luyten et al. 1999). The governing equations of this hydrodynamic model are based on the shallow-water equations used in Kämpf (2009). In the absence of wind and tidal forcing, it predicted the depth-averaged flow that follows from a barotropic pressure gradient due to a sloping sea surface. The model is governed by the momentum equations for  $(u, v)$  which are the components of the horizontal flow vector, and vertically integrated continuity equations that computes the rate of change of sea level elevation following from a divergence of horizontal equations. These momentum equations are separated into two parts: one with no frictional influence, and one that calculates flow deviations in a bottom Ekman layer with an assumed thickness of  $h_{ek} = 20$  m. The first part of the momentum equations can be written as:

$$\left(\frac{\delta}{\delta t} + u \frac{\delta}{\delta x} + v \frac{\delta}{\delta y}\right) u - f v = -g \frac{\delta}{\delta x} \eta + A_h \left(\frac{\delta^2}{\delta x^2} + \frac{\delta^2}{\delta y^2}\right) u \quad (3a)$$

$$\left(\frac{\delta}{\delta t} + u \frac{\delta}{\delta x} + v \frac{\delta}{\delta y}\right) v - f u = -g \frac{\delta}{\delta y} \eta + A_h \left(\frac{\delta^2}{\delta x^2} + \frac{\delta^2}{\delta y^2}\right) v \quad (3b)$$

For equation 3a, and 3b,  $(u, v)$  is zonal velocity ( $\text{ms}^{-1}$ ),  $t$  is time (h),  $(x, y)$  are Cartesian horizontal co-ordinates,  $\eta$  is sea-level elevation (m) and  $A_h$  is an assumed constant lateral eddy viscosity ( $1 \text{ m}^2\text{s}^{-1}$ ). The momentum equations for the bottom Ekman layer are:

$$\left(\frac{\delta}{\delta t} + u' \frac{\delta}{\delta x} + v' \frac{\delta}{\delta y}\right) u' - f v' = -g \frac{\delta}{\delta x} \eta + A_h \left(\frac{\delta^2}{\delta x^2} + \frac{\delta^2}{\delta y^2}\right) u' + \frac{r}{h_{ek}} u' \sqrt{u'^2 + v'^2} \quad (4a)$$

$$\left(\frac{\delta}{\delta t} + u' \frac{\delta}{\delta x} + v' \frac{\delta}{\delta y}\right) v' - f u' = -g \frac{\delta}{\delta y} \eta + A_h \left(\frac{\delta^2}{\delta x^2} + \frac{\delta^2}{\delta y^2}\right) v' + \frac{r}{h_{ek}} v' \sqrt{u'^2 + v'^2} \quad (4b)$$

For equations 4a, and 4b,  $(u', v')$  is the zonal velocity in the bottom Ekman layer, and  $r$  is the bottom friction parameter ( $r = 0.001$ ). The vertically integrated continuity equations can then be formulated as:

$$\frac{\delta}{\delta t} \eta + \frac{\delta}{\delta x} (uh) + \frac{\delta}{\delta y} (vh) + \frac{\delta}{\delta x} (\Delta u * h_{ek}) + \frac{\delta}{\delta y} (\Delta v * h_{ek}) = 0 \quad (5)$$

For  $z$ ,  $\Delta u = (u' - u)$  and  $\Delta v = (v' - v)$  are flow deviations in the bottom Ekman layer, and  $h$  is the total water depth. Density stratification was ignored in this model, though it can influence upwelling

(Kämpf, 2018). To assure the numerical model is stable, the timestep needs to meet the Courant-Friedrichs-Lewy Condition which states that the grid spacing used to shorten the bathymetry into a usable model domain needs to be less than the maximum water depth multiplied by gravity (Navon, 1979). This model is also absent of sub-scale diffusivity and frictional effects.

To drive change in the barotropic pressure gradient in this model, a forced sea level elevation change on the northern boundary was applied, and no change on the southern boundary. To adjust to the change in pressure which will result from changing the sea level elevation, the model was allowed to run for a few days to stabilise before calculating the resulting sea level gradient, as well as the resulting zonal and meridional velocity field at what the final state for sea level elevation is. As this would create a geostrophic flow due to the Coriolis force balancing out the pressure change, direction of flow can be controlled via increasing, or removing water, as well as magnitude via changing how much of a gradient is present.

Once both the zonal and meridional velocity field was obtained, it was used to simulate neutrally buoyant, passive Lagrangian particles, which in turn is used as a proxy for current flow. The Lagrangian particles module based on equations (3-5) used in the COHERENS hydrodynamic model (Luyten et al., 1999) and diffusion from turbulence is ignored in these calculations. Where particles are released was determined by randomising the horizontal location within the boundary, and by the maximum depth for the meridional location. For all simulations, boundary conditions were set so that a particle travelling through the model domain would not exit the model domain when at the eastern and western boundary to account for the possibility that flow direction could reverse. There was also a small section near the eastern and western boundary in which the bathymetry was set to stay constant to prevent the boundary influencing the pressure gradient or forming Kelvin waves.

#### 2.4.4 Calculations

A particle heatmap was created by counting how many particles entered a pre-defined area in the model domain (Figure 2.8, 2.9). The model domain was split into 120 squares of 1.28 km to 0.64 km for the shelf break model (Figure 2.8), and 80 squares of 10 km by 6 km for the deep upwelling modelling (Figure 2.9). To avoid the potential to double up particles should they land on a boundary between two squares, the eastern and southern square had priority. A limitation to using this method for heatmaps was the locations of the grid can cause an artificial error, thus causing a lower percentage to be visible. Another limitation is that depending on the velocity obtained by particles, it was possible they can bypass a grid cell, thus causing a lower percentage than what was occurring.

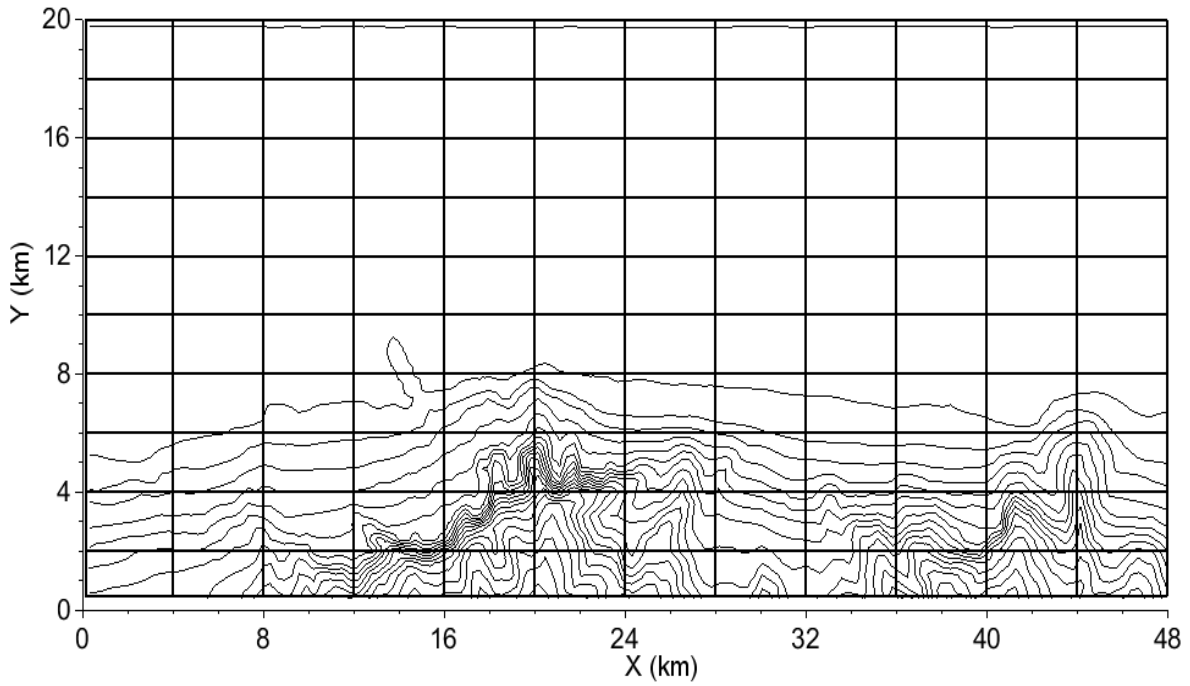


Figure 2.8: Grid spacing for the heat maps made for the shelf break upwelling chapter, with the first square starting at 1,1. The small spacing between points was due to particles are expected to be in the continental slope. Grey lines represent 100 m contours lines.

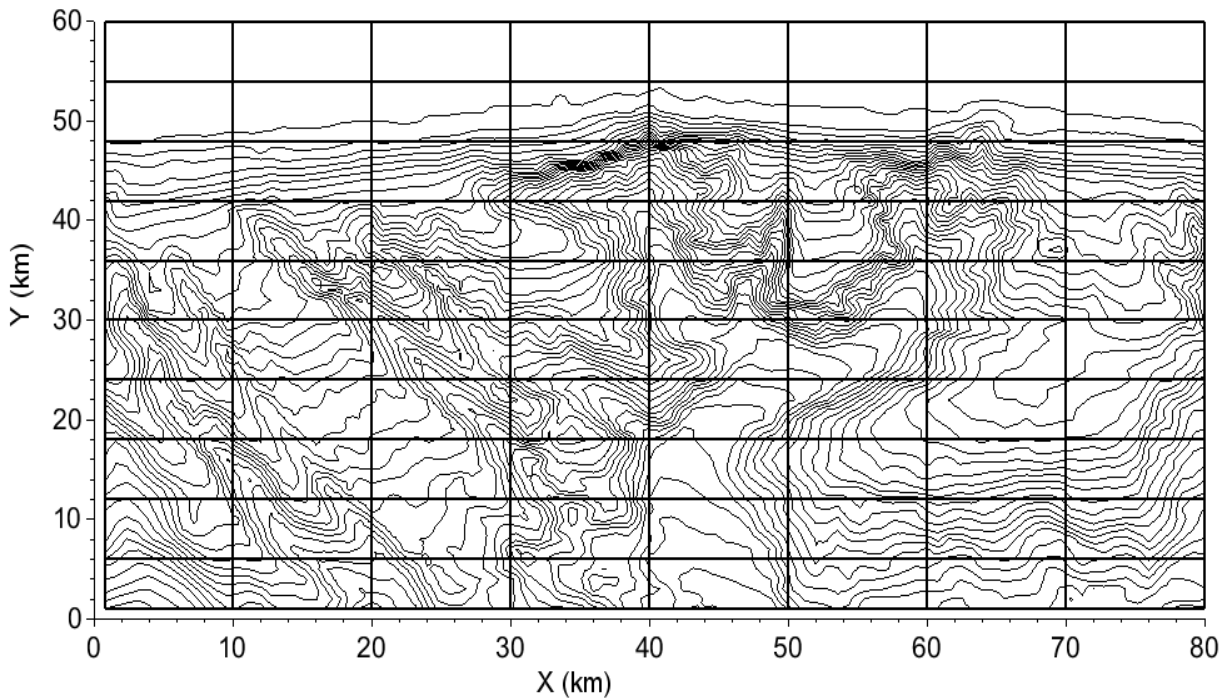


Figure 2.9: The grid spacing used for heat-map in the deeper upwelling modelling, with the first square starting at 1, 1. Black lines are representing contours of every 100 m of depth in between 100 m to 3800 m.

Due to the model being two dimensional, with particle depth being treated as the maximum depth of the location they were in, both zonal flow (east-west) and meridional flow (north-south) velocity was calculated by taking the distance travelled between two points. For an eastwards flow, the

last location a particle could be in the model prior to exiting it was either 48 km, or 80 km (depending on the model) and for the westwards flow the value used was  $1.0 \times 10^{-6}$  km. These timesteps were then converted to days and velocity was calculated by using a distance of 47.52 km for the shelf break model and 78 km for the deep canyon models, which were from the middle of the boundary to the end of the model. If a particle took longer than 60 days to exit the model, it was considered “trapped”, and were not considered in any velocity calculations. Velocities were also calculated for each group of particles (see 2.4.1 and 2.4.2) to test how an increase of depth impacted movement.

## 2.5 Temperature and Salinity Profiles

To obtain temperature and salinity data to test if a subsurface event did occur near the shelf break, a SonTek CastAway CTD was used during early February 2019. This device measures temperature, salinity, density, sound speed, and conductivity up to a maximum depth of 100 m in the ocean. To measure each station, the CastAway CTD was allowed to sit on the surface of the ocean for 10 seconds, before descending to either the maximum depth of the sea floor in that location, or 100 m depending on which came first, then pulled upwards at a similar rate. The rope was marked in 5 m intervals to track the water depth and the descent was stopped once maximum depth was reached to prevent it crashing into the seafloor. Data was taken from near the Bremer and Hood Canyons between the 5th of February 2019 to the 7th of February 2019 with the areas maximum depth ranging from 50 m to 900 m (Figure 2.10, Table 2.5). 72 m water depth was the primary focus of this study as it was close to the bottom edge of the continental shelf, with the areas with a maximum depth of 600 m and 900 m testing the temperature and salinity conditions that were occurring in the upper 100 m in the continental slope, and 50 m and 60 m acting to validate what was occurring on the continental shelf.

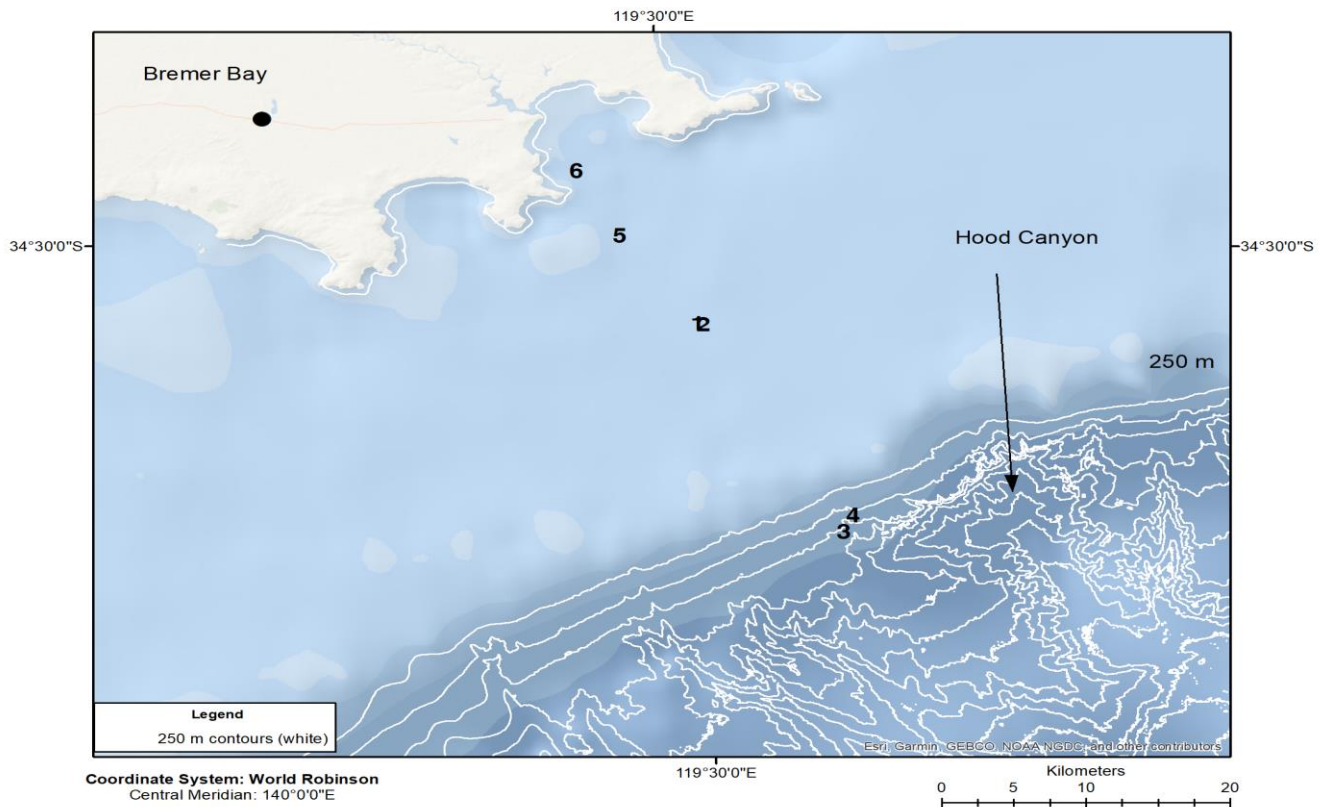


Figure 2.10: Stations used for SonTek CastAway CTD Casts in between the 5<sup>th</sup> of February 2019 to the 7<sup>th</sup> of February 2019, overlain on GEBCO 2012 bathymetry. Locations for each station are found in Table 2.5

Table 2.5: The locations where the CastAway CTD was launched, as well as the cast depth

Station	Date	Latitude	Longitude	Cast depth (m)	Ocean depth (m)
1	5/02/2019	-34.56	119.51	66.15	72
2	6/02/2019	-34.73	119.61	92.41	900
3	6/02/2019	-34.71	119.62	80.11	600
4	6/02/2019	-34.56	119.52	69.31	70
5	7/02/2019	-34.49	119.46	59.51	60
6	7/02/2019	-34.44	119.43	52.03	50

Additionally, temperature and salinity data were obtained from an autonomous sea glider through the IMOS (Integrated Marine Observation System) online portal (<https://portal.aodn.org.au/>). The sea glider measures temperature, salinity, as well as pressure (and therefore density), coloured dissolved organic matter, chlorophyll-a, dissolved oxygen, nitrate concentration, current velocity, and various forms of irradiance from the water column. Ocean gliders can only reach a maximum depth of 1000 m and are designed to take a diagonal path in the ocean with an average forward velocity of 25 cms<sup>-1</sup> instead of descending and then ascending in a fixed location (Woo, 2019). The February 21st to March 13th, 2013 sea glider deployment, which focused on an area from

34.67°S, and 117.6°E to 35.65°S and 120.01°E was used for temperature and salinity data (Figure 2.11).

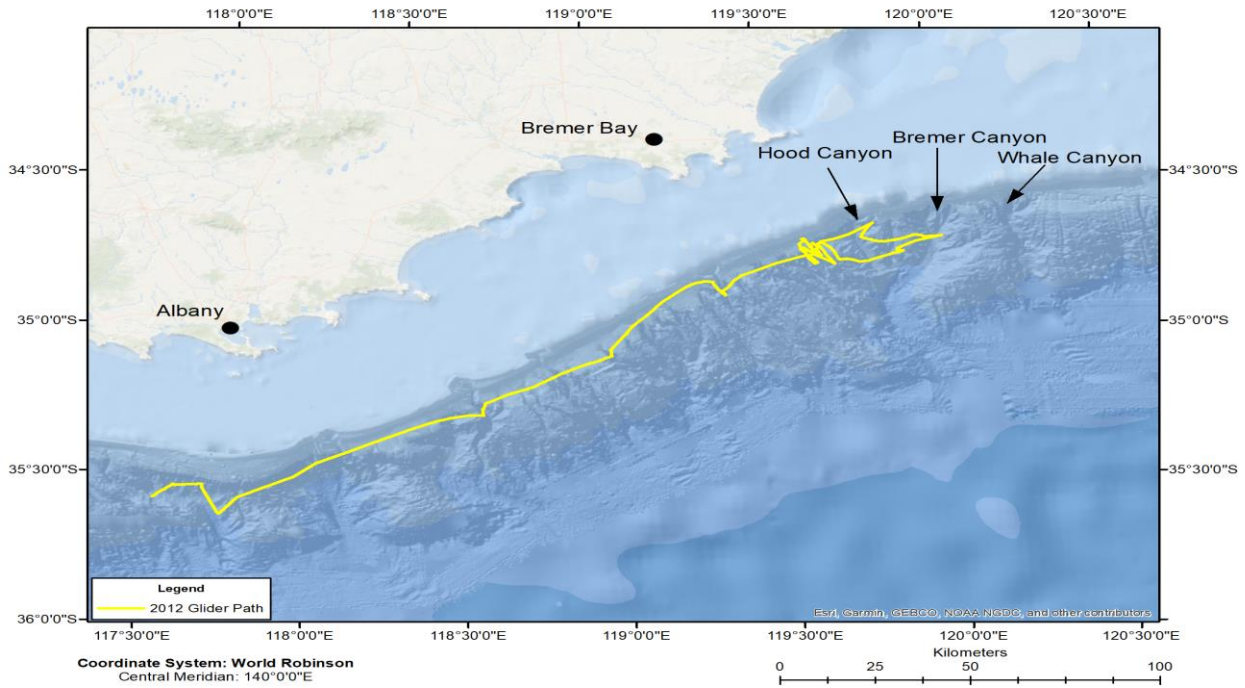


Figure 2.11: The glider track of the 2013 sea glider deployment in Bremer Bay, in yellow.

In the 2013 deployment, 0.32% of temperature data taken were rated by IMOS as either missing data or bad data, salinity was 0.49%, whereas chlorophyll-a was at 69.35%, and coloured dissolved organic matter was at 69.78%. Hence, the only usable and relevant data from the 2013 deployment was temperature and salinity. The areas used were 34.74°S, 119.63°E for the hotspot, 34.72°S, 119.71°E for the Hood Canyon, and 34.98°S, 119.12°E for the reference area near Bremer Bay.

Ship based measurements are an alternative to gliders to obtain temperature and salinity data, and there have been two cruises which have taken data in or around the Bremer and Hood Canyon. The first voyage was in July 2006 and was ruled out due to being in a period that was outside of the orca migratory season. The second voyage occurred during November 2017; however, it unfortunately did not take any casts within the hotspot, and only went to a depth of 1000 m, which meant the flexibility of a glider ended up being preferred in this study.

## CHAPTER 3 SHELF BREAK EXPERIMENTS

### 3.1 Coastal Current

A wind driven coastal current occurs seasonally in the region, driving flow westwards as shown in Figure 1.1 (Ridgway and Condie, 2004, Pattiaratchi, 2007, Cresswell and Domingues, 2009, Mondello, 2017). The altimetry data from AVISO that was between the Bremer Bay coastline and 167 km south of that coastline suggested evidence of a coastal current formation between September to March, with an average current velocity of  $2.96 \text{ cms}^{-1} \pm 6.76 \text{ cms}^{-1}$  westwards (Figure 3.1, 3.2). The peak average flow occurred in January with an average of  $4.79 \text{ cms}^{-1} \pm 7.21 \text{ cms}^{-1}$  westwards, with February slowing down to an average velocity of  $4.04 \text{ cms}^{-1} \pm 6.66 \text{ cms}^{-1}$  westwards, and December at  $3.34 \text{ cms}^{-1} \pm 6.48 \text{ cms}^{-1}$  westwards. Between April and August, the Leeuwin current was dominant in the area with an average velocity of  $4.39 \text{ cms}^{-1} \pm 8.12 \text{ cms}^{-1}$ . The high amount of variability showed that when a coastal current forms, it does so in “events”. Using the criteria described in the methods (chapter 2), a coastal current is present in the form of an event 70.1% of the time. The data showed that on average, there were 1.73 events a year between October to March with at least one four-week event occurring. The average amount of time that a coastal current is occurring each year was 11.77 weeks (Table 3.1). The longest event each year had an average of 8.55 weeks. The average current velocity within events was  $8.71 \text{ cms}^{-1}$  westward with events peaking at  $14.80 \text{ cms}^{-1}$  westward.

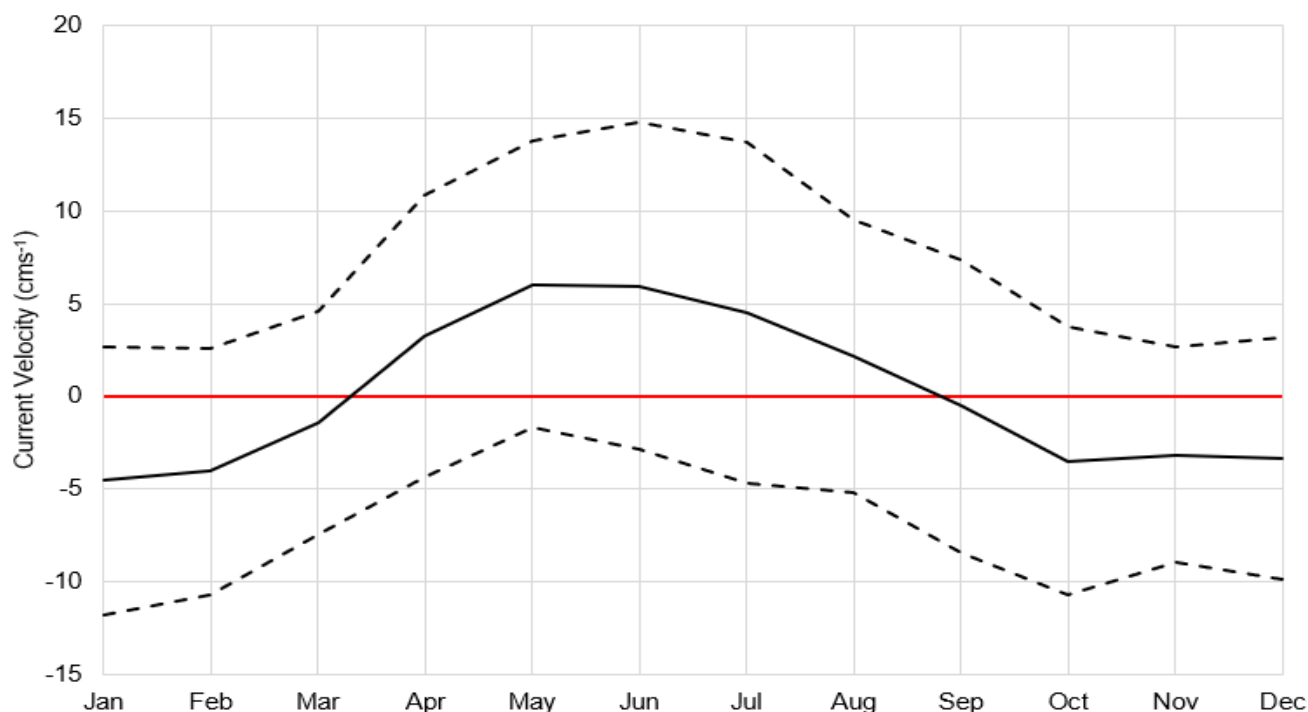


Figure 3.1: The monthly average current velocity for the sea at location 119.7°E, 34.1°S to 35.6°E, which was used to represent the shelf break off Bremer Bay. The dotted lines represent a  $\pm 1$  standard deviation, with positive values representing the presence the eastwards Leeuwin Current. Geostrophic data was derived from AVISO satellite data, which is available at <https://www.aviso.altimetry.fr/>

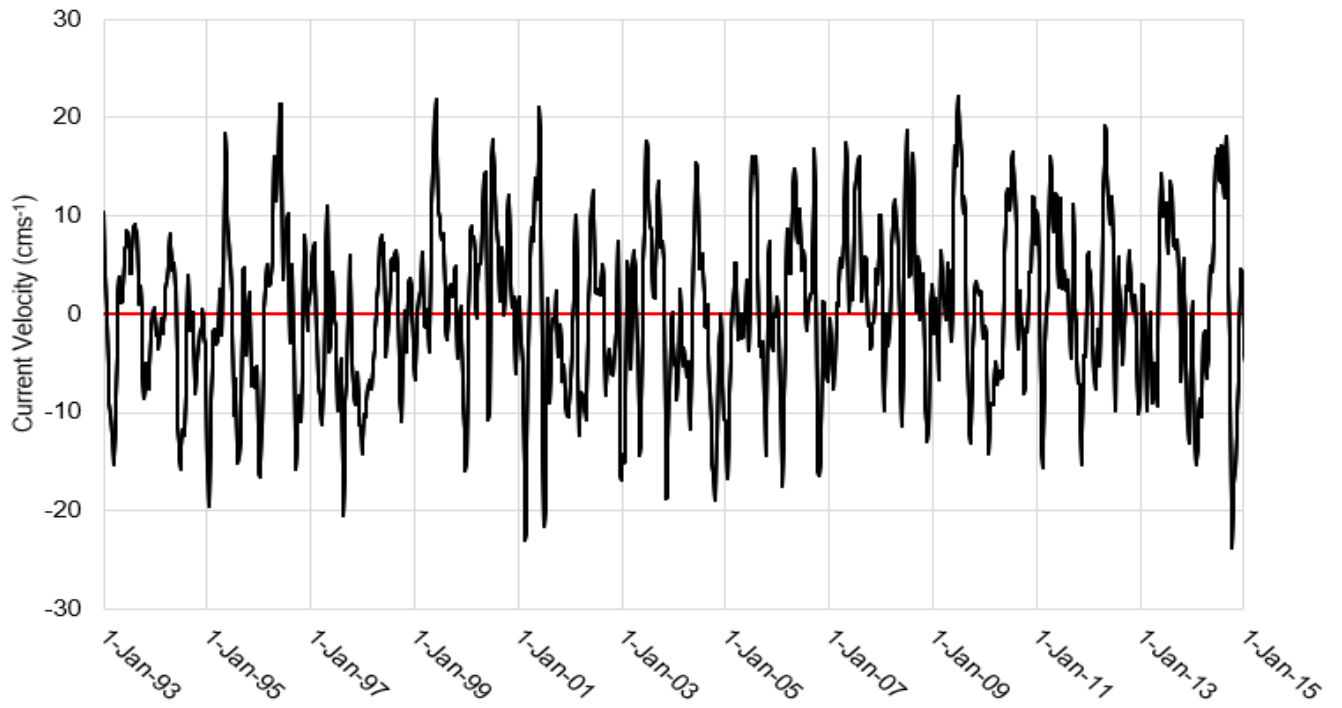


Figure 3.2: The weekly average current velocity for Bremer Bay with a 22-year time span from 1/1/1993 to 1/1/2015. Positive values indicating that the Leeuwin Current is present. The maximum coastal current velocity was 22.16 cms<sup>-1</sup> westwards while the maximum Leeuwin current velocity was 23.8 cms<sup>-1</sup> eastwards. Geostrophic data was derived from AVISO satellite data, which is available at <https://www.aviso.altimetry.fr/>

Table 3.1: The event analysis for altimetry data taken from Bremer Bay region (119.7°E, 34.1°S to 35.6°E).

Period	Number of weeks under event conditions	Total events	Maximum westwards velocity (cms <sup>-1</sup> )	Longest event (weeks)
Summer 93	10	1	15.27	10
93-94	7	1	8.62	7
94-95	13	2	19.63	8
95-96	16	3	16.6	13
96-97	11	2	11.21	7
97-98	24	1	14.15	24
98-99	4	1	6.64	4
99-00	7	1	15.97	7
00-01	8	1	22.97	8
01-02	18	2	12.29	12
02-03	13	2	16.97	7
03-04	17	3	18.85	6
04-05	17	2	18.91	10
05-06	9	2	17.55	6
06-07	15	3	16.49	6
07-08	3	1	9.9	3
08-09	6	1	12.90	6
09-10	15	1	14.26	15
10-11	6	1	15.59	6
11-12	14	2	15.37	9
12-13	11	3	10.22	4
13-14	15	2	15.27	10
Mean	11.77	1.73	14.8	8.55

There was a coastal current flow between the Esperance coastline and 167 km to the south of that coastline from November to March, with an average flow velocity during this time of 4.11 cms<sup>-1</sup> ± 4.55 cms<sup>-1</sup> westwards (Figure 3.3, 3.4). The coastal current flow reached its maximum in December at 5.82 cms<sup>-1</sup> westwards, with January at 4.56 cms<sup>-1</sup> westwards and February at 4.66 cms<sup>-1</sup> westwards. Months outside of this period were under the influence of the Leeuwin current, with an average current velocity of 5.48 cms<sup>-1</sup> ± 5.16 cms<sup>-1</sup> eastwards, and a maximum current average of 10.99 cms<sup>-1</sup> ± 4.8 cms<sup>-1</sup> during June. Similarly, at Bremer Bay, there was a high variability in monthly averages within this time span. 78.54% of times a coastal current was present off Esperance between October to March was within an event. There were 1.68 events

per year with the year having the lowest time under event conditions being 2011/2012 at 6 weeks (Table 3.2). The average amount of time October to March is under coastal current conditions was 14.14 weeks, with the longest event each year running for on average 11.32 weeks. The average flow occurring during an event was  $7.58 \text{ cms}^{-1}$  westwards, with events peaking at  $13.33 \text{ cms}^{-1}$  westwards.

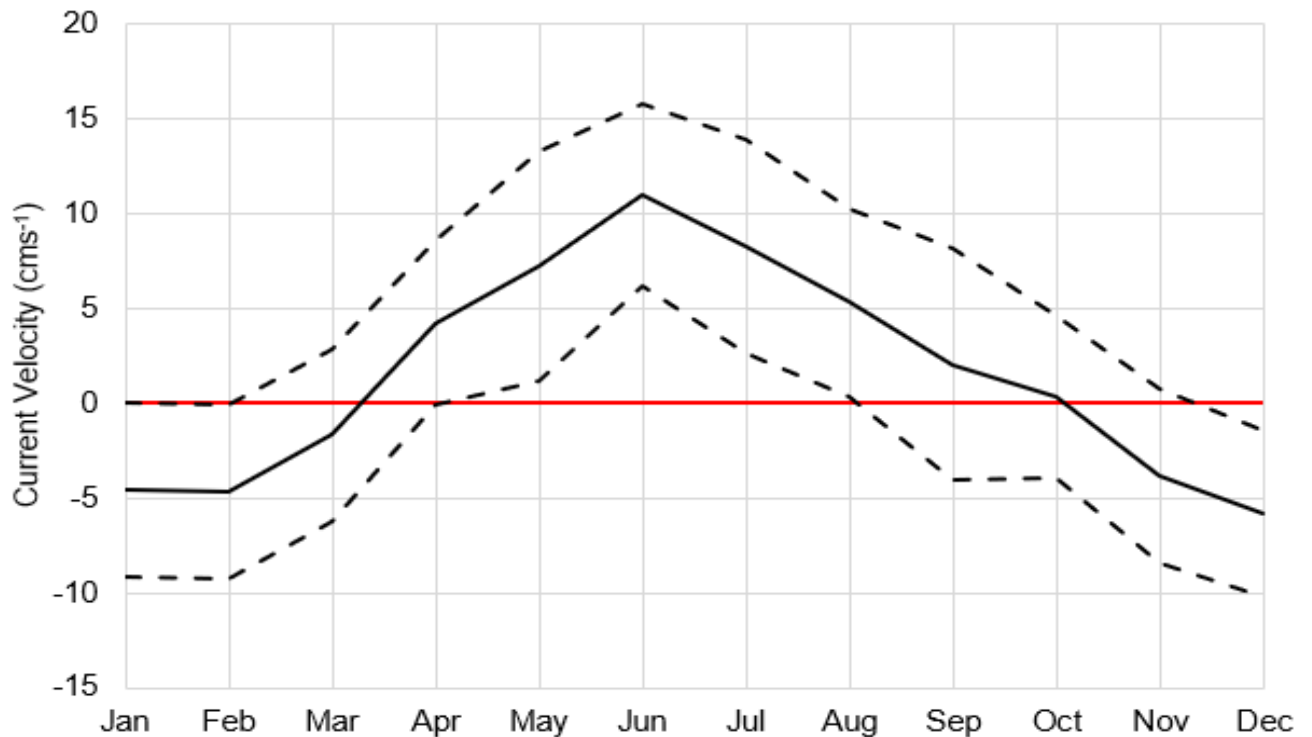


Figure 3.3: The monthly average current velocity for  $121.9^{\circ}\text{E}$ ,  $33.9^{\circ}\text{S}$  to  $35.4^{\circ}\text{S}$ , which represents changes in the shelf break off the Esperance Coastline, WA. The dotted lines represent a  $\pm 1$  standard deviation, with positive values showing the presence of a eastwards Leeuwin Current. Geostrophic data was derived from AVISO satellite data, which is available at <https://www.aviso.altimetry.fr/>

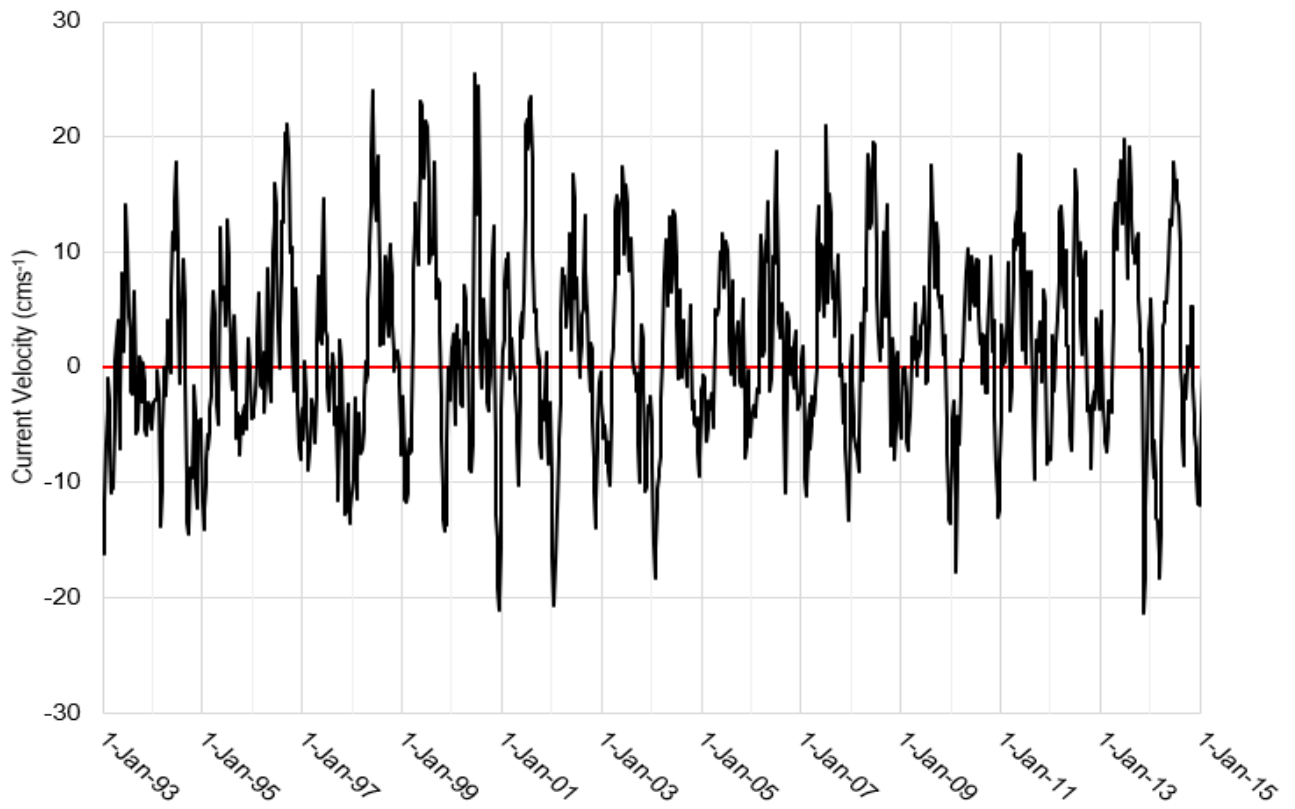


Figure 3.4: The weekly average current velocity for Esperance with a 22-year time span from 1/1/1993 to 1/1/2015. Positive values indicating that the Leeuwin Current is present. The maximum coastal current velocity was 21.39 cms<sup>-1</sup> westwards while the maximum Leeuwin current velocity was 25.47 cms<sup>-1</sup>. Geostrophic data was derived from AVISO satellite data, which is available at <https://www.aviso.altimetry.fr/>

Table 3.2: The event analysis for altimetry data taken from Esperance region in between 1993 to 2014 (121.9°E, 33.9°S to 35.4°S).

Period	Number of weeks under event conditions	Total events	Maximum westwards velocity (cms <sup>-1</sup> )	Longest event (weeks)
Summer 93	12	2	16.27	7
93-94	17	2	13.84	13
94-95	22	2	14.09	18
95-96	12	2	7.63	8
96-97	16	2	9.02	10
97-98	24	1	13.63	24
98-99	13	1	11.81	13
99-00	8	1	14.26	8
00-01	8	1	21.15	8
01-02	20	2	20.76	15
02-03	18	2	14	18
03-04	19	1	18.41	19
04-05	15	2	9.45	10
05-06	11	2	7.86	8
06-07	15	2	11.19	11
07-08	12	2	13.29	7
08-09	10	3	7.21	4
09-10	15	1	17.77	15
10-11	7	1	13.09	7
11-12	6	1	8.39	6
12-13	16	2	8.87	10
13-14	15	2	21.39	10
Average	14.14	1.68	13.33	11.32

There was a coastal current flow present between the Albany coastline and 189 km to the south of the Albany coastline between October to March with an average flow of  $2.46 \text{ cms}^{-1} \pm 7.98 \text{ cms}^{-1}$  westwards (Figure 3.5, 3.6). This coastal current flow tended to be stronger in February with an average velocity of  $3.99 \text{ cms}^{-1} \pm 8.42 \text{ cms}^{-1}$  westwards, with January having an average velocity of  $3.1 \text{ cms}^{-1} \pm 8.36 \text{ cms}^{-1}$  westwards, and December having an average velocity of  $2.88 \text{ cms}^{-1} \pm 7.27 \text{ cms}^{-1}$  westwards. From April to September Albany was under the influence of the Leeuwin Current which had an average current velocity of  $5.48 \text{ cms}^{-1} \pm 7.81 \text{ cms}^{-1}$  eastwards during this

time, with the maximum average velocity occurring in June at  $9.67 \text{ cms}^{-1} \pm 7.92 \text{ cms}^{-1}$ . Similar to Esperance and Bremer Bay, switching between Leeuwin Current and the coastal current appears to be driven by events, with an event analysis showing that 80.82% of the weeks where a coastal current was present between October to March was within an event. On average there were 1.7 events per year within the October to March period (Table 3.3). The years with the smallest number of weeks under event conditions were 1999/2000 and 2007/2008. These years had event conditions for 4 weeks of the year. The average time for October to March to have the coastal current present was 11.3 weeks, with the longest coastal current event each year lasting 8.26 weeks. The average flow for an event was  $9.46 \text{ cms}^{-1}$  westwards, with events peaking at  $16.79 \text{ cms}^{-1}$  westwards.

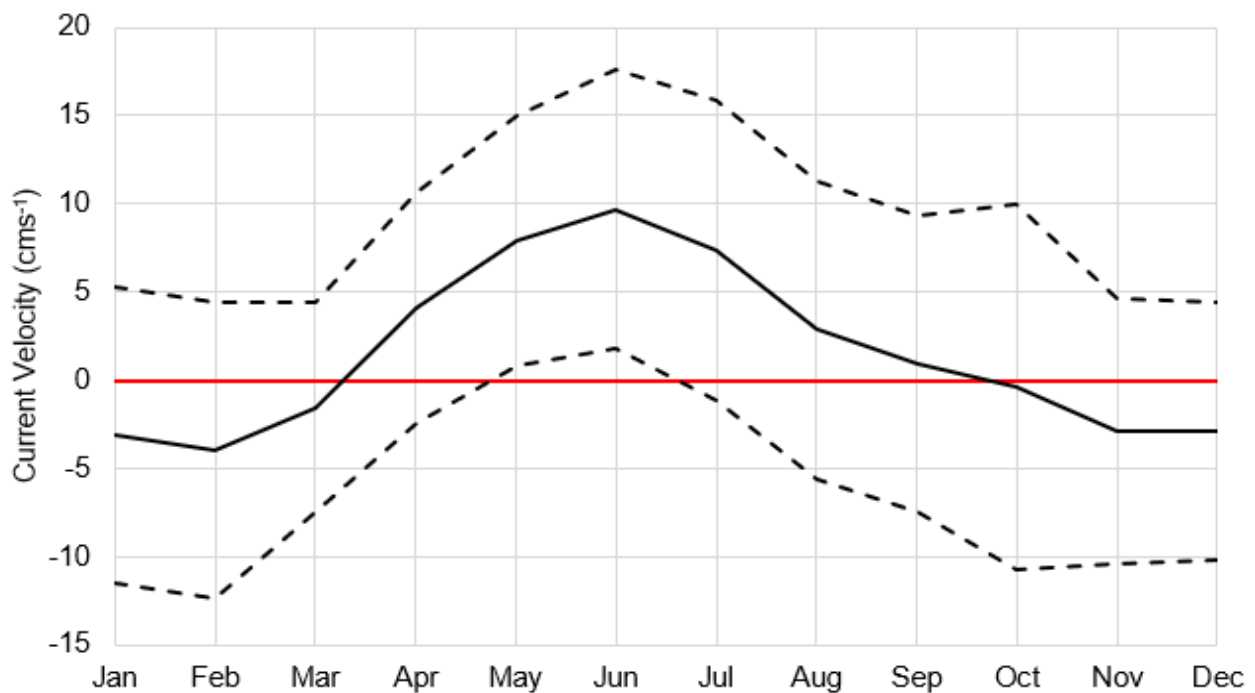


Figure 3.5: The average climatological current velocity for 118°E, 34.9°S to 36.6°S. This represents changes in the shelf break off Albany WA with positive values representing the Leeuwin Current. Dotted line represents  $\pm 1$  standard deviation of the current flow present in this area. Geostrophic data was derived from AVISO satellite data, which is available at <https://www.aviso.altimetry.fr/>

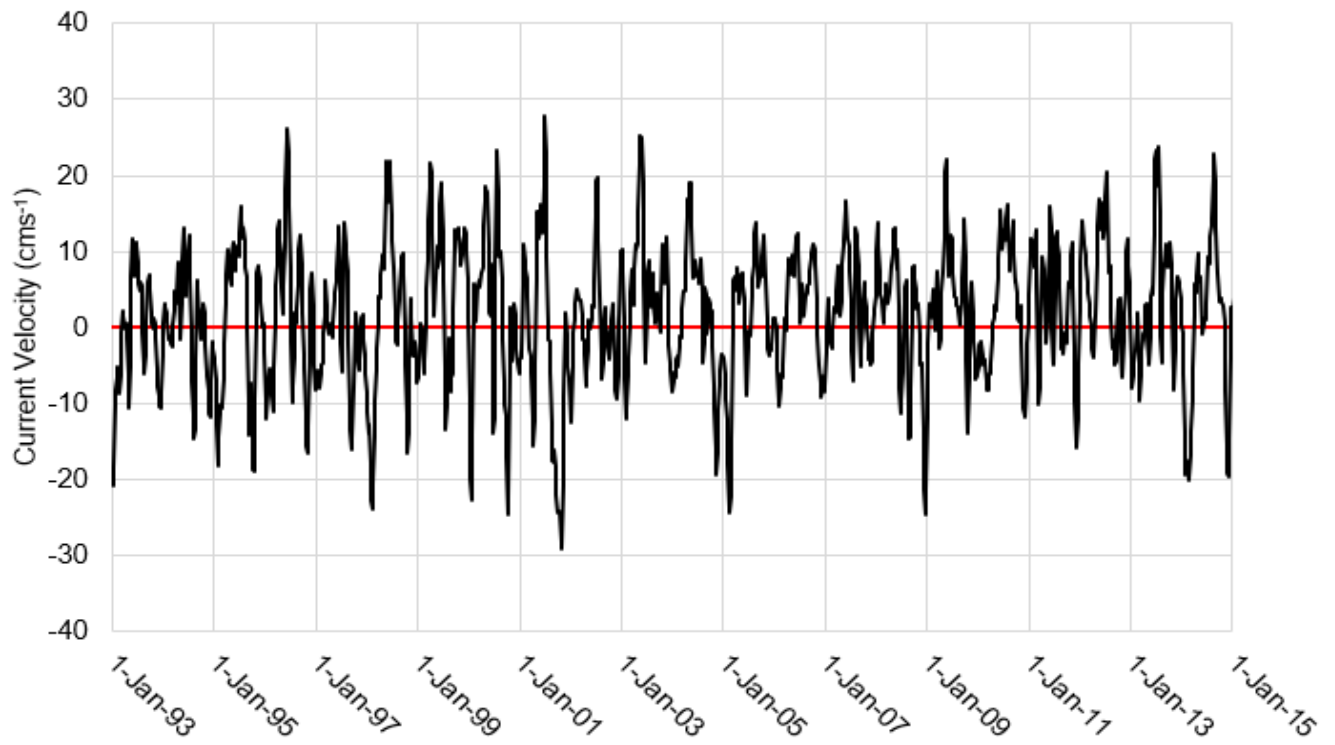


Figure 3.6: 22-year time series of the average weekly current velocity off the Albany Coastline, with positive values showing the presence of the Leeuwin Current. The maximum weekly velocity for the coastal current was 29.19 cms<sup>-1</sup> westwards, and the Leeuwin Current was 27.55 cms<sup>-1</sup> eastwards. Geostrophic data was derived from AVISO satellite data, which is available at <https://www.aviso.altimetry.fr/>

Table 3.3: Event analysis for altimetry data taken from the Albany region in between 1993 to 2014 (118°E, 34.9°S to 36.6°S).

Time	Total weeks	Total events	Maximum westwards velocity (cms <sup>-1</sup> )	Largest event (weeks)
Summer 93	9	1	20.82	9
93-94	7	1	10.48	7
94-95	18	2	18.13	12
95-96	15	2	18.86	10
96-97	17	2	16.49	10
97-98	17	2	23.88	14
98-99	12	3	16.52	5
99-00	4	1	22.58	4
00-01	14	3	24.58	6
01-02	14	2	29.19	8
02-03	10	2	12.05	5
03-04	11	1	8.54	11
04-05	20	1	24.25	20
05-06	7	1	10.27	7
06-07	9	1	9.07	9
07-08	4	1	4.83	4
08-09	8	1	24.58	8
09-10	18	3	13.98	9
10-11	8	2	11.67	5
11-12	5	1	15.90	5
12-13	9	2	9.69	5
13-14	14	2	20.10	11
14-15	10	2	19.63	6
Mean	11.30	1.70	16.79	8.26

## 3.2 Experiment SB1

### 3.2.1 Sea Level Elevation and Velocity Fields

For experiment SB1 the sea level elevation was forcibly decreased by 2 cm on the northern boundary, and the sea level was allowed to adjust to that change over a six-day period. This was designed to create an average flow of 10 cms<sup>-1</sup> westwards to represent the average conditions of

a coastal current event. The Coriolis force was set to  $-1 \times 10^{-4} \text{ s}^{-1}$  to represent the Coriolis force at  $\sim 40^\circ\text{S}$ . Particles were released on the western boundary after five days and allowed to run for fifty-five days.

The average sea level elevation throughout the SB1 model was  $-0.81 \text{ cm} \pm 0.63 \text{ cm}$  (Figure 3.7, Table 3.1). This change in sea level elevation resulted in an average zonal Eulerian velocity of  $10.32 \text{ cm s}^{-1} \pm 4.97 \text{ cm s}^{-1}$  westwards (Figure 3.8). Compared to altimetry data in the region, the Eulerian velocity was  $7.36 \text{ cm s}^{-1}$  faster than the average velocity for the Bremer Bay region,  $1.61 \text{ cm s}^{-1}$  faster than the average velocity for events where the coastal current forms and  $4.48 \text{ cm s}^{-1}$  faster than the maximum velocity for an event. The average meridional velocity for SB1 was  $0.71 \text{ cm s}^{-1} \pm 2.74 \text{ cm s}^{-1}$  southwards (Figure 3.9).

The entire 100 m to 1000 m depth range supported a westwards flow, which would be conducive for upwelling in the Bremer Bay region. The Whale Canyon averaged a northwards Eulerian velocity of  $1.51 \text{ cm s}^{-1} \pm 1.78 \text{ cm s}^{-1}$ , and the eastern perimeter of the Bremer Canyon supported a northwards Eulerian velocity of  $1.84 \text{ cm s}^{-1} \pm 3.07 \text{ cm s}^{-1}$ . The remainder of the region averaged a southwards flow. As both the Whale and Bremer Canyon supported a northwards flow, this indicated both canyons could support the formation of a topographic Rossby wave (Table 3.1).

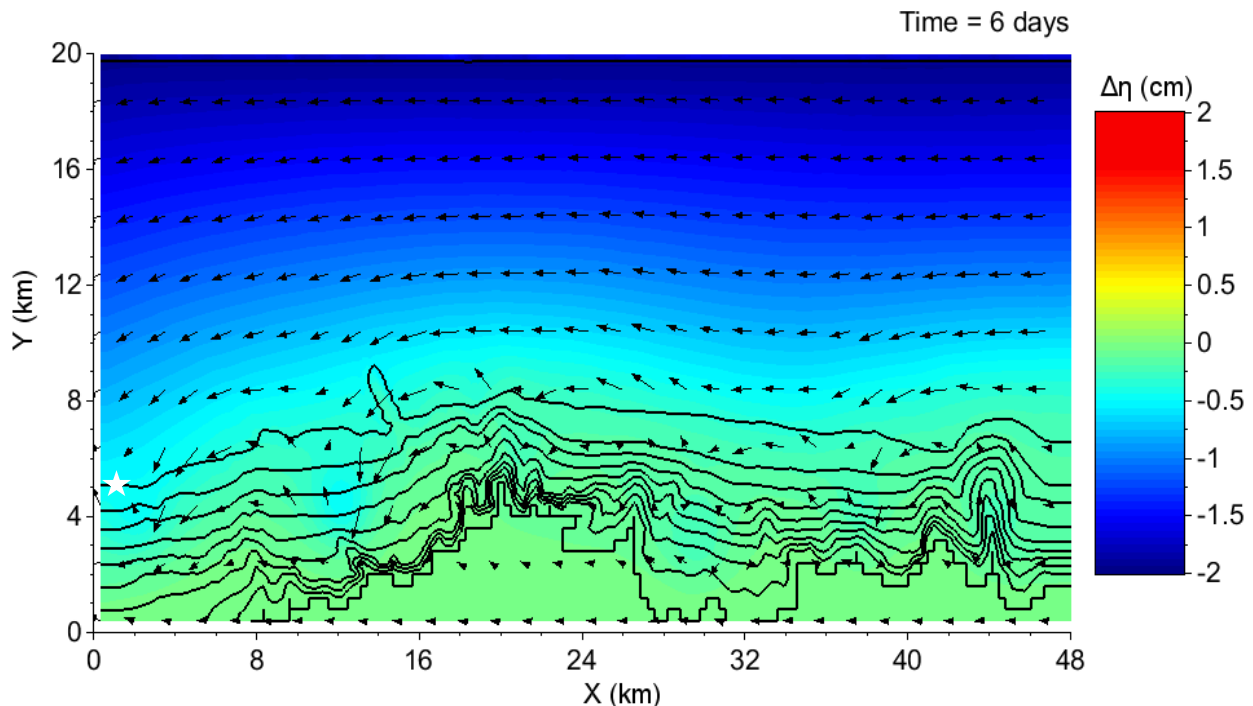


Figure 3.7: The change in sea level for experiment SB1, with positive values representing an increase in sea level. Black lines are 100 m contour lines up until 1000 m, and arrows are the flow vector. The white star is representative of the 100 m contour line. The northern boundary had an average sea level decrease of  $-1.78 \text{ cm} \pm 0.18 \text{ cm}$ , while the southern boundary had an average decrease of  $-0.01 \text{ cm} \pm 7.2 \times 10^{-3} \text{ cm}$

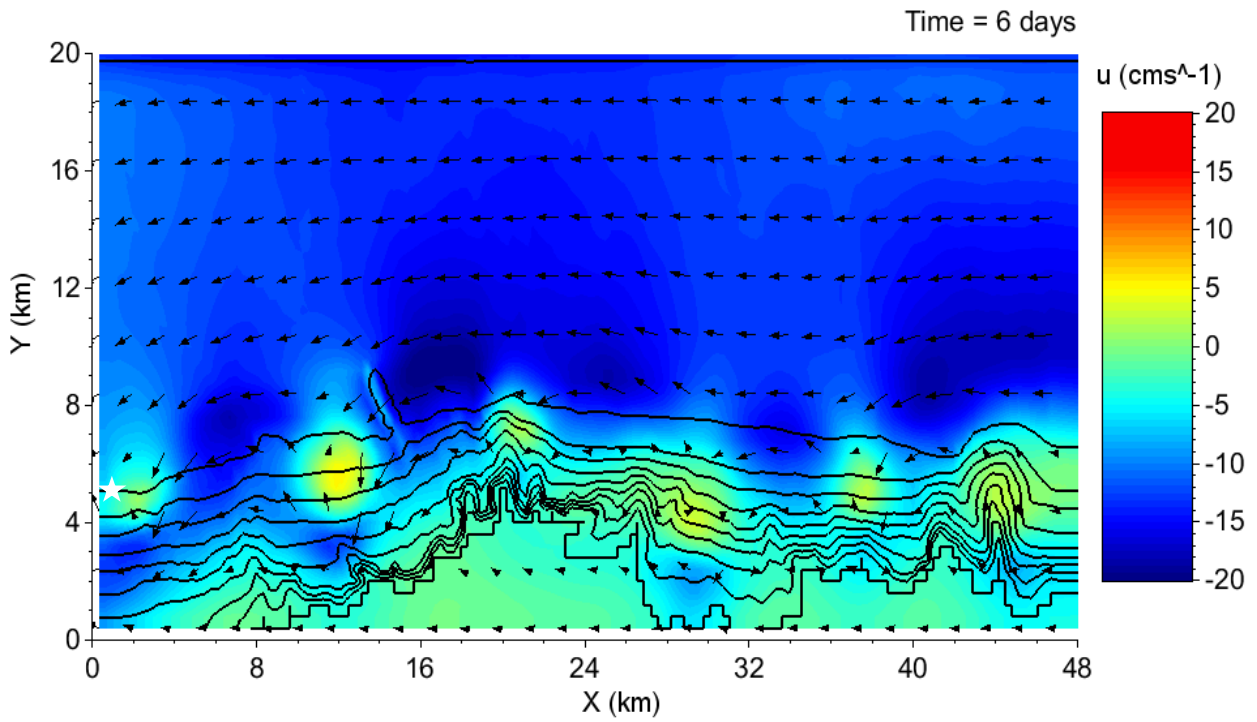


Figure 3.8: The zonal Eulerian velocity for experiment SB1, with positive values representing an eastwards flow. Black lines are 100 m contour lines up until 1000 m, and arrows are the flow vector. The white star is notating the 100 m contour line. The median flow present in the model is  $12.25 \text{ cm s}^{-1}$  westwards.

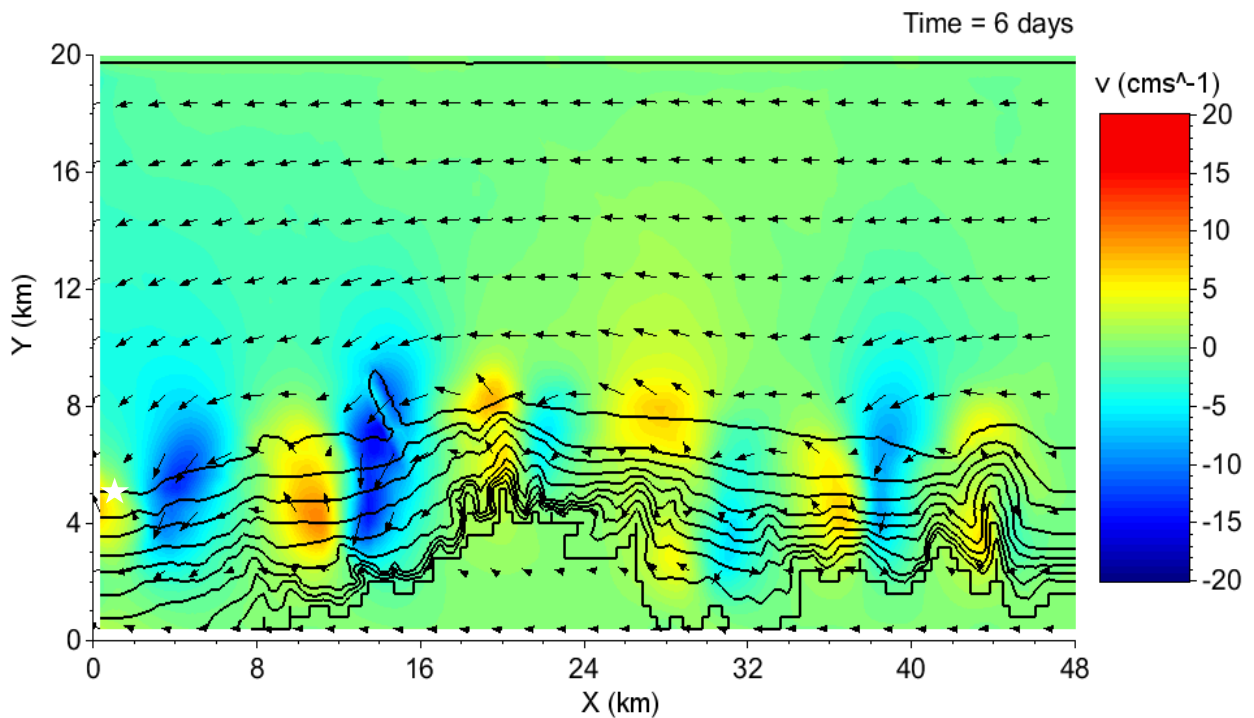


Figure 3.9: The meridional Eulerian velocity for experiment SB1, with positive values representing a northwards flow. Black lines are 100 m contour lines up until 1000 m, and arrows are the flow vector. The white star is denoting the 100 m contour line. The median flow present is  $0.33 \text{ cm s}^{-1}$  southwards.

Table 3.4: The average sea level elevation (Figure 3.7), zonal Eulerian velocity (Figure 3.8), and meridional Eulerian velocity (Figure 3.9) for areas of interest within experiment SB1 model domain. Positive values where an increase in sea level elevation, an eastward zonal flow, and a northward meridional flow. W.C. stands for Whale Canyon. B.C. stands for Bremer Canyon.

Location	Average sea level elevation (cm)	Average zonal Eulerian velocity (cms <sup>-1</sup> )	Average meridional Eulerian velocity (cms <sup>-1</sup> )
Mean	-0.81 ± 0.63	-10.32 ± 4.97	-0.71 ± 2.74
Continental shelf	-1.27 ± 0.36	-13.8 ± 4.73	-0.58 ± 1.64
W.C.	-0.15 ± 0.07	-4.34 ± 4.11	1.51 ± 1.78
Between W.C. & B.C.	-0.17 ± 0.12	-6.46 ± 4.31	-1.23 ± 3.37
B.C. eastern perimeter	-0.21 ± 0.09	-7.37 ± 5.28	1.84 ± 3.07
B.C. western perimeter	-0.22 ± 0.14	-7.34 ± 5.01	-1.67 ± 5.35
B.C. head	-0.05 ± 0.04	-2.36 ± 1.17	0.74 ± 0.85

### 3.2.2 Lagrangian Particle Tracker

After sixty days of run time, 100% of particles passed through Whale Canyon, and from that, 71.76% of particles entered the continental shelf north of the Whale Canyon (Figure 3.10, 3.11, Table 3.2). This 71.76% was made up of >50% of particles released from each of the 100 m to 500 m release point, and 0% from below 500 m. After these particles returned to the continental slope, 99.54% entered the eastern perimeter of the Bremer Canyon with the missing percentage being particles which were released between 100 m to 400 m. 83.58% of particles entered the continental shelf from the eastern perimeter of the Bremer Canyon. This consisted of every particle which entered the perimeter in between 100 m to 500 m, and 25.3% of particles released >500 m. These results indicated that a topographic Rossby wave had formed in the Whale and Bremer Canyons.

The average time for particles released in the SB1 model domain was 11.92 days which translated to an average velocity of 4.61 cms<sup>-1</sup> westwards (Table 3.3). The average particle velocity was 5.71 cms<sup>-1</sup> slower than the average Eulerian zonal velocity, and 4.1 cms<sup>-1</sup> slower than the average event velocity in the Bremer Bay. Particles were at their quickest in between 100 m to 200 m travelling through the model domain at 5.58 cms<sup>-1</sup> westwards, and slowest in between 300 m to 400 m at 4.03 cms<sup>-1</sup> westwards. Particles speed up by 0.38 cms<sup>-1</sup> when in between 400 m to 500 m travelling through at 4.41 cms<sup>-1</sup> before reaching 4.57 cms<sup>-1</sup> when at depths > 500 m.

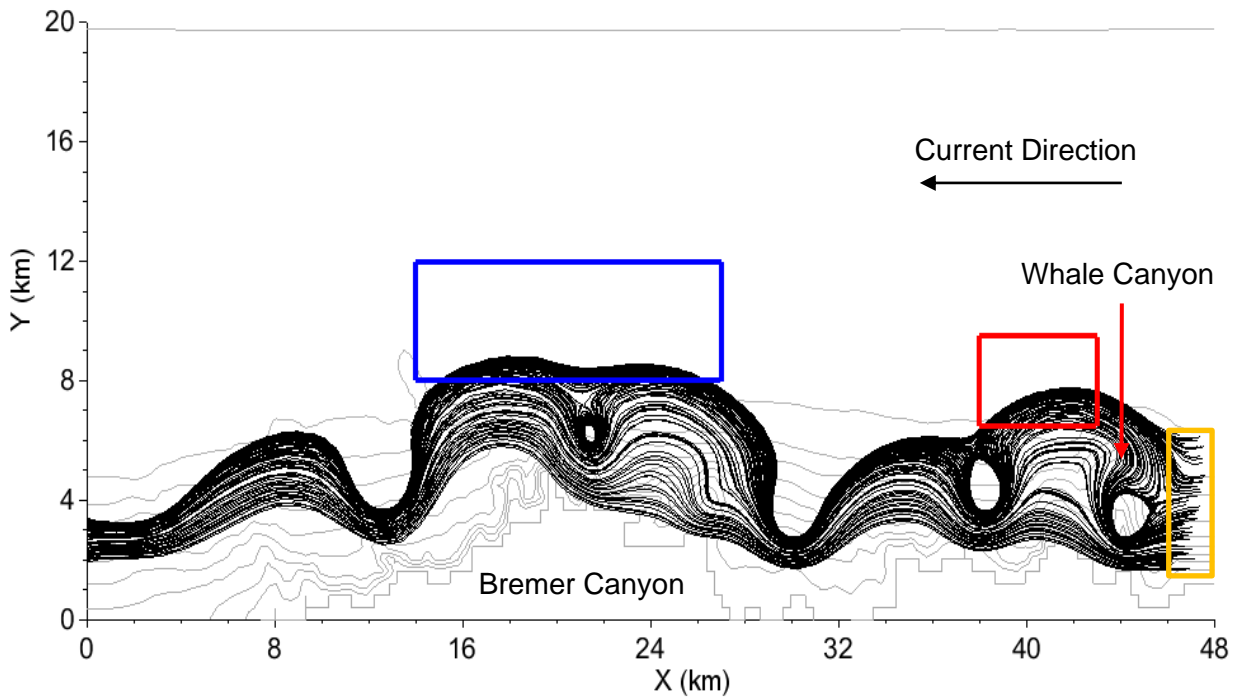


Figure 3.10: The trajectory for every 40<sup>th</sup> particle released on the eastern boundary of experiment SB1 (orange square is where). The sections of the continental shelf where particles would upwell into if a topographic Rossby wave formed in red (Whale Canyon), and blue (Bremer Canyon), which were based on locations 3 and 6 in section 2.5.1. The grey lines are 100 m contour lines.

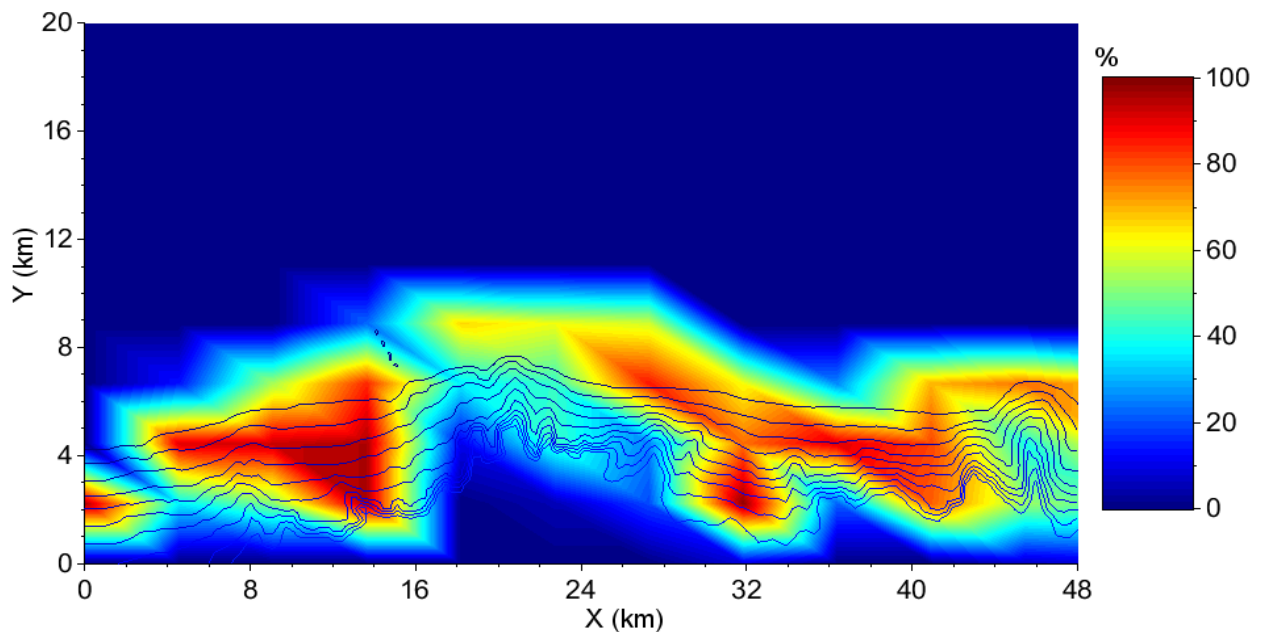


Figure 3.11: Heat map of particle concentrations for experiment SB1, and the blue lines are 100 m contour lines. The maximum percentage concentration was 98.52%, which occurred just after the Whale Canyon, indicating particles are reverting to their contoured depth. A similar effect occurred to the west of the Bremer Canyon, which had a maximum concentration of 95.54%

Table 3.5: Percentage of particles passing through each area of interest within the SB1 model domain, as well as how the release depth had affected this percentage (Figure 3.11). W.C. stands for Whale Canyon. B.C. stands for Bremer Canyon. PG1 is the particles that had a starting depth of 100 m to 200 m, PG2 had a starting depth of 200 m to 300 m, PG3 had a starting depth of 300 m to 400 m, PG4 had a starting depth of 400 m to 500 m and PG5 had a starting depth of 500 m to 1000 m.

Location	Total (%)	PG1 (%)	PG2 (%)	PG3 (%)	PG4 (%)	PG5 (%)
W.C.	100	100	100	100	100	100
Continental shelf north of the W.C.	71.76	100	100	97.7	61.1	0
Between W.C. & B.C.	99.54	100	100	97.7	100	100
B.C. eastern perimeter	98.52	99	95.9	97.7	100	100
Continental shelf north of the B.C.	83.58	99	95.9	97.7	100	25.3
B.C. western perimeter	95.54	99	95.9	86.4	96.4	100
B.C. head	8.22	0	0	0	0	41.1

Table 3.6: Time and the range of velocities for particles travelling through the SB1 model domain and a breakdown for each particle group. PG1 is the particles that had a starting depth of 100 m to 200 m, PG2 had a starting depth of 200 m to 300 m, PG3 had a starting depth of 300 m to 400 m, PG4 had a starting depth of 400 m to 500 m and PG5 had a starting depth of 500 m to 1000 m.

Particle group	Average time (days)	Minimum velocity (cms <sup>-1</sup> )	Average velocity (cms <sup>-1</sup> )	Maximum velocity (cms <sup>-1</sup> )
All	11.92	-2.8	-4.61	-6.88
PG1	9.86	-4.15	-5.58	-6.88
PG2	11.82	-4	-4.65	-5.79
PG3	13.65	-2.8	-4.03	-5.06
PG4	12.46	-3.89	-4.41	-4.73
PG5	12.03	-4.15	-4.57	-4.89

### 3.3 Experiment SB2

#### 3.3.1 Sea Level Elevation and Velocity Fields

Experiment SB2 was focused around reversing the flow regime in experiment SB1 to test the Bremer and Whale Canyon with an eastwards flow present in the southern hemisphere. To achieve this, the sea level elevation was increased by 2 cm on the northern boundary, and similarly, allowed to run for six days before sea level elevation was considered to be at its final state for the model. Instead of being released on the eastern boundary, the particles release points were shifted to the western boundary, and everything else was kept constant with experiment SB1.

After six days of run time, the average sea level elevation showed  $0.77 \text{ cm} \pm 0.68 \text{ cm}$  (Figure 3.12). This resulted in an average zonal Eulerian velocity of  $9.8 \pm 5.21 \text{ cms}^{-1}$  eastwards (Figure 3.12). The average meridional Eulerian velocity was  $0.13 \text{ cms}^{-1} \pm 0.72 \text{ cms}^{-1}$  northwards (Figure 3.13). All measured locations in the SB2 model domain had an eastwards velocity ranging from  $0.56 \text{ cms}^{-1} \pm 0.47 \text{ cms}^{-1}$  in the head of the Bremer Canyon compared to  $13.68 \text{ cms}^{-1} \pm 0.94 \text{ cms}^{-1}$  in the continental shelf. The western Bremer Canyon perimeter had an eastwards velocity of  $5.19 \text{ cms}^{-1} \pm 3.92 \text{ cms}^{-1}$  and the Whale Canyon had a velocity of  $6.03 \text{ cms}^{-1} \pm 5.63 \text{ cms}^{-1}$  eastwards. The western Bremer Canyon perimeter had an average northwards velocity of  $0.73 \text{ cms}^{-1} \pm 0.74 \text{ cms}^{-1}$  and the Whale Canyon had an average northwards velocity of  $0.29 \text{ cms}^{-1} \pm 1.67 \text{ cms}^{-1}$ . The northwards velocity indicated that formation of a topographic Rossby wave was possible (Table 3.4).

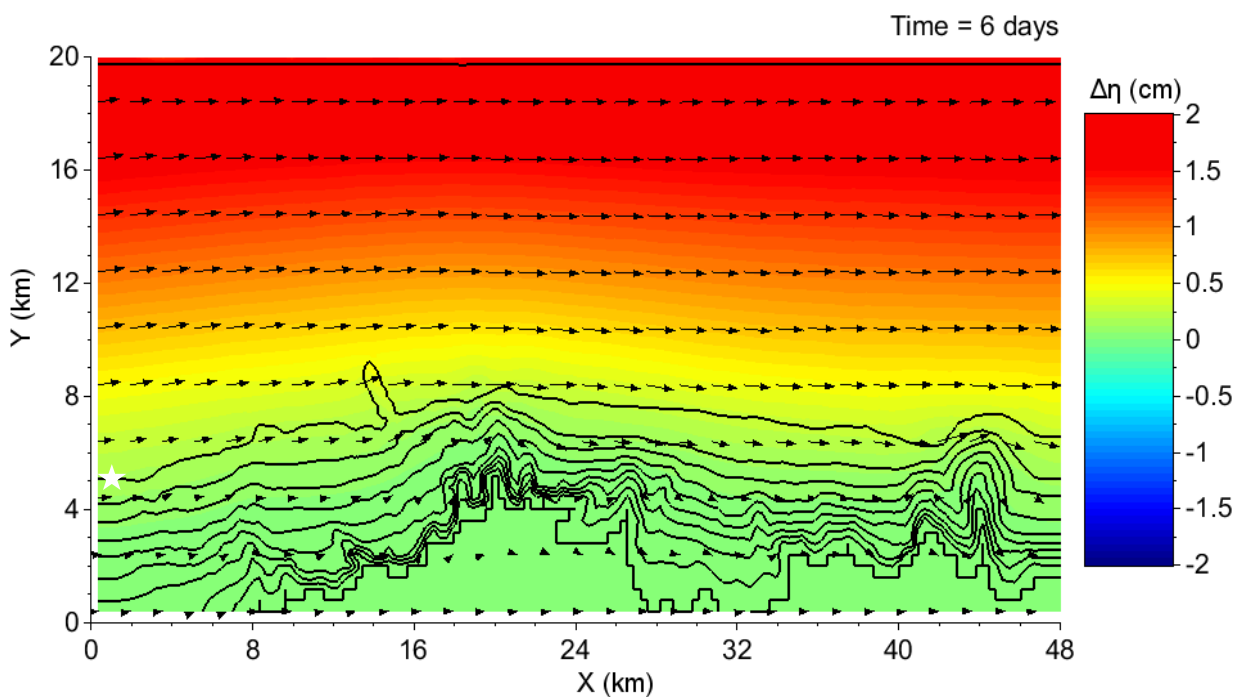


Figure 3.12: The resulting sea level increase for experiment SB2 after six days of run time. Black lines are 100 m contour lines up until 1000 m, and arrows are flow vector. The white star denotes where the 100 m contour line is. The northern boundary had an average sea level increase of  $1.77 \text{ cm} \pm 0.21 \text{ cm}$ , while the southern boundary had an average increase of  $2.7 \cdot 10^{-3} \text{ cm} \pm 1.5 \cdot 10^{-3} \text{ cm}$ .

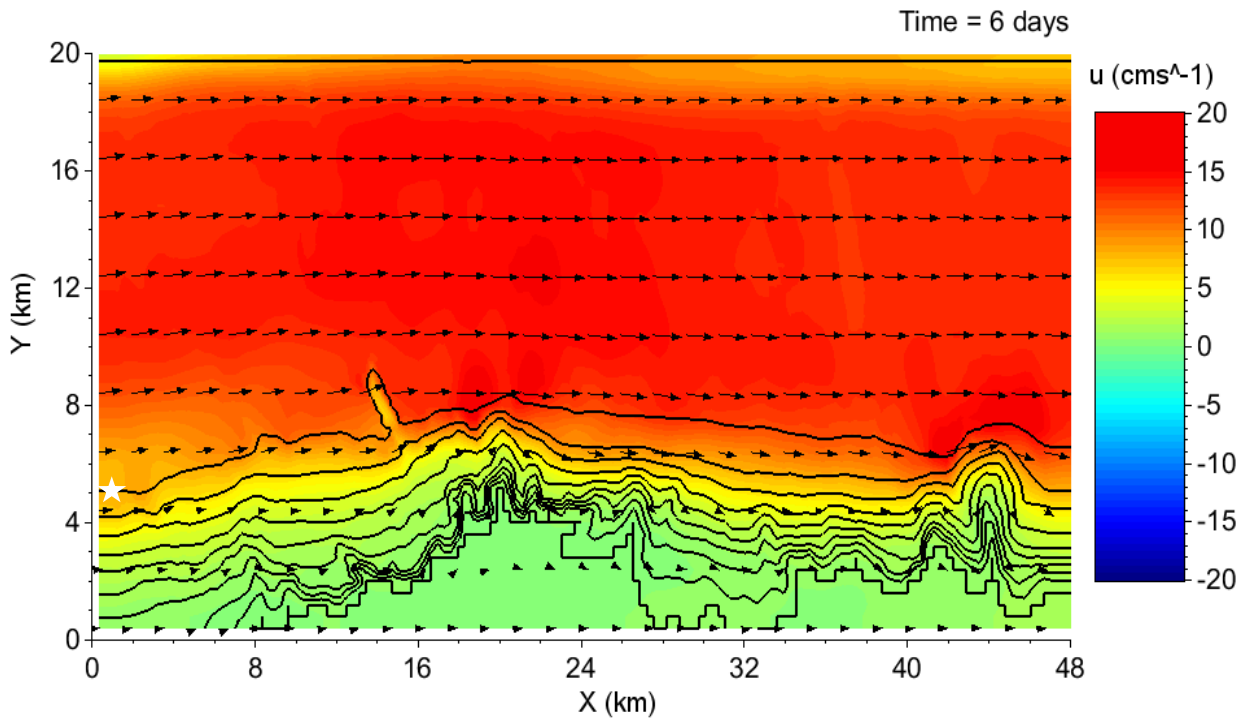


Figure 3.13: The zonal Eulerian velocity for experiment SB2, with positive values representing an eastwards flow. Black lines are 100 m contour lines up until 1000 m, and arrows are flow vectors. The white star denotes the 100 m contour line. The median flow was  $12.89 \text{ cms}^{-1}$  eastwards.

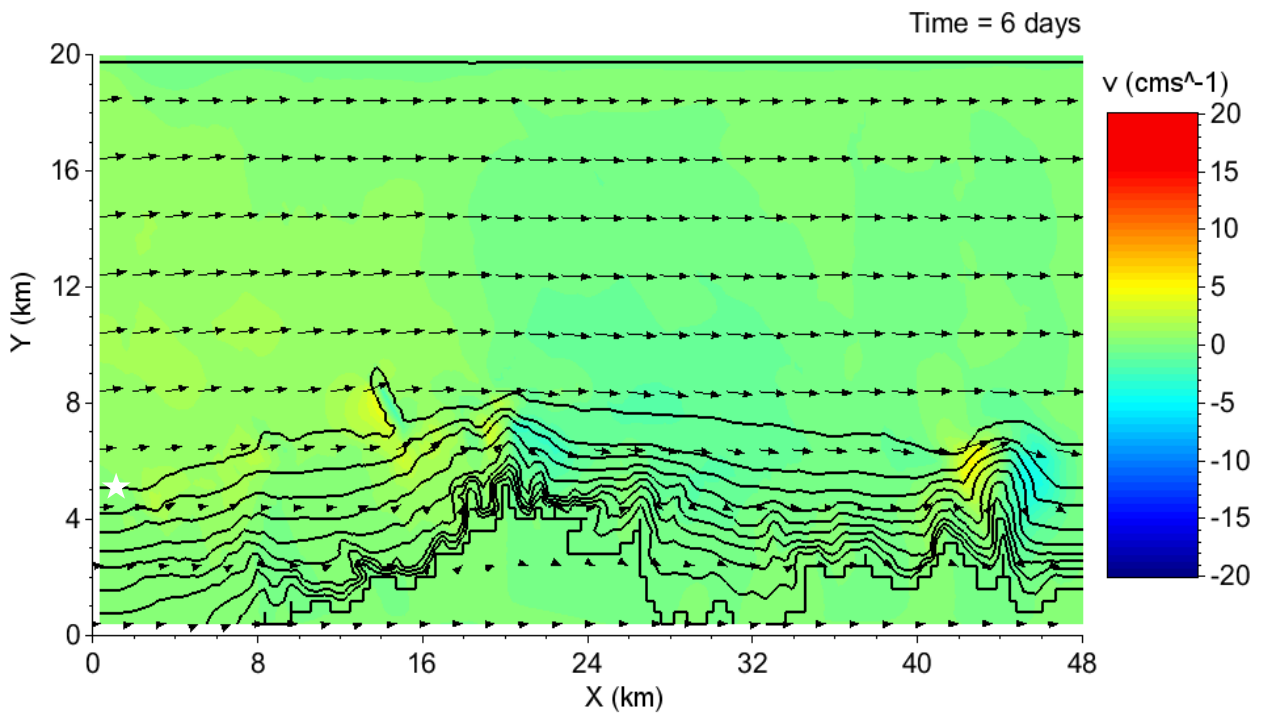


Figure 3.14: The meridional Eulerian velocity for experiment SB2 after six days of run time, with positive values representing a northwards flow. Black lines are 100 m contour lines up until 1000 m, and arrows are flow vectors. The white star indicates where the 100 m contour line is. The median velocity was  $0.03 \text{ cms}^{-1}$  northwards.

Table 3.7: The average sea level elevation (Figure 3.12), zonal Eulerian velocity (Figure 3.13), and meridional Eulerian velocity (Figure 3.14) for areas of interest within experiment SB2 model domain. Positive values were an increase in sea level elevation, an eastward zonal flow, and a northward meridional flow. W.C. stands for Whale Canyon. B.C. stands for Bremer Canyon.

Location	Average sea level elevation (cm)	Average zonal Eulerian velocity (cms <sup>-1</sup> )	Average meridional Eulerian velocity (cms <sup>-1</sup> )
Mean	0.77 ± 0.68	9.8 ± 5.21	0.13 ± 0.72
Continental shelf	1.27 ± 0.38	13.68 ± 0.94	0.21 ± 0.54
W.C.	0.12 ± 0.13	6.03 ± 5.63	0.29 ± 1.67
Between W.C. & B.C.	0.13 ± 0.13	6 ± 4.64	0.28 ± 0.42
B.C. eastern perimeter	0.16 ± 0.12	8.62 ± 4.70	0.53 ± 0.96
B.C. western perimeter	0.11 ± 0.10	5.19 ± 3.92	0.73 ± 0.74
B.C. head	0.01 ± 0.01	0.56 ± 0.47	0.01 ± 0.31

### 3.4.2 Lagrangian Particle Tracker

100% of particles entered the western perimeter of the Bremer Canyon, with 0% of these particles entering the continental shelf (Figure 3.15, 3.16). These particles instead entered the eastern perimeter of the Bremer Canyon. 100% of particles also entered the Whale Canyon. None of those particles entered the continental shelf via the Whale Canyon (Table 3.5).

The average time taken for particles to exit the eastern boundary was 23.81 days, which gave an overall average velocity of 2.31 cms<sup>-1</sup> eastwards (Table 3.6). Particles released between 100 m to 200 m were the fastest on average with an average velocity of 7.2 cms<sup>-1</sup> eastwards. Particle velocities decreased with an increase in depth, culminating at an average velocity of 1.16 cms<sup>-1</sup> eastwards at depths > 500 m.

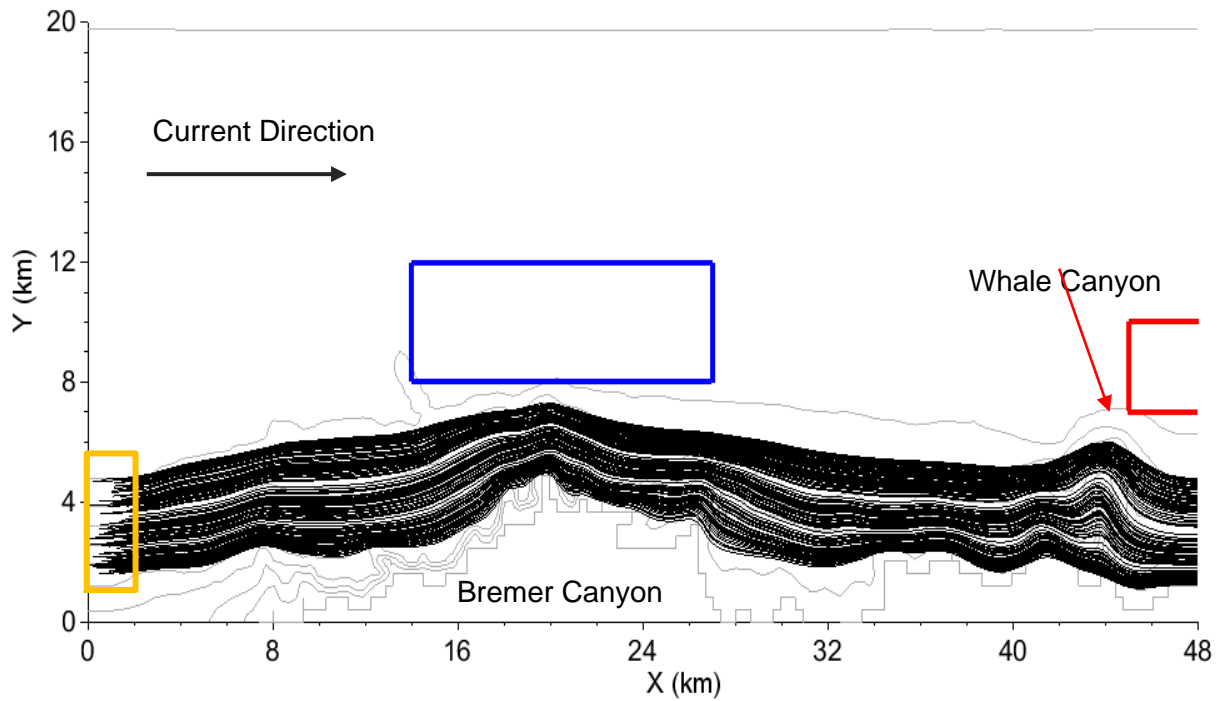


Figure 3.15: The average trajectory of every 40<sup>th</sup> particle released on the western boundary for experiment SB2 (orange square). The sections of the continental shelf where particles would upwell into if a topographic Rossby wave formed in red (Whale Canyon), and blue (Bremer Canyon), which are based on locations 4 and 6 in section 2.5.1. The grey lines are 100 m contours. The maximum velocity that particles reached was  $8.59 \text{ cm s}^{-1}$  eastwards. As a result, no topographic Rossby wave formed.

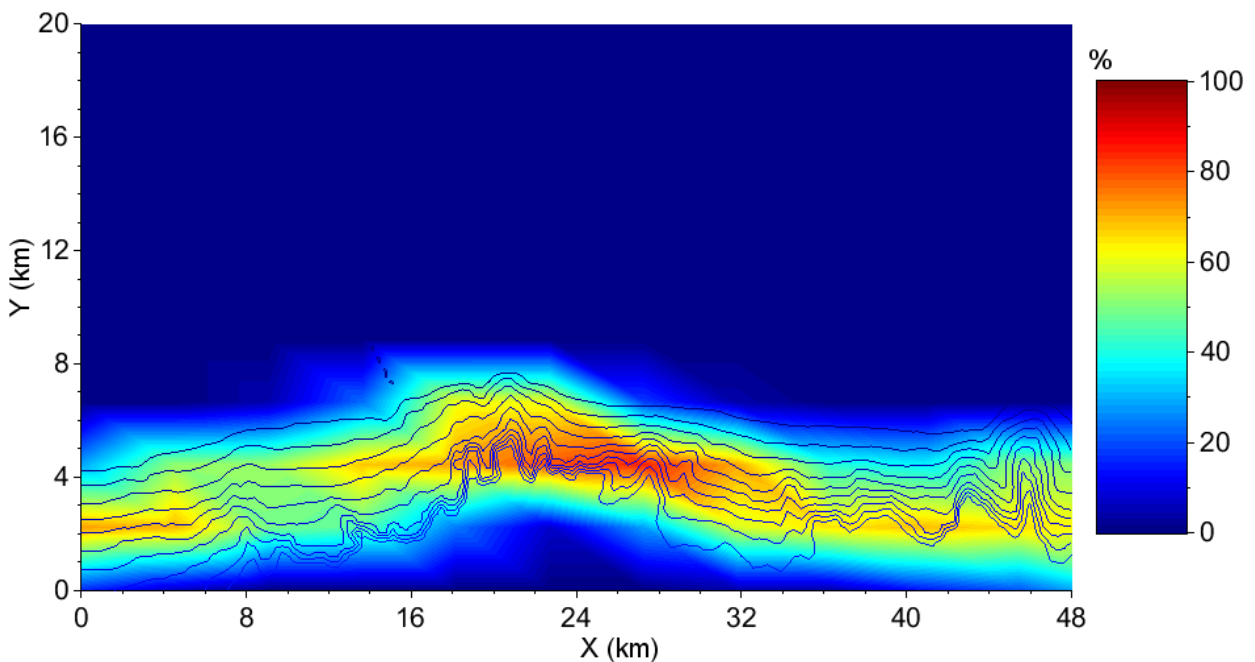


Figure 3.16: Average concentration of particles within the model domain. The blue lines represent 100 m contour lines in the model from 100 m to 1000 m. Particles tended to be evenly spread around the first 1000 m with maximum concentrations of 81% occurring within the eastern perimeter of the Bremer Canyon.

Table 3.8: Percentage of particles passing through each area of interest within the SB2 model domain, as well as how the release depth had affected this percentage (Figure 3.16). W.C. stands for Whale Canyon, and B.C. stands for Bremer Canyon. PG1 is the particles that had a starting depth of 100 m to 200 m, PG2 had a starting depth of 200 m to 300 m, PG3 had a starting depth of 300 m to 400 m, PG4 had a starting depth of 400 m to 500 m and PG5 had a starting depth of 500 m to 1000 m.

Location	Total (%)	PG1 (%)	PG2 (%)	PG3 (%)	PG4 (%)	PG5 (%)
W.C.	100	100	100	100	100	100
Continental shelf north of the W.C.	0	0	0	0	0	0
Between W.C. & B.C.	100	100	100	100	100	100
B.C. eastern perimeter	100	100	100	100	100	100
Continental shelf north of the B.C.	0	0	0	0	0	0
B.C. western perimeter	100	100	100	100	100	100
B.C. head	11.6	0	0	0	0	58

Table 3.9: Time and the range of velocities for particles travelling through the SB2 model domain, and a breakdown for each particle group. PG1 is the particles that had a starting depth of 100 m to 200 m, PG2 had a starting depth of 200 m to 300 m, PG3 had a starting depth of 300 m to 400 m, PG4 had a starting depth of 400 m to 500 m and PG5 had a starting depth of 500 m to 1000 m.

Particles	Average Time (days)	Minimum Velocity (cms <sup>-1</sup> )	Average Velocity (cms <sup>-1</sup> )	Maximum Velocity (cms <sup>-1</sup> )
All	23.81	0.95	2.31	8.8
PG1	7.64	5.71	7.2	8.8
PG2	13.16	2.96	4.18	5.87
PG3	19.91	2.29	2.76	4.04
PG4	31.12	1.3	1.77	2.3
PG5	47.22	0.95	1.16	1.73

### 3.5 Experiment SB3

#### 3.5.1 Sea Level Elevation and Velocity Fields

The aim of experiment SB3 was to test what would occur if the Whale and Bremer Canyon experienced a westwards flow in the northern hemisphere. The Coriolis force was changed to  $1 \times 10^{-4} \text{ s}^{-1}$  to represent  $\sim 40^\circ \text{N}$ . The sea level elevation was increased by 2 cm on the northern

boundary over a six-day period, and particles were set to be released on the eastern boundary. Outside of those two changes, everything else was kept constant with experiment SB1.

After reaching its final state, the average sea level elevation in SB3 showed  $0.75 \text{ cm} \pm 0.68 \text{ cm}$  (Figure 3.17), and from this change in sea level elevation, the average Eulerian zonal velocity was  $9.86 \text{ cm s}^{-1} \pm 6.37 \text{ cm s}^{-1}$  westwards (Figure 3.18). The average meridional Eulerian velocity in SB3 was  $0.11 \text{ cm}^{-1} \pm 0.65 \text{ cm s}^{-1}$  southwards (Figure 3.19).

The Whale Canyon had an average westwards velocity of  $3.48 \text{ cm s}^{-1} \pm 4.74 \text{ cm s}^{-1}$ . The eastern perimeter had an average westwards velocity of  $4.1 \text{ cm s}^{-1} \pm 4.44 \text{ cm s}^{-1}$ . The Whale Canyon had an average northwards velocity of  $3.9 \cdot 10^{-3} \text{ cm s}^{-1} \pm 0.99 \text{ cm s}^{-1}$ . The eastern perimeter of the Bremer Canyon had an average northwards velocity of  $0.09 \text{ cm s}^{-1} \pm 0.23 \text{ cm s}^{-1}$ .

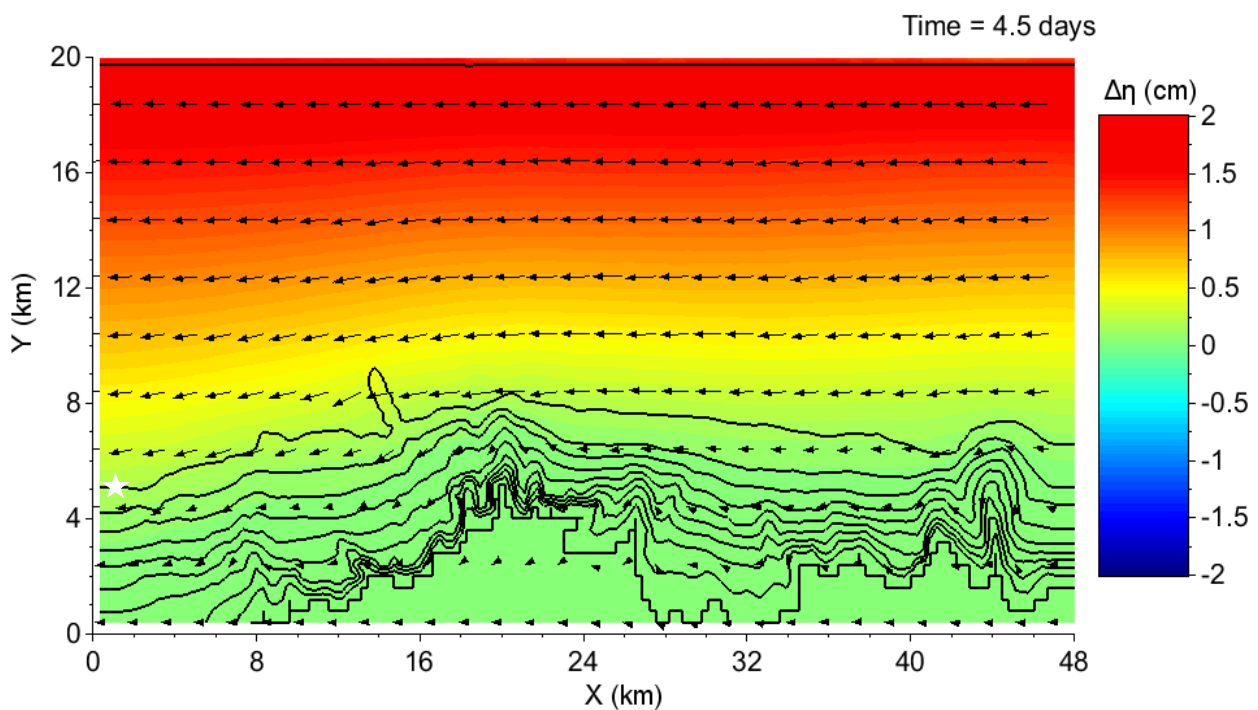


Figure 3.17: The resulting sea level change from experiment SB3, with positive values representing an increase in sea surface height. Black lines are contours, which represent 100 m lines up until 1000 m, star is where the 100 m contour line is located, and arrows are representing flow direction. The average sea level increase in the northern boundary was  $1.55 \text{ cm} \pm 0.47 \text{ cm}$ , while the southern boundary was  $5.49 \cdot 10^{-4} \text{ cm} \pm 1.2 \cdot 10^{-3} \text{ cm}$ .

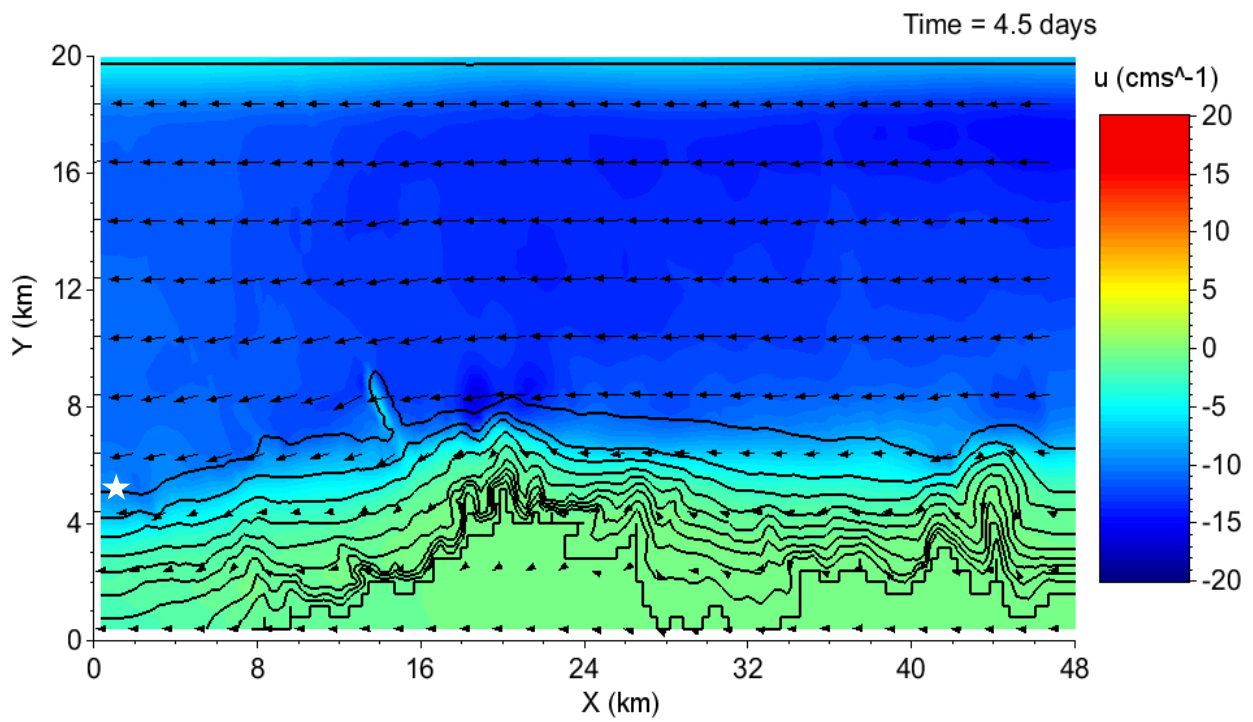


Figure 3.18: The resulting zonal Eulerian velocity from experiment SB3, with positive values representing an eastwards flow. Black lines are contours, which represent 100 m lines up until 1000 m, the white star is where the 100 m contour line is, and arrows are representing flow direction. The median velocity was  $-13.07 \text{ cms}^{-1}$  westwards. There was an issue on the northern boundary as the zonal velocity lowered to an average of  $1.35 \text{ cms}^{-1} \pm 1.15 \text{ cms}^{-1}$ .

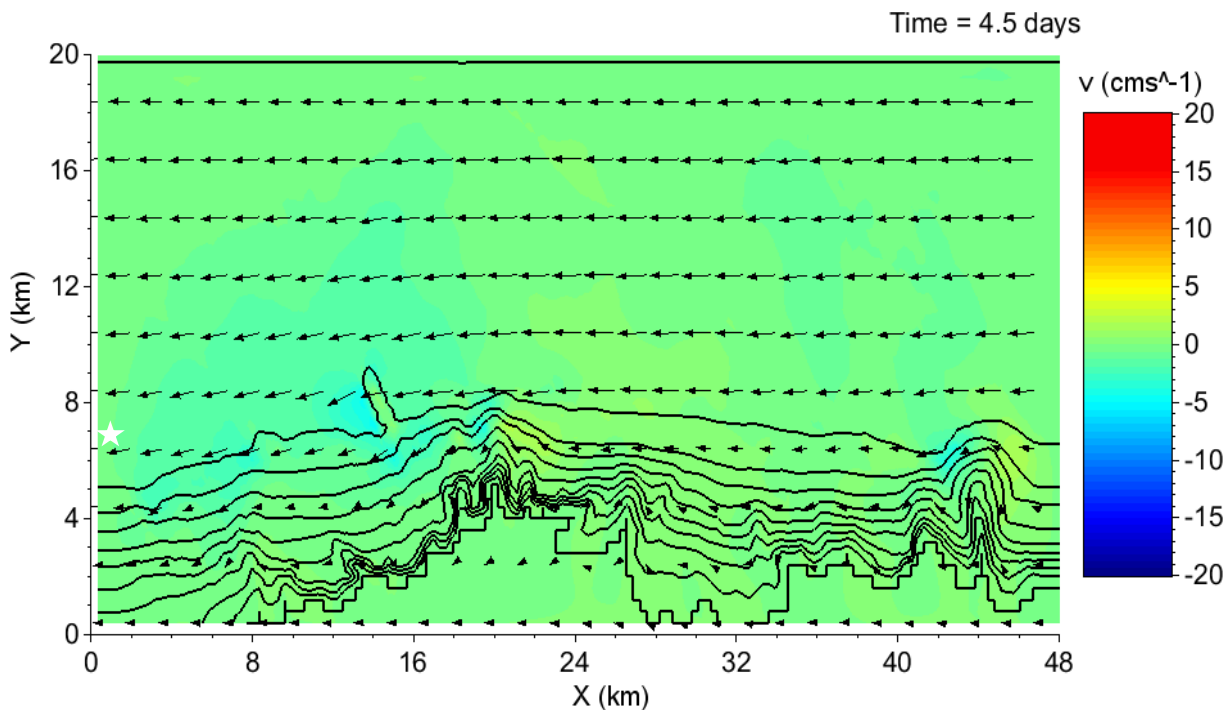


Figure 3.19: The resulting meridional Eulerian velocity for experiment SB3, with positive values representing a northwards flow. Black lines are contours which represent 100 m lines up until 1000 m, the white star is the 100 m contour line, and arrows are representing flow direction. The median flow is  $-0.25$  southwards.

Table 3.10: The average sea level elevation (Figure 3.17), zonal Eulerian velocity (Figure 3.18), and meridional Eulerian velocity (Figure 3.19) for areas of interest within experiment SB3 model domain. Positive values were for an increase in sea level elevation, an eastward zonal flow, and a northward meridional flow. W.C. stands for Whale Canyon, and B.C. stands for Bremer Canyon.

Location	Average sea level elevation (cm)	Average zonal Eulerian velocity (cms <sup>-1</sup> )	Average meridional Eulerian velocity (cms <sup>-1</sup> )
Mean	0.75 ± 0.68	-9.86 ± 6.37	-0.11 ± 0.65
Continental shelf	1.27 ± 0.42	-14.97 ± 1.58	-0.24 ± 0.41
W.C.	0.04 ± 0.07	-3.48 ± 4.74	3.9*10 <sup>-3</sup> ± 0.99
Between W.C. & B.C.	0.12 ± 0.12	-8.33 ± 5.61	0.25 ± 0.88
B.C. eastern perimeter	0.06 ± 0.08	-4.1 ± 4.44	0.09 ± 0.23
B.C. western perimeter	0.11 ± 0.12	-5.92 ± 5.18	-0.97 ± 0.96
B.C. head	9.39*10 <sup>-4</sup> ± 2.13*10 <sup>-3</sup>	-0.09 ± 0.29	7.6*10 <sup>-3</sup> ± 0.17

### 3.5.2 Lagrangian Particle Tracker

After sixty days of run time, 100% of particles had passed through the Whale Canyon, and from that, 0.2% of particles entered the continental shelf from the Whale Canyon. This 0.2% was made up of 1% released in between 100 m to 200 m, and 0% > 200 m. (Figure 3.20, 3.21, Table 3.8). 91.54% of particles entered the eastern perimeter of the Bremer Canyon, with no particles entering the continental shelf north of the Bremer Canyon. These results indicate that a topographic Rossby wave is not forming in SB3.

The times that it took particles to reach the western boundary ranged from 7.38 days to > 60 days, giving an average time of 27.72 days (Table 3.9). This gave a maximum average velocity for a particle of 7.46 cms<sup>-1</sup> westwards, with an average velocity of 1.98 cms<sup>-1</sup> westwards. As in experiment SB2 velocity decreases as depth increases with 100 m to 200 m having a velocity of 4.47 cms<sup>-1</sup> westwards, and 400 m to 500 m having an average velocity of 1.16 cms<sup>-1</sup> westwards. Depths > 500 m did not have a recorded velocity as 99.75% did not exit the model domain within the 60-day run time and were therefore ignored.

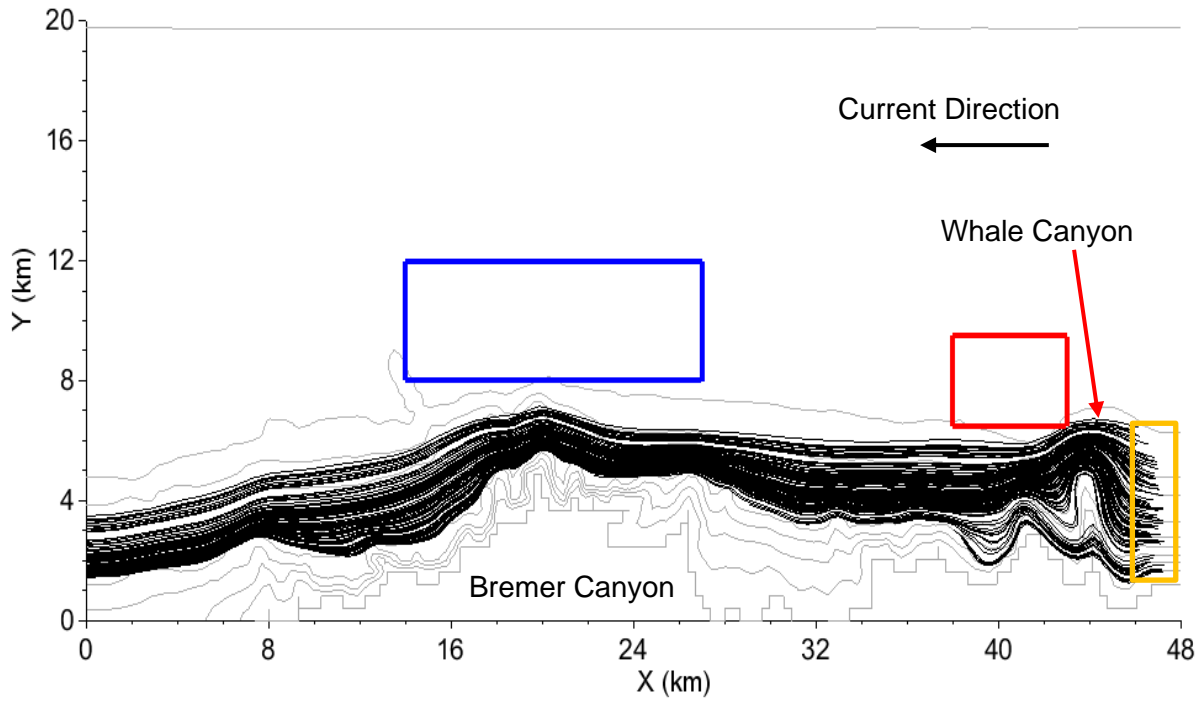


Figure 3.20: The trajectory for every 40<sup>th</sup> particle released on the eastern boundary for experiment SB3 (orange square shows release point). The sections of the continental shelf where particles would upwell into if a topographic Rossby wave formed in red (Whale Canyon), and blue (Bremer Canyon), which were based on locations 3 and 6 in section 2.5.1. The grey lines are 100 m contours. The maximum velocity that particles reach was 7.81  $\text{cm s}^{-1}$  westwards. No topographic Rossby waves formed during the model run time.

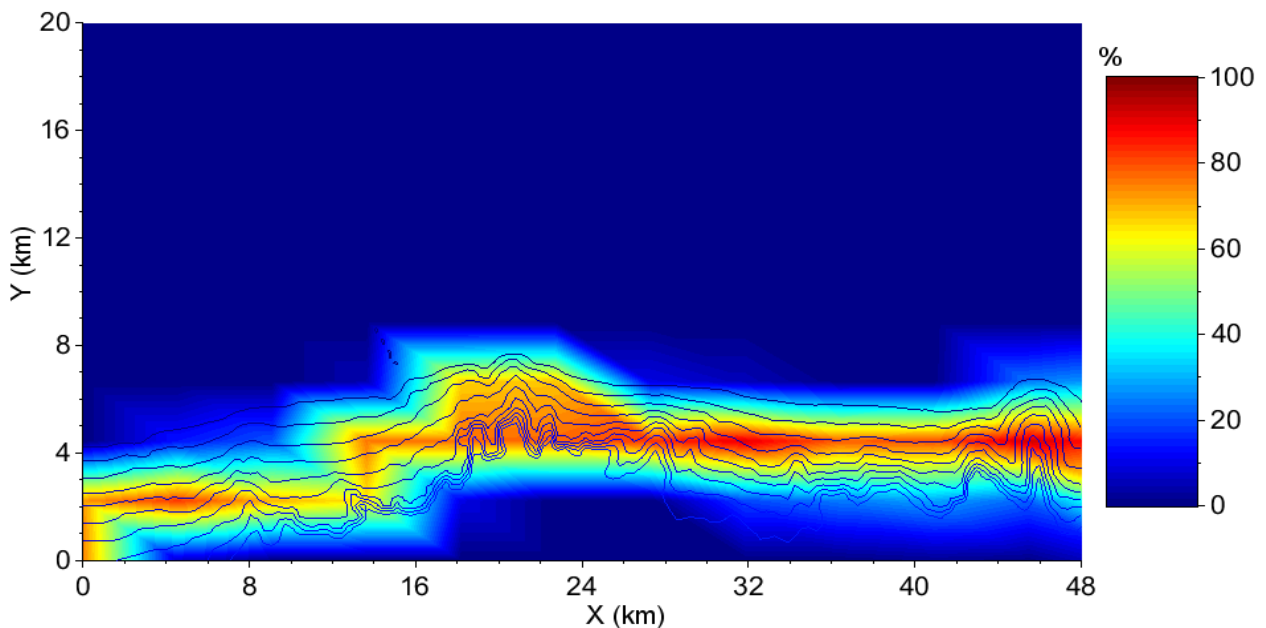


Figure 3.21: A heat map of particles concentration whilst travelling through the model domain. The blue lines represent 100 m contour lines in the model from 100 m to 1000 m. The maximum percentage of concentration was 91.48%, which was in the Whale Canyon.

Table 3.11: Percentage of particles passing through each area of interest within the SB3 model domain, as well as how the release depth affected this percentage (Figure 3.21). W.C. stands for Whale Canyon. B.C. stands for Bremer Canyon. PG1 is the particles that had a starting depth of 100 m to 200 m, PG2 had a starting depth of 200 m to 300 m, PG3 had a starting depth of 300 m to 400 m, PG4 had a starting depth of 400 m to 500 m and PG5 had a starting depth of 500 m to 1000 m.

Location	Total (%)	PG1 (%)	PG2 (%)	PG3 (%)	PG4 (%)	PG5 (%)
W.C.	100	100	100	100	100	100
Continental shelf north of the W.C.	0.2	1	0	0	0	0
Between W.C. & B.C.	99.8	100	100	100	100	99
B.C. eastern perimeter	91.54	100	100	100	100	57.7
Continental shelf north of the B.C.	0	0	0	0	0	0
B.C. western perimeter	86.96	100	100	100	100	34.8
B.C. head	0	0	0	0	0	0

Table 3.12: Time and the range of velocities for particles travelling through the SB3 model domain and a breakdown for each particle group. PG1 is the particles that had a starting depth of 100 m to 200 m, PG2 had a starting depth of 200 m to 300 m, PG3 had a starting depth of 300 m to 400 m, PG4 had a starting depth of 400 m to 500 m and PG5 had a starting depth of 500 m to 1000 m.

Particle group	Average time (days)	Minimum velocity (cms <sup>-1</sup> )	Average velocity (cms <sup>-1</sup> )	Maximum velocity (cms <sup>-1</sup> )
All	27.72	-0.92	-1.98	-7.46
PG1	12.31	-2.49	-4.47	-7.46
PG2	23.25	-2.07	-2.37	-3.19
PG3	31.22	-1.39	-1.76	-2.15
PG4	47.29	-0.92	-1.16	-1.41
PG5	> 60	N/A	N/A	N/A

### 3.6 Experiment SB4

#### 3.6.1 Sea Level Elevation and Velocity Fields

The aim of experiment SB4 was to test what would occur if the Whale and Bremer Canyon experienced an eastward flow in the northern hemisphere. Like SB3, the Coriolis force was changed to  $1 \times 10^{-4} \text{ s}^{-1}$  to represent  $\sim 40^\circ \text{N}$ . To create an eastward flow, the sea level elevation was decreased by 2 cm on the northern boundary, and particles were released on the western

boundary. The run time for sea level elevation change was lowered to three days prior due to instability issues present in the model.

The average sea level elevation for SB4 at its final state was  $-0.39 \text{ cm} \pm 0.39 \text{ cm}$  (Figure 3.22), which resulted in an average zonal Eulerian velocity of  $4.87 \text{ cm s}^{-1} \pm 2.76 \text{ cm s}^{-1}$  eastwards (Figure 3.23). The average meridional Eulerian velocity was  $0.12 \text{ cm s}^{-1} \pm 0.68 \text{ cm s}^{-1}$  northwards (Table 3.10). The western perimeter of the Bremer Canyon had an average eastwards velocity of  $3.18 \text{ cm s}^{-1} \pm 2.38 \text{ cm s}^{-1}$  (Table 3.10). The western perimeter had an average meridional velocity of  $0.57 \text{ cm s}^{-1} \pm 0.71 \text{ cm s}^{-1}$ . The Whale Canyon had an average Eulerian velocity of  $2.15 \text{ cm s}^{-1} \pm 1.51 \text{ cm s}^{-1}$  eastwards. The Whale Canyon had an average meridional velocity of  $0.16 \text{ cm s}^{-1} \pm 1.22 \text{ cm s}^{-1}$  southwards.

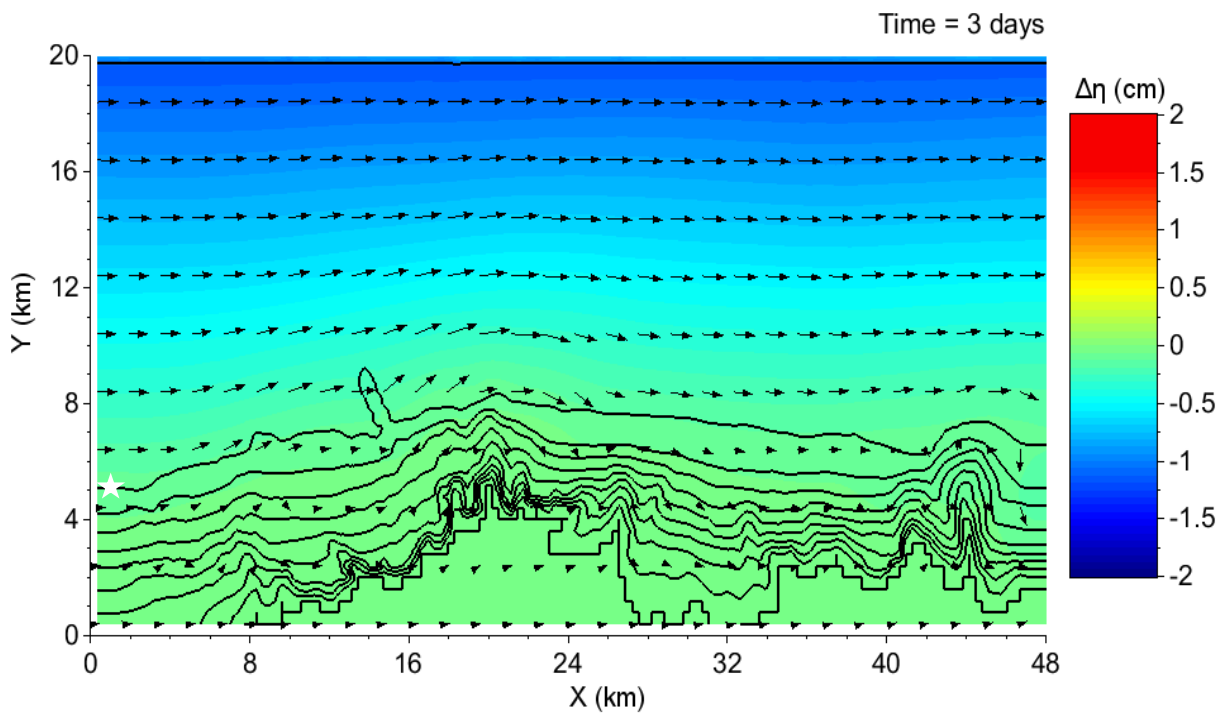


Figure 3.22: The resulting sea level change from experiment SB4, with positive values representing an increase in sea surface height. Black lines are 100 m contour lines up until 1000 m, the white star is the location of the 100 m contour line and arrows are flow direction. The average sea level decrease in the northern boundary was  $-1.49 \text{ cm} \pm 0.51 \text{ cm}$ , while the southern boundary was  $-3.5 \cdot 10^{-3} \text{ cm} \pm 2.6 \cdot 10^{-3} \text{ cm}$ .

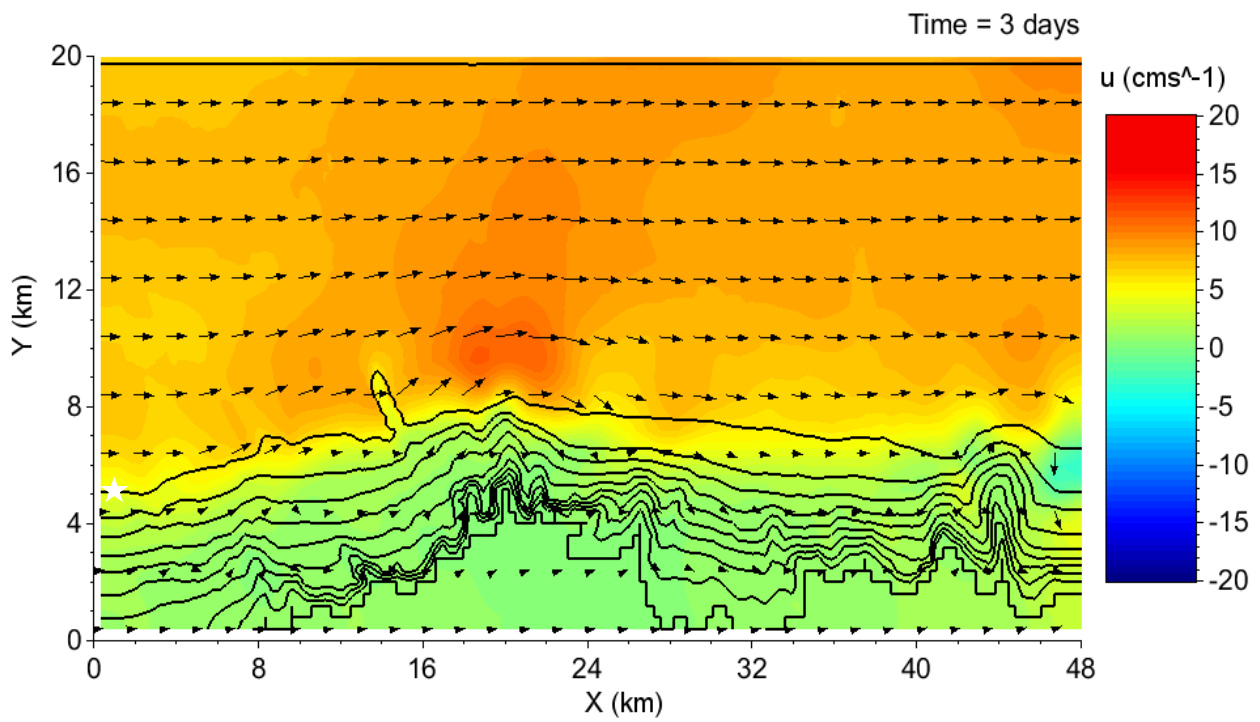


Figure 3.23: The resulting zonal Eulerian velocity from experiment SB4, with positive values representing an eastwards flow. Black lines are 100 m contour lines up until 1000 m, the white star is the location of the 100 m contour line and arrows are flow direction. The median flow was  $10.67 \text{ cms}^{-1}$  eastwards.

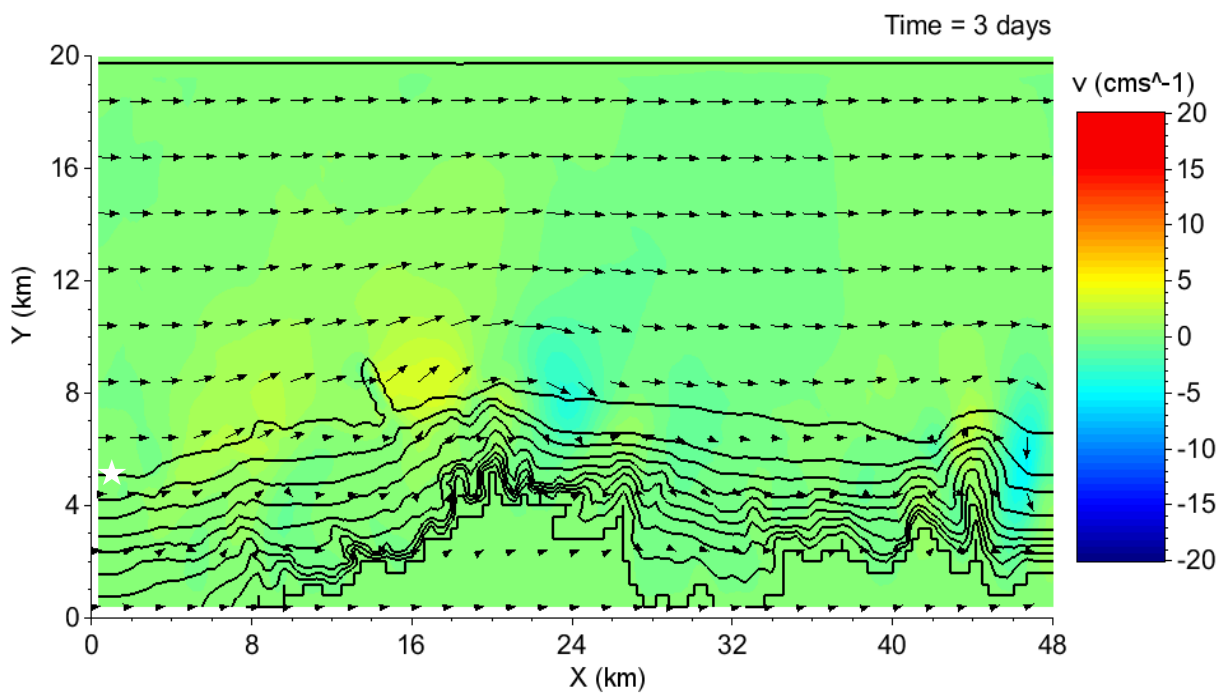


Figure 3.24: The meridional Eulerian velocity for experiment SB4, with positive values representing a northwards flow. Black lines are 100 m contour lines up until 1000 m, the white star is the location of the 100 m contour line and arrows are flow direction. The median flow is  $0.61 \text{ cms}^{-1}$  northwards.

Table 3.13: The average sea-level elevation (Figure 3.22), zonal Eulerian velocity (Figure 3.23), and meridional Eulerian velocity (Figure 3.24) for areas of interest within experiment SB4 model domain. Positive values were for an increase in sea level elevation, an eastwards zonal flow, and a northwards meridional flow. W.C. stands for Whale Canyon, and B.C. stands for Bremer Canyon.

Location	Average sea level elevation (cm)	Average zonal Eulerian velocity (cms <sup>-1</sup> )	Average meridional Eulerian velocity (cms <sup>-1</sup> )
Mean	-0.39 ± 0.39	4.87 ± 2.76	0.12 ± 0.68
Continental shelf	-0.59 ± 0.19	6.97 ± 0.57	0.16 ± 0.43
W.C.	-0.06 ± 0.04	2.15 ± 1.51	-0.16 ± 1.22
Between W.C. & B.C.	-0.06 ± 0.04	2.14 ± 1.63	-0.08 ± 0.26
B.C. eastern perimeter	-0.06 ± 0.04	3.18 ± 2.38	-0.19 ± 1.06
B.C. western perimeter	-0.05 ± 0.05	2.44 ± 2.05	0.57 ± 0.71
B.C. head	-0.01 ± 6.1*10 <sup>-3</sup>	0.37 ± 0.18	0.09 ± 0.14

### 3.6.2 Lagrangian Particle Tracker

100% particles entered the western Bremer Canyon perimeter, of which 50.58% entered the continental shelf from the Bremer Canyon (Figure 3.25, 3.26, Table 3.11). Of this 50.58%, the majority were released in between 100 m to 300 m. The Whale Canyon had 89.22% of particles entering the canyon of which 46.1% were upwelled into the continental slope from the Whale Canyon. Most particles upwelled were released in between 100 m to 300 m, and particles returned to the continental slope after the whale canyon. These results indicate a topographic Rossby wave did not form in either the Bremer Canyon or the Whale Canyon.

The average time it took particles to exit the eastern boundary for experiment SB4 was 24.38 days, which gave an average zonal velocity of 2.26 cms<sup>-1</sup> eastwards (Table 3.12). Particle velocity decreased with depth, with 100 m to 200 m having an average velocity of 4.74 cms<sup>-1</sup> eastwards, whereas > 500 m had an average velocity of 1.3 cms<sup>-1</sup> eastwards. The biggest decrease in velocity occurred in SB4 in between 100 m to 200 m at 2.46 cms<sup>-1</sup>.

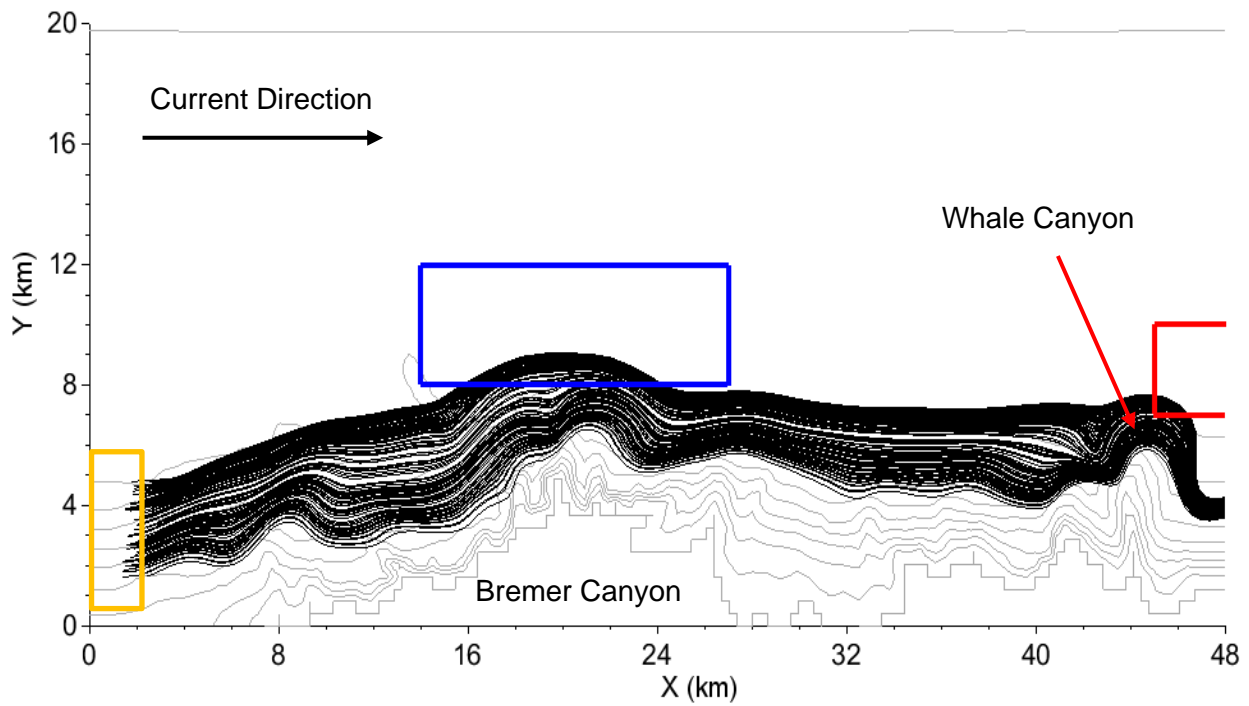


Figure 3.25: The trajectory of every 40<sup>th</sup> particle that was released within experiment SB4. The sections of the continental shelf where particles would upwell into if a topographic Rossby wave formed in red (Whale Canyon), and blue (Bremer Canyon), which are based on locations 4 and 6 in section 2.5.1 The grey lines are 100 m contours. The minimum velocity was 5.18 cms<sup>-1</sup> eastwards and the maximum velocity was 3.28 cms<sup>-1</sup> eastwards.

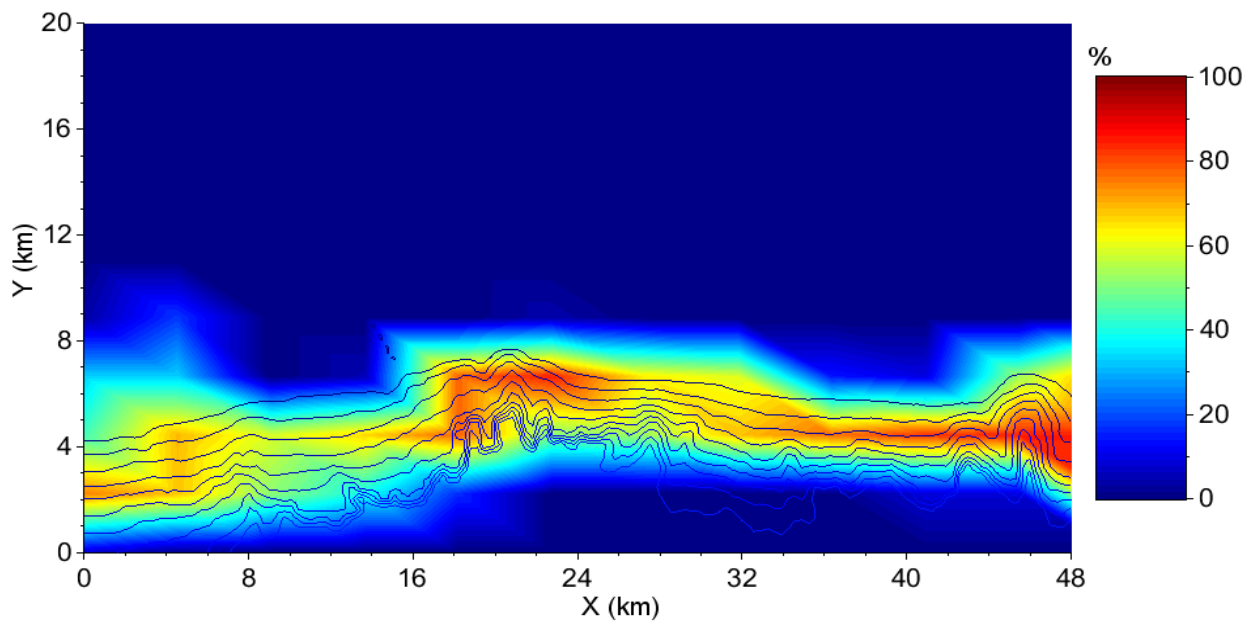


Figure 3.26: A heat map of particles concentration whilst travelling through the experiment SB4 model domain. The blue lines are 100 m contour lines in the model from 100 m to 1000 m. The maximum percentage of concentration was 84.48% which is in the Whale Canyon.

Table 3.14: Percentage of particles passing through each area of interest within the SB4 model domain, as well as how the release depth had affected this percentage (Figure 3.26). W.C. stands for Whale Canyon. B.C. stands for Bremer Canyon. PG1 is the particles that had a starting depth of 100 m to 200 m, PG2 had a starting depth of 200 m to 300 m, PG3 had a starting depth of 300 m to 400 m, PG4 had a starting depth of 400 m to 500 m and PG5 had a starting depth of 500 m to 1000 m.

Location	Total (%)	PG1 (%)	PG2 (%)	PG3 (%)	PG4 (%)	PG5 (%)
W.C.	89.22	47	99.1	100	100	100
Continental shelf north of the W.C.	46.1	100.0	99.7	30.9	0.0	0.0
Between W.C. & B.C.	53.16	0.0	0.0	65.8	100	100
B.C. eastern perimeter	61.88	0.0	10.8	98.6	100	100
Continental shelf north of the B.C.	50.58	100	100	52.9	0	0
B.C. western perimeter	100	100	100	100	100	100
B.C. head	0	0	0	0	0	0

Table 3.15: Time and the range of velocities for particles travelling through the SB4 model domain, and a breakdown for each particle group. PG1 is the particles that had a starting depth of 100 m to 200 m, PG2 had a starting depth of 200 m to 300 m, PG3 had a starting depth of 300 m to 400 m, PG4 had a starting depth of 400 m to 500 m and PG5 had a starting depth of 500 m to 1000 m.

Particle group	Average time (days)	Minimum velocity (cms <sup>-1</sup> )	Average velocity (cms <sup>-1</sup> )	Maximum velocity (cms <sup>-1</sup> )
All	24.38	0.98	2.26	5.30
PG1	11.61	3.7	4.74	5.30
PG2	15.06	2.98	3.65	4.84
PG3	21.92	1.70	2.51	3.28
PG4	30.94	1.49	1.78	2.07
PG5	42.40	0.98	1.3	1.68

### 3.7 Experiment SB5

#### 3.7.1 Sea Level Elevation and Velocity Fields

The aim of experiment SB5 is to test what would happen if a greater depression in sea level occurred around the Whale and Bremer Canyons. The intention was to calculate an upper limit of flow speed for upwelling to occur. To achieve this, the sea level elevation was decreased by 4 cm

on the northern boundary with everything else kept constant. The sea level elevation was allowed to run for six days, before the sea level gradient was treated as a constant in the model.

After reaching its final state in SB5, the average sea level elevation was  $-1.58 \text{ cm} \pm 1.29 \text{ cm}$  (Figure 3.27) which resulted in an average zonal Eulerian velocity of  $21.51 \text{ cms}^{-1} \pm 11.52 \text{ cms}^{-1}$  westwards (Figure 3.28). When compared to the average event velocity for Bremer Bay, SB5 was faster by  $12.8 \text{ cms}^{-1}$ . When compared to the maximum event velocity SB5 was faster by  $6.71 \text{ cms}^{-1}$  (Table 3.1, 3.13). The average meridional velocity for SB5 was  $1.39 \text{ cms}^{-1} \pm 7.04 \text{ cms}^{-1}$  southwards (Figure 3.29).

The Whale Canyon had an average zonal Eulerian velocity of  $6.87 \text{ cms}^{-1} \pm 6.01 \text{ cms}^{-1}$  westwards (Table 3.13). The eastern perimeter of the Bremer Canyon had an average westwards velocity of  $11.47 \text{ cms}^{-1} \pm 7.66 \text{ cms}^{-1}$ . The Whale Canyon had an average meridional velocity of  $3.54 \text{ cms}^{-1} \pm 4.38 \text{ cms}^{-1}$  northwards. The eastern perimeter had a northwards velocity of  $7.88 \text{ cms}^{-1} \pm 5.07 \text{ cms}^{-1}$ .

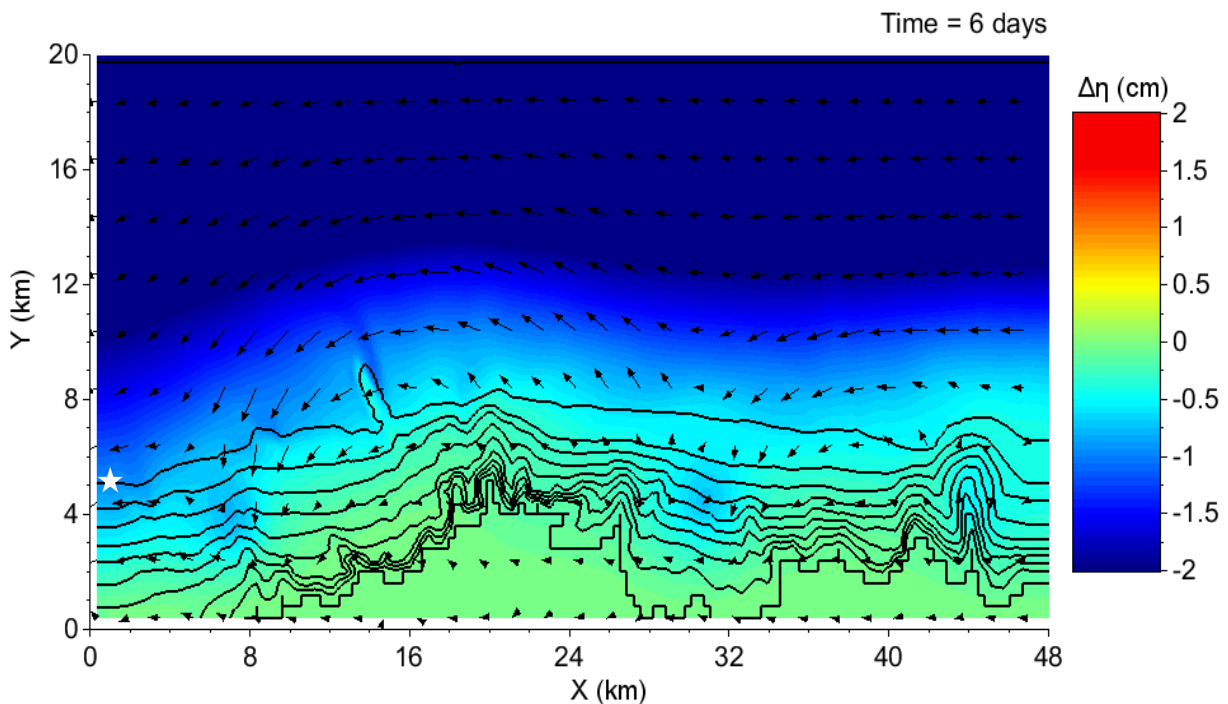


Figure 3.27: The resulting sea level change after experiment SB5, with positive values representing an increase in sea level. Black lines are 100 m contour lines up until 1000 m, and arrows are flow vectors. The white star indicates where the 100 m contour line is. The average sea level decrease in the northern boundary was  $-3.88 \text{ cm} \pm 0.27 \text{ cm}$ , while the southern boundary was  $-0.23 \text{ cm} \pm 0.2 \text{ cm}$

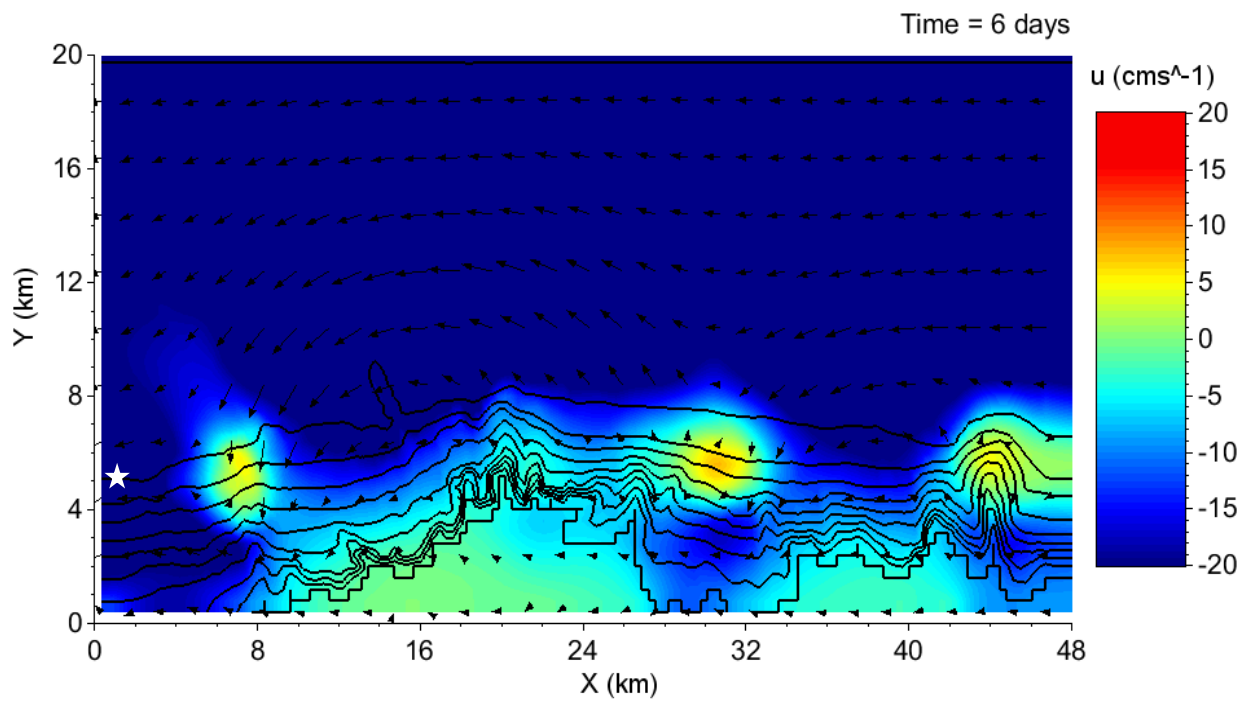


Figure 3.28: The average zonal Eulerian velocity for experiment SB5, with positive values representing an eastwards value. Black lines are 100 m contour lines up until 1000 m, and arrows are flow vectors. The white star indicates where the 100 m contour line is. The median flow velocity was  $24.14 \text{ cm s}^{-1}$  westwards.

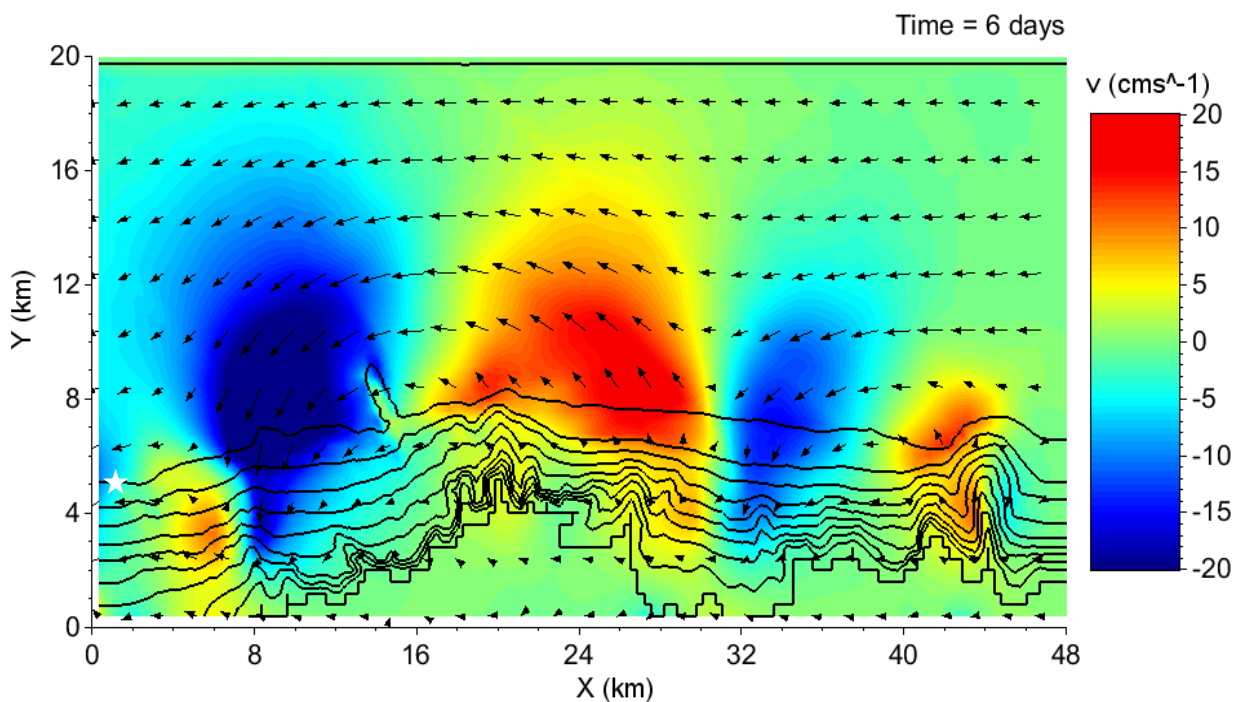


Figure 3.29: The meridional Eulerian velocity for experiment SB5, with positive values representing a northwards velocity. Black lines are 100 m contour lines up until 1000 m, and arrows are flow vectors. The white star indicates where the 100 m contour line is. The median flow velocity was  $0.43 \text{ cm s}^{-1}$  southwards.

Table 3.16: The average sea-level elevation (Figure 3.27), zonal Eulerian velocity (Figure 3.28), and meridional Eulerian velocity (Figure 3.29) for areas of interest within experiment SB5 model domain. Positive values were for an increase in sea level elevation, an eastward zonal flow, and a northward meridional flow. W.C. stands for Whale Canyon. B.C. stands for Bremer Canyon.

Location	Average sea level elevation (cm)	Average zonal Eulerian velocity (cms <sup>-1</sup> )	Average meridional Eulerian velocity (cms <sup>-1</sup> )
Mean	-1.58 ± 1.29	-21.51 ± 11.52	-1.39 ± 7.04
Continental shelf	-2.48 ± 0.77	-29.96	-1.69 ± 6.07
W.C.	-0.33 ± 0.15	-6.87 ± 6.01	3.54 ± 4.38
Between W.C. & B.C.	-0.34 ± 0.22	-11.47 ± 7.66	-3.48 ± 5.4
B.C. eastern perimeter	-0.39 ± 0.19	-11.3 ± 6.88	7.88 ± 5.07
B.C. western perimeter	-0.38 ± 0.29	-11.74 ± 8.32	-8.25 ± 9.36
B.C. head	-0.08 ± 0.08	-4.36 ± 2.94	1.16 ± 1.5

### 3.7.2 Lagrangian Particle Tracker

During the 60-day run time, 99.04% of particles have entered the Whale Canyon and from there, 73.28% entered the continental shelf from the Whale Canyon, which was an increase of 1.52% on SB1 (Figure 3.30, 3.31, Table 3.14). The 73.28% consisted of 100% of particles released between 100 m to 400 m, and 71.2% of particles released between 400 m to 500 m. 99.04% of particles entered the eastern perimeter of the Bremer Canyon, and from there, 91.28% entered the continental shelf from the Bremer Canyon. This was made up of 100% particles released < 500 m, and 61.2 % of particles > 500 m.

Particles released on the eastern boundary took on average 5.17 days to reach the western boundary, which gave an average velocity of 10.64 cms<sup>-1</sup> westwards (Table 3.15). Particles released between 100 m to 200 m had an average velocity of 7.48 cms<sup>-1</sup> westward which was the slowest recorded depth range, with 400 m to 500 m being the quickest at 13.82 cms<sup>-1</sup> westwards. The reason that the 100 m to 200 m changed from the quickest depth range in SB1 to the slowest in SB5 is that 4.8 % of particles released between these depths did not exit the model domain.

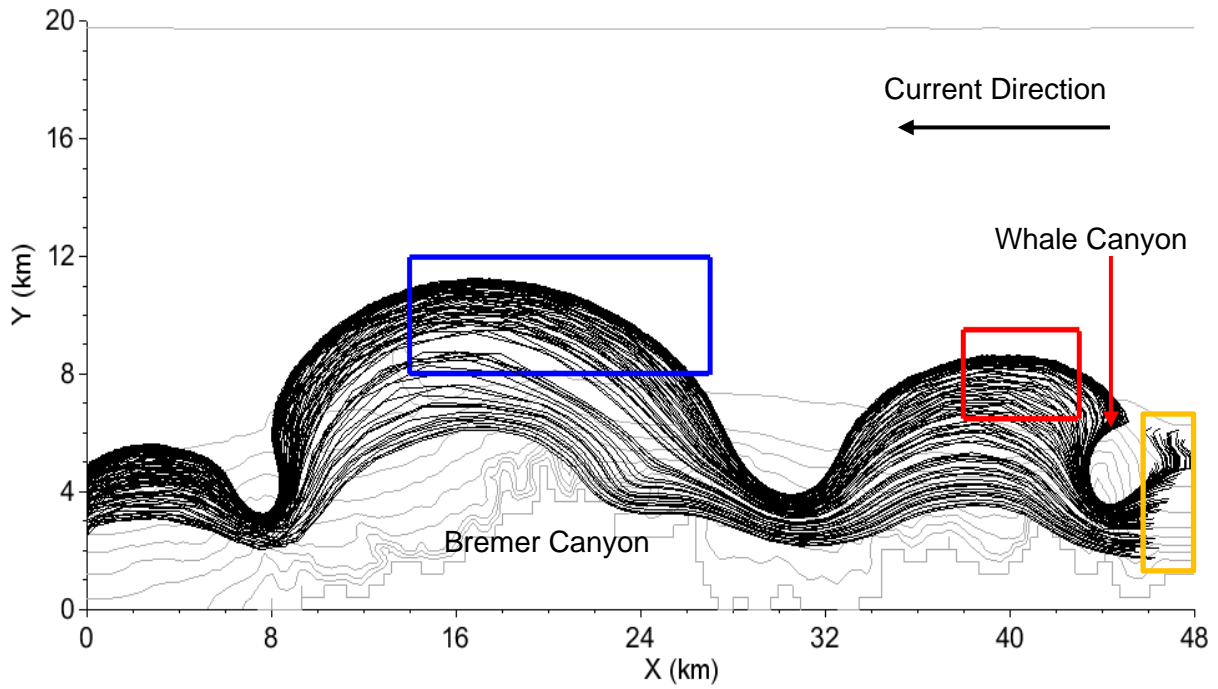


Figure 3.30: The trajectory of every 40<sup>th</sup> particle that was released within experiment SB5 (orange square is starting location). The sections of the continental shelf where particles would upwell into if a topographic Rossby wave formed in red (Whale Canyon), and blue (Bremer Canyon), which were based on locations 3 and 6 in section 2.5.1. The grey lines are 100 m contour. The wave was still in motion when it exited the model (green circle).

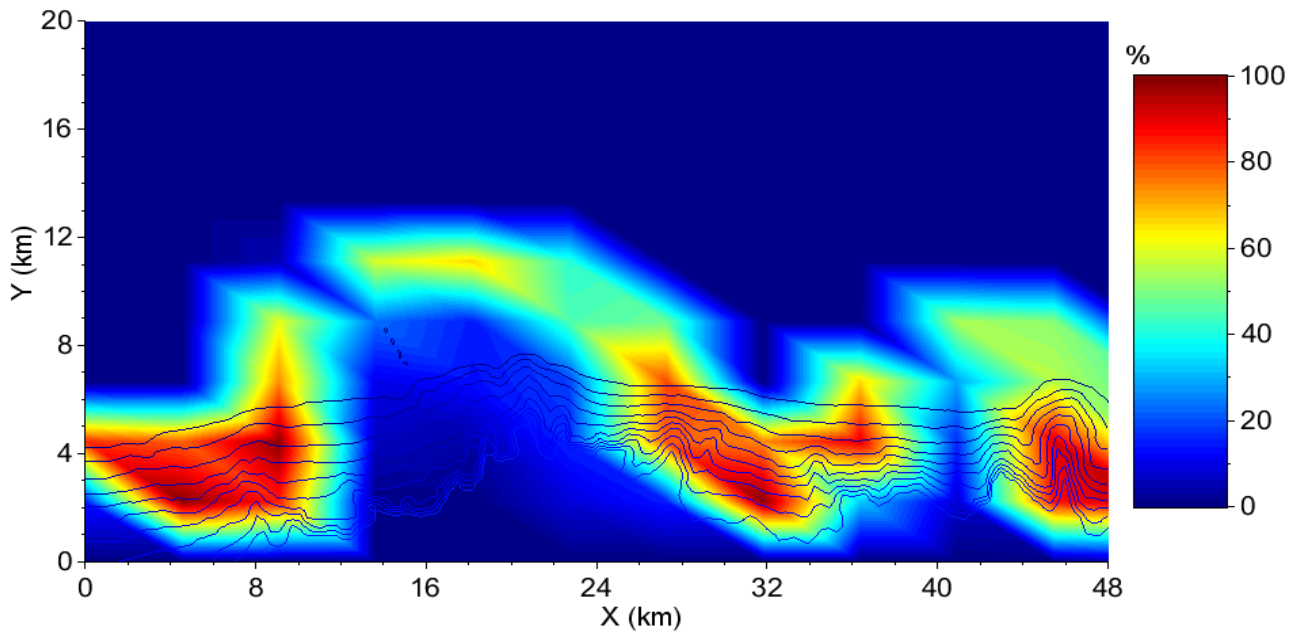


Figure 3.31: The heat-map of particle concentrations within experiment SB5. The blue lines are 100 m contour lines in the model. The maximum concentration of particles is 99.04%, which occurred around both Bremer Canyon perimeters.

Table 3.17: Percentage of particles passing through each area of interest within the SB5 model domain, as well as how the release depth had affected this percentage (Figure 3.31). W.C. stands for Whale Canyon. B.C. stands for Bremer Canyon. PG1 is the particles that had a starting depth of 100 m to 200 m, PG2 had a starting depth of 200 m to 300 m, PG3 had a starting depth of 300 m to 400 m, PG4 had a starting depth of 400 m to 500 m and PG5 had a starting depth of 500 m to 1000 m.

Location	Total (%)	PG1 (%)	PG2 (%)	PG3 (%)	PG4 (%)	PG5 (%)
W.C.	99.04	95.2	100	100	100	100
Continental shelf north of the W.C.	73.28	95.2	100	100	71.2	0
Between W.C. & B.C.	99.04	95.2	100	100	100	100
B.C. eastern perimeter	99.04	95.2	100	100	100	100
Continental shelf north of the B.C	91.28	95.2	100	100	100	61.2
B.C. western perimeter	32.06	0	0	0	60.3	100
B.C. head	1.66	0	0	0	0	8.3

Table 3.18: Time and the range of velocities for particles travelling through the SB5 model domain, and a breakdown for each particle group. PG1 is the particles that had a starting depth of 100 m to 200 m, PG2 had a starting depth of 200 m to 300 m, PG3 had a starting depth of 300 m to 400 m, PG4 had a starting depth of 400 m to 500 m and PG5 had a starting depth of 500 m to 1000 m.

Particle group	Average time (days)	Minimum velocity (cms <sup>-1</sup> )	Average velocity (cms <sup>-1</sup> )	Maximum velocity (cms <sup>-1</sup> )
Total	5.17	-5.24	-10.64	-14.19
PG1	7.36	-5.24	-7.48	-10
PG2	5.29	-8.98	-10.4	-11.58
PG3	4.35	-11.28	-12.63	-13.75
PG4	3.98	-13.33	-13.82	-14.19
PG5	4.98	-9.36	-11.05	-13.75

### 3.8 Experiment SB6

#### 3.8.1 Sea Level Elevation and Velocity Fields

The aim of experiment SB6 was to test what would occur to the Whale and Bremer Canyon should the coastal current flow observed in experiment SB1 be halved. The intention was to calculate a lower limit of flow speed that the canyon would be able to support upwelling. To achieve this, the sea level elevation was decreased by 1 cm on the northern boundary with

everything else kept constant. The sea level gradient was given six days to run, before it was treated as a constant.

After SB6 reached its final state, it had an average sea level elevation of  $-0.42 \text{ cm} \pm 0.31$  (Figure 3.32), which caused an average zonal Eulerian velocity of  $5.03 \text{ cm s}^{-1} \pm 2.18 \text{ cm s}^{-1}$  westwards (Figure 3.33). SB6 was also slower than the average coastal current velocity by  $3.68 \text{ cm s}^{-1}$  (Table 3.1, 3.16). The average meridional velocity for SB6 was  $0.28 \text{ cm s}^{-1} \pm 1.32 \text{ cm s}^{-1}$  southwards, (Figure 3.34). The average zonal Eulerian velocity in the Whale Canyon for SB6 was  $2.82 \text{ cm s}^{-1} \pm 2.76 \text{ cm s}^{-1}$  westwards (Table 3.16). The eastern perimeter of the Bremer Canyon had an average velocity of  $4.7 \text{ cm s}^{-1} \pm 2.49 \text{ cm s}^{-1}$  westwards. The Whale Canyon had an average meridional Eulerian velocity of  $0.23 \text{ cm s}^{-1} \pm 1.6 \text{ cm s}^{-1}$  northwards. The eastern perimeter had an average northwards velocity of  $0.36 \text{ cm s}^{-1} \pm 1.98 \text{ cm s}^{-1}$ .

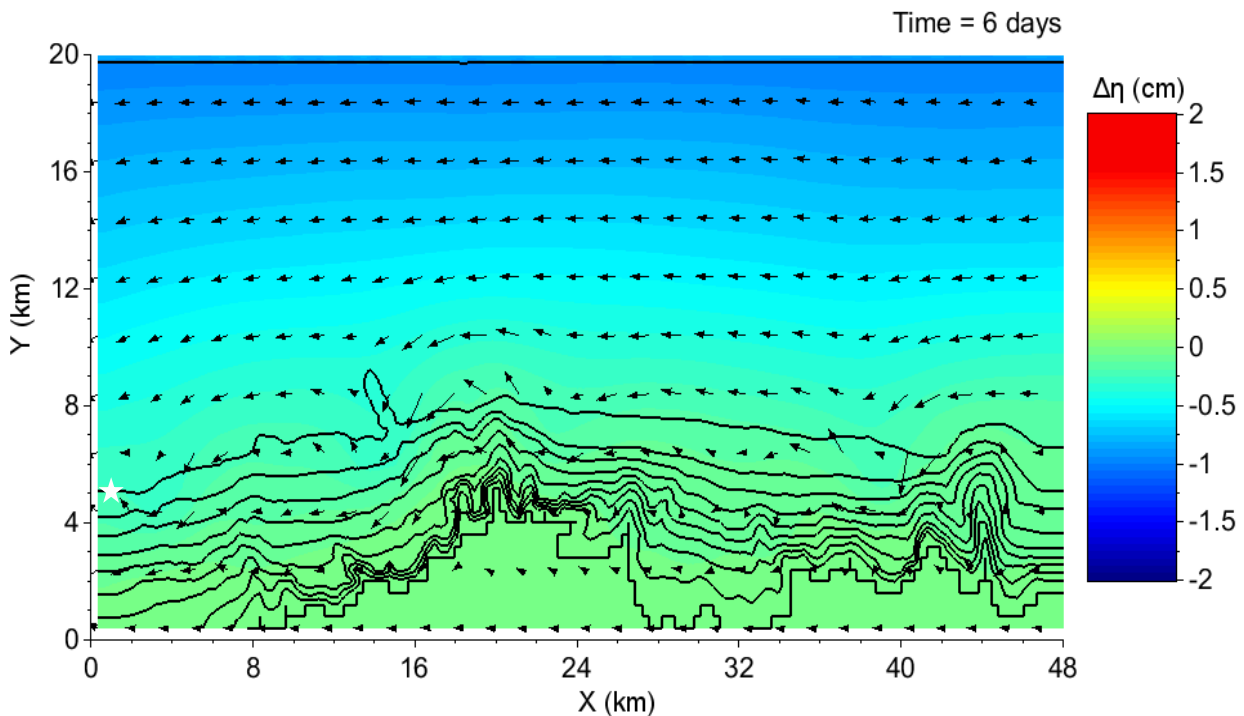


Figure 3.32: The average sea level decrease in experiment SB6, with positive values representing an increase in sea level. Black lines are 100 m contour lines up until 1000 m, and arrows are flow vectors. The white star indicates where the 100 m contour line is. The northern boundary had an average sea level decrease of  $-0.89 \text{ cm} \pm 0.09 \text{ cm}$ , while the southern boundary was  $-6.1 \cdot 10^{-3} \text{ cm} \pm 2.5 \cdot 10^{-3} \text{ cm}$ .

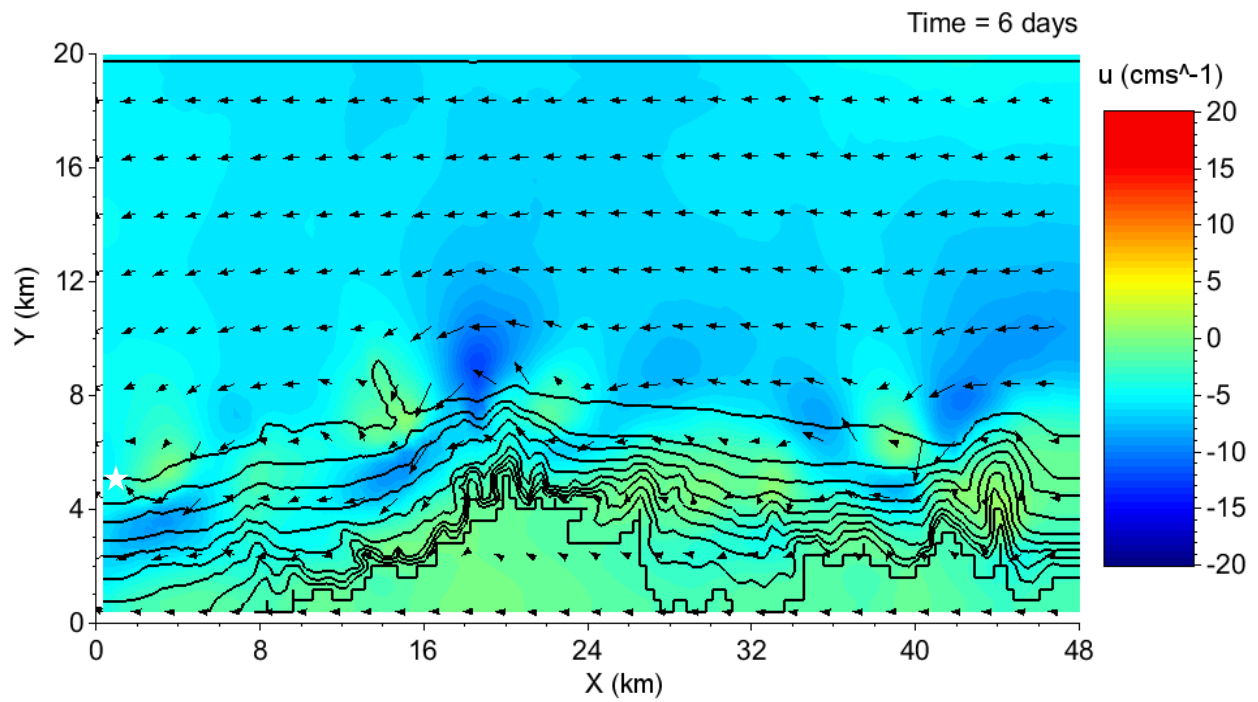


Figure 3.33: The average zonal Eulerian velocity for experiment SB6, with positive values representing an eastwards flow. Black lines are 100 m contour lines up until 1000 m, and arrows are flow vectors. The white star indicates where the 100 m contour line is. The median flow was  $5.73 \text{ cms}^{-1}$  westwards.

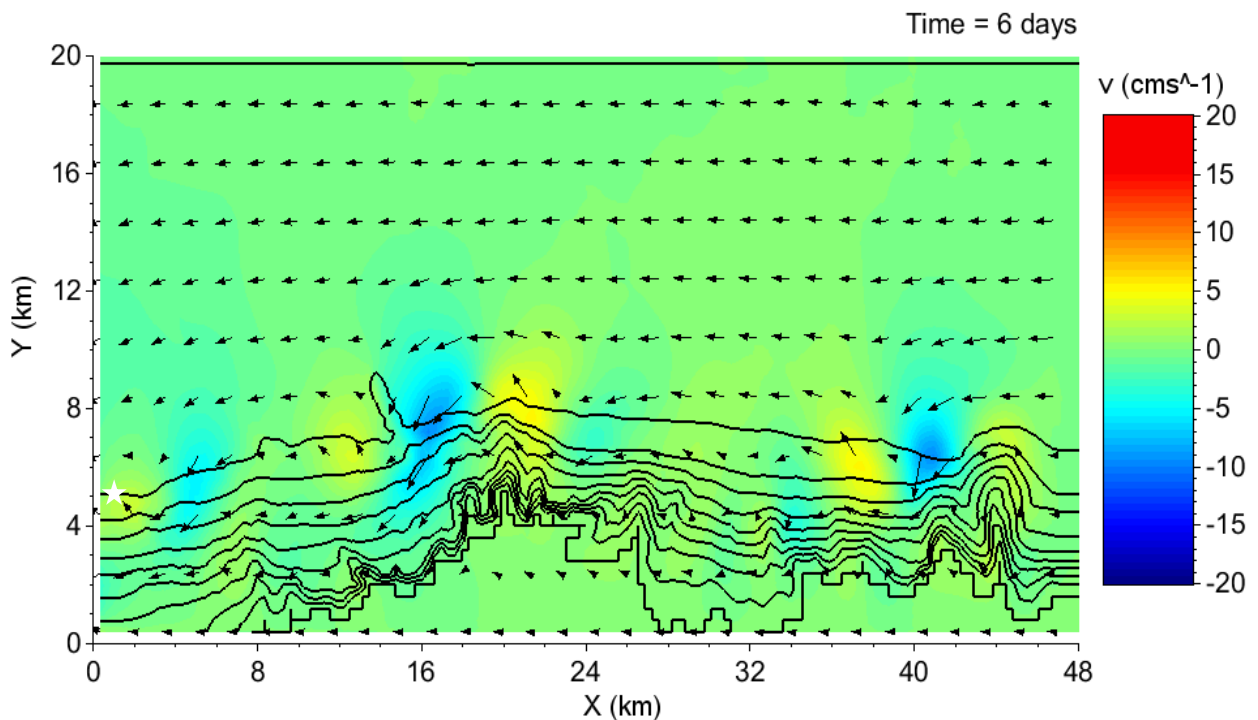


Figure 3.34: The average meridional Eulerian velocity for experiment SB6, with positive values representing a northwards flow. Black lines are 100 m contour lines up until 1000 m, and arrows are flow vectors. The white star indicates where the 100 m contour line is. The median velocity was  $0.12 \text{ cms}^{-1}$  southwards.

Table 3.19: The average sea-level elevation (Figure 3.32), zonal Eulerian velocity (Figure 3.33), and meridional Eulerian velocity (Figure 3.34) for areas of interest within experiment SB6 model domain. Positive values were for an increase in sea level elevation, an eastward zonal flow, and a northward meridional flow. W.C. stands for Whale Canyon. B.C. stands for Bremer Canyon.

Location	Average sea level elevation (cm)	Average zonal Eulerian velocity (cms <sup>-1</sup> )	Average meridional Eulerian velocity (cms <sup>-1</sup> )
Mean	-0.42 ± 0.31	-5.03 ± 2.18	-0.28 ± 1.32
Continental shelf	-0.66 ± 0.17	-6.26 ± 0.8	-0.29 ± 0.55
W.C.	-0.09 ± 0.04	-2.82 ± 2.76	0.23 ± 1.6
Between W.C. & B.C.	-0.11 ± 0.08	-3.44 ± 2.18	-0.12 ± 2.04
B.C. eastern perimeter	-0.14 ± 0.06	-4.7 ± 2.49	0.36 ± 1.98
B.C. western perimeter	-0.15 ± 0.09	-4.06 ± 2.11	-1.02 ± 2.24
B.C. head	-0.03 ± 0.02	-1.28 ± 0.67	0.3 ± 0.51

### 3.8.2 Lagrangian Particle Tracker

100% of particles entered the Whale Canyon, of which only 71.76% of particles were upwelled onto the continental shelf (Figure 3.35, 3.36, Table 3.17). That 71.76% consisted of 100% of particles released in between 100 m to 300m, and > 50% between 300 m to 500 m. 98.52% of particles entered the eastern perimeter of the Bremer Canyon of which 83.58% of particles ended up on the continental shelf. This consisted of 100% of particles released < 500 m, and 74.7% of particles released > 500 m.

The average time that particles took to reach the western boundary was 11.92 days, which gave an overall average velocity of 4.61 cms<sup>-1</sup> westwards (Table 3.18). The 100 m to 200 m was the fastest depth range at 5.58 cms<sup>-1</sup> westwards, and the slowest occurring in between 300 m to 400 m at 4.03 cms<sup>-1</sup> westwards. 4.46% of particles that were released did not exit the model domain, with trapped particles spread between 100 m to 500 m.

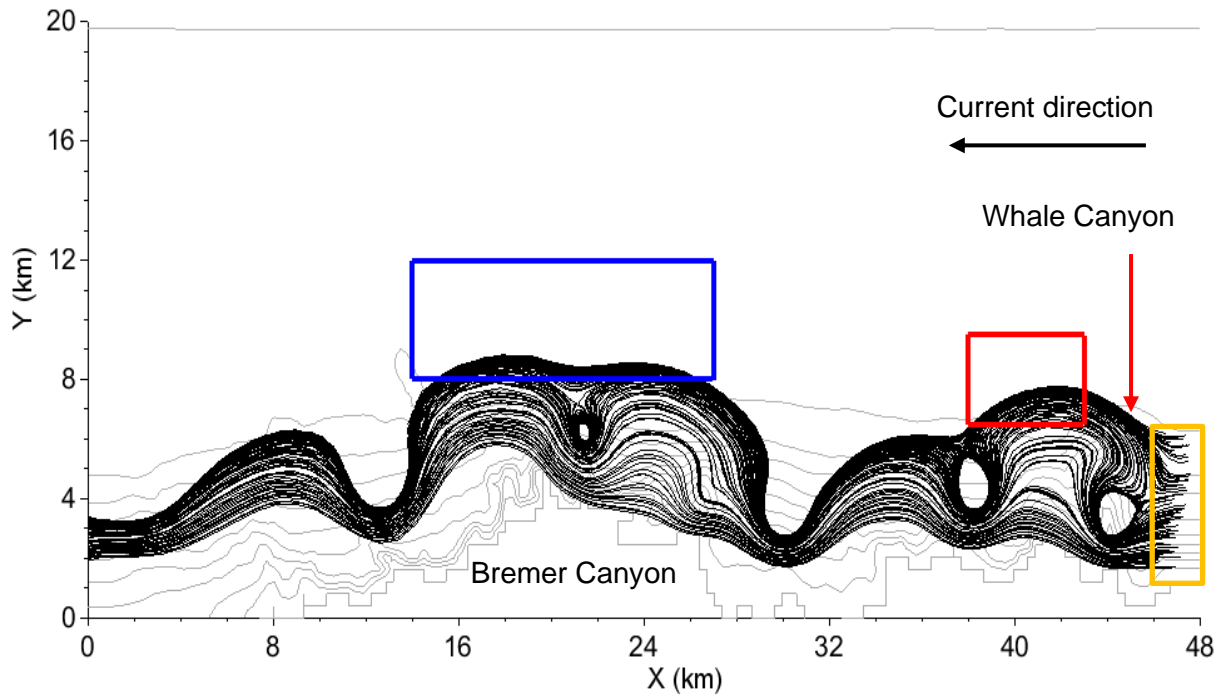


Figure 3.35: The trajectory of every 40<sup>th</sup> particle released on the eastern boundary (orange box) in experiment SB6. The sections of the continental shelf where particles would upwell into if a topographic Rossby wave formed in red (Whale Canyon), and blue (Bremer Canyon), which were based on locations 3 and 6 in section 2.5.1. The grey lines are 100 m contour lines. The minimum velocity was 2.74 cms<sup>-1</sup> westwards and the maximum velocity was 6.71 cms<sup>-1</sup> westwards. Like SB1, the topographic Rossby wave which formed only travelled for ~20 km after entering the Bremer Canyon (green circle).

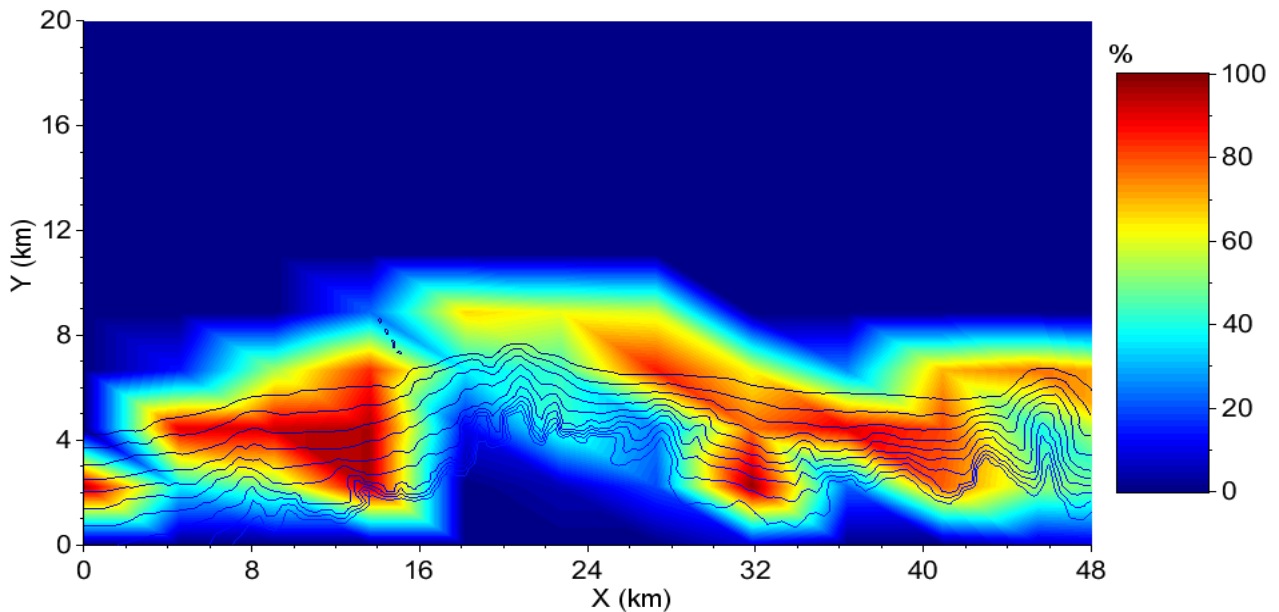


Figure 3.36: The heat-map of particle concentrations within experiment SB6. The blue lines are 100 m contour lines in the model from 100 m to 1000 m. The maximum concentration of particles was 98.52%, which occurred around the western Bremer Canyon perimeter.

Table 3.20: Percentage of particles passing through each area of interest within the SB6 model domain, as well as how the release depth affected this percentage (Figure 3.36). W.C. stands for Whale Canyon. B.C. stands for Bremer Canyon. PG1 is the particles that had a starting depth of 100 m to 200 m, PG2 had a starting depth of 200 m to 300 m, PG3 had a starting depth of 300 m to 400 m, PG4 had a starting depth of 400 m to 500 m and PG5 had a starting depth of 500 m to 1000 m.

Location	Total (%)	PG1 (%)	PG2 (%)	PG3 (%)	PG4 (%)	PG5 (%)
W.C.	100	100	100	100	100	100
Continental shelf north of the W.C.	71.76	100	100	97.7	61.1	0
Between W.C. & B.C.	99.54	100	100	97.7	100	100
B.C. eastern perimeter	98.52	99	95.9	97.7	100	100
Continental shelf north of the B.C.	83.58	99	95.9	97.7	100	25.3
B.C. western perimeter	95.54	99	95.9	86.4	96.4	100
B.C. head	8.22	0	0	0	0	41.1

Table 3.21: Time and the range of velocities for particles travelling through the SB6 model domain, and a breakdown for each particle group. PG1 is the particles that had a starting depth of 100 m to 200 m, PG2 had a starting depth of 200 m to 300 m, PG3 had a starting depth of 300 m to 400 m, PG4 had a starting depth of 400 m to 500 m and PG5 had a starting depth of 500 m to 1000 m.

Particle group	Average time (days)	Minimum velocity (cms <sup>-1</sup> )	Average velocity (cms <sup>-1</sup> )	Maximum velocity (cms <sup>-1</sup> )
Total	11.92	-2.74	-4.51	-6.71
PG1	9.86	-4.05	-5.45	-6.71
PG2	11.82	-3.91	-4.54	-5.65
PG3	13.65	-2.74	-3.93	-4.94
PG4	12.46	-3.8	-4.31	-4.62
PG5	12.03	-4.05	-4.46	-4.77

### 3.9: Temperature and Salinity Profiles

Temperature data from off the Bremer Bay coastline (Figure 2.10, 3.37) on average showed a decrease from the surface to the bottom of the profile of ~ 3.81°C. There was also a decrease of 2.19 °C in between 49.44 m to 59.25 m at station one, which became more pronounced a few days later with a temperature decrease of 3.53 °C between 52.73 m to 61.09 m at station two. This rapid decrease in temperature was also observed at stations three and four, despite them being in the continental slope with a 4.49 °C change occurring between 50.04 m to 64.37 m at station three, and a 3.43°C change between 61.09 m to 74.23 m at station four. This rapid temperature change was also observed closer to the coastline, as a 2.83 °C temperature change

occurred between 44.35 m to 54.2 m at station five, and a 2.36°C decrease occurred between 33.91 m to 46.15 m at station six.

Salinity data from the Bremer Bay coastline had an average decrease 0.54 PSU from the surface to the final depth of the CTD profiles (Figure 2.10, 3.38). Similarly, to temperature, station one and two had a salinity decrease of 0.23 PSU and 0.58 PSU between 49.44 m to 59.25 m and 60.49 m to 73.33 m, respectively. On the continental slope, station three had a salinity change of 0.53 PSU between 50.04 m to 64.37 m, and station four had a salinity change of 0.65 PSU between 60.49 m to 73.33 m. Closer to the coastline, station five had a salinity decrease of 0.66 PSU between 47.05 m to 57.21 m and station six had a decrease of 0.32 PSU between 33.91 m to 46.15 m. All stations experienced an  $\geq 0.08$  PSU increase of salinity between this decrease and the depth the measurement ended. The indication from these decreases in temperature and salinity is that these changes are not as a response to upwelling, but the thermocline adjusting to the change in maximum depth.

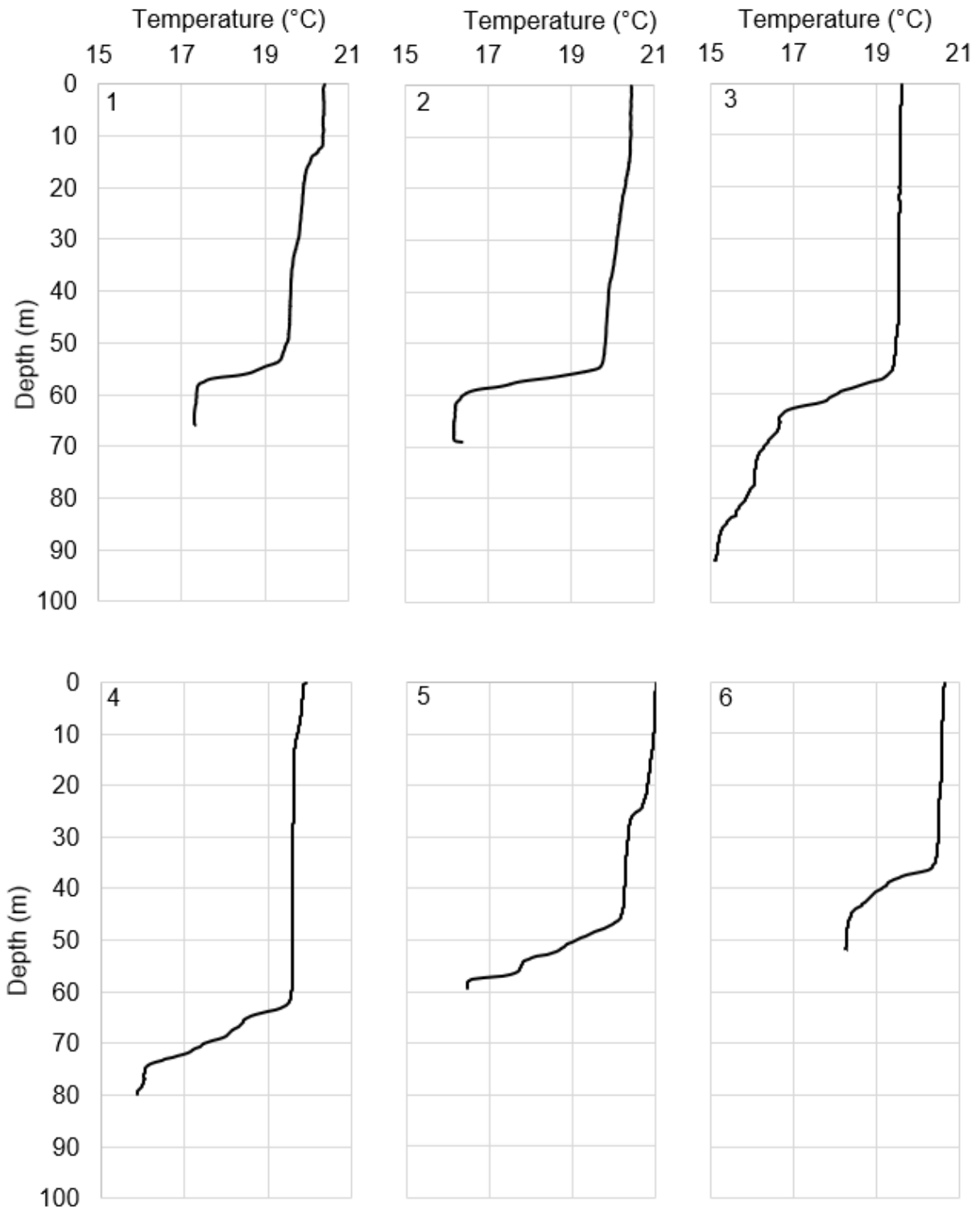


Figure 3.37: Temperature data for the stations used in CTD measurements off the Bremer Bay coastline (refer to Figure 2.10 for locations) for the 5<sup>th</sup> of February to the 7<sup>th</sup> of February. The maximum depth of each station is: 1) 72 m, 2) 72 m, 3) 900 m, 4) 600 m, 5) 60 m and 6) 50 m. The maximum depth the CTD probe could reach is 100 m.

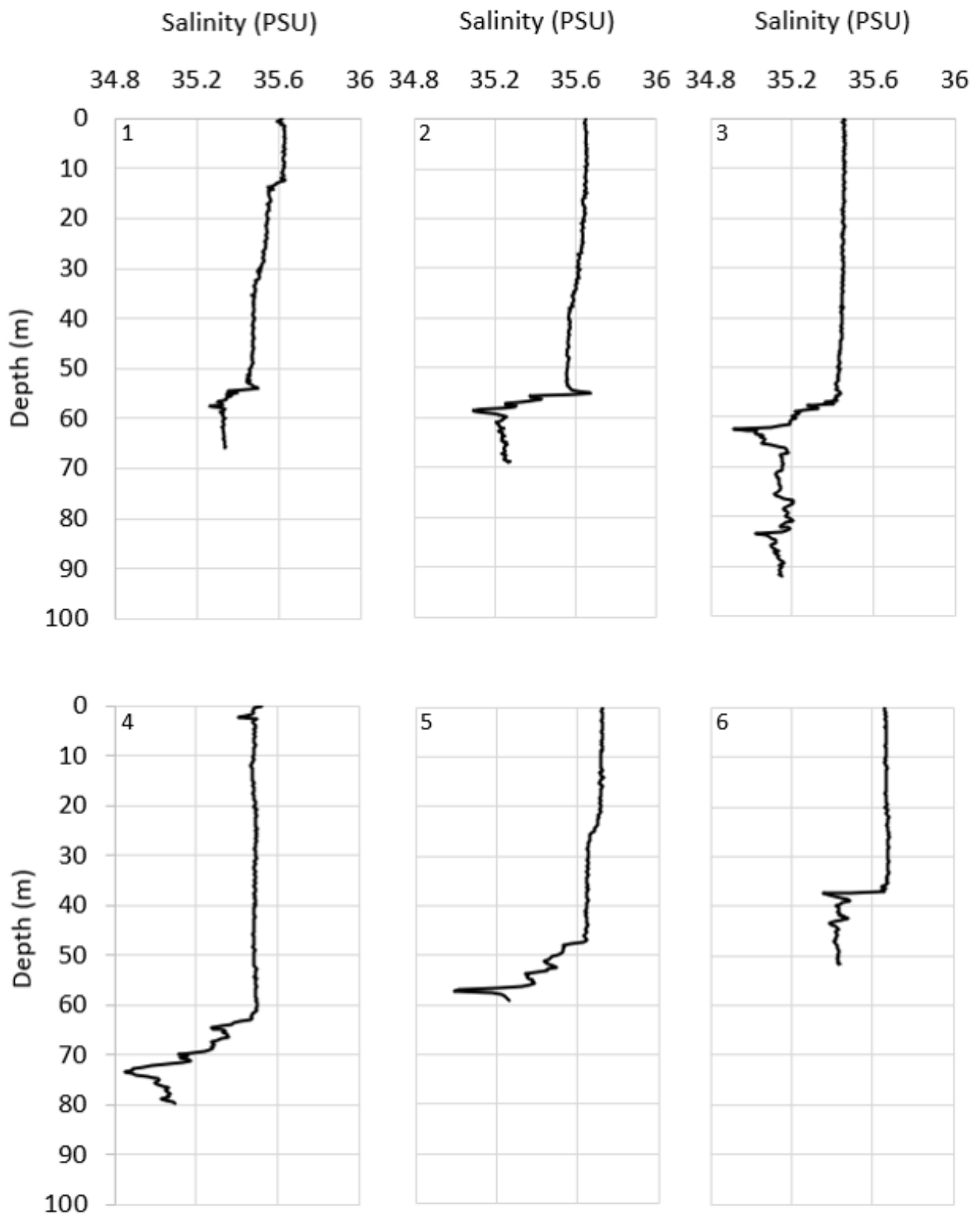


Figure 3.38: Salinity profiles for each station off the Bremer Bay coastline from 5<sup>th</sup> to the 7<sup>th</sup> of February 2009 (refer to Figure 2.10 for station locations). Maximum depth for each station is: 1) 72 m, 2) 900 m, 3) 600 m, 4) 72 m, 5) 60 m and 6) 50 m.

## CHAPTER 4 DEEP CANYON EXPERIMENTS

### 4.1 Experiment DC1

#### 4.1.1 Sea Level Elevation and Velocity Fields

The intention of experiment DC1 was to test if upwelling occurs as the Flinders Current flows past the Hood Canyon. To simulate this, the Coriolis force was set to  $-1 \times 10^{-4} \text{ s}^{-1}$ , which was analogous to the amount of Coriolis force that was experienced at  $\sim 40^\circ\text{S}$ . The sea surface level for the northern boundary was decreased by 5 cm over the six-day run time, with the model adjusting to the resulting pressure change for six days in three-hour increments. Once six days had elapsed, the resulting sea level was considered to be at its final state and particles were released on the western boundary after five days.

The mean sea level elevation throughout the domain was  $-1.95 \text{ cm} \pm 1.45 \text{ cm}$  (Table 4.1). There were two eddies on the western side of the domain at  $\sim 1000 \text{ m}$  to  $\sim 1400 \text{ m}$  of depth which caused the maximum sea level elevation to decrease by 6.6 cm within the output (Figure 4.1). This change in sea level elevation created an average Eulerian zonal velocity field of  $8.87 \text{ cms}^{-1} \pm 11.16 \text{ cms}^{-1}$  westwards (Figure 4.2), and a meridional velocity field of  $0.92 \text{ cms}^{-1} \pm 7.74 \text{ cms}^{-1}$  southwards (Figure 4.3). This average zonal velocity field was lower than the Flinders Current velocity by  $1.13 \text{ cms}^{-1}$  and cannot be compared meridionally (Arthur, 2006).

A flow structure present in experiment DC1 velocity field was a jet formation west of the Hood Canyon. This had an average zonal velocity of  $43.1 \text{ cms}^{-1} \pm 8.14 \text{ cm}$  westwards (Figure 4.2, Table 4.1), and an average meridional velocity of  $21.33 \text{ cms}^{-1} \pm 5.08 \text{ cms}^{-1}$  southwards (Figure 4.3). Above this lies an eddy which had an average velocity of  $19.4 \text{ cms}^{-1} \pm 9.13 \text{ cm}$  eastwards, and  $19.29 \text{ cms}^{-1} \pm 7.48 \text{ cms}^{-1}$  northwards. This jet was formed in the Hood Canyon outlet which had an average velocity of  $25.36 \text{ cms}^{-1} \pm 8 \text{ cms}^{-1}$  westwards, and  $5.06 \text{ cms}^{-1} \pm 3.26 \text{ cms}^{-1}$  northwards. The hotspot slows the jet down to  $15.7 \text{ cms}^{-1} \pm 21.3 \text{ cms}^{-1}$  westwards, and a southwards velocity of  $13.9 \text{ cms}^{-1} \pm 10.9 \text{ cms}^{-1}$ . When compared to the mean Eulerian velocity for DC1, the average flow velocity was  $34.23 \text{ cms}^{-1}$  faster in the jet and  $16.49 \text{ cms}^{-1}$  faster in the Hood Canyon outlet.

The Bremer Canyon was able to isolate itself from the rest of the model domain with its zonal Eulerian velocity, with flow in the lower slope having an average velocity of  $2.05 \text{ cms}^{-1} \pm 3.07 \text{ cms}^{-1}$  eastwards and the flow in the mid-slope having an average velocity of  $4.06 \text{ cms}^{-1} \pm 1.25 \text{ cms}^{-1}$  eastwards (Table 4.1). Flow in the lower slope of the Hood Canyon was also able to isolate itself, with an average velocity of  $5.03 \text{ cms}^{-1} \pm 2.27 \text{ cms}^{-1}$  eastwards. All sections of the Hood and Bremer Canyon supported a northwards flow, ranging from  $4.25 \text{ cms}^{-1} \pm 3.33 \text{ cms}^{-1}$  to  $12.72 \text{ cms}^{-1} \pm 3.18 \text{ cms}^{-1}$  in the bottom slope and the lower slope of the Bremer Canyon respectively.

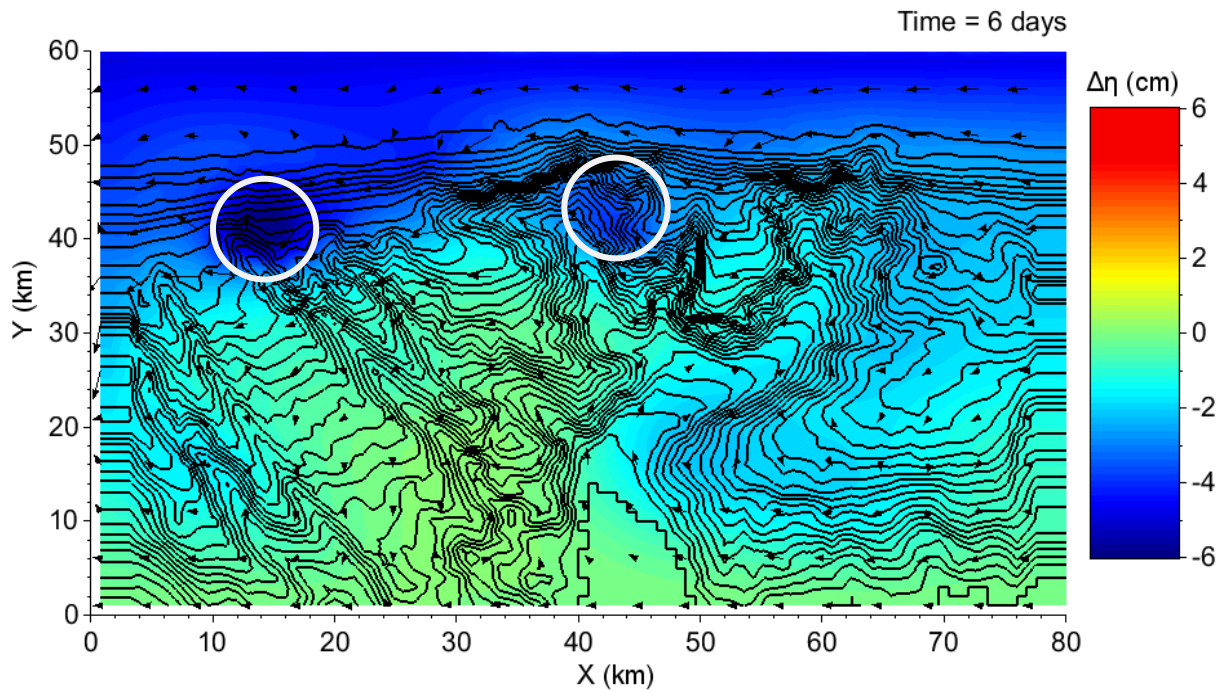


Figure 4.1: The resulting sea level decrease after 6 days for experiment DC1, with positive values indicating a decrease in sea level. Two eddy formations are circled in white, with one of them being present in the Hood Canyon. The black lines are 100 m contours lines, and the arrows are the flow direction. The northern boundary had an average sea level decrease of  $-4.59 \text{ cm} \pm 0.22 \text{ cm}$ , whereas the southern boundary had an average sea level decrease of  $-0.19 \text{ cm} \pm 0.04 \text{ cm}$ .

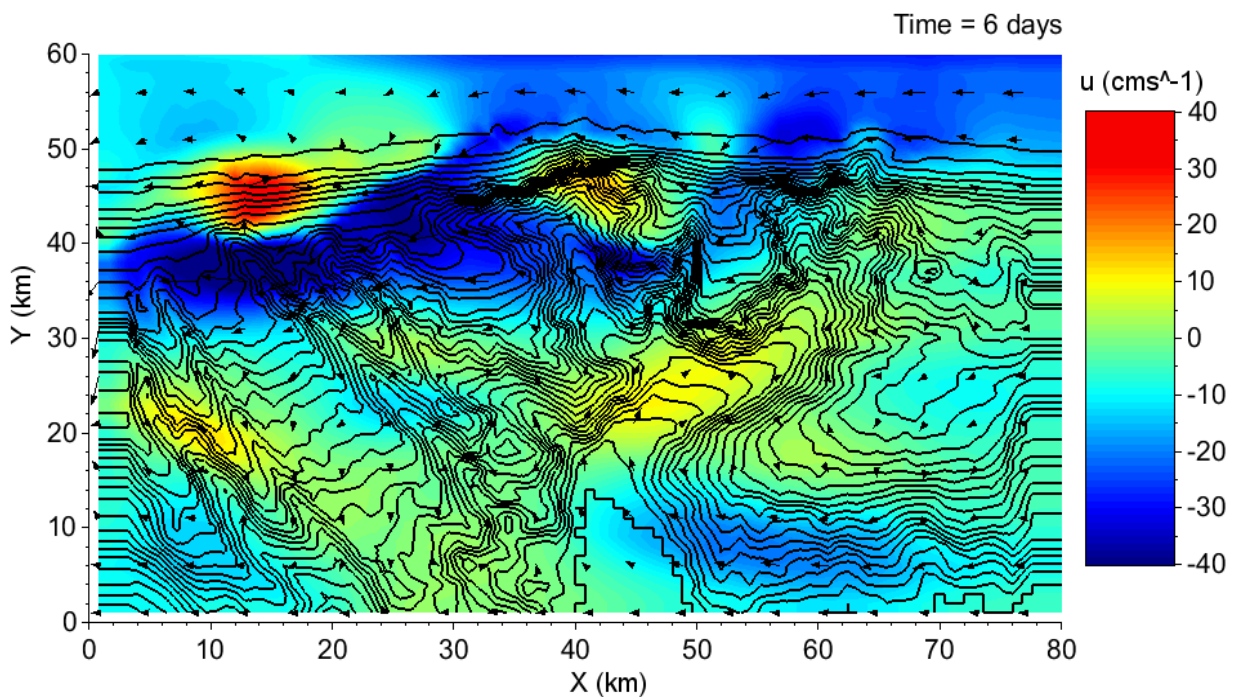


Figure 4.2: The resulting zonal velocity field after the sea level change, with positive values indicating an eastwards flow. The black lines are 100 m contours and the arrows are the flow direction. The median velocity was  $7.08 \text{ cm s}^{-1}$  westwards.

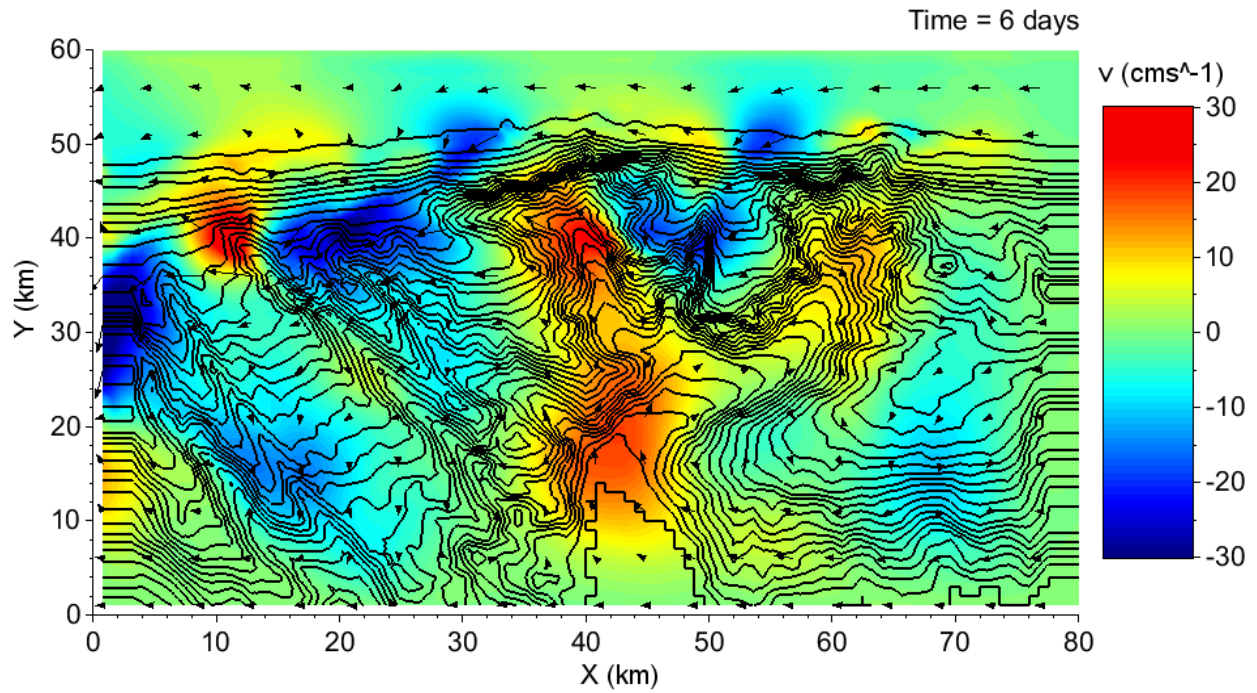


Figure 4.3: The resulting meridional velocity field for experiment DC1 after 6 days of run time, and positive values are a northwards flow. The black lines are 100 m contours lines and the arrows are the flow direction. The median velocity was  $0.24 \text{ cms}^{-1}$  southwards.

Table 4.1: The average sea-level elevation (Figure 4.1), as well as the average zonal (Figure 4.2) and meridional Eulerian velocity (Figure 4.3) for areas of interest in experiment DC1. Positive values represent an increase in sea level elevation, eastwards flow in average zonal Eulerian velocity, and northwards in average meridional Eulerian velocity. H.C. stands for Hood Canyon. B.C. stands for Bremer Canyon.

Location	Average sea level elevation (cm)	Average zonal Eulerian velocity ( $\text{cms}^{-1}$ )	Average meridional Eulerian velocity ( $\text{cms}^{-1}$ )
Mean	$-1.95 \pm 1.45$	$-8.87 \pm 11.16$	$-0.92 \pm 7.74$
Hotspot	$-3.83 \pm 0.81$	$-15.7 \pm 21.3$	$-13.9 \pm 10.9$
H.C. outlet	$-2.24 \pm 0.43$	$-25.36 \pm 8$	$5.06 \pm 3.26$
H.C. northern wall	$-2.85 \pm 0.14$	$1.72 \pm 15.68$	$1.66 \pm 4.84$
H.C. eastern wall	$-3.07 \pm 0.58$	$-10.6 \pm 16.6$	$0.01 \pm 13.7$
H.C. mid-slope	$-0.92 \pm 0.28$	$-10.12 \pm 5.88$	$10.45 \pm 1.97$
H.C. lower slope	$-1.16 \pm 0.15$	$5.03 \pm 2.27$	$8.16 \pm 2.43$
B.C. head	$-1.91 \pm 0.21$	$-4.11 \pm 3.57$	$7.61 \pm 3.02$
B.C. mid-slope	$-1.66 \pm 0.21$	$4.06 \pm 1.25$	$6.63 \pm 1.05$
B.C. lower slope	$-1.62 \pm 0.14$	$2.05 \pm 3.07$	$12.72 \pm 3.18$
B.C. bottom slope	$-0.28 \pm 0.28$	$-7.74 \pm 4.54$	$4.25 \pm 3.33$
Plateau	$-1.31 \pm 0.63$	$-10.42 \pm 7.2$	$-0.67 \pm 3.89$
Headland	$-1.95 \pm 0.45$	$-15.2 \pm 4.86$	$-6.34 \pm 6.12$
Eastern hotspot	$-2.11 \pm 0.09$	$-2.59 \pm 2.16$	$-0.80 \pm 2.61$

#### 4.1.2 Lagrangian Particle Tracker Results

The Bremer Canyon was shown to push particles northwards, with ~ 89.1% of released particles finding their way into the hotspot, and 90.48% of released particles coming from the Hood Canyon outlet, or just south of it. This indicates that both canyons have the necessary structure to upwell the Flinders Current (Figure 4.4, 4.5, Table 4.2). The difference in particles percentage between the hotspot and the outlet was that some particles were flowing south of the hotspot after exiting the outlet. Outside of the Hood Canyon the other major aggregate point for particles was the head of the Bremer Canyon, which ended up with 75.03% of particles entering the area. This result was unexpected with 55.75% of particles entering the lower slope of the Bremer Canyon, showing there was transition between the two locations prior to moving on into the Hood Canyon, instead of just having particles that were entering the lower slopes bypass the head of the Bremer Canyon.

That connection did reveal that there were three distinct pathways that particles followed through the model domain prior to entering the Hood Canyon outlet (Figure 4.6):

- 1) Particles would enter in or around the head of the Bremer Canyon, prior to exiting the canyon, then enter the Hood Canyon and pass through the Hood Canyon outlet.
- 2) Particles would enter the lower slope of the Bremer Canyon, travel northwards to the head of the Bremer Canyon before following path one.
- 3) Particles would enter the lower slope of the Bremer Canyon; however, unlike path 2 they entered the Hood Canyon where it formed and travelled up the Hood Canyons mid-slope until entering the outlet.

The percentage breakdown of particles taking path 1 was 44.2%, path 2 was 29.5%, path 3 was 25% and 1.7% of particles unaccounted for until the outlet. The path that a particle took was due to the depth they were released in, with particles from 600 m to 1200 m opting for path 1, 1800 m to 2400 m opting for path 2, and 2400 m to 3000 m opting for path 3. Particles released in between 1200 m to 1800 m ended up travelling through a mixture of path 1 and path 2 at a ratio of 3:1, showing that the depth particles started pushing into the lower slope was ~1650 m. Even though 100% of particles entered the Hood Canyon outlet, path 3 was the only one which did not have 100% of particles entering the hotspot. Path 3 had 10.1% of particles missing the hotspot which ended up being due to particles bypassing the hotspot to the south.

The average velocity for particles travelling through the model domain was 8.06  $\text{cms}^{-1}$  westwards, with velocities ranging from 3.51  $\text{cms}^{-1}$  westwards to 13.13  $\text{cms}^{-1}$  westwards (Table 4.3). The average particle velocity was only 0.81  $\text{cms}^{-1}$  slower than the corresponding average Eulerian velocity in experiment DC1 and only 1.94  $\text{cms}^{-1}$  slower than the Flinders Current. Velocity varied throughout the model with the fastest velocity measured in particles released between 600 m to 1200 m with an average velocity of 9.11  $\text{cms}^{-1}$  westwards. The slowest velocity was from particles

released between 1800 m to 2400 m at  $7.35 \text{ cms}^{-1}$  westwards. It was expected that the pathway with the longest distance would end up being the slowest.

Particles which enter the lower slope of the Bremer Canyon end up generating an average northwards velocity of  $9.45 \text{ cms}^{-1} \pm 0.46 \text{ cms}^{-1}$  from the velocity field present. This lowers to  $6.01 \text{ cms}^{-1} \pm 1.46 \text{ cms}^{-1}$  northwards when directly entering the Hood Canyon. When exiting the head of the Bremer Canyon particles can generate an average velocity of  $5.41 \text{ cms}^{-1} \pm 0.7 \text{ cms}^{-1}$  westwards. The average velocity to exit the Hood Canyon outlet was  $16.02 \text{ cms}^{-1}$  westwards  $\pm 2.32 \text{ cms}^{-1}$  westward. Most of these particles enter the hotspot and have an average velocity of  $21.83 \text{ cms}^{-1} \pm 3.29 \text{ cms}^{-1}$  westwards whilst travelling through the area.

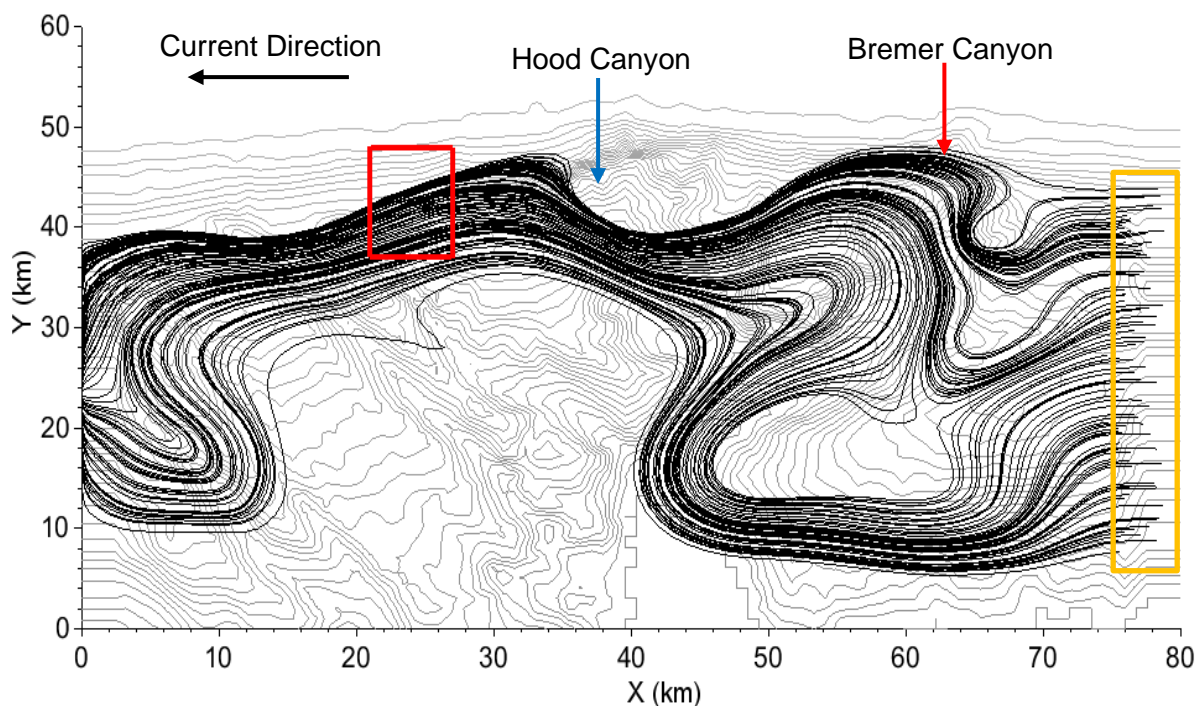


Figure 4.4: The resulting trajectory of every 40<sup>th</sup> particle released within 600 m to 3500 m (starting point showed with an orange square), with the red square noting the hotspot location. The grey lines are 100 m contour lines. 75% of particles end up traversing the northern section of the Bremer Canyon before entering the Hood Canyon.

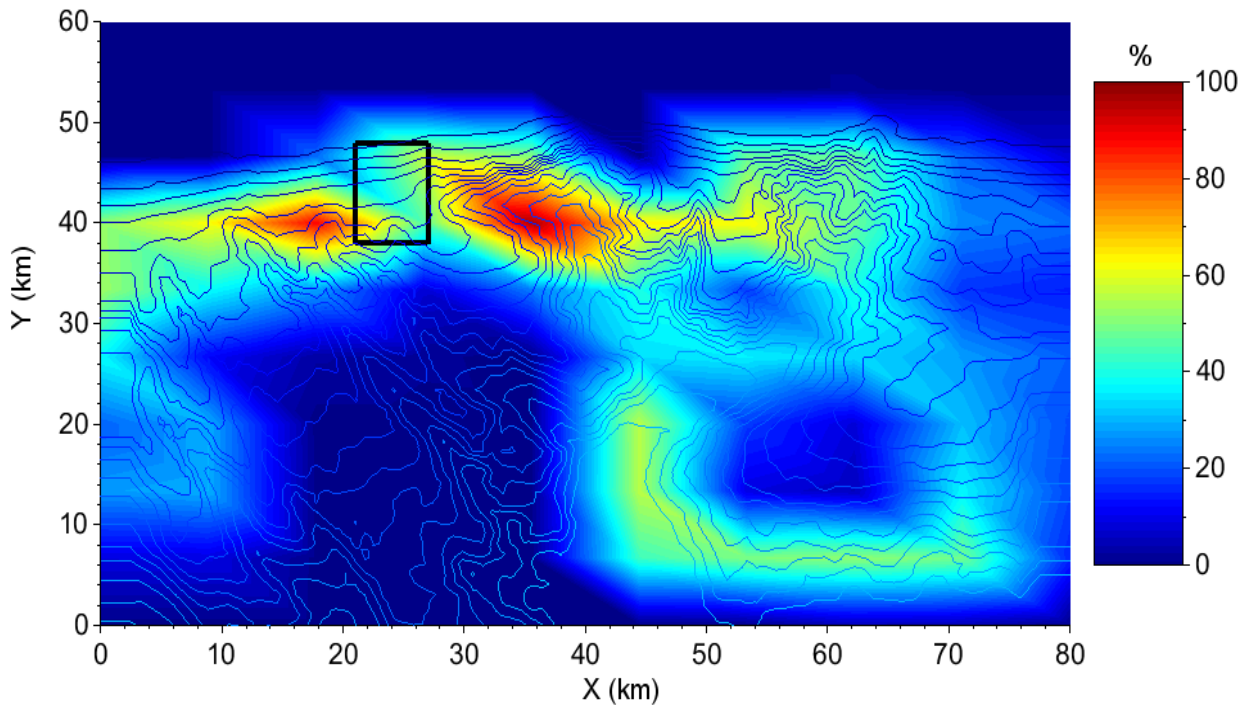


Figure 4.5: Heat map of particle locations for experiment DC1 calculated by counting each unique particle that enters a location, overlain on 175 m contours in blue. The black square is the location of the hotspot. The percentage of particle concentration in the hotspot was artificially lowered by intersecting multiple grid section. For the orca hotspot, it ends up being 81.7% of particles which enter the area.

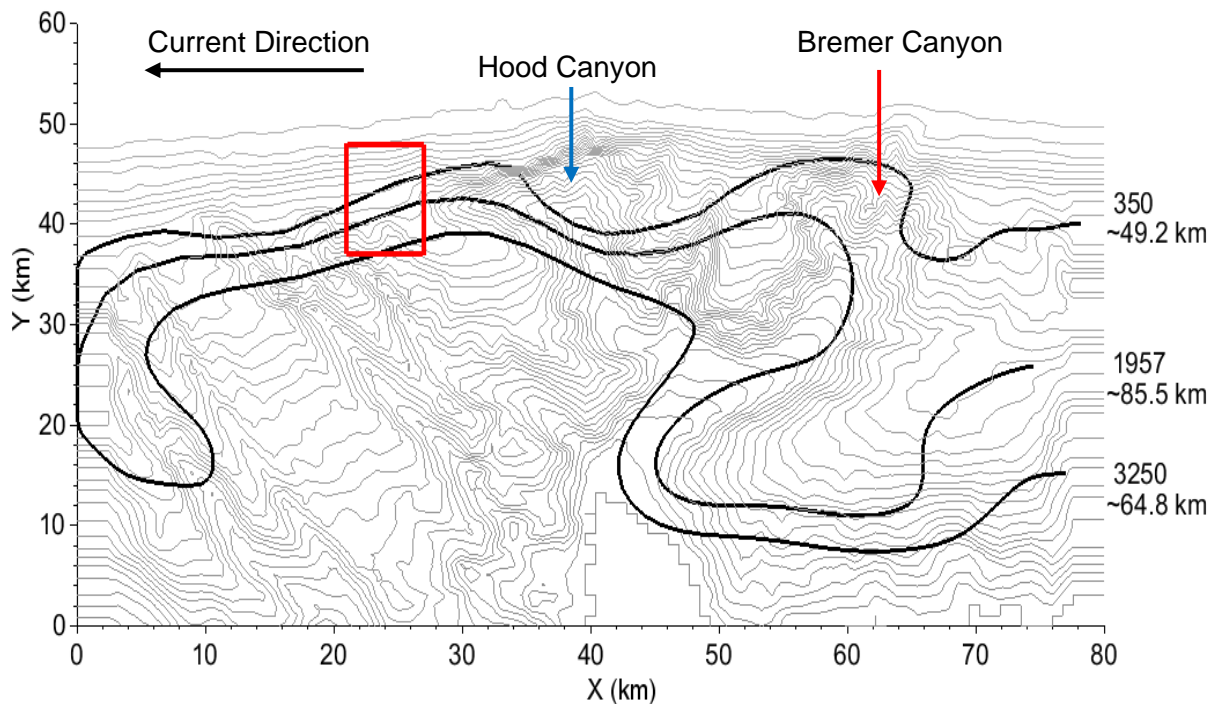


Figure 4.6: The three noted pathways that particles took, with particle 350 showing path 1, particle 1957 for path 2, and particles 3250 for path 3. Grey lines are 100 m contours. The location of the hotspot is the red square. The approximate distance of all three paths to the hotspot are shown below the particle number.

Table 4.2: Approximate percentage of particles entering areas of interest within the DC1 model domain, as well as a breakdown on where particles originated from (Figure 4.5, and Figure 4.6). H.C. stands for Hood Canyon. B.C. for Bremer Canyon. PG1 consisted of particles with a starting depth of 600 m to 1200 m, PG2 was particles which had a starting depth of 1200 m to 1800 m, PG3 was particles which had a starting depth of 1800 m to 2400 m and PG4 was particles which had a starting depth that was > 2400 m.

Location	Total %	PG1 (%)	PG2 (%)	PG3 (%)	PG4 (%)
Hotspot	89.1	100	100	100	56.3
H.C. outlet	90.48	100	100	100	61.9
H.C. mid-slope	25.37	0	0	5.7	95.8
B.C. head	75.03	100	100	94.7	5.4
B.C. mid-slope	29.54	0	23	91.8	0.8
B.C. lower slope	55.75	0	23	100	100
Eastern hotspot	39.3	100	57.2	0	0

Table 4.3: Average time, and velocity for particles released on the eastern boundary and a breakdown for each particle group. Positive values are an eastwards flow. PG1 consisted of particles with a starting depth of 600 m to 1200 m, PG2 was particles which had a starting depth of 1200 m to 1800 m, PG3 was particles which had a starting depth of 1800 m to 2400 m and PG4 was particles which had a starting depth that was > 2400 m.

Particle group	Average time (days)	Minimum velocity (cms <sup>-1</sup> )	Average velocity (cms <sup>-1</sup> )	Maximum velocity (cms <sup>-1</sup> )
All	11.2	-3.51	-8.06	-13.13
PG1	9.91	-4.13	-9.11	-13.13
PG2	10.87	-3.51	-8.3	-12.67
PG3	12.28	-5.02	-7.35	-8.6
PG4	11.72	-5.27	-7.7	-8.81

## 4.2 Experiment DC2

### 4.2.1 Sea Level Elevation and Velocity Fields

The intention of experiment DC2 was to test how the Hood and Bremer Canyons influence an eastwards flow in the southern hemisphere. To achieve this, the sea level elevation was increased by 5 cm on the northern boundary, and due to this, particles were released on the western boundary. The rest of the model was set up with the same specifications as DC1.

The average sea level elevation in experiment DC2 was  $2.02 \text{ cm} \pm 1.55 \text{ cm}$  (Figure 4.7). This change created an average zonal Eulerian velocity field of  $8.31 \text{ cms}^{-1} \pm 4.33 \text{ cms}^{-1}$  eastwards (Figure 4.8) and an average meridional Eulerian velocity field of  $0.34 \text{ cms}^{-1} \pm 3.40 \text{ cms}^{-1}$  northwards (Figure 4.9). The average horizontal Eulerian velocities for flow in the Hood Canyon ranged from  $8.11 \text{ cms}^{-1} \pm 1.45 \text{ cms}^{-1}$  eastwards in the lower slopes to  $15.44 \text{ cms}^{-1} \pm 1.97 \text{ cms}^{-1}$  eastwards in the Hood Canyon northern wall (Figure 4.7, Table 4.4). The average meridional Eulerian velocity had a southwards flow in the lower-slope of  $0.99 \text{ cms}^{-1} \pm 2.12 \text{ cms}^{-1}$ , while the outlet had a northwards flow of  $5.07 \text{ cms}^{-1} \pm 1.63 \text{ cms}^{-1}$ . Flow in the Bremer Canyon followed a similar pattern with its average zonal Eulerian velocities ranging from  $0.07 \text{ cms}^{-1} \pm 0.44 \text{ cms}^{-1}$

eastwards in the bottom slope to  $10.93 \text{ cm s}^{-1} \pm 2.56 \text{ cm s}^{-1}$  eastwards in the head. The Bremer Canyon however, supported a downwelling flow, with a southwards flow varying from  $0.29 \text{ cm s}^{-1} \pm 2.16 \text{ cm s}^{-1}$  in the lower slopes to  $2.8 \text{ cm s}^{-1} \pm 3.7 \text{ cm s}^{-1}$  in the mid-slope. These results indicate there was no unique behaviour occurring in zonal velocities of either canyon when compared to the rest of the model domain. Outside of mid-slope, outlet, and northern wall of the Hood Canyon, the rest of the canyon structures supported a downwelling flow.

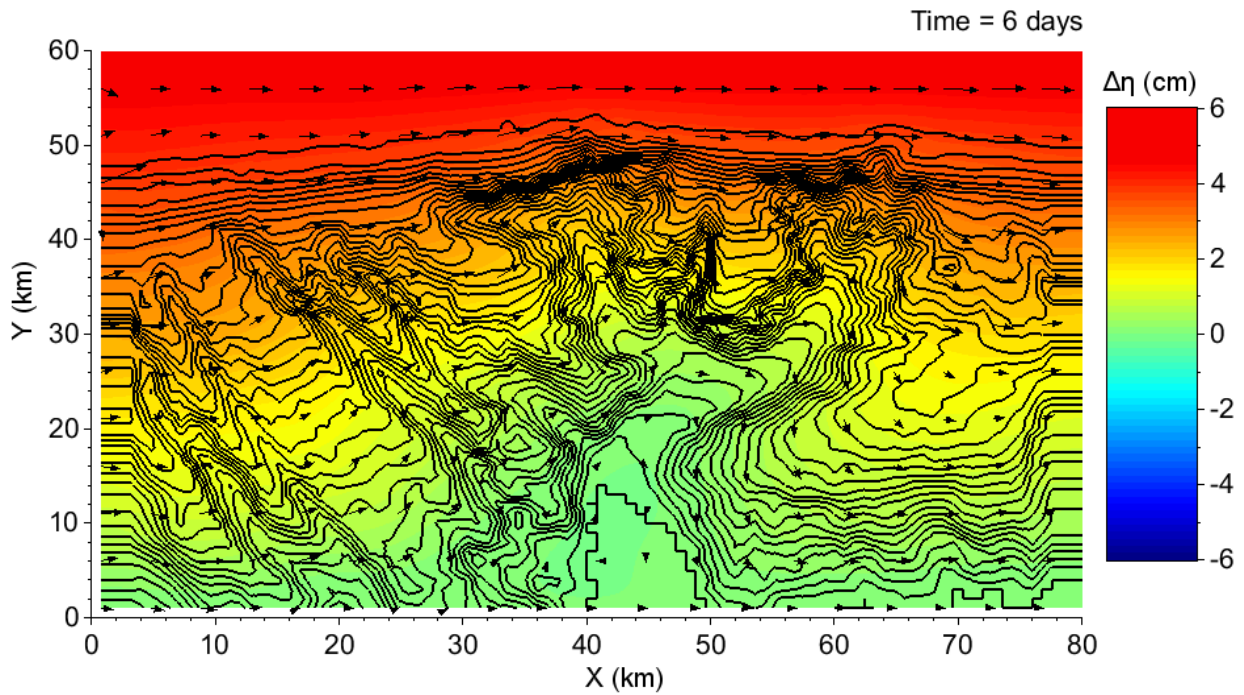


Figure 4.7: The change in sea level after 6 days of run time for experiment DC2. Positive values indicate an increase in sea level in a cell. The black lines are 100 m contours lines, and the arrows are the flow direction. The northern boundary had an average increase of  $4.97 \text{ cm} \pm 0.03 \text{ cm}$ , while the southern boundary had an average sea level increase of  $0.11 \text{ cm} \pm 0.03 \text{ cm}$ .

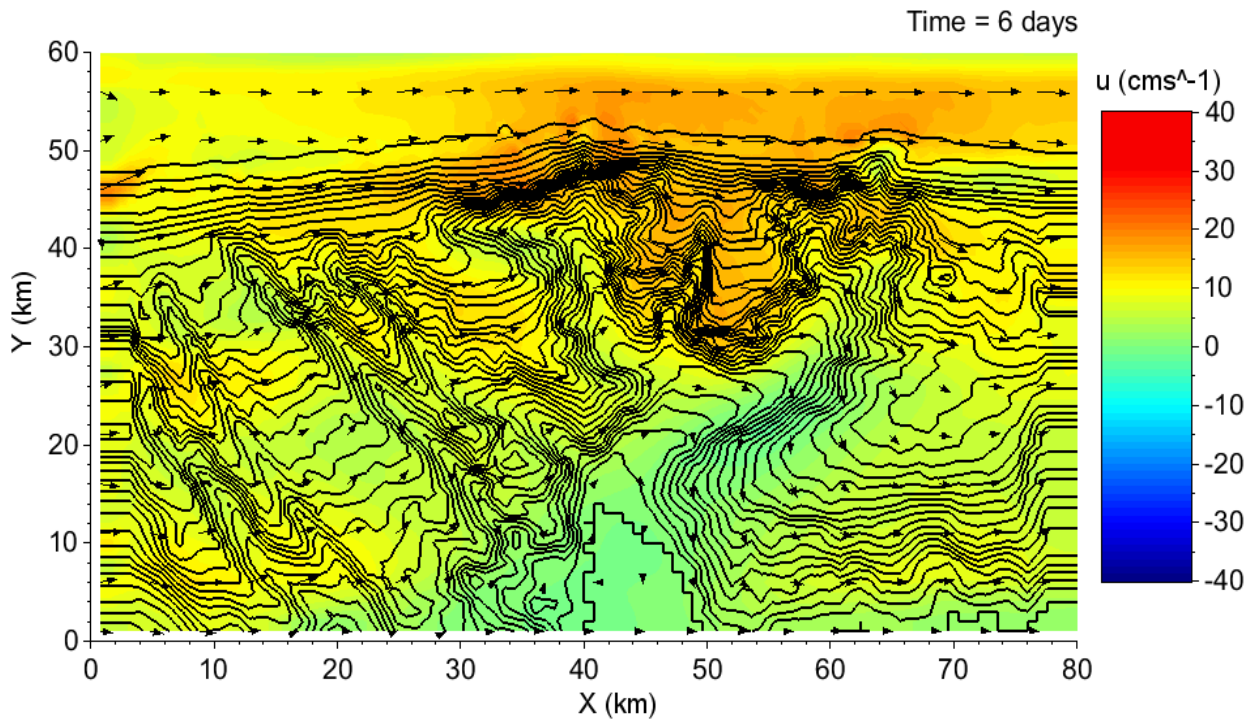


Figure 4.8: The resulting zonal Eulerian velocity field for experiment DC2 after 6 days of run time, with positive values indicate an eastwards flow. The black lines are 100 m contours lines, and the arrows are the flow direction. The median velocity was  $8.08 \text{ cm s}^{-1}$  eastwards.

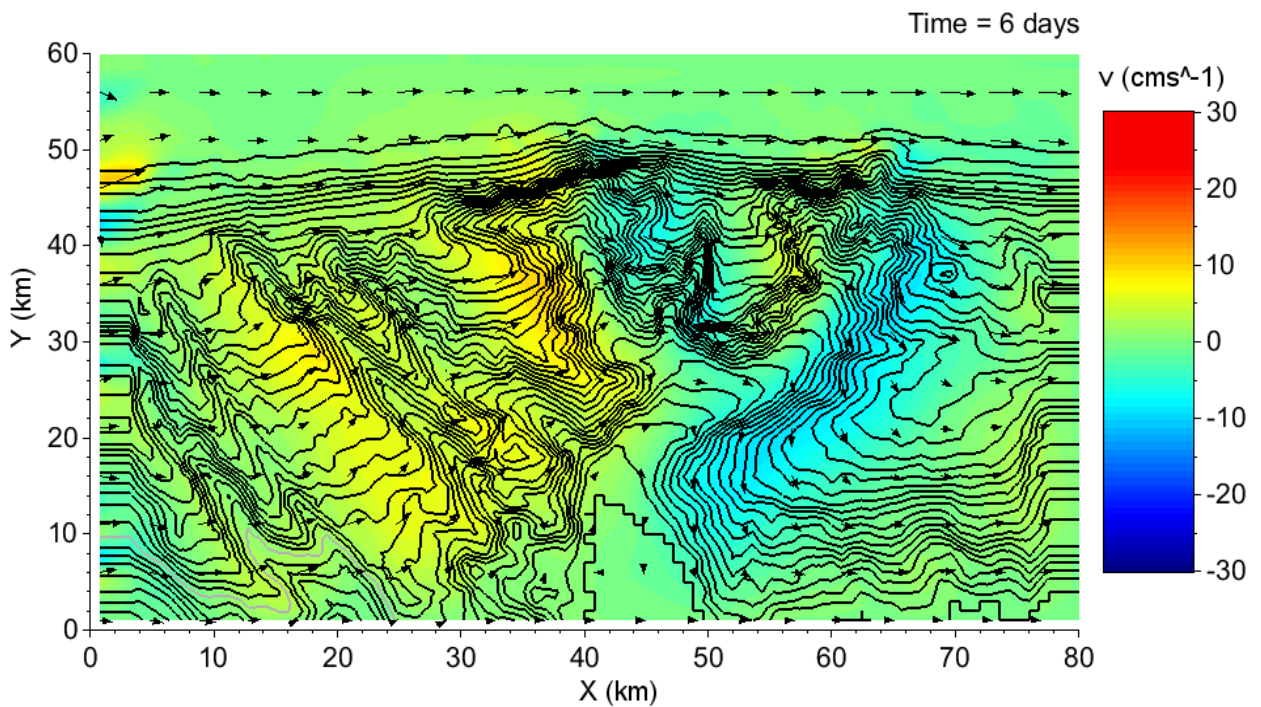


Figure 4.9: The resulting meridional Eulerian velocity field for experiment DC2 after 6 days of run time. Positive values represent a northwards flow. The black lines are 100 m contours, and the arrows are the flow direction. The median velocity was  $0.19 \text{ cm s}^{-1}$  northwards.

Table 4.4: The average sea-level elevation (Figure 4.7), as well as the average zonal (Figure 4.8), and meridional Eulerian velocity (Figure 4.9) for areas of interest in the DC2 model domain. Positive values represent an increase in sea level elevation, eastwards flow in average zonal Eulerian velocity, and northwards in average meridional Eulerian velocity. H.C. stands for Hood Canyon. B.C. for Bremer Canyon.

Location	Average sea level elevation (cm)	Average zonal Eulerian velocity (cms <sup>-1</sup> )	Average meridional Eulerian velocity (cms <sup>-1</sup> )
Mean	2.02 ± 1.55	8.31 ± 4.33	0.34 ± 3.40
Hotspot	3.17 ± 0.41	10.98 ± 1.46	2.13 ± 0.70
H.C. outlet	2.51 ± 0.28	9.71 ± 3.88	5.07 ± 1.63
H.C. northern wall	3.17 ± 0.25	15.44 ± 1.97	0.29 ± 3.69
H.C eastern wall	2.12 ± 0.34	12.43 ± 2.56	-3.8 ± 2.12
H.C. mid-slope	1.06 ± 0.22	8.83 ± 2.11	2.77 ± 3.37
H.C. lower slope	0.55 ± 0.07	8.11 ± 1.45	-0.99 ± 2.12
B.C. head	2.32 ± 0.38	10.93 ± 2.56	-2.03 ± 2.98
B.C. mid-slope	1.11 ± 0.17	6.49 ± 2.9	-2.8 ± 3.7
B.C. lower slope	0.15 ± 0.07	2.5 ± 1.47	-0.29 ± 2.16
B.C. bottom slope	0.01 ± 0.02	0.07 ± 0.44	-0.82 ± 1.08
Plateau	0.44 ± 0.28	4.26 ± 2.15	-2.94 ± 2.66
Headland	2.46 ± 0.47	14.63 ± 1.24	0.01 ± 2.29
Eastern hotspot	2.45 ± 0.26	10.3 ± 1.40	-5.37 ± 2.64

#### 4.2.2 Lagrangian Particle Tracker Results

The largest concentration of particles was found in the head of the Bremer Canyon at 46%, which contained >80% of the particles released between 600 m to 1800 m. Despite an average southward velocity in the head of the Bremer Canyon, 32.3% of particles made it out into the eastern hotspot (Figure 4.10, 4.11, Table 4.5). 37.13% of particles entered the Bremer Canyon mid-slope, however, only 13% of that 37.13% originated from depths of < 1800 m. The lower slope of the Bremer Canyon had 10.1% of particles enter the area, with all originating from depths > 2400 m. The Hood Canyon outlet had a particle concentration of 35.9% with all originating from < 1800 m depth, whereas the mid-slope of the Hood Canyon had a particle concentration of 31.58% with > 80% of particles released in between 1800 m to 2400 m. These results indicate that there was limited at best particle retention in both canyons, and from this, it is unlikely that either upwelling or downwelling is occurring.

Particles travelling through the DC2 model domain had an average velocity of 8 cms<sup>-1</sup> eastwards, with a range of velocities from 5.12 cms<sup>-1</sup> to 12.67 cms<sup>-1</sup> eastwards (Table 4.6). Depth plays a key role in this decrease in velocity with particles released from 600 m to 1200 m being the fastest on average of 11.42 cms<sup>-1</sup> eastwards, and particles released in between 2400 m to 3000 m being

the slowest at an average of  $6.26 \text{ cms}^{-1}$  eastwards. This combined with the limited impact of the Bremer and Hood Canyon in retaining particles implies that flow direction was a response to a change in depth within the model domain (Figure 4.12).

Particles travelling through the hotspot had an average eastwards velocity of  $10.56 \text{ cms}^{-1} \pm 0.77 \text{ cms}^{-1}$ , which lowered to an eastward velocity of  $9.32 \text{ cms}^{-1} \pm 1.87 \text{ cms}^{-1}$  eastwards when it entered the Hood Canyon outlet. Particles that ended up in the northern section of the Bremer Canyon had an average velocity of  $10.73 \text{ cms}^{-1} \pm 0.47 \text{ cms}^{-1}$  travelling through the area. Finally, particles that entered the southern section of the Hood Canyon had an average velocity of  $2.29 \text{ cms}^{-1} \pm 1.35 \text{ cms}^{-1}$  northwards. The area used for the eastern jet had an average velocity of  $8.77 \text{ cms}^{-1}$  eastwards.

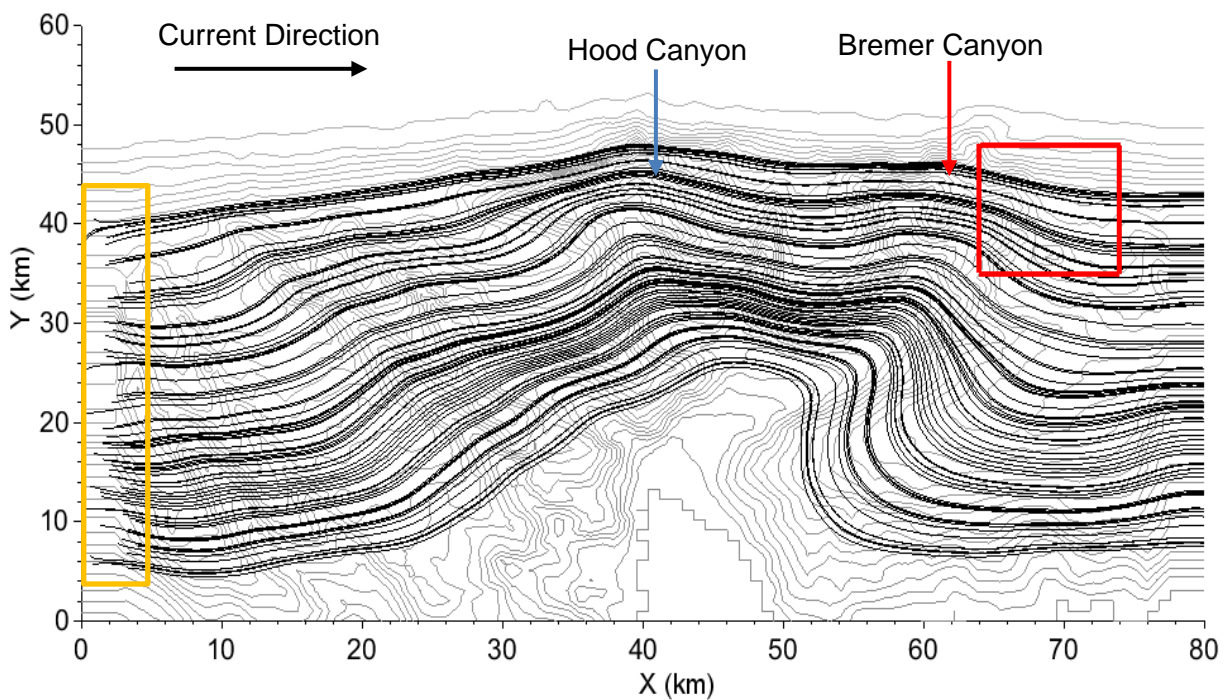


Figure 4.10: The trajectory of every 40<sup>th</sup> particle released near the western boundary (release point indicated by the orange square) after 60 days of run time. Black lines are particle paths and grey lines are 100 m contour lines. The maximum eastwards flow obtained by particles was  $12.67 \text{ cms}^{-1}$  eastwards.

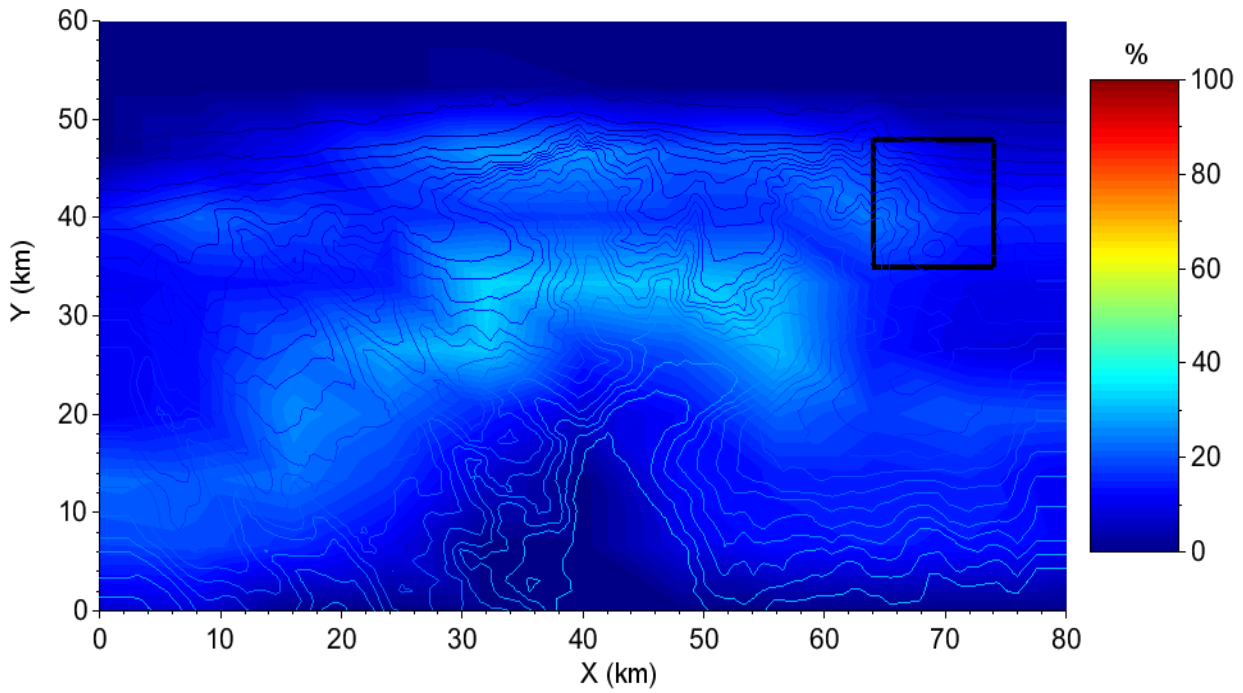


Figure 4.11: The heat-map of particles released on the western boundary in experiment DC2, with the black box being the “eastern hotspot” overlain on 175 m contour lines (blue). The maximum percentage of particles in any 10 km by 6 km section was 36.4%, which indicates only a small number of particles are converging on any location throughout the model.

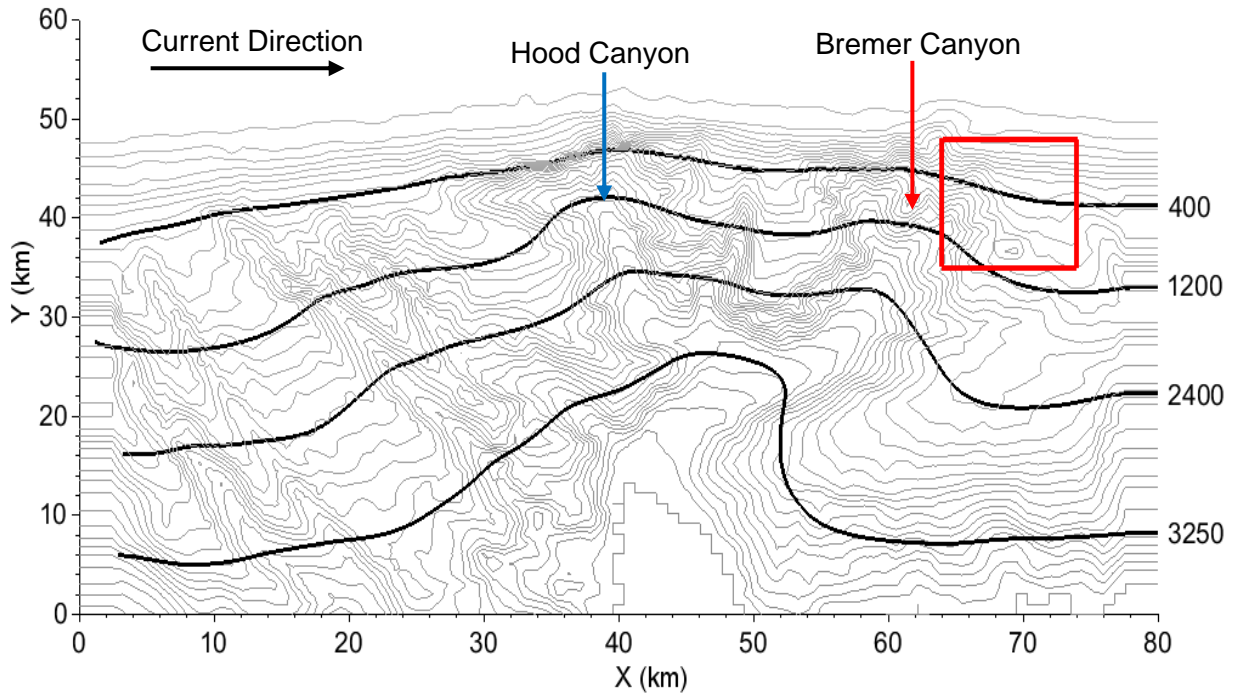


Figure 4.12: A representation of the pathways taken by a particle in between 600 m to 1200 m (particle 400), 1200 m to 1800 m (particle 1200), 1800 m to 2400 m (particle 2400) and 2400 m to 3000 m (particle 3250). Grey lines are 100 m contours. The red square is the location of the eastern hotspot.

Table 4.5: Approximate percentage of particles entering areas of interest within the DC2 model domain, as well as a breakdown on where particles originated from (Figure 4.11, and Figure 4.12). H.C. stands for Hood Canyon. B.C. stands for Bremer Canyon. PG1 consisted of particles with a starting depth of 600 m to 1200 m, PG2 was particles which had a starting depth of 1200 m to 1800 m, PG3 was particles which had a starting depth of 1800 m to 2400 m and PG4 was particles which had a starting depth that was > 2400 m.

Location	Total (%)	PG1 (%)	PG2 (%)	PG3 (%)	PG4 (%)
Hotspot	24	81.7	14.3	0	0
H.C. outlet	35.9	81.7	61.9	0	0
H.C. mid-slope	31.58	0	16.4	80.1	29.8
B.C. head	46	81.7	80.7	20.6	0
B.C. mid-slope	37.13	0	19.3	80.1	49.1
B.C. lower slope	10.1	0	0	0	40.1
Eastern hotspot	32.3	81.7	49.6	0	0

Table 4.6: Average time and velocity for particles released on the western boundary and a breakdown for each particle group. Positive values were an eastwards flow. PG1 consisted of particles with a starting depth of 600 m to 1200 m, PG2 was particles which had a starting depth of 1200 m to 1800 m, PG3 was particles which had a starting depth of 1800 m to 2400 m and PG4 was particles which had a starting depth that was > 2400 m.

Particle group	Average time (days)	Minimum velocity (cms <sup>-1</sup> )	Average velocity (cms <sup>-1</sup> )	Maximum velocity (cms <sup>-1</sup> )
Total	11.29	5.12	8	12.67
PG1	7.91	8.81	11.42	12.67
PG2	9.62	7.37	9.38	10.32
PG3	13.21	6.17	6.84	7.6
PG4	14.41	5.12	6.26	6.69

## 4.3 Experiment DC3

### 4.3.1 Sea Level Elevation and Velocity Fields

The intention of experiment DC3 was to test how the Hood and Bremer Canyon were affected by a westwards flow in the northern hemisphere. The Coriolis force was switched to  $+1.0 \times 10^{-4} \text{ s}^{-1}$ , which represents the amount of Coriolis force experienced at  $\sim 40^\circ \text{N}$ . To get a westwards flow in the northern hemisphere, the sea level elevation at the northern boundary was increased by 5 cm. The model was allowed to adjust to this change for four and a half days, due to instability issues in the model that occurred at five and a half days of run time.

The average sea level elevation for DC3 was  $2.32 \text{ cm} \pm 1.22 \text{ cm}$  (Figure 4.13, Table 4.7). DC3 had an average zonal Eulerian velocity of  $7.57 \text{ cms}^{-1}$  westwards (Figure 4.14). When compared

to the velocity of the Flinders Current, DC3 was slower by  $2.43 \text{ cm s}^{-1}$  (Figure 4.15). Flow in the Hood Canyon varied in average zonal velocity from  $2.98 \text{ cm s}^{-1}$  westwards in the mid-slope to  $12.85 \text{ cm s}^{-1}$  westwards at the northern wall of the head of the canyon (Table 4.7). A westwards flow also occurs in the Bremer Canyon with velocity varying from  $3.56 \text{ cm s}^{-1}$  westwards in the mid-slope to  $7.27 \text{ cm s}^{-1}$  westwards in the Bremer Canyon.

The average Eulerian meridional velocity for the Hood Canyons' northern and eastern wall supported a northwards velocity ranging from  $0.11 \text{ cm s}^{-1}$  to  $3.09 \text{ cm s}^{-1}$ , whereas the outlet, mid-slope and lower slope supported a southwards velocity ranging from  $1.15 \text{ cm s}^{-1}$  to  $3.77 \text{ cm s}^{-1}$  (Figure 4.15, Table 4.7). The Bremer Canyon followed a similar trend with the head and mid-slope having a northwards velocity ranging from  $1.11 \text{ cm s}^{-1}$  to  $2.6 \text{ cm s}^{-1}$ . Once in the lower slope, flow in the Bremer Canyon reversed to a southward velocity of  $3.07 \text{ cm s}^{-1}$ , which lowered to a velocity of  $1.79 \text{ cm s}^{-1}$  in the bottom slope. Despite supporting a westward flow throughout, the meridional velocity would prevent the canyon from supporting either an upwelling or downwelling flow.

Flow in the Hood Canyon supported an outflow of  $4.63 \text{ cm s}^{-1}$  westwards and  $3.77 \text{ cm s}^{-1}$  southwards, which became  $7.99 \text{ cm s}^{-1}$  westwards and  $0.82 \text{ cm s}^{-1}$  southwards when in the hotspot. As the outlet and hotspot velocities were not  $> 10 \text{ cm s}^{-1}$  larger than the mean Eulerian velocity, which indicated that the canyon was not forming a jet.

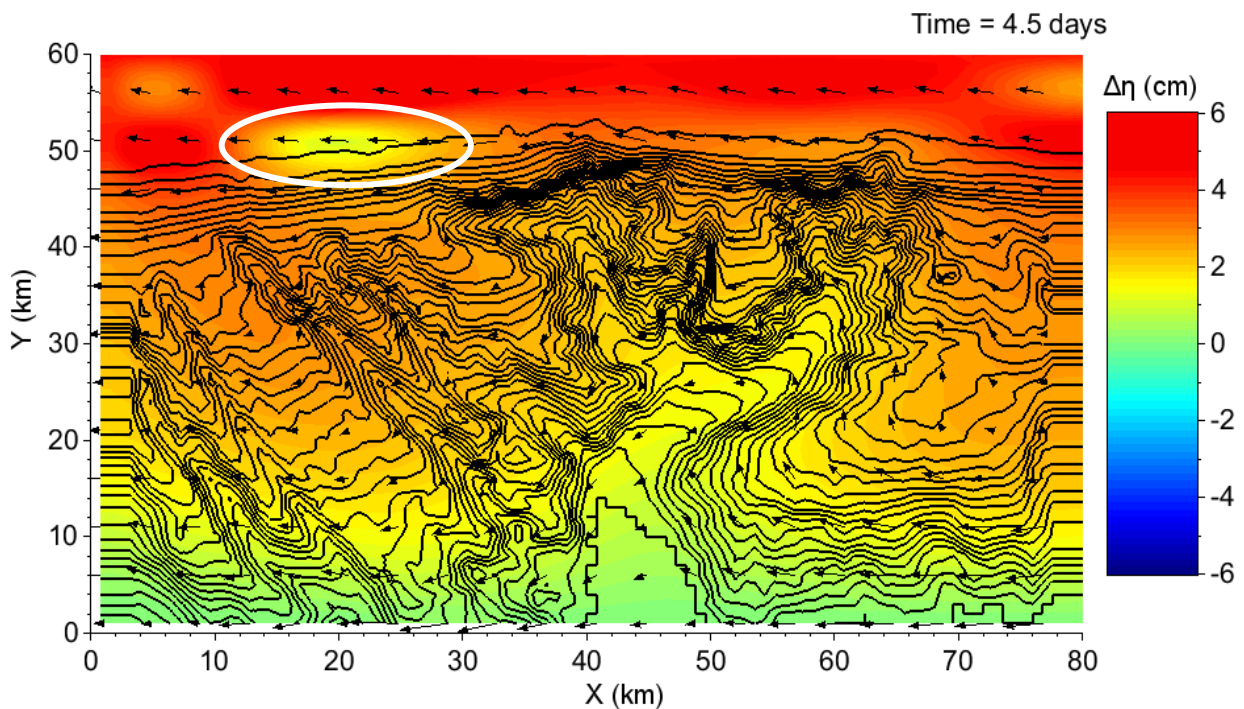


Figure 4.13: The average change in sea level for experiment DC3 after 4.5 days of run time, with positive values representing an increase in sea level. The black lines are 100 m contours lines and the arrows are the flow direction. The northern boundary had an average increase of  $4.64 \text{ cm} \pm 0.82 \text{ cm}$ , while the southern boundary had an average increase of  $0.36 \text{ cm} \pm 0.23 \text{ cm}$ . There was also a potential eddy, which had a sea level that was  $\sim 0.8 \text{ cm}$  lower than its surroundings. This eddy is circled in white.

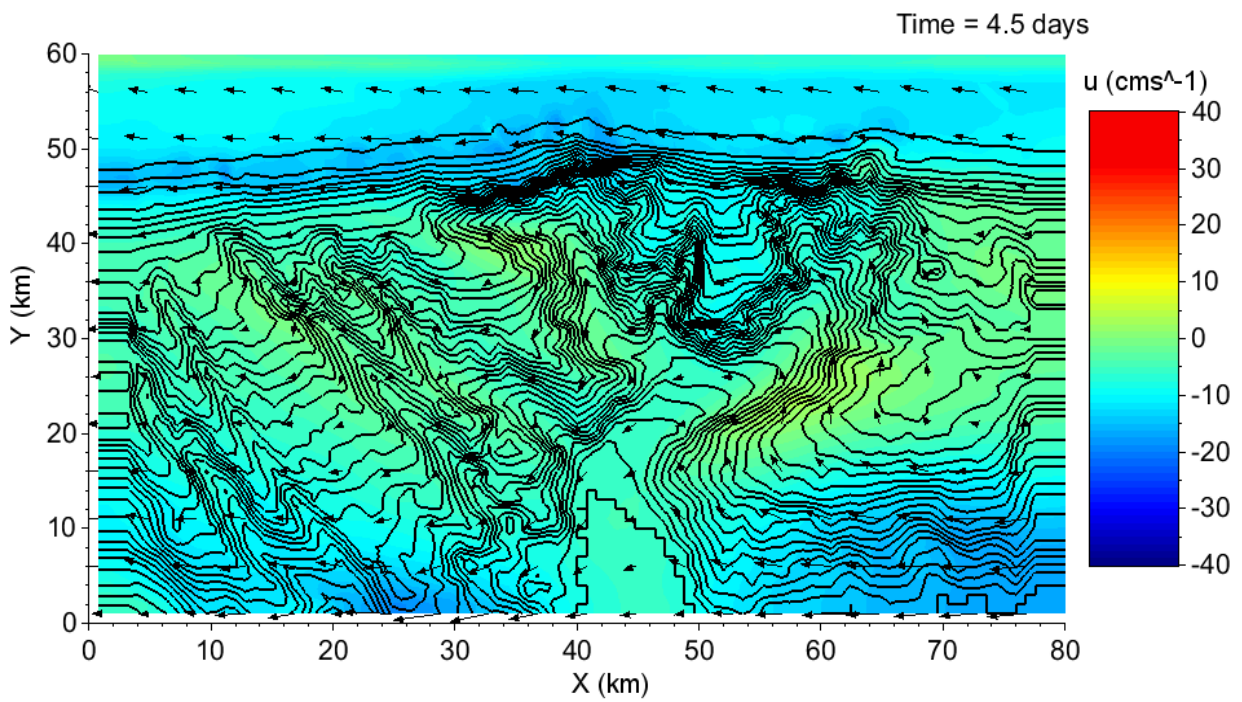


Figure 4.14: The average zonal Eulerian velocity for experiment DC3 after 4.5 days, with positive values representing an eastwards flow. The black lines are 100 m contours lines and the arrows are the flow direction. The median velocity was  $6.07 \text{ cm s}^{-1}$  westwards.

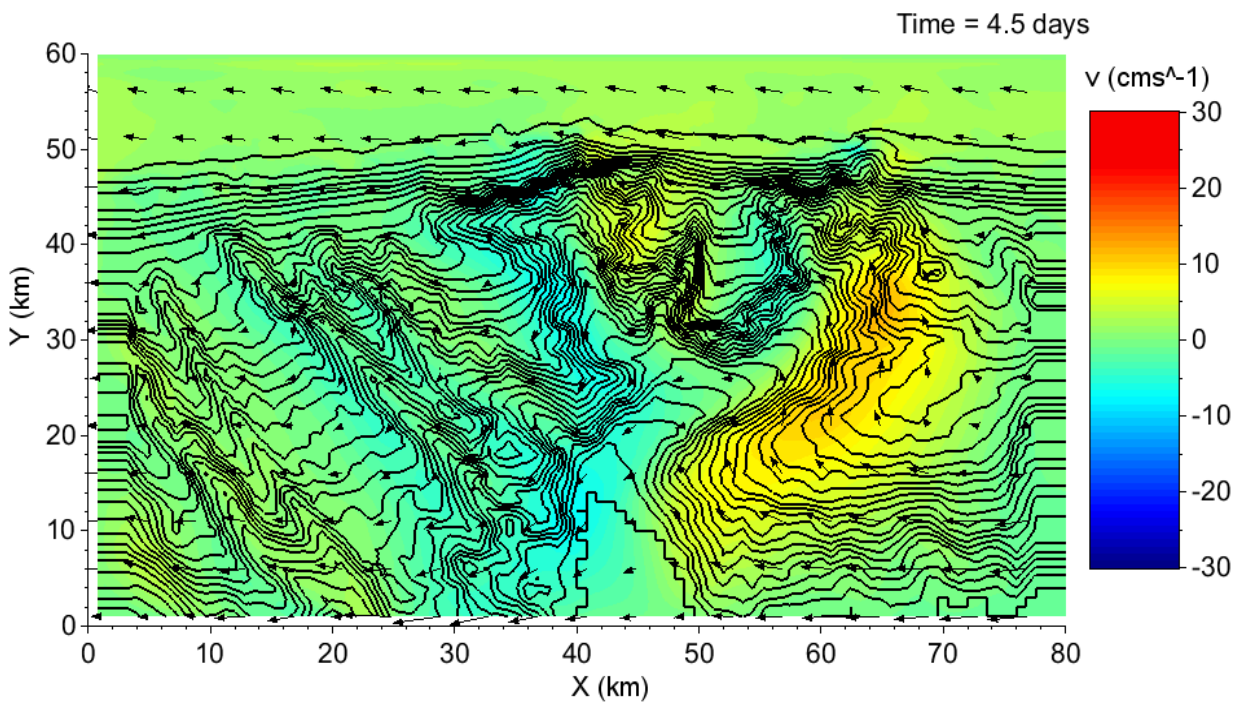


Figure 4.15: The average meridional Eulerian velocity for experiment DC3, with positive values representing a northwards velocity. The black lines are 100 m contours lines, and the arrows are the flow direction. The median velocity was  $0.2 \text{ cm s}^{-1}$  northwards.

Table 4.7: The average sea level elevation (Figure 4.13), as well as the average zonal (Figure 4.14), and meridional Eulerian velocity (Figure 4.15) for areas of interest in experiment DC3. Positive values represent an increase in sea level elevation, eastwards flow in average zonal Eulerian velocity, and northwards in average meridional Eulerian velocity. H.C. stands for Hood Canyon. B.C. stands for Bremer Canyon.

Location	Average sea level elevation (cm)	Average zonal Eulerian velocity (cms <sup>-1</sup> )	Average meridional Eulerian velocity (cms <sup>-1</sup> )
Mean	2.32 ± 1.22	-7.57 ± 4.31	0.44 ± 3.1
Hotspot	2.61 ± 0.22	-7.99 ± 3.89	-0.82 ± 0.62
H.C. outlet	2.46 ± 0.13	-4.63 ± 4.55	-3.77 ± 1.14
H.C. northern wall	2.81 ± 0.17	-12.85 ± 2.1	0.11 ± 3.32
H.C. eastern wall	2.27 ± 0.13	-6.79 ± 2.18	3.09 ± 2.3
H.C. mid-slope	2.02 ± 0.1	-2.98 ± 1.32	-3.17 ± 2.49
H.C. lower slope	1.71 ± 0.06	-5.01 ± 1.23	-1.15 ± 1.25
B.C. head	2.23 ± 0.2	-7.27 ± 1.63	2.6 ± 3.05
B.C. mid-slope	1.65 ± 0.06	-3.56 ± 2.31	1.11 ± 3.78
B.C. lower slope	1.29 ± 0.13	-5.24 ± 0.83	-3.07 ± 1.90
B.C. bottom slope	0.39 ± 0.23	-6.15 ± 0.73	-1.79 ± 2.29
Plateau	1.01 ± 0.53	-9.8 ± 3.75	3.79 ± 2.53
Headland	2.37 ± 0.21	-9.22 ± 0.83	-0.63 ± 2.05
Eastern hotspot	2.65 ± 0.18	-2.91 ± 1.1	4.78 ± 3.06

#### 4.3.2 Lagrangian Particle Tracker

62.23% and 63.05% of particles entered the hotspot and Hood Canyon outlet respectively (Figure 4.16, 4.17, Table 4.8). Only 32.5% of particles which entered the hotspot in between 600 m to 1200 m entered the Hood Canyon outlet, and of the 98% of particles which entered the outlet between 1800 m to 2400 m, 49.1% entered the hotspot. The hotspot and the eastern hotspot were near identical with the only difference being that the eastern hotspot had 1.6% more particles entering between 1800 m to 2400 m. This similarity indicated there was a lack of upwelled flow from the canyon.

The head of the Bremer Canyon had 86.55% of released particles enter with 100% of particles released between 600 m to 2400 m, and 46.2 % from > 2400 m. This was compared to the mid-slope of the Bremer Canyon receiving 13.98% with 54.3% coming from below 2400 m, and the lower slope of the Bremer Canyon receiving 13.35% with 53.4% of particles released >2400 m. These results indicate that there was some minor transport of deep particles, with minimal travelling upwards.

The average velocity for particles travelling through the DC3 model domain was 5.64 cms<sup>-1</sup> westwards, with a range of velocities from 4.1 cms<sup>-1</sup> to 10.71 cms<sup>-1</sup> westwards (Table 4.9). The

depth range having the fastest particles on average was 600 m to 1200 m with a velocity of  $6.93 \text{ cms}^{-1}$  westwards, with particles released between 2400 m to 3000 m being the second fastest at  $5.88 \text{ cms}^{-1}$  westwards. The slowest depth range for particles was 1800 m to 2400 m with an average velocity of  $4.53 \text{ cms}^{-1}$  westwards.

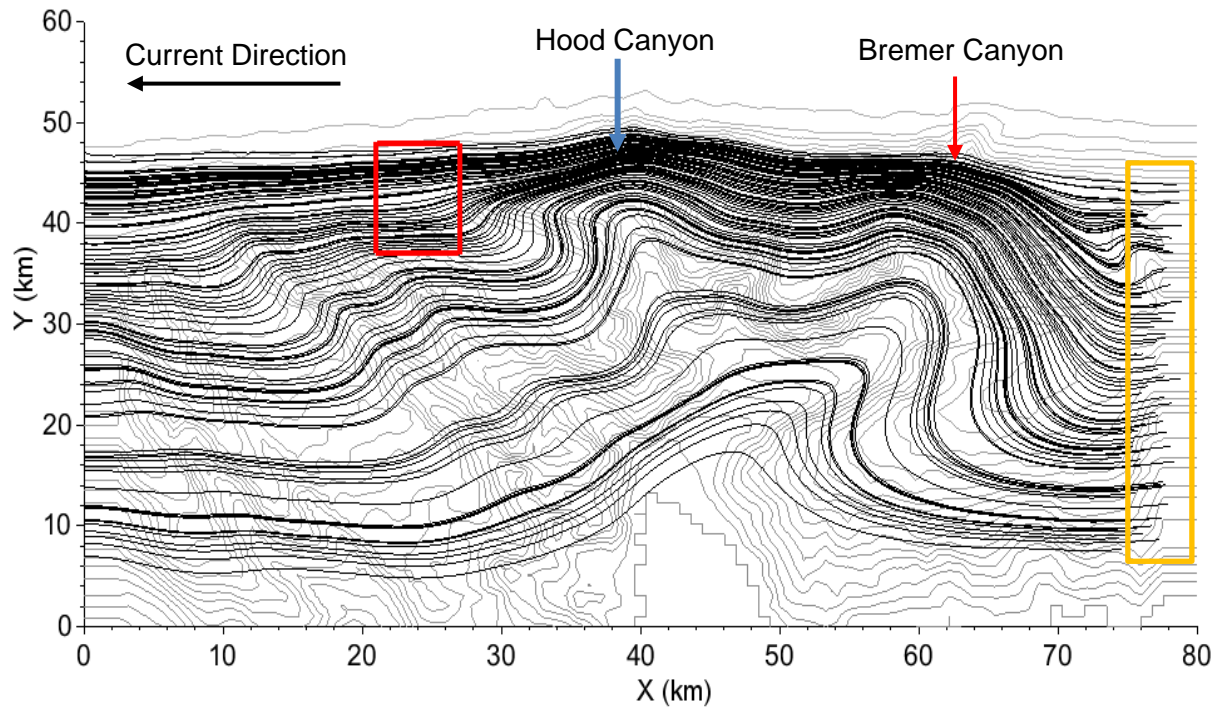


Figure 4.16: The trajectory of every 40<sup>th</sup> particle released on the eastern boundary (orange box) for experiment DC3. The red box is where the hotspot is located. Black lines are where particles have travelled, and grey lines are 100 m contours. The highest average particle speed for a particle travelling through the domain was  $10.78 \text{ cms}^{-1}$  westwards.

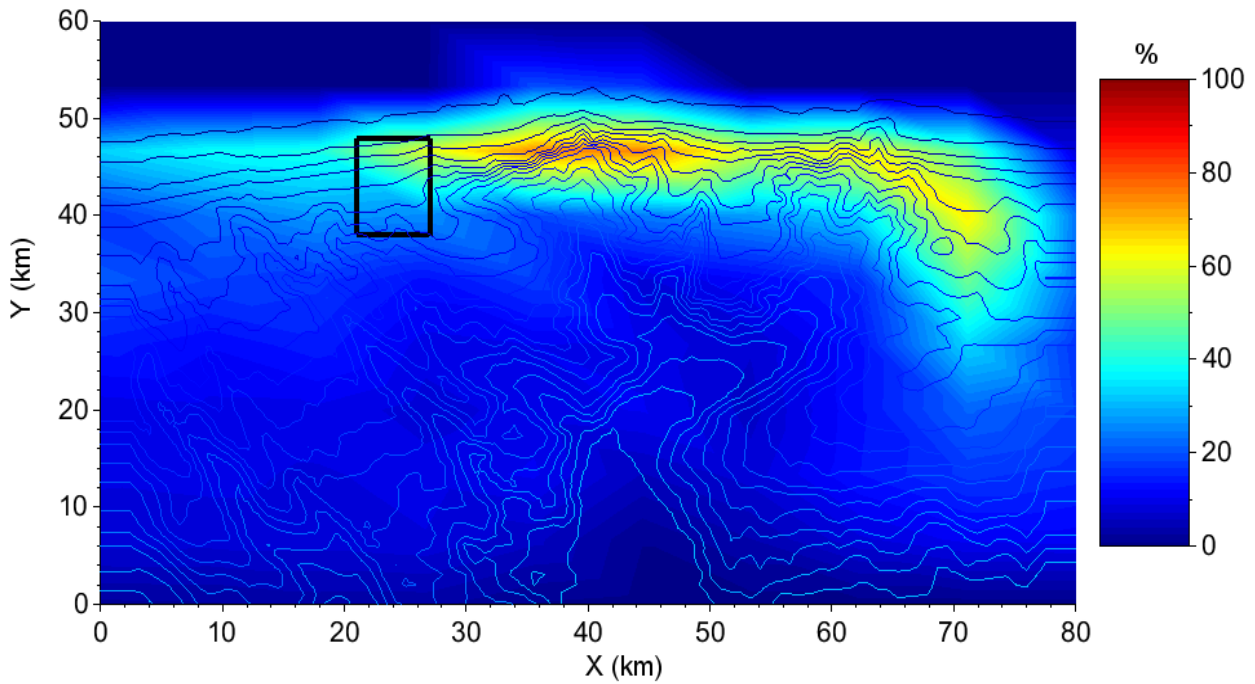


Figure 4.17: Heat map of particle concentration for experiment DC3. Most particles congregated around the heads of the Hood and Bremer Canyon; however, particles dispersed when travelling through the western section of the domain.

Table 4.8: Approximate percentage of particles entering areas of interest within the DC3 model domain, as well as a breakdown on where particles originated from (Figure 4.16, and Figure 4.17). H.C. stands for Hood Canyon. B.C. for Bremer Canyon. PG1 consisted of particles with a starting depth of 600 m to 1200 m, PG2 was particles which had a starting depth of 1200 m to 1800 m, PG3 was particles which had a starting depth of 1800 m to 2400 m and PG4 was particles which had a starting depth that was > 2400 m.

Location	Total (%)	PG1 (%)	PG2 (%)	PG3 (%)	PG4 (%)
Hotspot	62.23	100	100	49.1	0
H.C. outlet	63.05	32.5	100	98	22.6
H.C. mid-slope	14.63	0	0	6.9	51.6
B.C. head	86.55	100	100	100	46.2
B.C. mid-slope	13.98	0	0	1.6	54.3
B.C. lower slope	13.35	0	0	0	53.4
Eastern hotspot	62.68	100	100	50.7	0

Table 4.9: Average time and velocity for particles released on the eastern and a breakdown for each particle group. Positive values were an eastwards flow. PG1 consisted of particles with a starting depth of 600 m to 1200 m, PG2 was particles which had a starting depth of 1200 m to 1800 m, PG3 was particles which had a starting depth of 1800 m to 2400 m and PG4 was particles which had a starting depth that was > 2400 m.

Particle group	Average time (days)	Minimum velocity (cms <sup>-1</sup> )	Average velocity (cms <sup>-1</sup> )	Maximum velocity (cms <sup>-1</sup> )
All	16.02	-2.84	-5.64	-10.71
PG1	13	-3.42	-6.93	-9.57
PG2	15.78	-2.91	-5.72	-7.32
PG3	19.94	-2.84	-4.53	-5.09
PG4	15.36	-3.05	-5.88	-10.71

## 4.4 Experiment DC4

### 4.4.1 Sea Level Elevation and Velocity Fields

Experiment DC4 was designed to test how the Hood and Bremer Canyon are affected by an eastwards flow in the northern hemisphere. To create an eastwards flow in the northern hemisphere, the sea level elevation was decreased by 5 cm. The model was allowed to adjust to this change for four and a half days, due to instability issues in the model that occurred at five to six days of run time.

The average sea level elevation for DC4 was  $-3.35 \text{ cm} \pm 1.51 \text{ cm}$  (Figure 4.18). From this change it created an average velocity of  $7.79 \text{ cms}^{-1} \pm 9.31 \text{ cms}^{-1}$  eastwards (Figure 4.19) and  $1.83 \text{ cms}^{-1} \pm 6.77 \text{ cms}^{-1}$  southwards (Figure 4.20). Flow in the Hood Canyon had an average eastwards Eulerian velocity with its lowest being an average of  $1.05 \text{ cms}^{-1} \pm 2.13 \text{ cms}^{-1}$  in the outlet and the maximum being in the northern wall at  $10.51 \text{ cms}^{-1} \pm 9.63 \text{ cms}^{-1}$ , with the lower slopes also being slightly slower at  $10.26 \text{ cms}^{-1} \pm 0.87 \text{ cms}^{-1}$  (Table 4.10). Flow in the Bremer Canyon follows suit with the entire canyon having an eastward velocity, with the head being the slowest at  $7.34 \text{ cms}^{-1} \pm 5.15 \text{ cms}^{-1}$  and the mid-slope having the highest velocity at  $18.16 \text{ cms}^{-1} \pm 1.68 \text{ cms}^{-1}$ .

The Hood Canyon had a northwards flow present everywhere bar the northern wall, which had a southward velocity of  $1.61 \text{ cms}^{-1} \pm 6.66 \text{ cms}^{-1}$  (Figure 4.20, Table 4.10). Of the northward velocities, the lower-slopes were the quickest at  $7.87 \text{ cms}^{-1} \pm 1.05 \text{ cms}^{-1}$ . The Bremer Canyon northwards flow velocity peaked in the lower slopes at  $9.75 \text{ cms}^{-1} \pm 2.16 \text{ cms}^{-1}$ ; however, the mid-slope had an average southward velocity of  $0.32 \text{ cms}^{-1} \pm 2.16 \text{ cms}^{-1}$  which potentially can impede any particle retention. In terms of a coastal jet formation, flow in the head of the Bremer Canyon had an average velocity of  $7.34 \text{ cms}^{-1} \pm 5.15 \text{ cms}^{-1}$  eastward, and  $5.86 \text{ cms}^{-1} \pm 5.04 \text{ cms}^{-1}$  northward (Figure 4.19, 4.20, Table 4.10). Flow in the eastern hotspot had an average velocity of  $18.81 \text{ cms}^{-1} \pm 4.27 \text{ cms}^{-1}$  eastward, and  $11.14 \text{ cms}^{-1} \pm 10.08 \text{ cms}^{-1}$  southward which was  $11.02$

$\text{cm s}^{-1}$  faster than the mean zonal velocity, and indicative that a coastal jet had formed.

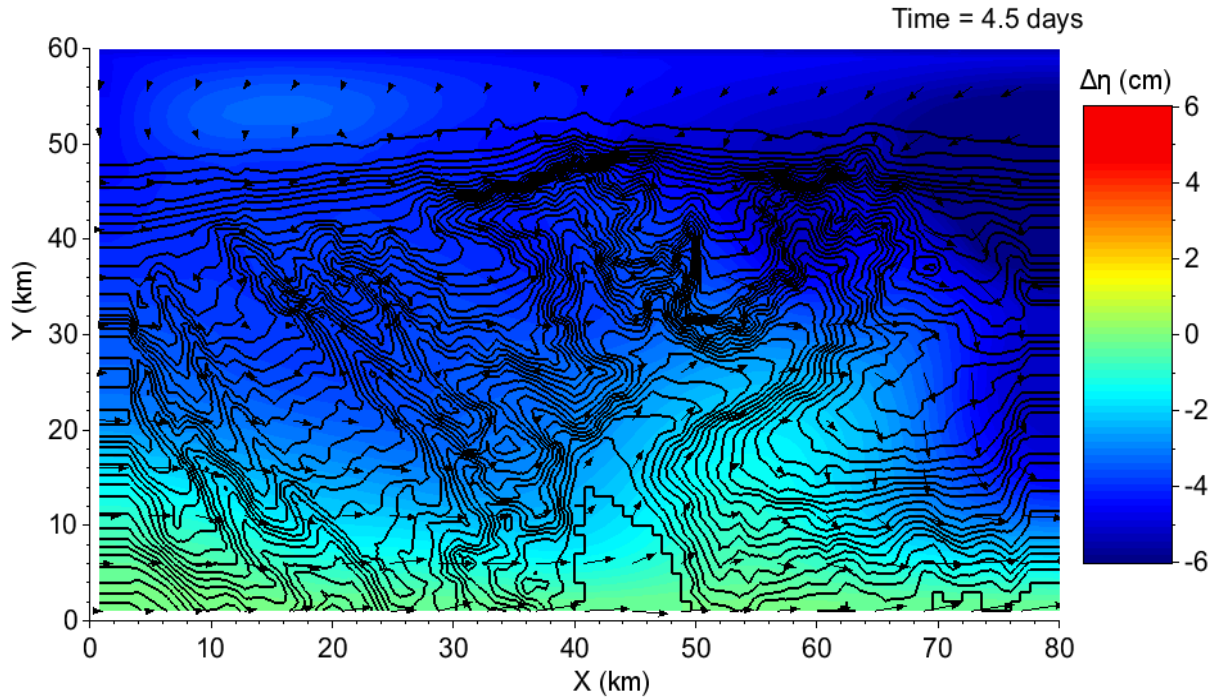


Figure 4.18: The resulting sea level decrease after 4.5 days of runtime with a positive number representing an increase of sea level. The black lines are 100 m contours lines and the arrows are the flow direction. The northern boundary averaged a sea level decrease of  $-3.91 \text{ cm} \pm 1.09 \text{ cm}$  and the southern boundary averaged  $-0.11 \text{ cm} \pm 0.02 \text{ cm}$ .

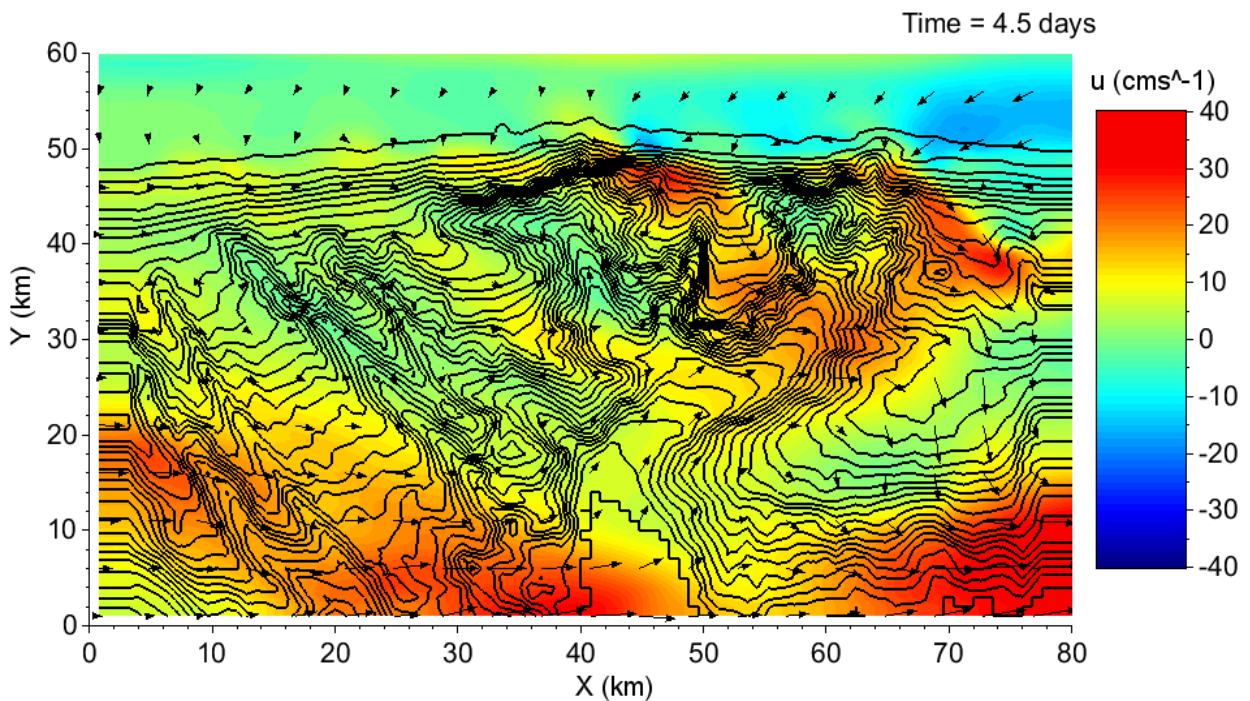


Figure 4.19: The resulting zonal velocity after 4.5 days of run time, with positive values representing an eastwards flow. The black lines are 100 m contour lines, and the arrows are the flow direction. The median velocity was  $6.57 \text{ cm s}^{-1}$  eastwards.

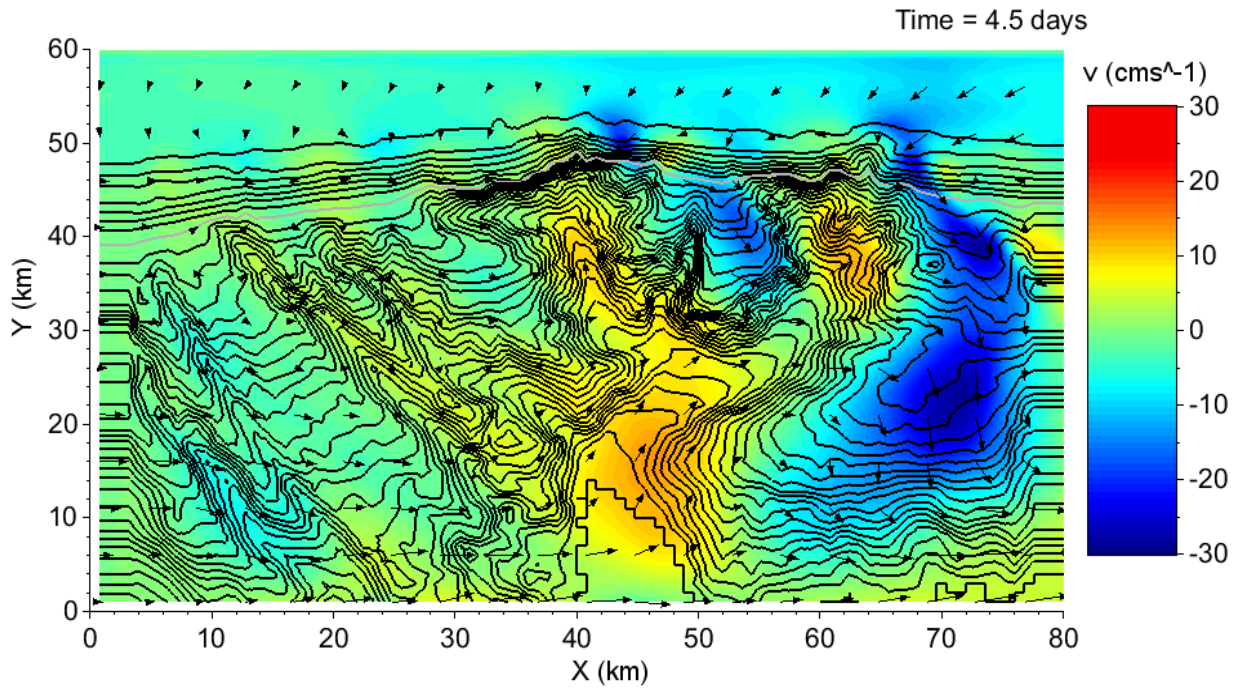


Figure 4.20: The resulting meridional velocity for experiment DC4, with positive values representing a northwards velocity. The black lines are 100 m contour lines, and the arrows are the flow direction. The median velocity was  $0.95 \text{ cm s}^{-1}$  southwards.

Table 4.10: The average sea level elevation (Figure 4.18), as well as the average zonal (Figure 4.19), and meridional Eulerian velocity (Figure 4.20) for areas of interest in experiment DC4. Positive values represent an increase in sea level elevation, eastwards flow in average zonal Eulerian velocity, and northwards in average meridional Eulerian velocity. H.C. stands for Hood Canyon, and B.C. for Bremer Canyon.

Location	Average sea level elevation (cm)	Average zonal Eulerian velocity ( $\text{cm s}^{-1}$ )	Average meridional Eulerian velocity ( $\text{cm s}^{-1}$ )
Mean	$-3.35 \pm 1.51$	$7.79 \pm 9.31$	$-1.83 \pm 6.77$
Hotspot	$-3.94 \pm 0.05$	$3.9 \pm 1.36$	$0.84 \pm 1.46$
H.C. outlet	$-4.12 \pm 0.04$	$1.05 \pm 2.13$	$1.16 \pm 2.18$
H.C. northern wall	$-4.45 \pm 0.32$	$10.51 \pm 9.63$	$-1.61 \pm 6.66$
H.C. eastern wall	$-3.86 \pm 0.14$	$5.74 \pm 4.78$	$4.32 \pm 4.08$
H.C. mid-slope	$-3.69 \pm 0.17$	$4.3 \pm 4.64$	$6.03 \pm 2.7$
H.C. lower slope	$-3.05 \pm 0.15$	$10.26 \pm 0.87$	$7.87 \pm 1.05$
B.C. head	$-4.89 \pm 0.27$	$7.34 \pm 5.15$	$5.86 \pm 5.04$
B.C. mid-slope	$-3.21 \pm 0.35$	$18.16 \pm 1.68$	$-0.32 \pm 2.16$
B.C. lower slope	$-2.38 \pm 0.24$	$8.06 \pm 1.02$	$9.75 \pm 2.16$
B.C. bottom slope	$-1 \pm 0.55$	$17.35 \pm 7.12$	$5.30 \pm 3.6$
Plateau	$-1.34 \pm 0.64$	$10.18 \pm 6.49$	$-2.64 \pm 7.73$
Headland	$-4.58 \pm 0.45$	$11.83 \pm 5.81$	$-9.87 \pm 5.15$
Eastern hotspot	$-4.76 \pm 0.57$	$18.81 \pm 4.27$	$-11.14 \pm 10.08$

#### 4.4.2 Lagrangian Particle Tracker

After sixty days of run time, 53.6% of particles had entered the eastern hotspot with > 95% of particles originating from depths of 600 m to 1800 m (Figure 4.21, 4.22, Table 4.11). This was like the head of the Bremer Canyon where 52.4% of particles had entered over the runtime, with > 90 % of particles released in between 600 m to 1800 m entering. This indicates that particles that are entering the head of the Bremer Canyon are transitioning to the eastern hotspot. The Bremer mid-slope had 56.6% of particles entering it with 73.1% of particles released in between 1200 m to 1800 m, as well as 100% of particles entering between 1800 m to 2400 m, indicating there was some northwards transport throughout the canyon. This shows that upwelling was possible, though there is a limited number of particles originating from depths  $\geq 1800$  m upwelling into the head the Bremer Canyon. What acted to prevent this was that the mid-slope of the Bremer Canyon was also a location where particles could exit the canyon, with 84.6% of particles released between 1800 m to 2400 m exiting at the mid-slope. This result was also like the result obtained on the lower slope of the Bremer Canyon with 46.4% of particles released at > 2400 m exiting the canyon.

The average velocity for particles travelling through the DC4 model domain was  $7.98 \text{ cms}^{-1}$  eastwards, with a range of velocities of  $2.82 \text{ cms}^{-1}$  to  $14.44 \text{ cms}^{-1}$  eastwards (Table 4.12). The fastest release point for particle velocity on average was 2400 m to 3000 m with a velocity of  $13.7 \text{ cms}^{-1}$  eastwards, with the slowest being  $4.76 \text{ cms}^{-1}$  eastwards in between 600 m to 1200 m, with particles progressively getting faster as they get deeper. The southern section of the Bremer Canyon had a northward velocity of  $1.21 \text{ cms}^{-1} \pm 0.93 \text{ cms}^{-1}$ . The head of the Bremer Canyon had an exit velocity of  $3.52 \text{ cms}^{-1} \pm 1.54 \text{ cms}^{-1}$  eastward.

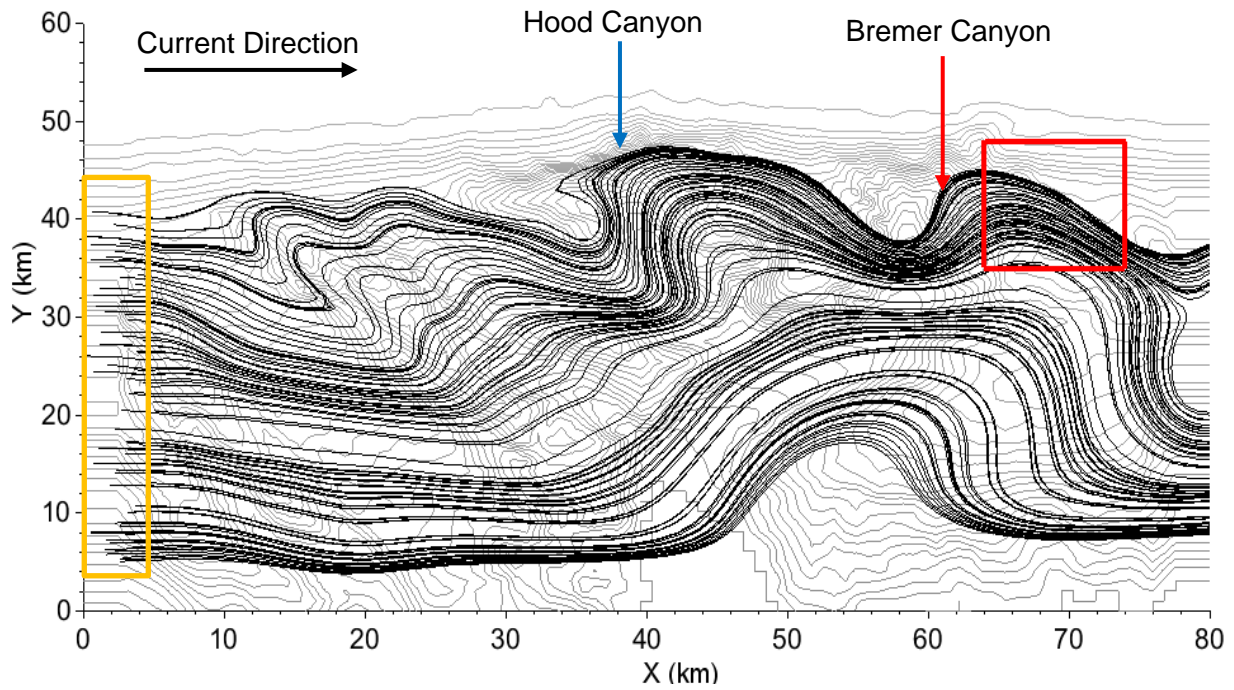


Figure 4.21: The trajectory of every 40<sup>th</sup> particle that was released on the western boundary (orange box indicates release point). The red box is where the eastern hotspot is located. Black lines are where particles have travelled, and grey lines is 100 m contours. The maximum eastern velocity for particles travelling through the model was 14.44  $\text{cm s}^{-1}$  eastwards.

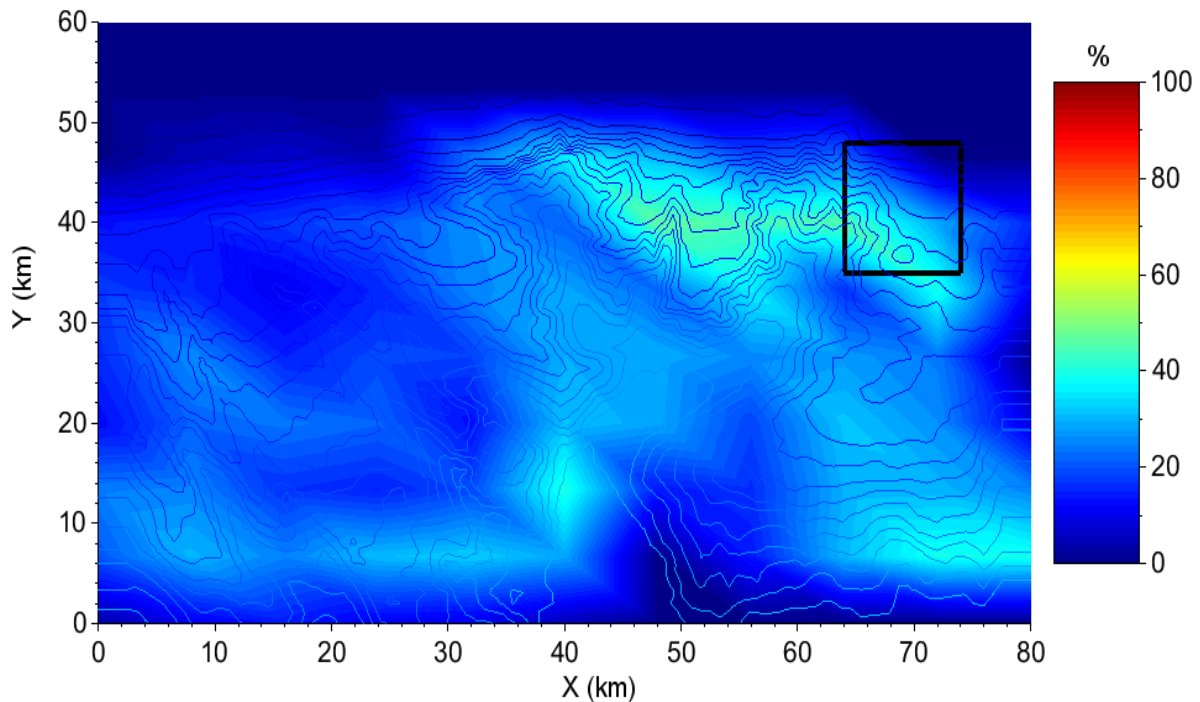


Figure 4.22: Heat map of particles travelling through the model domain for experiment DC4, with the black square being the “eastern hotspot”, and blue lines being 175 m contour lines. The maximum concentration of particles in one of the grid cells was 48.5%, which was located near the head of the Bremer Canyon.

Table 4.11: Approximate percentage of particles entering areas of interest within the DC4 model domain, as well as a breakdown on where particles originated from (Figure 4.21, and Figure 4.22). H.C. stands for Hood Canyon. B.C. stands for Bremer Canyon. PG1 consisted of particles with a starting depth of 600 m to 1200 m, PG2 was particles which had a starting depth of 1200 m to 1800 m, PG3 was particles which had a starting depth of 1800 m to 2400 m and PG4 was particles which had a starting depth that was > 2400 m.

Location	Total (%)	PG1 (%)	PG2 (%)	PG3 (%)	PG4 (%)
Hotspot	18.1	72.4	0	0	0
H.C. outlet	26.13	98.1	6.4	0	0
H.C. mid-slope	34.5	21.6	99	17.4	0
B.C. head	52.4	100	94.2	15.4	0
B.C. mid-slope	56.68	0	73.1	100	53.6
B.C. lower slope	51.73	0	22.3	84.6	100
Eastern hotspot	53.6	100	98.4	16	0

Table 4.12: Average time and velocity for particles released on the western boundary and a breakdown for each particle group. Positive values were an eastwards flow. PG1 consisted of particles with a starting depth of 600 m to 1200 m, PG2 was particles which had a starting depth of 1200 m to 1800 m, PG3 was particles which had a starting depth of 1800 m to 2400 m and PG4 was particles which had a starting depth that was > 2400 m.

Particle group	Average time (days)	Minimum velocity (cms <sup>-1</sup> )	Average velocity (cms <sup>-1</sup> )	Maximum velocity (cms <sup>-1</sup> )
All	11.32	2.82	7.98	14.44
PG1	18.96	2.82	4.76	6.75
PG2	12.03	5.12	7.5	12.67
PG3	7.68	6.88	11.75	14.16
PG4	6.59	12.04	13.7	14.44

## 4.5 Experiment DC5

### 4.5.1 Sea Level Elevation and Velocity Fields

Experiment DC5 was designed to test what would occur if the velocity of the Flinders Current were doubled. The intention was to calculate an upper limit of flow speed for upwelling to occur. In terms of set up, the sea level elevation was decreased by 10 cm on the northern boundary, and every other condition was kept constant with experiment DC1.

The result of doubling the change in sea level elevation in DC5 produced an average sea level elevation of  $-4.59 \text{ cm} \pm 3.08$ , which was 2.64 cm larger than experiment DC1 (Figure 4.23, Table 4.13). This decrease in sea level elevation resulted in an average zonal Eulerian velocity  $20.22 \text{ cms}^{-1} \pm 44.35 \text{ cms}^{-1}$  westward and  $0.73 \text{ cms}^{-1} \pm 16.53 \text{ cms}^{-1}$  northward (Figure 4.24, 4.25).

Within the DC5 domain the Hood Canyon supported a westward flow until the northern wall with the slowest flow being the mid-canyon at  $2.61 \text{ cms}^{-1} \pm 4.55 \text{ cms}^{-1}$ , and the fastest being the Hood

Canyon outlet at  $39.43 \text{ cms}^{-1} \pm 10.18 \text{ cms}^{-1}$  (Figure 4.24, Table 4.13). The Bremer Canyon supported an eastwards flow in the head and the mid-slope, ranging from  $0.59 \text{ cms}^{-1} \pm 5.26 \text{ cms}^{-1}$  to  $5.41 \text{ cms}^{-1} \pm 4.88 \text{ cms}^{-1}$ , and a westwards flow in the lower slope and the bottom slope, ranging from  $7.83 \text{ cms}^{-1} \pm 5.42 \text{ cms}^{-1}$  to  $28.78 \text{ cms}^{-1} \pm 8.7 \text{ cms}^{-1}$ . The plateau had a westwards flow velocity of  $25.9 \text{ cms}^{-1} \pm 7.51 \text{ cms}^{-1}$ . A jet formation was present in DC5 with the Hood Canyon outlet having the zonal velocity of  $39.43 \text{ cms}^{-1} \pm 10.18 \text{ cms}^{-1}$  and a northwards velocity of  $3.3 \text{ cms}^{-1} \pm 9.22 \text{ cms}^{-1}$  (Figure 4.25, Table 4.13). This fed into the hotspot which had an eastward velocity of  $22.40 \text{ cms}^{-1} \pm 44.35 \text{ cms}^{-1}$  and a southward velocity of  $34.79 \text{ cms}^{-1} \pm 18.29$ . This jet attains a maximum eastward velocity of  $65.15 \text{ cms}^{-1}$  and a southwards velocity of  $55.91 \text{ cms}^{-1}$ .

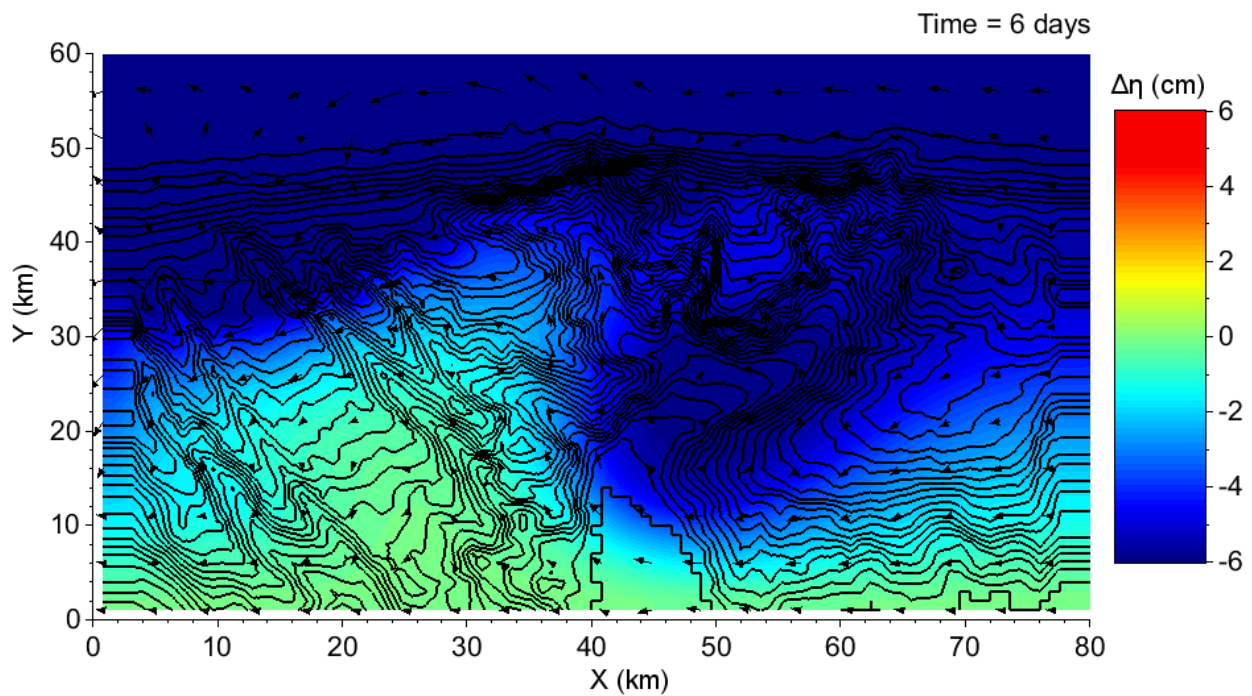


Figure 4.23: The resulting sea level change for experiment DC5 after four days of run time. The black lines are 100 m contours lines and the arrows are the flow direction. The maximum increase in sea level observed from the extra forcing was 2.24 cm, and the maximum decrease was -5.97 cm.

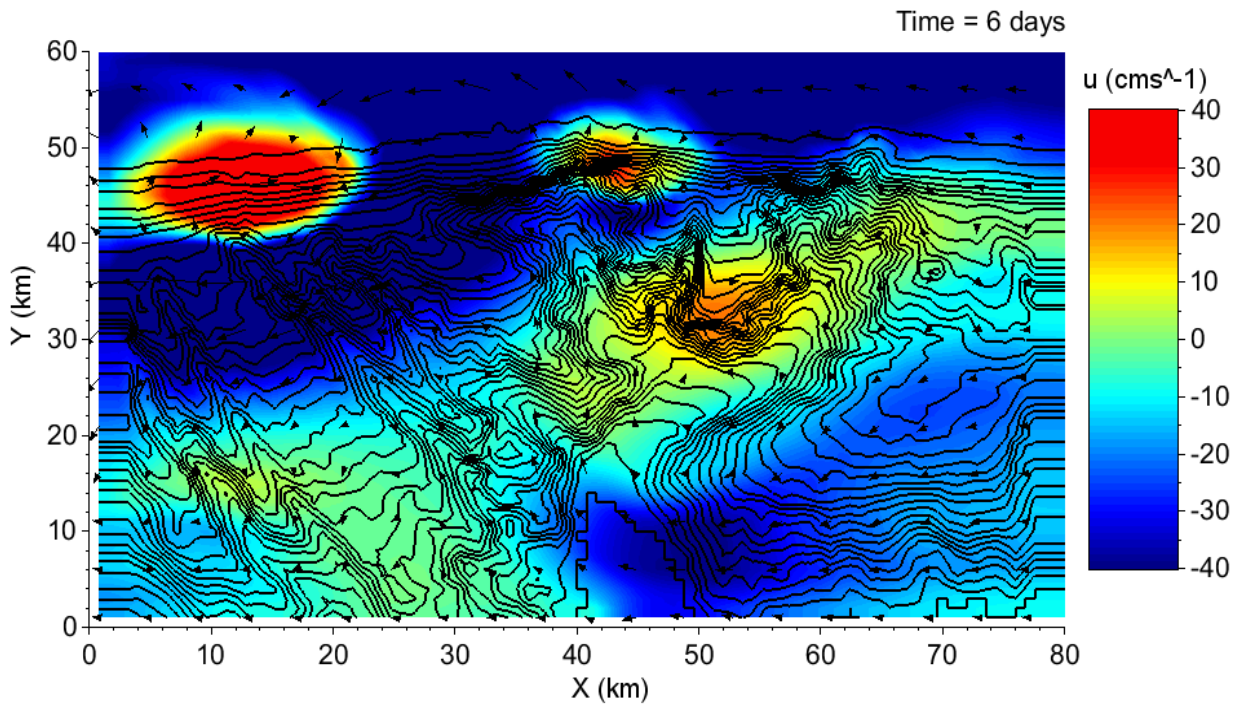


Figure 4.24: The resulting zonal velocity from experiment DC5 after six days of run time. The black lines are 100 m contours lines and the arrows are the flow direction. The median velocity was  $16.33 \text{ cm s}^{-1}$  westwards.

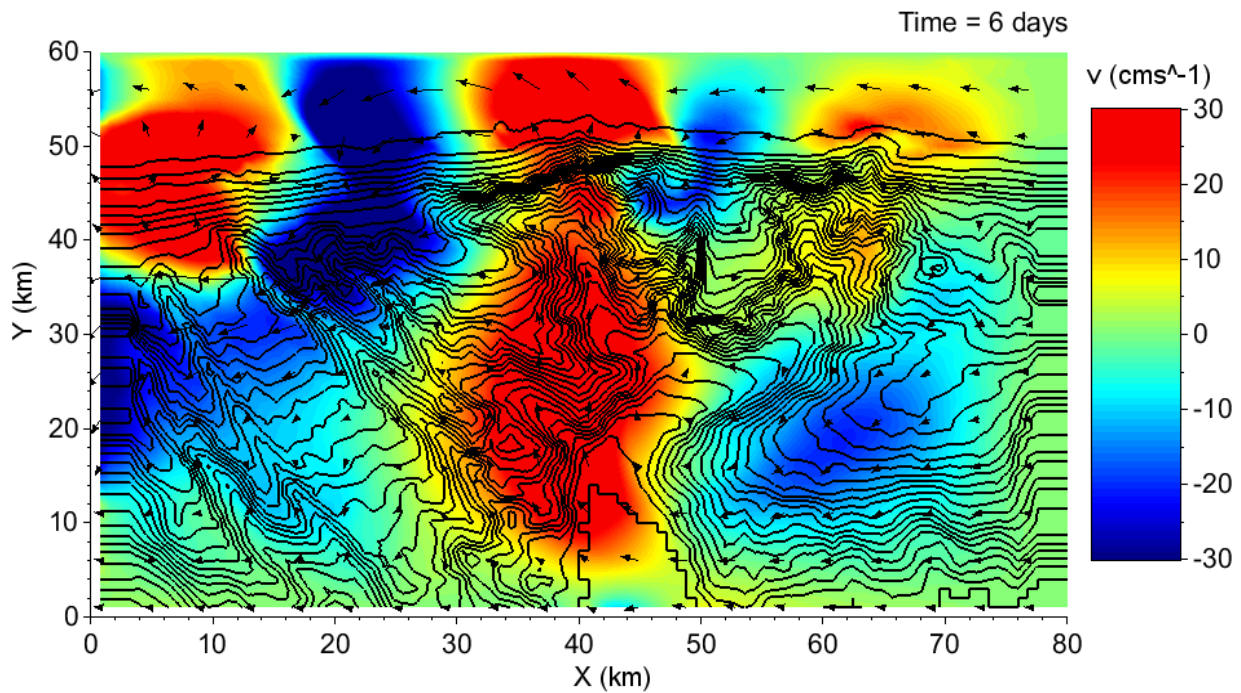


Figure 4.25: The resulting meridional velocity from a 10 cm decrease in sea level on the northern boundary and 6 days of run time. The black lines are 100 m contours lines and the arrows are the flow direction. The maximum change caused by this increase in forcing was  $55.91 \text{ cm s}^{-1}$  southward and  $50.04 \text{ cm s}^{-1}$  northward. This resulted in a median velocity of 0.

Table 4.13: The average change in sea level elevation (Figure 4.23), as well as the average zonal (Figure 4.24), and meridional Eulerian velocity (Figure 4.25) for areas of interest in experiment DC5. Positive values represent an increase in sea level elevation, eastwards flow in average zonal Eulerian velocity, and northwards in average meridional Eulerian velocity. H.C. stands for Hood Canyon, and B.C. stands for Bremer Canyon.

Location	Average sea level elevation (cm)	Average zonal Eulerian velocity (cms <sup>-1</sup> )	Average meridional Eulerian velocity (cms <sup>-1</sup> )
Mean	-4.59 ± 3.08	-20.22 ± 23.81	0.73 ± 16.53
Hotspot	-9.33 ± 2.03	-22.20 ± 44.35	-34.79 ± 18.29
H.C. outlet	-4.7 ± 0.62	-39.43 ± 10.18	3.3 ± 9.22
H.C. northern wall	-6.11 ± 0.5	1.83 ± 19.3	8.41 ± 10.43
H.C. eastern wall	-5.27 ± 1	-20.46 ± 12.72	9.72 ± 12.44
H.C. mid-slope	-4.34 ± 0.55	-2.61 ± 4.55	27.16 ± 6.09
H.C. lower slope	-6.1 ± 0.31	-7.44 ± 2.85	13.94 ± 6.14
B.C. head	-5.3 ± 0.2	0.59 ± 5.26	7.92 ± 2.34
B.C. mid-slope	-5.83 ± 0.2	5.41 ± 4.88	2.12 ± 3.32
B.C. lower slope	-5.49 ± 0.48	-7.83 ± 5.42	16.90 ± 9.99
B.C. bottom slope	-1.24 ± 1.01	-28.78 ± 8.7	8.08 ± 8.03
Plateau	-2.74 ± 1.6	-25.90 ± 7.51	-6.79 ± 6.62
Headland	-5.06 ± 0.27	-7.89 ± 13.1	-1.86 ± 6.01
Eastern hotspot	-5.62 ± 0.15	-3.08 ± 5.30	-3.99 ± 3.41

#### 4.5.2 Lagrangian Particle Tracker Results

After doubling the sea level elevation from DC1, 60.1% of particles that were released on the eastern boundary entered the hotspot and 74.5% of particles entered the Hood Canyon outlet (Figure 4.26, 4.27, Table 4.14). > 50% of particles entered the hotspot and Hood Canyon outlet from depths originating from 600 m to 2400 m, with only 5% entering both locations from depths originating at > 2400 m. 49.2% of particles released between 600 m to 1200 m bypassed the hotspot after entering the Hood Canyon outlet. A way that 17.1% of particles released within 600 m to 1200 m bypass the hotspot was by exiting at the northern wall. Only 49.75% of particles entered the head of the Bremer Canyon with 1.6% of particles that entered the head came from > 1800 m. The reason for why this occurred was that the concentration on the lower slope of the Bremer Canyon was 72.43%. This consisted of 89.7% of particles released between 1200 m to 1800 m and 100% of particles released > 1800 m. The Hood Canyon mid-slope had 100% of particles released in between 1800 m to 2400 m entering it at some stage during the model run time, as well as 80% from > 2400 m. 23.8% of released particles were exiting through the Henry Canyon, which consisted of 95.1% of particles released between 2400 m to 3000 m (Figure

4.28). Also particles that were released between 600 m to 1200 m were able to bypass the hotspot by exiting through the northern wall of the Hood Canyon.

The average velocity of particles travelling through the DC5 model domain was  $16.6 \text{ cm s}^{-1}$  westwards, with particles having a range of velocities between  $6.63 \text{ cm s}^{-1}$  to  $26.75 \text{ cm s}^{-1}$  westwards (Table 4.15). The fastest particle range was between 1800 m to 2400 m with a velocity of  $23.2 \text{ cm s}^{-1}$  westwards, and the slowest was 1200 m to 1800 m at  $12.48 \text{ cm s}^{-1}$  westwards. Particles travelling through the hotspot had an average velocity of  $26.34 \text{ cm s}^{-1} \pm 5.25 \text{ cm s}^{-1}$  westwards which was higher than the average exit velocity of the Hood Canyon outlet, which was at  $20.78 \text{ cm s}^{-1} \pm 5.53 \text{ cm s}^{-1}$  westwards. Particles exiting the head of the Bremer Canyon had an average velocity of  $4.97 \text{ cm s}^{-1} \pm 2.25 \text{ cm s}^{-1}$  westwards. Particles travelling through the lower slope of the Bremer Canyon had an average velocity of  $17.59 \text{ cm s}^{-1} \pm 1.77 \text{ cm s}^{-1}$  northwards. This northwards velocity slowed down as it approached the Hood Canyon outlet, as the entry speed into the Hood Canyon was  $6.78 \text{ cm s}^{-1} \pm 1.58 \text{ cm s}^{-1}$  northwards.

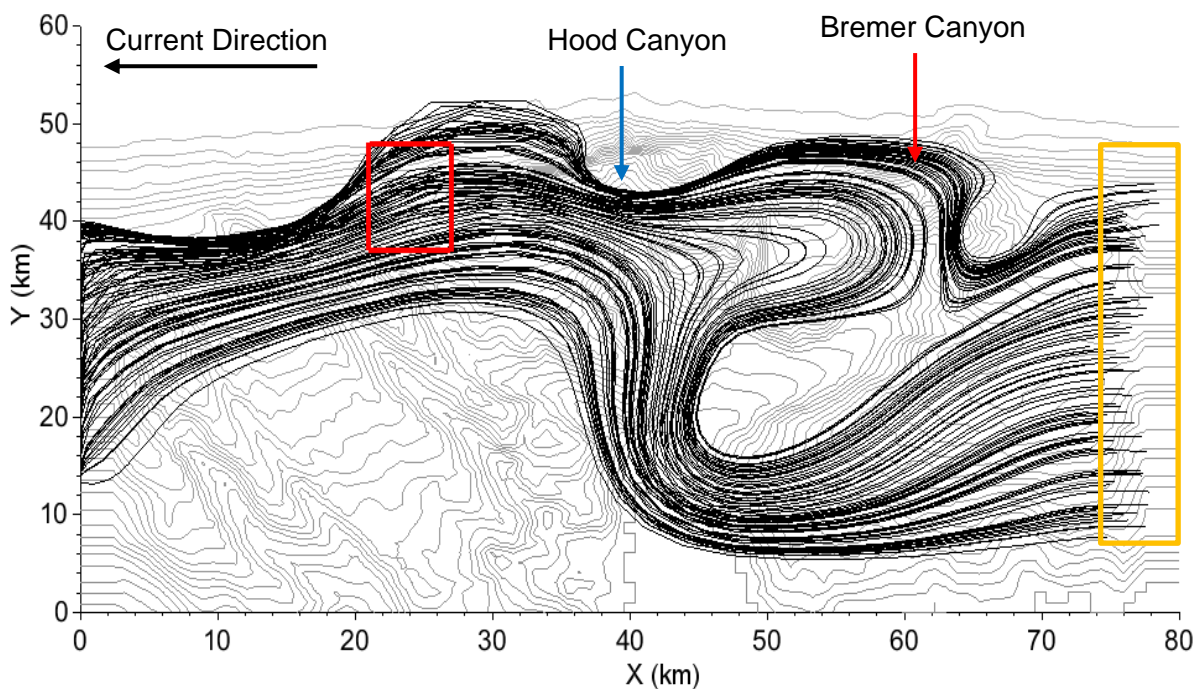


Figure 4.26: The trajectory of every 40<sup>th</sup> particle released near the eastern boundary (orange box) with the hotspot highlighted with a red box. The black lines represent the path taken by each particle and grey lines are 100 m contour lines. The maximum average westwards velocity was  $26.75 \text{ cm s}^{-1}$ .

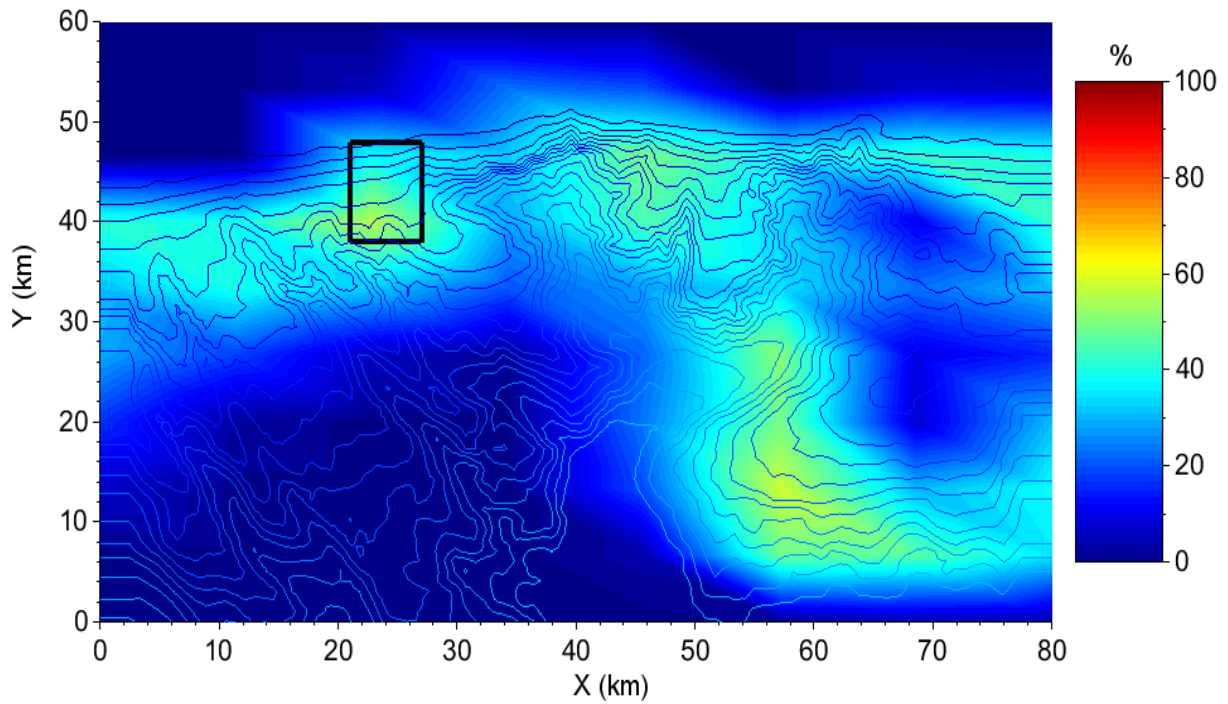


Figure 4.27: Heat map of particles trajectories for experiment DC5 with the hotspot location in black and 175 m contours in blue. The doubling of forcing on the northern boundary had spread out particles with a maximum concentration of 57.65% present in the lower slope of the Bremer canyon.

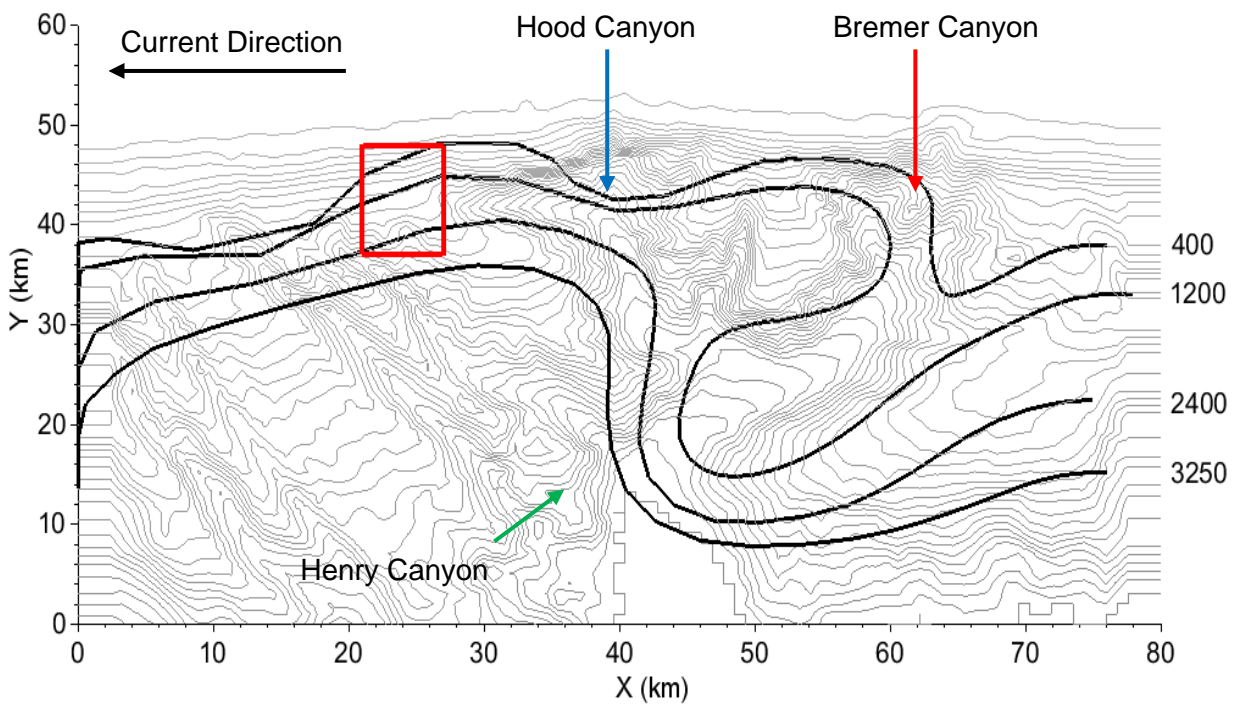


Figure 4.28: The pathway that particles have taken in DC5, with grey lines being 100 m contour lines. The red box is the location of the hotspot. Whilst particles 400, 1200, and 2400 follow paths described in 4.1.2, 3200 exits the Bremer Canyon where the Henry Canyon tributary forms before leaving the canyon system entirely.

Table 4.14: Approximate percentage of particles entering areas of interest within the DC5 model domain, as well as a breakdown on where particles originated from (Figure 4.27, and Figure 4.28). H.C. stands for Hood Canyon. B.C. stands for Bremer Canyon. PG1 consisted of particles with a starting depth of 600 m to 1200 m, PG2 was particles

which had a starting depth of 1200 m to 1800 m, PG3 was particles which had a starting depth of 1800 m to 2400 m and PG4 was particles which had a starting depth that was > 2400 m.

Location	Total (%)	PG1 (%)	PG2 (%)	PG3 (%)	PG4 (%)
Hotspot	60.1	50.8	96.6	82.7	2.2
H.C. outlet	74.5	100	100	93.9	4.2
H.C. mid-slope	58.53	0	54.1	100	80
B.C. head	49.75	100	97.4	1.6	0
B.C. mid-slope	19.5	0	78	0	0
B.C. lower slope	72.43	0	89.7	100	100
Eastern hotspot	39.33	100	57.3	0	0

Table 4.15: Average time and velocity for particles released on the eastern boundary, as well as a breakdown of each group. Positive values were an eastwards flow. PG1 consisted of particles with a starting depth of 600 m to 1200 m, PG2 was particles which had a starting depth of 1200 m to 1800 m, PG3 was particles which had a starting depth of 1800 m to 2400 m and PG4 was particles which had a starting depth that was > 2400 m.

Particle group	Average time (days)	Minimum velocity (cms <sup>-1</sup> )	Average velocity (cms <sup>-1</sup> )	Maximum velocity (cms <sup>-1</sup> )
Total	6.1	-6.63	-16.6	-26.75
PG1	7.06	-9.5	-13.71	-18.06
PG2	7.67	-6.63	-12.48	-19.01
PG3	4.62	-14.74	-23.2	-26.75
PG4	5.05	-15.7	-22.31	-25.79

## 4.6 Experiment DC6

### 4.6.1 Sea Level Elevation and Velocity Fields

Experiment DC6 was designed to test what would occur if the velocity of the Flinders Current were halved. The intention was to calculate a lower limit of flow speed for upwelling to occur. To test this, the sea level elevation was decreased by 2.5 cm with everything else kept constant with experiment DC1.

DC6 had an average sea level elevation of  $-0.96 \text{ cm} \pm 0.69 \text{ cm}$  (Figure 4.29, Table 4.16). This resulted in an average velocity field of  $4.31 \text{ cms}^{-1} \pm 5.49 \text{ cms}^{-1}$  westwards and  $0.49 \text{ cms}^{-1} \pm 4.7 \text{ cms}^{-1}$  southwards (Figure 4.30, 4.31). The zonal velocity field was slower than the Flinders Current by  $5.44 \text{ cms}^{-1}$ .

The hotspot had an average westwards velocity field of  $5.87 \text{ cms}^{-1} \pm 7.46 \text{ cms}^{-1}$  and the Hood Canyon outlet had an average velocity field of  $15.94 \text{ cms}^{-1} \pm 6.29 \text{ cms}^{-1}$  westwards (Figure 4.30, Table 4.16). This culminated into a jet formation that had a maximum westwards velocity of  $35.14 \text{ cms}^{-1}$ . The entire Hood Canyon supported a westwards flow velocity ranging from  $1.89 \text{ cms}^{-1} \pm$

1.55  $\text{cms}^{-1}$  in the lower slopes to  $15.94 \text{ cms}^{-1} \pm 6.29 \text{ cms}^{-1}$  in the outlet. The Bremer Canyon supported an eastwards flow in the mid-slope and the lower slope, ranging from  $0.88 \text{ cms}^{-1} \pm 0.74 \text{ cms}^{-1}$  to  $2.52 \text{ cms}^{-1} \pm 0.93 \text{ cms}^{-1}$ . The head of the Bremer Canyon as well as the bottom slope supported a westwards flow, with the head at  $2.99 \text{ cms}^{-1} \pm 2.8 \text{ cms}^{-1}$  and the bottom slope at  $4.92 \text{ cms}^{-1} \pm 2.03 \text{ cms}^{-1}$ .

Flow in the Hood Canyon Outlet had a southwards velocity of  $0.36 \text{ cms}^{-1} \pm 5.63 \text{ cms}^{-1}$ , which varied from other sections of the Hood Canyon, as they had a northwards velocity ranging from  $0.25 \text{ cms}^{-1} \pm 3.04 \text{ cms}^{-1}$  in the northern wall, to a maximum of  $6.06 \text{ cms}^{-1} \pm 3.81 \text{ cms}^{-1}$  in the eastern wall (Figure 4.31, Table 4.16). The entirety of the Bremer Canyon supported a northwards flow velocity ranging from  $2.81 \text{ cms}^{-1} \pm 1.51 \text{ cms}^{-1}$  in the mid-slope to  $5.81 \text{ cms}^{-1} \pm 1.34 \text{ cms}^{-1}$  in the lower slope.

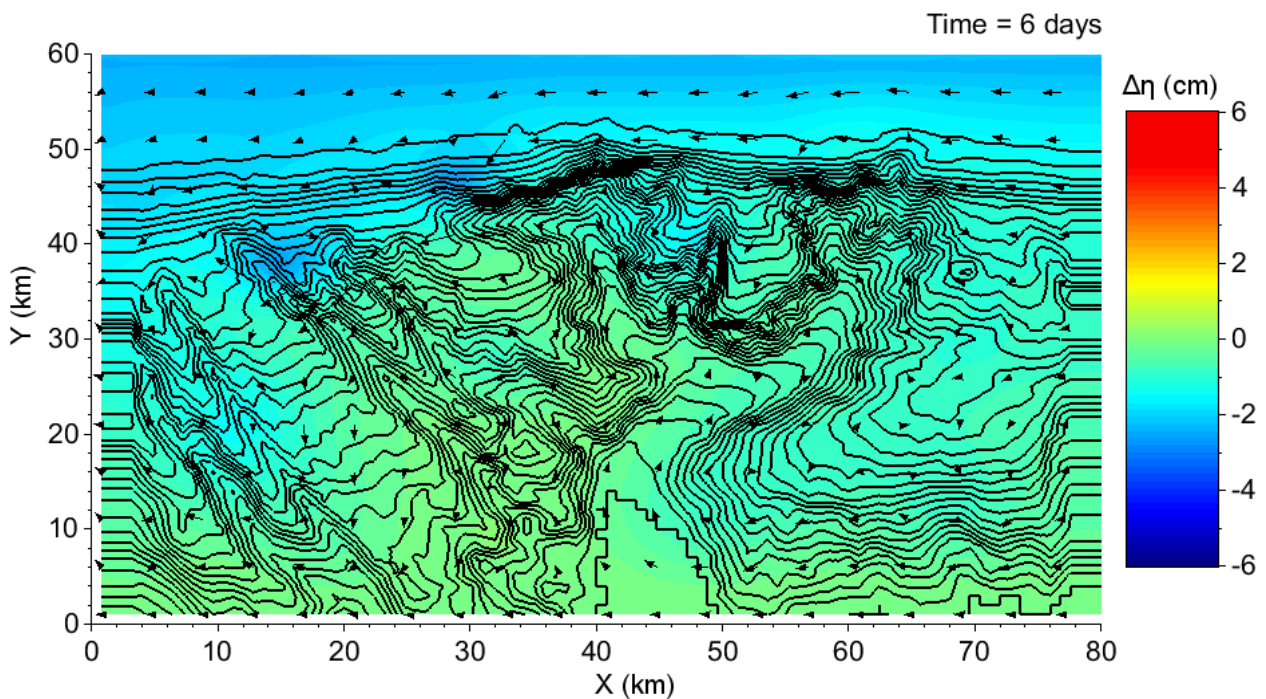


Figure 4.29: The average sea level decrease for DC6 after six days of run time with positive values indicating an increase in sea level. The black lines are 100 m contours lines, and the arrows are the flow direction. The maximum sea level decrease in the region was -2.66 cm, whereas the minimum increase was 0.01 cm.

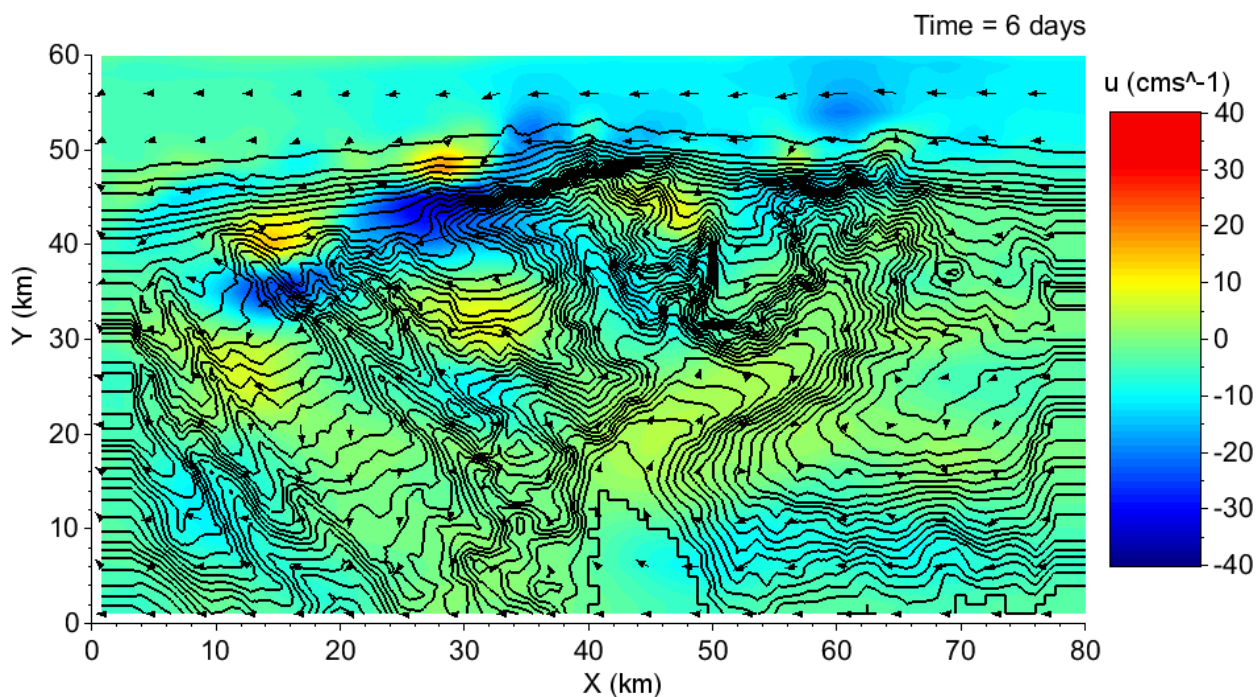


Figure 4.30 The average zonal velocity for experiment DC6 with positive values representing an eastwards flow. The black lines are 100 m contours lines, and the arrows are the flow direction. The median velocity was  $3.61 \text{ cm s}^{-1}$  westwards.

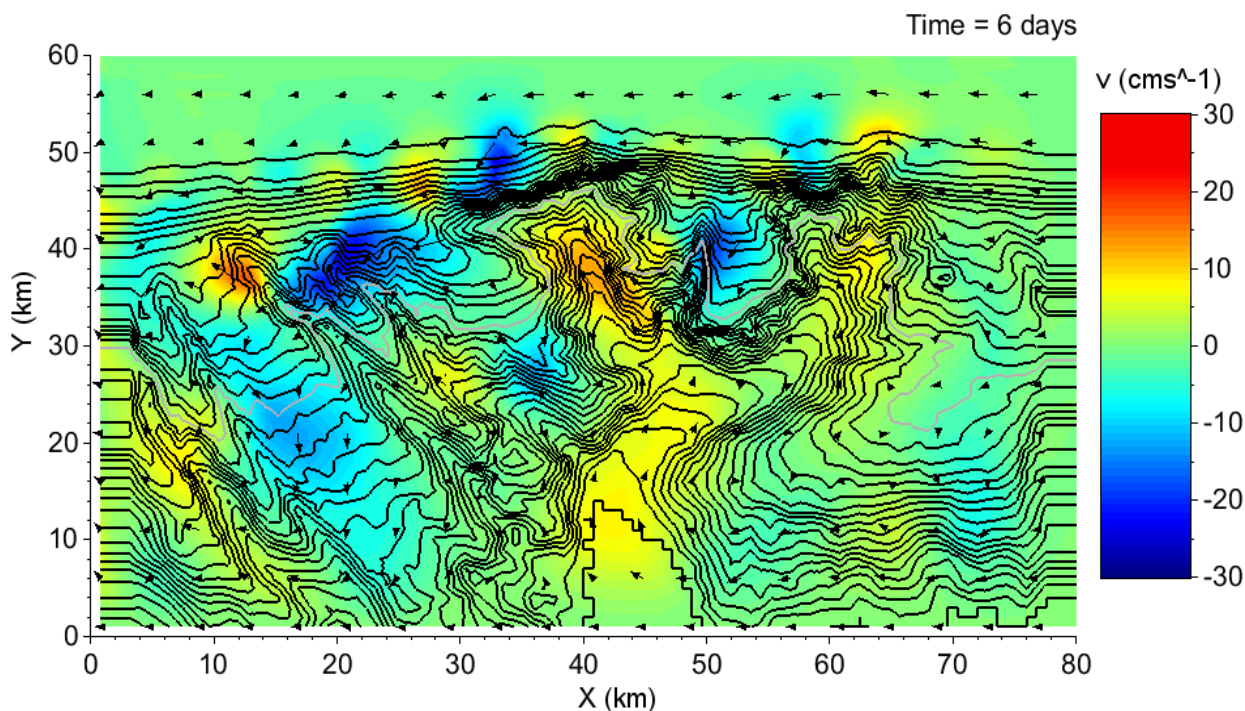


Figure 4.31: The average meridional Eulerian velocity for experiment DC6 with positive values representing a northwards flow. The black lines are 100 m contours lines and the arrows are the flow direction. The median velocity was  $0.09 \text{ cm s}^{-1}$  southwards.

Table 4.16: The average change in sea level elevation (Figure 4.29), the average zonal (Figure 4.30, and meridional Eulerian velocity (Figure 4.31) for areas of interest in experiment DC6. Positive values represent an increase in sea level elevation, eastwards flow in average zonal Eulerian velocity, and northwards in average meridional Eulerian velocity. H.C. stands for Hood Canyon. B.C. stands for Bremer Canyon.

Location	Average sea level elevation (cm)	Average zonal Eulerian velocity (cms <sup>-1</sup> )	Average meridional Eulerian velocity (cms <sup>-1</sup> )
Mean	-0.96 ± 0.69	-4.31 ± 5.49	-0.49 ± 4.7
Hotspot	-1.67 ± 0.28	-5.87 ± 7.46	-7.55 ± 8.94
H.C. outlet	-0.83 ± 0.36	-15.94 ± 6.29	-0.36 ± 5.63
H.C. northern wall	-1.22 ± 0.09	-6.30 ± 6.07	0.25 ± 3.04
H.C. eastern wall	-1.14 ± 0.21	-3.45 ± 5.36	6.06 ± 3.81
H.C. mid-slope	-0.36 ± 0.17	-6.05 ± 2.94	6.03 ± 3.58
H.C. lower slope	-0.39 ± 0.17	-1.89 ± 1.55	4.88 ± 1.08
B.C. head	-0.9 ± 0.21	-2.99 ± 2.8	3.95 ± 2.47
B.C. mid-slope	-0.46 ± 0.53	0.88 ± 0.74	2.81 ± 1.51
B.C. lower slope	-0.46 ± 0.14	2.52 ± 0.93	5.81 ± 1.34
B.C. bottom slope	-0.22 ± 0.19	-4.92 ± 2.03	3.05 ± 2.22
Plateau	-0.56 ± 0.27	-4.73 ± 3.52	0.12 ± 1.87
Headland	-0.81 ± 0.13	-6.86 ± 3.41	0.01 ± 2.29
Eastern hotspot	-0.99 ± 0.05	-1.71 ± 1.20	0.09 ± 1.69

#### 4.6.2 Lagrangian Particle Tracker

96.33% of particles released in the model domain entered the hotspot, and 99.33% of particles entered the Hood Canyon outlet (Figure 4.32, 4.33, Table 4.17). This decrease in concentration at the hotspot compared to the Hood Canyon outlet came from the 2400 m to 3000 m depth range. The Bremer Canyon had 71.85% of particles entering the section. This coincided with 50.2% of particles entering from the Hood Canyon mid-slope, which was primarily made up of 97.4% particles released between 1800 m to 2400 m.

The average velocity of particles travelling through the DC6 model domain was 3.59 cms<sup>-1</sup> westwards, with a range of velocity from 1.53 cms<sup>-1</sup> to 5.64 cms<sup>-1</sup> westwards (Table 4.18). Particle velocity was fastest between 600 m to 1200 m with an average velocity of 4.49 cms<sup>-1</sup> westwards. Particle velocity was also the slowest between 1800 m to 2400 m with an average velocity of 2.89 cms<sup>-1</sup> westwards. The average velocity for particles that were travelling through the hotspot was 13.41 cms<sup>-1</sup> ± 1.82 cms<sup>-1</sup> westwards, and the Hood Outlet was at 13.78 cms<sup>-1</sup> ± 1.56 cms<sup>-1</sup>. Feeding the Hood Canyon outlet, particles had an exit velocity of 2.61 cms<sup>-1</sup> ± 0.86 cms<sup>-1</sup> westwards from the head of the Bremer Canyon. Particles had a northwards flow velocity of 4.65 cms<sup>-1</sup> ± 0.27 cms<sup>-1</sup> from the lower slope of the Bremer Canyon, which increased to a northward

velocity of  $6.95 \text{ cms}^{-1} \pm 0.98 \text{ cms}^{-1}$  when entering the lower slope of the Hood Canyon.

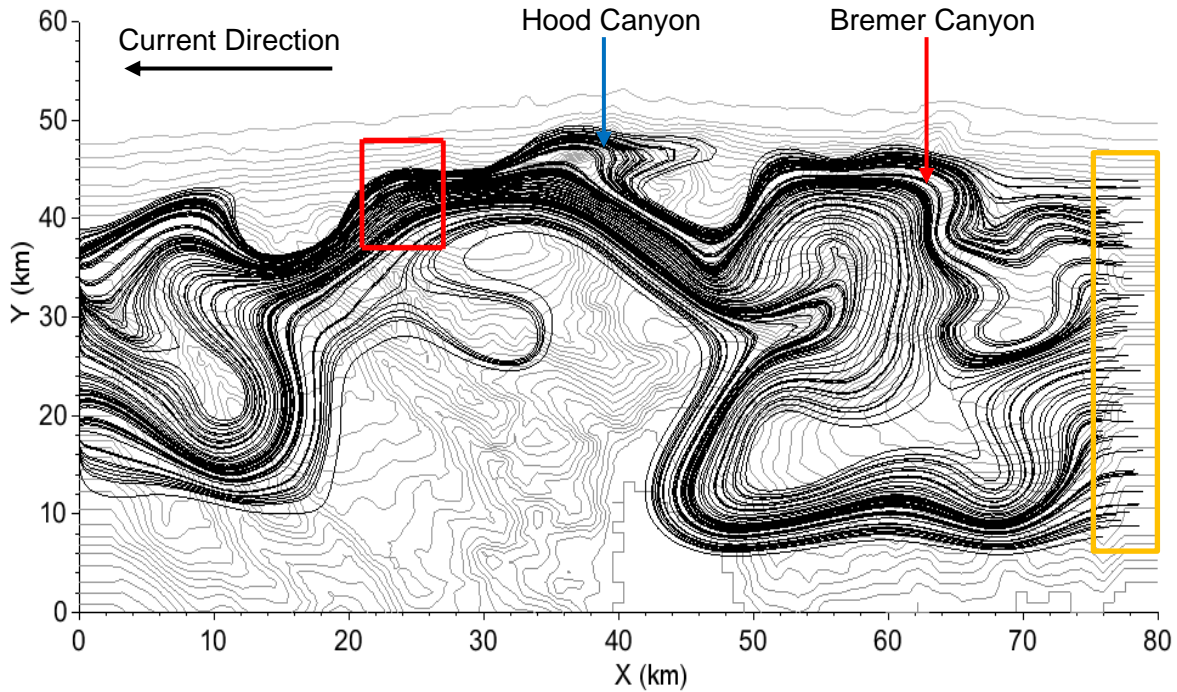


Figure 4.32: The trajectory of every 40<sup>th</sup> particle released within the eastern boundary (indicated by the orange box) for experiment DC6. The trajectory of particles is black, and the 100 m contour lines are in grey. The velocity of the fastest particle was  $5.61 \text{ cms}^{-1}$  westwards.

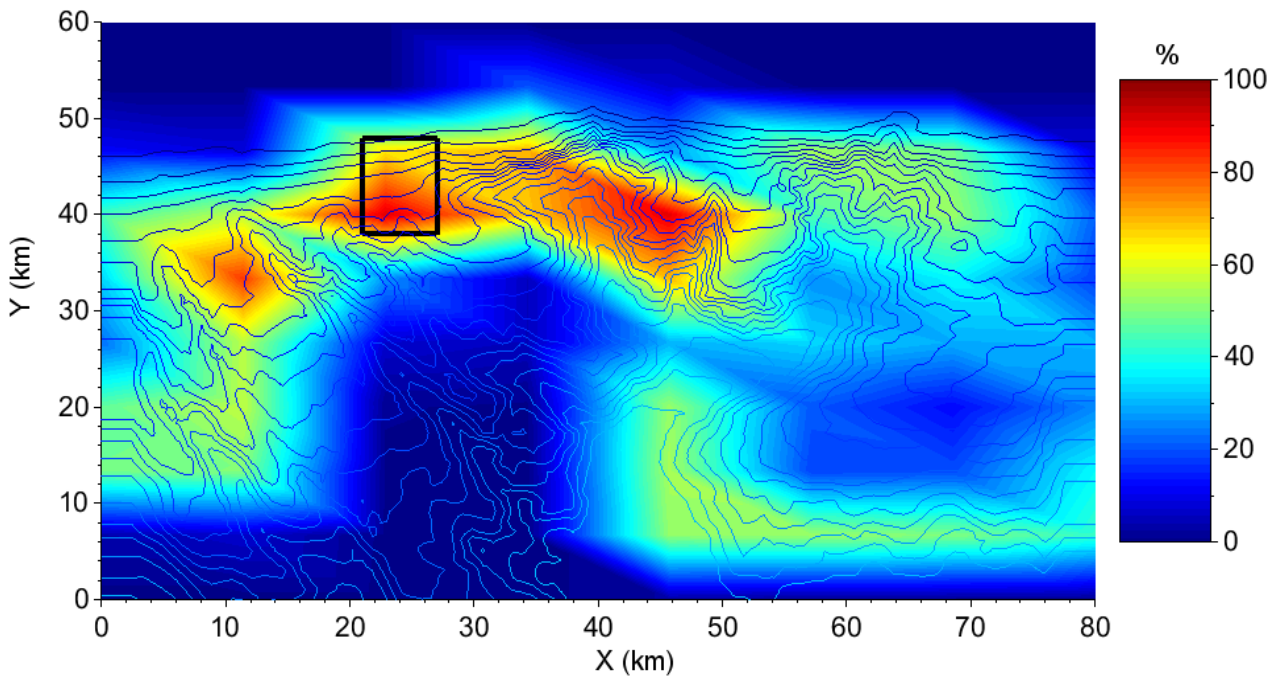


Figure 4.33: The concentration of particles travelling through the model domain for experiment DC6 with the hotspot location in a black square. The maximum concentration of particles was 91.6%, which was in the Hood Canyon outlet.

Table 4.17: Approximate percentage of particles that entered areas of interest within the DC6 model domain, as well as a breakdown on where particles originated from (Figure 4.32, and Figure 4.33). H.C. stands for Hood Canyon. B.C. stands for Bremer Canyon. PG1 consisted of particles with a starting depth of 600 m to 1200 m, PG2 was particles which had a starting depth of 1200 m to 1800 m, PG3 was particles which had a starting depth of 1800 m to 2400 m and PG4 was particles which had a starting depth that was > 2400 m.

Location	Total %	PG1 (%)	PG2 (%)	PG3 (%)	PG4 (%)
Hotspot	96.33	100	99.9	100	85.4
H.C. outlet	99.33	100	99.9	100	97.4
H.C. mid-slope	50.2	0	2.4	98.4	100
B.C. head	71.85	100	100	87.4	0
B.C. mid-slope	29.55	0	2.5	97.5	18.2
B.C. lower slope	53.9	0	15.6	100	100
Eastern hotspot	39.1	100	56.4	0	0

Table 4.18: Average time and velocity for particles released on the eastern boundary and a breakdown for each particle group. Positive values were an eastwards flow. PG1 consisted of particles with a starting depth of 600 m to 1200 m, PG2 was particles which had a starting depth of 1200 m to 1800 m, PG3 was particles which had a starting depth of 1800 m to 2400 m and PG4 was particles which had a starting depth that was > 2400 m

Particle group	Average time (days)	Minimum velocity (cms <sup>-1</sup> )	Average velocity (cms <sup>-1</sup> )	Maximum velocity (cms <sup>-1</sup> )
All	34.65	-1.53	-3.59	-5.64
PG1	20.09	-3.65	-4.49	-5.43
PG2	27.06	-1.53	-3.34	-5.64
PG3	31.24	-2.01	-2.89	-4.43
PG4	22.3	-3	-4.05	-4.95

#### 4.7 Glider Temperature and Salinity Data

The average temperature of the hotspot from the IMOS ocean glider was 10.42°C, which cooled down to an average of 6.33°C from 500 m onwards (Figure 4.34). In the same depth range, the average salinity for the hotspot was 34.82 PSU (Figure 4.35), which became fresher as it approached 500 m. After 500 m the average salinity was 34.44 PSU. This differed from the Hood Canyon outlet which had an average temperature of 10.89°C and after 500 m had a temperature of 6.43°C. The average salinity in the Hood Canyon outlet was 34.87 PSU which lowered to 34.44 PSU below 500 m. The difference was that the hotspot was on average 0.47°C colder throughout the depth profile and below 500 m the difference in temperature was on average 0.10°C colder. The average difference between the two profiles in salinity was that the hotspot was 0.05 PSU fresher, however below 500 m that difference lowers to  $2.0 \times 10^{-3}$  PSU. Below 650 m this change gets smaller with the difference between the hotspot and outlet being  $\sim 0.03^\circ\text{C}$ . The reference area had an average temperature of 11.61°C, which was 0.91°C warmer than the hotspot (Figure 4.34). The reference area had an average salinity of 34.92 PSU which was 0.08

PSU saltier than the hotspot (Figure 4.35). Below 500 m the average temperature cooled to 6.92°C for the reference area, however, it was still 0.38°C warmer than the hotspot. From 750 m onwards, the reference area was 0.14°C warmer. Below 500 m the reference area was at an average salinity of 34.48 PSU, which was 0.04 PSU saltier than the hotspot. When below 750 m the hotspot was fresher than the reference area by  $8.3 \times 10^{-4}$  PSU.

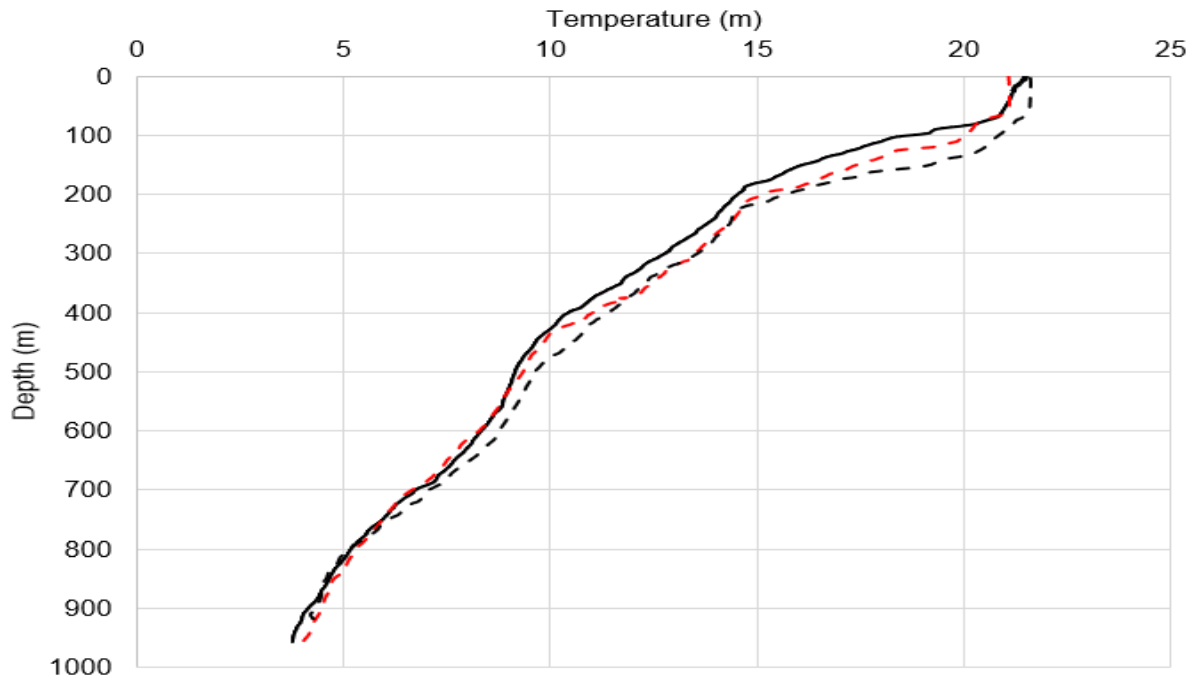


Figure 4.34: Comparison of temperatures against depth for the hotspot (black dotted line), the reference area (red dotted line) and the Hood Canyon outlet (black). The maximum depth for the hotspot was 959.18 m, reference area was 918.31 m and the Hood Canyon outlet was 958.45 m. The total change in temperature for the Hotspot throughout this profile was 17.39°C, the reference area had a change of 17.47°C while the Hood Canyon outlet had an average change of 17.07°C.

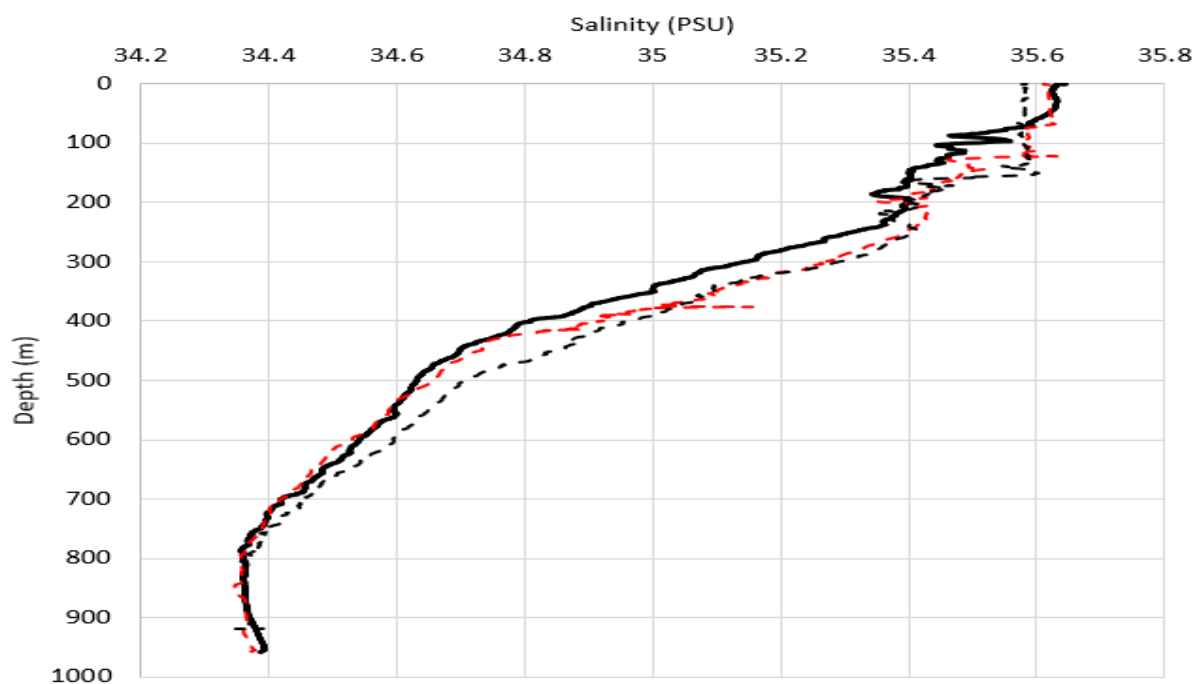


Figure 4.35: Comparison of salinity against depth for the hotspot (dotted line) and the Hood Canyon outlet. The total salinity change for the hotspot was 1.3 PSU, which was slightly higher than the Hood Canyon outlet as it had an average change of 1.28 PSU. The maximum change in salinity for the reference area was 1.28 PSU, which was slightly lower than the hotspot salinity change.

## CHAPTER 5 DISCUSSION

### 5.1 Shelf Break Experiments

The altimetry data obtained between 1993 to 2015 for Albany, Bremer Bay and Esperance showed that the Leeuwin Current was dominant between April to September. During October to March, the data showed that a localised coastal current could supersede the Leeuwin Current. October and March tended to be transitional months in Albany and Bremer Bay, while Esperance had November as its transitional month. This weakening in the Leeuwin Current was observed in other research undertaken in the western Great Australian Bight (Rochford, 1986, Feng et al., 2003, Ridgway and Condie, 2004, Koslow et al., 2008). The formation of a coastal current in altimetry data has also been observed in the western Great Australian Bight (Ridgway and Condie, 2004, Pattiaratchi, 2007, Mondello, 2017). The coastal current formed events from 8.26 weeks in Albany to 11.32 weeks in Esperance; however, the average velocity of events in Albany was  $9.46 \text{ cms}^{-1}$  westwards which decreased to a velocity of  $7.58 \text{ cms}^{-1}$  westwards in Esperance. This could be result of the Leeuwin current receding in the summer months, as it is indicating that weaker westwards current is able to form the more east a location is (Ridgway and Condie, 2004, Pattiaratchi, 2007, Mondello, 2017). The width of this coastal current ranged from 167 km to 189 km which was within the 150-200 km range of widths that Ridgway and Condie (2004) gave for this coastal current.

After 60-days of run time with a westwards current in the southern hemisphere, SB1 showed that the Whale and Bremer Canyon had the necessary structure to force particles into the continental shelf from where the canyons are located, with 71.76% and 83.58% of the particles being upwelled into the continental slope respectively from between 100 m to 1000 m. This indicates that a difference of  $> 300 \text{ m}$  of water depth between the canyon and the surrounding continental slope, a width ranging from 2.5 km to 9 km and a slope of  $5.95^\circ$  meet the deep, steep and narrow conditions to support upwards movement of water particles (Hickey, 1997, Allen et al., 2001, Allen and Durrieu de Madron, 2009, Allen and Hickey, 2010).

When an eastwards flow was present in the southern hemisphere in SB2 neither the Whale nor Bremer Canyon supported any particles upwelling into the continental shelf. As this was designed to imitate the Leeuwin Current, which is a current that acts to transport warm water poleward and should prevent any upwelling from occurring; it indicates that the modelling is replicating what occurs in real life. Despite the same change in sea level, and run time however, the eastwards flow in SB2 ended up being slower than SB1 by  $0.52 \text{ cms}^{-1}$  which could also indicate that the Bremer and Whale Canyon are acting to speed up current flow when an upwelling conducive current is present.

When the model was switched to the northern hemisphere for SB3 and SB4, the eastwards flow in SB4 ended up upwelling 50.58% and 41% of released particles when interacting with the Bremer and Whale Canyon, and the westwards flow prevented any upwelling from occurring. This was the expected result from these models as the switch of hemispheres should cause the flow in the opposite direction to upwell/downwell (Hickey, 1997, Allen et al., 2001). Despite the similar sea level gradient to SB1, there was a decrease of >20% of particles which were upwelled in the northern hemisphere, with upwelling being localised between particles which were in a starting depth range of 100 m to 300 m. A potential reason for why there is a decrease in particles being upwelled could be due to both the Whale and Bremer Canyon being steeper on the western side of the canyon by  $> 5^\circ$  compared to the eastern side. This drop off in steepness at the back wall of the canyon could be impacting the amount of force generated by the stretching and squashing motion of water particles by allowing particles to gradually adjust to the depth gradient, though future research is needed to test out this idea of how an asymmetric canyon drives flow.

Experiments SB5 and SB6 focused on altering the sea level gradient present in SB1, with the intention of at least calculating a range of velocities which could support upwelling. The doubling of this sea level gradient lead to an overall increase of particle velocity of  $5.78 \text{ cms}^{-1}$  throughout SB5. As a result of this increase, the number of particles which upwelled by the Bremer Canyon increased by 7.7% to 91.28% and upwelling from the Whale Canyon increased by 1.6% to 73.28% of particles being upwelled. This result wasn't expected as both canyons should have been increasing at a similar rate with the increase of velocity, as the change in depth is  $\sim 300 \text{ m}$  for both canyons around the area the flow would have been entering. A potential reason for the change is due to the larger width in the Bremer Canyon might be the driver, being 2.5 km to 4 km wide instead of 0.3 km to 0.8 km, however that goes against the narrow component that Hickey (1997) stated. It could indicate there is an ideal length for a narrow canyon in idealised modelling instead of the narrower the better. Decreasing the sea level gradient by half however does not make any difference to the zonal velocity of particles, and equally, the % of upwelled particles remained the same in both canyons compared to SB1. This indicates with that this % of upwelled particles is potentially the lowest it will get whilst there is a westwards velocity which is capable of supporting upwelling. Overall, in an idealised two-dimensional model, the range of average particle velocity which can support upwelling in the Bremer and Whale Canyon is  $4.51 \text{ cms}^{-1}$  westwards to  $10.39 \text{ cms}^{-1}$  westwards. This indicates the average event velocity measured for coastal current events in Albany, Bremer Bay and Esperance would support upwelling in these canyons. This does not cover the maximum westwards velocity that Cresswell and Domingues (2009) observed which was  $25 \text{ cms}^{-1}$  as a daily current speed, though it was considered that focusing on average weekly velocities was a better representation of if upwelling could occur.

The minimum velocity in SB1 and SB6 occurred in between 300 m to 400 m at  $4.03 \text{ cm s}^{-1}$  westward. This minimum velocity did not reflect what occurs in the ocean, as the westwards Flinders Current would form at around 300 m (Bye, 1983, Middleton and Cirano, 2002, Arthur, 2006, Ridgway and Dunn, 2007, Middleton and Bye, 2007). A reason for this lack of Flinders Current formation was due to the model only having one layer, and from that was unable to account for the formation of the Flinders Current. Conversely, SB2 follows what occurs in the Leeuwin Current in the upper 300 m with the eastward velocity slowing down as depth increases (Church et al., 1989, Arthur, 2006). Considering that it was a one-layer model, particle velocity slowing down at depths  $> 300 \text{ m}$  is an acceptable compromise that reflects the upper-conditions in the western Great Australian Bight.

In temperature and salinity profiles taken on early February 2019 (locations of stations are in Figure 2.10), a decrease of temperature of  $\geq 2^\circ\text{C}$  had occurred between 49.44 m to 59.29 m in station one, and 52.73 m to 61.09 m in station two. This decrease is expected if a flow is being stretched into the canyon, mixing with deeper water, and then generating enough uplift to enter the continental shelf (Kämpf and Chapman, 2016). An issue arose though as stations 3, 4, 5 and 6 also had a  $\geq 2^\circ\text{C}$  decrease of temperature within a similar depth range which indicates that for at least when this data was taken, that change was not caused by a sub-surface upwelling event from a canyon, but a thermohaline adjustment. It does throw into doubt the possibility of a sub-surface upwelling event being localised in the continental shelf, via a topographic Rossby wave. It is worth noting that it is likely that any temperature and salinity data would need to be expanded on in future research, as there is a possibility that the canyon was not under event conditions.

Another factor is a topographic Rossby wave would be supporting growth by increasing the concentration of phytoplankton within the euphotic zone. However, the likely food source for orcas in the region baleen whales and squid. Both baleen whales and squid predate on creatures which are benthic in origin and would not respond to changes in phytoplankton concentration (MacLeod et al., 2003, Wellard et al., 2016, Meeuwig and Turner, 2017). Orca sightings also tend to be focused around the 1000 m depth contour. This is  $\sim 900 \text{ m}$  deeper than the continental shelf, which indicates that orcas are not aggregating here due to any biological response occurring in the shelf. Despite the Whale and Bremer Canyon having the potential structure which is capable of forming of a topographic Rossby wave, the likely prey, the thermohaline adjustment and the depths that orcas are sighted makes it unlikely that an upwelling event caused by the formation of a topographic Rossby wave is the root cause for orcas to migrate to the western Great Australian Bight.

## 5.2 Deep Upwelling Experiments

DC1 supported a current which had an average particle velocity of  $8.06 \text{ cms}^{-1}$  westwards throughout its sixty-day run time, which was  $1.94 \text{ cms}^{-1}$  slower than the average velocity of the Flinders Current (Arthur, 2006, Middleton and Bye, 2007). This was considered acceptable, as it was expected that particles would lose some velocity as they interacted with the Bremer and Hood Canyon. This current flow ended up resulting in 90.48% of released particles entering the Hood Canyon outlet and 89.1% of particles to enter the hotspot, with the difference being that an 5.3% of particles released between 2400 m to 3000 m bypassed the hotspot to the south after entering the outlet. This indicated that when the Flinders Current enters the Bremer and Hood Canyon, the flow is able to be manipulated by interacting with the topology and exit out into the orca hotspot, which in turn, could be used for marine organisms to use as a pathway to travel northwards in the canyon (Hickey, 1997, Allen et al., 2001, Allen and Durrieu de Madron, 2009, Allen and Hickey, 2010).

An intriguing result that is paired with 90.48% of particles entering the outlet is that 55.8% of released particles entered the Bremer Canyon via its lower slope including 25% of the particles released from 1200 m to 1800 m. Seeing the expectation was that particles would enter the canyon at, or near their starting depth, it's likely that the eddy which formed to push particles southwards is a model artefact, though it was decided that it was more a nice coincidence as it pushed particles into the areas this study was interested in. >75% of particles which entered the Bremer Canyon lower slopes would end up in the Hood Canyon outlet, which was backed up by the entirety of the Hood and Bremer Canyon supporting a northwards flow ranging from  $0.01 \text{ cms}^{-1} \pm 13.7 \text{ cms}^{-1}$  to  $12.72 \text{ cms}^{-1} \pm 3.18 \text{ cms}^{-1}$ . To create an upwards flow in a canyon, there needs to be upwelling conducive conditions (Macquart-Moulin and Patriti, 1996, Hickey, 1997, Allen et al., 2001, Genin, 2004), and an interaction between a current and the change in topography to form an inertial wave, which will in-turn flow towards the shelf (Shepard et al., 1974, Gordon and Marshall, 1976). The interaction which drove this likely inertial wave formation was particles entering from the plateau into the lower slopes. This would increase the amount of water flowing into the lower slope of the Bremer Canyon as the model runs. The reason why the flow was prevented from moving westwards was that the western wall of the Bremer Canyon was  $4.02^\circ$  steeper than the entry point from the plateau, which was steep enough to prevent any alongshore flow in the canyon, a pre-requisite for upwelling (Klinck, 1996, Dawe and Allen, 2010). The Hood Canyon outlet was only  $0.5^\circ$  degrees less steep than the western wall of the Bremer Canyon, however, the northern and eastern walls of the Hood Canyon were  $4.67^\circ$  and  $4.24^\circ$  steeper than the outlet, making outflowing into the hotspot the easiest path to travel for particles.

A factor that also supports the notion that the canyons topography was the defining factor of why an upwelling flow was occurring, was in DC4 which was based on having upwelling conducive flow in the northern hemisphere. Only 53.6% of particles entered the eastern equivalent of the

hotspot, with only 16 % of particles released between 1800 m to 2400 m managing to push up that far north. Upwelling was prevented due to the mid-slope of the Bremer Canyon acting as an exit point for particles released at depths  $\geq 1800$  m instead of travelling into the head of the Bremer Canyon. The reasons why the mid-slope of the Bremer Canyon acted as an exit point was due to a sharp bank northward when it moved towards the head of the canyon, as well as an average eastward Eulerian velocity of  $18.16 \text{ cms}^{-1} \pm 4.27 \text{ cms}^{-1}$  which did not give particles enough time to adjust to the change of direction in the canyon.

Once particles entered the Hood Canyon, it acted as a catalyst for the formation of a localised jet into the hotspot, with average velocity ranging from  $16.02 \text{ cms}^{-1}$  to  $21.83 \text{ cms}^{-1}$  westwards. This was an increase of  $7.96 \text{ cms}^{-1}$  to  $13.77 \text{ cms}^{-1}$  on the average particle velocity. The meridional direction of flow reversed in the hotspot, having a southward Eulerian velocity of  $13.9 \text{ cms}^{-1} \pm 10.9 \text{ cms}^{-1}$ , indicating particles are being pushed back towards their starting depths. Despite the mid-slope of the Bremer Canyon preventing upwelling, an eastward jet forms in the head of the Bremer Canyon with a Eulerian velocity of  $18.81 \text{ cms}^{-1}$ , before having a southward velocity of  $> 10 \text{ cms}^{-1}$  once out of the canyon. The formation of this jet did not occur in experiments DC2 and DC3 which were designed to support a downwelling conducive flow. This indicates this jet formation is reliant on upwelling conditions, though due to its formation in DC4, it is not likely to be reliant on a northward movement of water in the canyon. It is likely that this jet forms in a similar manner to a topographic Rossby wave, in that water entering from the headland enters the canyon stretches, proceeds to mix with the deeper water, then squashes which is causing an acceleration of particles.

When downwelling conditions were present for the southern hemisphere (DC2), 46% of particles were counted to have passed through the head of the Bremer Canyon, which was made up of 81.2% of particles released between 600 m to 1800 m. The Bremer mid-slope had 37.13% of particles pass through the area, with  $< 20\%$  of the particles released between 600 m to 1800 m. A similar trend was seen in the northern hemisphere (DC3) where whilst 86.55% of particles entered the head of the Bremer Canyon, however only 13.35% and 13.98% entered the lower slope and the mid-slope of the Bremer Canyon respectively. This indicates that either downwelling is creating a minor downwards/southwards flow in the canyon or it is not at all. This result is surprising seeing that the expected result was a downwards flow path forming for detritus to support life in the canyon (Stefanescu et al., 1994, Cartes et al., 1994, Vetter and Dayton, 1998, Vetter and Dayton, 1999, Moors-Murphy, 2014).

DC5 and DC6 were focused around giving a range of velocities which can cause upwelling to occur in the Bremer and Hood Canyon. The average particle velocity in DC5 was  $6.6 \text{ cms}^{-1}$  faster than the Flinders Current, and  $8.54 \text{ cms}^{-1}$  faster than DC1. Despite this increase in velocity, the number of particles that entered the hotspot and Hood Canyon outlet had decreased by 29.1%

and 15.5% respectively. One reason for this decrease is that < 5% of particles released at depths  $\geq 2400$  m entered either of the hotspot, or Hood Canyon outlet, instead having enough zonal velocity to exit just after it entered the Hood Canyon mid-slope, or to even enter the Henry Canyon instead of being pushed upwards in the Bremer Canyon. Another cause for the decrease in particles entering the hotspot was from 49.2% of particles released between 600 m to 1200 m being able to exit the Hood Canyon by the northern wall of the canyon, compared to 100% in DC1. This might be due to generating enough meridional/downward velocity in this case that when vorticity spun it back upwards, it had enough force to overcome the steeper northern wall, instead of using that wall like a half-pipe. DC6 ended up supporting an average velocity of  $7.41 \text{ cms}^{-1}$  slower than the Flinders current, and  $4.47 \text{ cms}^{-1}$  slower than DC1. This slower average velocity ended up increasing the number of particles which entered both the hotspot and Hood Canyon outlet by 7.22% and 8.85% respectively, which indicates that its easier for a flow to upwell due to a canyons topography if the entering velocity is slower. It is worth mentioning that it potentially could take too long to traverse through the canyon to support upwelling if it becomes too slow, though that is beyond the scope of these models.

Comparing temperature and salinity data from the 2012 glider profile, the hotspot was colder compared to the Hood Canyon by  $0.44^\circ\text{C}$  throughout the 959 m profile however this change decreased to  $0.03^\circ\text{C}$  once past 650 m. The hotspot being colder than the Hood Canyon was surprising seeing that if a pathway had formed, the temperature between the outlet and hotspot should be near identical, though below 650 m is very promising in this regard. Compared to the reference location however, the hotspot was on average  $0.91^\circ\text{C}$  colder and 0.08 PSU fresher throughout, with depths  $\geq 750$  m still having the hotspot cooler by  $0.14^\circ\text{C}$  on average. This backs up the assertion that the hotspot could be getting fed colder water from the Hood Canyon outlet, though the change isn't large enough to be definite indicator of a pathway forming in the area (Allen et al., 2001, Rennie et al., 2007, Connolly and Hickey, 2014).

### 5.3 Improvements/Justification

An issue which occurred in all experiments was that the northern boundary did not decrease by the planned amount, which potentially caused model simulations to underestimate velocity. It was unlikely that this had any impact on results other than to influence the number of particles which were trapped (Table 7.1, 7.2). This was due to the sea level elevation calculations not reaching a true steady state after six days and instead being stopped prior due to models becoming unstable with a longer run time of sea elevation. The SB models also had the depth increased to 100-200 m on the most northern row due to an error in the model which may have lessened the sea level gradient. This was likely either an error from how the bathymetries were melded, or an issue with the calculation to condense the bathymetry for the shelf break model. However, as this was

occurring at the point where the sea level change is forced and due to time constraints, it was included.

Even though the cubic convolution technique was used to smooth out the composite bathymetry, it did create the occasional difference in depth which resulted in a slope that was  $> 60^\circ$  where the converted GEBCO data was placed. This usually occurred in areas where only a small amount of GEBCO data was needed to fill out an area that was surrounded by high-resolution data. As the composite bathymetry was condensed for both shelf break experiments and deep canyon experiments, this issue potentially impacted both Eulerian and particle velocity.

An issue with this model was that the northern hemisphere was more unstable than the southern hemisphere. To get these models running, the time given for the model to calculate sea level elevation was decreased to four and a half days for SB3, SB4, DC3 and DC4. In addition, a calculation to assist with making the sea level elevation uniform on the northern boundary was turned off. To confirm the results obtained in SB4, DC3 and DC4, a model which was not based on the COHERENS framework should be used. They were included due to time constraints, and seeing that less time spent iterating the sea level gradient would result in slower particle velocities, they could still be an adequate representation of what is occurring if a canyon with a similar structure to the Bremer and Hood Canyon was found in the northern hemisphere.

An improvement would be to devise a method that can calculate the average northward particle velocity for every particle released. When compared to using a random sub-set of particles, it would make any northwards velocity measurement more accurate due to a larger sample size. Another potential improvement would be a method that assigned the original depth to each particle instead of using a range of depths, which could be used in conjunction with the percentage of particles entering an area to better show if upwelling is occurring.

A potential improvement in the shelf break modelling was that the model domain should have been expanded by 5-7 km to the east. By doing this, it would have allowed neutrally buoyant particles more time to adjust the calculated velocity field prior to the Whale Canyon, which could have increased the amount of upwelling occurring with a westward flow for SB1, SB5, and SB6. It also would have made it easier to determine the length of a topographic wave if it formed when an eastward current was present. Considering neither SB2 nor SB4 did end up supporting upwelling from the Whale Canyon, the end result of this change would have a visual change with an eastwards flow.

The temperature and salinity profiles from the ocean glider were not deep enough to be a proper test for if upwelling was occurring at the depths the deeper upwelling study was primarily focused on, which was 1000 m to 1400 m. This was due to the IMOS Ocean Glider having a maximum sampling depth of 1000 m (Woo, 2019). An improvement on this would be organise measuring

the temperature and salinity at depths > 1000 m in the area in and around the Bremer and Hood Canyons.

Another factor that would improve the quality of results would be to increase the amount of orca sighting surveys, which would help better identify where points of interest are in the western Great Australian Bight. This would show if orcas are concentrating in areas that are experiencing a higher amount of prey concentration, and from that, it would give a clearer indication if this migration was due to region specific changes, or isolated to topographic structure within a region. Expanding the number of orca sightings could potentially remove any accidental bias which could have occurred, as the majority of sightings originate from ecotourism ventures, which focus on areas they know to be a reliable source of sightings. In addition to expanding on orca sightings, expanding research on what prey was being hunted, as well as the frequency of prey that orcas predate on would also prove beneficial to confirm if the orcas are there to feed on an increase in productivity in the benthic zone. This could be expanded further by investigating the migration path of this pod of orcas, as well as what they are predated on in any other locations that they visit, as pods of orcas tend to be specialised in what they hunt (Ford, 2009). Confirming if there was an increase in biological productivity in the benthic zone would help to solidify if a deeper upwelling event were the reason orcas migrate to the western Great Australia Bight.

As the Hood and Bremer Canyon structure can support an upwelling flow, the next step in model development would be the addition of a density layer to the deeper upwelling modelling, as changes in density can influence upwelling. Another addition would be to add different flow directions, which would enable the Indian Deep Ocean Boundary Current to be included in this model. This current could be affecting upwelling of particles released at depths > 1500 m (Tamsitt et al., 2019).

The importance of this research is that, whilst it is an idealised model, it does make some progress to unravelling the mystery behind why orcas are migrating to the western Great Australian Bight in the austral summer. Solving this is important as it expands on the knowledge on what drives orca migratory patterns as well as expanding on how topographic features can support them. Identifying the mechanisms which is causing this migration is also important to marine park management as this study was focused on an area just outside of the Bremer commonwealth marine park (Figure 1.5), in which expanding the protection to include the study area could protect this migration from mining and exploration for resources. Expanding the marine park protection could also have the flow on effects of helping to safeguard the tourism industry which supports 14.1% of jobs in regional West Australia (Tourism Western Australia, 2018), as whale watching is a drawcard to the region.

## CHAPTER 6 CONCLUSION

The aim of this thesis was to test if upwelling events could be caused by any of the Bremer, Hood and Whale Canyons and if this is the reason why orcas are aggregating in the western Great Australian Bight. There were two hypothesises with how upwelling could form from these canyons. The first being the formation of a topographic Rossby wave which could support an upwelling event in the lower continental shelf. The second being that the Flinders Current may cause an upwelling event through the canyons at depth.

For a topographic Rossby wave to occur a coastal current must replace the Leeuwin Current in between October to March. This occurred in “events”, with an event defined as a minimum of 3 successive weeks in October to March, with all weeks having an average current velocity of  $> 2.5 \text{ cms}^{-1}$  westwards. Off the Bremer Bay coastline, there was on average 11.77 weeks in a year where the coastal current had formed (Figure 3.2). The average velocity for an event that occurred off the Bremer Bay coastline was  $8.71 \text{ cms}^{-1}$  westwards.

To test if a topographic Rossby wave could form in the western Great Australian Bight, a model using a particle velocity that was similar to the average coastal current velocity, showed that 71.76% and 83.58% of particles were upwelled on to the continental shelf from the Whale and Bremer Canyon respectively from the canyon (Figure 3.10). This showed that both the Whale and Bremer Canyon have the necessary structure to cause upwelling. When using differing sea level elevations to vary particle velocity, it was found that upwelling was supported between  $4.51 \text{ cms}^{-1}$  westwards to  $10.77 \text{ cms}^{-1}$  westwards in the southern hemisphere (Figure 3.30, 3.35, Table 3.15, 3.18).

Temperature and salinity data showed that the water column had a decrease of  $> 2^{\circ}\text{C}$  within a depth range of 30 m to 70 m, regardless of the depth individual measurements were taken. This occurrence is likely to be a result of thermohaline expansion instead of a topographic Rossby wave, as a topographic Rossby wave would have caused a localised decrease in sea water temperature (Figure 3.37, 3.38, 3.39). When also factoring in what prey drives this orca aggregation was likely to originate from deeper in the water column in origin, and thus would not be affected by an increase of phytoplankton concentration which would occur if an upwelling event was formed by a topographic Rossby wave. Orca sightings tend to be around the 1000 m depth contour which indicates they are not preying on marine organisms which are reliant on phytoplankton (Wellard et. al., 2016). Whilst this does not rule out a topographic Rossby wave forming, it does make it unlikely it is the root cause of why orcas are migrating to the western Great Australia Bight.

To test if a deeper upwelling event was occurring, a model which had a similar velocity to the Flinders Current was used. From this 89.1% of particles entered the area where the highest concentration of orca sightings occurred (“hotspot”), which contained 100% of particles that were released from depths < 2400 m. This indicates that the Flinders Current can travel through the Bremer and Hood Canyon structure to cause an upwelling event. When a downwelling conducive flow was present in the model domain, the Bremer and Hood Canyon only supported a minimal downwelling of particles. When the northern hemisphere was simulated with upwelling conditions, upwelling was prevented by particles being able to exit the Bremer Canyon prior to entering the head of the canyon. When varying the change in sea level elevation, upwelling occurred with velocities ranging from 3.59 cms<sup>-1</sup> westwards to 16.6 cms<sup>-1</sup> westwards.

For temperature data taken below 650 m of depth, the hotspot was 0.03°C cooler than the head of the Hood Canyon. The difference in salinity after 650 m of depth was that the hotspot was fresher by 2.0x10<sup>-3</sup> PSU. Compared to a reference location to the west of the Hood Canyon, the Hood Canyon was 0.14°C cooler, and fresher by 8.3x10<sup>-4</sup> PSU after 750 m of depth. These results indicated that the Hood Canyon was feeding water into the hotspot, and that this caused a pool of cooler water forming in the hotspot, when compared to the reference area. The formation of colder water supports the modelling that indicates the Bremer and Hood Canyon is upwelling deeper water.

To answer the question “does an upwelling event form from a current interacting with a canyon in the western Great Australian Bight?”, the Bremer and Hood Canyon has the structure to support deep water being upwelled into the area orcas are aggregating. This upwards movement could be acting to give a pathway for deeper creatures to end up in an area where they can be predated on.

## BIBLIOGRAPHY

- Ahumada-Sempoal, M.-A., Flexas, M. D. M., Bernardello, R., Bahamon, N., Cruzado, A. & Reyes-Hernández, C. 2015. Shelf-slope exchanges and particle dispersion in Blanes submarine canyon (NW Mediterranean Sea): A numerical study. *Continental Shelf Research*, vol. 109, pp. 35-45, DOI: 10.1016/j.csr.2015.09.012
- Allen, J.S., Newberger, P.A. and Federiuk, J., 1995. Upwelling circulation on the Oregon continental shelf. Part I: Response to idealized forcing. *Journal of Physical Oceanography*, vol. 25, no. 8, pp.1843-1866, DOI: 10.1175/1520-0485(1995)025<1843:UCOTOC>2.0.CO;2
- Allen, S. E. 1996. Topographically generated, subinertial flows within a finite length canyon. *Journal of Physical Oceanography*, vol. 26, no. 8, pp. 1608-1632, DOI: 10.1175/1520-0485(1996)026<1608:TGSFWA>2.0.CO;2.
- Allen, S., Vindeirinho, C., Thomson, R., Foreman, M. G. & Mackas, D. 2001. Physical and biological processes over a submarine canyon during an upwelling event. *Canadian Journal of Fisheries and Aquatic Sciences*, vol. 58, no. 4, pp. 671-684, DOI: 10.1139/f01-008.
- Allen, S. E., Dinniman, M., Klinck, J., Gorby, D., Hewett, A. & Hickey, B. 2003. On vertical advection truncation errors in terrain-following numerical models: Comparison to a laboratory model for upwelling over submarine canyons. *Journal of Geophysical Research: Oceans*, vol. 108, no. C1, pp. 3-1-3-16, DOI: 10.1029/2001JC000978.
- Allen, S. & Durrieu De Madron, X. 2009. A review of the role of submarine canyons in deep-ocean exchange with the shelf. *Ocean Science*, vol. 5, no. 4, pp. 607-620, DOI: 10.5194/os-5-607-2009
- Allen, S. E. & Hickey, B. 2010. Dynamics of advection-driven upwelling over a shelf break submarine canyon. *Journal of Geophysical Research: Oceans*, vol. 115, no. C8, pp. 1-20, DOI: 10.1029/2009JC005731.
- Ardhuin, F., Pinot, J.M. and Tintoré, J., 1999. Numerical study of the circulation in a steep canyon off the Catalan coast (western Mediterranean). *Journal of Geophysical Research: Oceans*, vol. 104, no. C5, pp. 11115-11135, DOI: 10.1029/1999JC900029
- Arthur, W. C. 2006. 'The Flinders Current and Upwelling in Submarine Canyons', MSc thesis, University of New South Wales, NSW, <http://unsworks.unsw.edu.au/fapi/datastream/unsworks:1363/SOURCE02?view=true>

- Auclair, F., Marsaleix, P. and Estournel, C., 2000. Sigma coordinate pressure gradient errors: evaluation and reduction by an inverse method. *Journal of Atmospheric and Oceanic Technology*, vol. 17, no. 10, pp.1348-1367, DOI: 10.1175/1520-0426(2000)017<1348:SCPGEE>2.0.CO;2
- Barrett-Lennard, L. G. & Heise, K. A. 2006. The natural history and ecology of killer whales. Whales, whaling, and ocean ecosystems. University of California Press, Berkeley, CA, 163-173. ISBN: 978-0-520-93320-0
- Bazzino, G., Gilly, W. F., Markaida, U., Salinas-Zavala, C. A. & Ramos-Castillejos, J. 2010. Horizontal movements, vertical-habitat utilization and diet of the jumbo squid (*Dosidicus gigas*) in the Pacific Ocean off Baja California Sur, Mexico. *Progress in Oceanography*, vol. 86, no 1-2, pp. 59-71, DOI: 10.1016/j.pocean.2010.04.017.
- Blevin, J. 2005. Geological framework of the Bremer and Denmark sub-basins, southwest Australia, R/V Southern Surveyor Survey SS03/2004, Geoscience Australia Survey 265, post-survey report and GIS. Geoscience Australia, Record, 5, ISBN: 1 920871 30 6.
- Boyer, D.L., Haidvogel, D.B. and Pérenne, N., 2004. Laboratory–numerical model comparisons of canyon flows: A parameter study. *Journal of Physical Oceanography*, vol. 34, no. 7, pp.1588-1609, DOI: 10.1175/1520-0485(2004)034<1588:LMCOCF>2.0.CO;2
- Boyer, D. L., Sommeria, J., Mitrovic, A. S., Pakala, V. C., Smirnov, S. A. & Etling, D. 2006. The effects of boundary turbulence on canyon flows forced by periodic along-shelf currents. *Journal of Physical Oceanography*, vol. 36, no. 5, pp. 813-826, DOI: 10.1175/JPO2866.1.
- Bradshaw, B. E. 2003. A revised structural framework for frontier basins on the southern and southwestern Australian continental margin, Geoscience Australia, Department of Industry, Tourism & Resources, ISBN 0 642 46761 7.
- Brault, S. & Caswell, H. 1993. Pod-specific demography of killer whales (*Orcinus orca*). *Ecology*, vol. 74, no. 5, pp.1444-1454, DOI: 10.2307/1940073.
- Bye, J. A. 1983. The general circulation in a dissipative ocean basin with longshore wind stresses. *Journal of Physical Oceanography*, vol. 13, no. 9, pp. 1553-1563, DOI: 10.1175/1520-0485(1983)013<1553:TGCIAD>2.0.CO;2.
- Bye, J. A. 1986. Simulation of shelf-averaged water properties with application to the south coast of Australia. *Estuarine, Coastal and Shelf Science*, vol. 23, no. 3, pp. 317-338, DOI: 10.1016/0272-7714(86)90031-4.
- Cartes, J., Company, J. & Maynou, F. 1994. Deep-water decapod crustacean communities in the Northwestern Mediterranean: influence of submarine canyons and season. *International Journal on Life in Oceans and Coastal Waters*, vol. 120, pp. 221-229. DOI: 10.1007/BF00349682

Castelao, R.M. and Luo, H., 2018. Upwelling jet separation in the California Current System. *Scientific reports*, vol. 8, no. 1, pp.1-8. DOI: 10.1175/2007JPO3679.1

Chapman, D.C. and Lentz, S.J., 2005. Acceleration of a stratified current over a sloping bottom, driven by an alongshelf pressure gradient. *Journal of Physical Oceanography*, vol. 35, no. 8, pp.1305-1317, DOI: 10.1175/JPO2744.1

Chen, Z., Yan, X.H. and Jiang, Y., 2014. Coastal cape and canyon effects on wind-driven upwelling in northern Taiwan Strait. *Journal of Geophysical Research: Oceans*, vol. 119, no. 7, pp.4605-4625. DOI: 10.1002/2014JC009831

Church, J. A., Cresswell, G. R. & Godfrey, J. S. 1989. The Leeuwin Current. Poleward flows along eastern ocean boundaries. Springer, ISBN: 978-1-4613-8965-1.

Clavel-Henry, M., Solé, J., Ahumada-Sempoal, M.Á., Bahamon, N., Briton, F. and Rotllant, G., 2019. Influence of the summer deep-sea circulations on passive drifts among the submarine canyons in the northwestern Mediterranean Sea. *Ocean Science*, vol. 15, no. 6, pp. 1745-1759, DOI: 10.5194/os-15-1745-2019

Connolly, T. P. & Hickey, B. M. 2014. Regional impact of submarine canyons during seasonal upwelling. *Journal of Geophysical Research: Oceans*, vol. 119, no. 2, pp. 953-975, DOI: 10.1002/2013JC009452.

Cresswell, G. R. & Golding, T. 1980. Observations of a south-flowing current in the southeastern Indian Ocean. *Deep Sea Research Part A. Oceanographic Research Papers*, vol. 27, no. 6, pp. 449-466, DOI: 10.1016/0198-0149(80)90055-2.

Cresswell, G. & Domingues, C. 2009. The Leeuwin Current south of Western Australia. *Journal of the Royal Society of Western Australia*, vol. 92, pg. 83-100, [https://www.rswa.org.au/publications/Journal/92\(2\)/ROY%20SOC%2092.2%20LEEWIN%2083-100.pdf](https://www.rswa.org.au/publications/Journal/92(2)/ROY%20SOC%2092.2%20LEEWIN%2083-100.pdf).

Cullen J.J., Yang X., MacIntyre H.L. (1992) Nutrient Limitation of Marine Photosynthesis. In: Falkowski P.G., Woodhead A.D., Vivirito K. (eds) Primary Productivity and Biogeochemical Cycles in the Sea. Environmental Science Research, vol 43. Springer, Boston, MA, ISBN: 978-1-4899-0762-2  
Currie, R. 1953. Upwelling in the Benguela current. *Nature*, vol. 171, pp. 497-500, DOI: 10.1038/171497a0.

D'Asaro, E.A., 2004. Lagrangian trajectories on the Oregon shelf during upwelling. *Continental shelf research*, vol. 24, no. 13-14, pp.1421-1436, DOI: 10.1016/j.csr.2004.06.003

De Baar, H. 1994. von Liebig's law of the minimum and plankton ecology (1899–1991). *Progress in Oceanography*, vol. 33, no. 4, pp. 347-386, DOI: 10.1016/0079-6611(94)90022-1.

Dibarboure, G., Pujol, M.-I., Briol, F., Traon, P. L., Larnicol, G., Picot, N., Mertz, F. & Ablain, M. 2011. Jason-2 in DUACS: Updated system description, first tandem results and impact on processing and products. *Marine Geodesy*, vol. 34, no. 3-4, pp. 214-241, DOI: 10.1080/01490419.2011.584826.

Ducet, N., Le Traon, P.-Y. & Reverdin, G. 2000. Global high-resolution mapping of ocean circulation from TOPEX/Poseidon and ERS-1 and-2. *Journal of Geophysical Research: Oceans*, vol. 105, no. C8, pp. 19477-19498, DOI: 10.1029/2000JC900063.

Dugdale, R. 1972. Chemical oceanography and primary productivity in upwelling regions. *Geoforum*, vol. 3, no. 3, pp. 47-61, DOI: 10.1016/0016-7185(72)90085-1.

Eppley, R. W. & Peterson, B. J. 1979. Particulate organic matter flux and planktonic new production in the deep ocean. *Nature*, vol. 282, pp. 677, DOI: 10.1038/282677a0.

Estrade, P., Marchesiello, P., De Verdière, A.C. and Roy, C., 2008. Cross-shelf structure of coastal upwelling: A two—dimensional extension of Ekman's theory and a mechanism for inner shelf upwelling shut down. *Journal of marine research*, vol. 66, no. 5, pp.589-616, DOI: 10.1357/002224008787536790

Exon, N., Hill, P., Mitchell, C. & Post, A. 2005. Nature and origin of the submarine Albany canyons off southwest Australia. *Australian Journal of Earth Sciences*, vol. 52, no. 1, pp. 101-115, DOI: 10.1080/08120090500100036.

Feng, M., Meyers, G., Pearce, A. & Wijffels, S. 2003. Annual and interannual variations of the Leeuwin Current at 32 S. *Journal of Geophysical Research: Oceans*, vol. 108, no. C11, pp. 1-21, DOI: 10.1029/2002JC001763.

Fildani, A. 2017. Submarine Canyons: A brief review looking forward. *Geology*, vol. 45, no. 4, pp. 383-384, DOI: 10.1130/focus042017.1.

Flexas, M.D.M., Boyer, D.L., Espino, M., Puigdefàbregas, J., Rubio, A. and Company, J.B., 2008. Circulation over a submarine canyon in the NW Mediterranean. *Journal of Geophysical Research: Oceans*, vol. 113, no. C12, pp 1-18, DOI: 10.1029/2006JC003998.

Ford, J.K., 2009. Killer whale: *Orcinus orca*. In *Encyclopedia of marine mammals* (pp. 650-657). Academic Press, ISBN: 978-0-12-373553-9

Frost, B. 1987. Grazing control of phytoplankton stock in the open subarctic Pacific Ocean: a model assessing the role of mesozooplankton, particularly the large calanoid copepods *Neocalanus* spp. *Marine Ecology Progress Series*. *Oldendorf*, vol. 39, no. 1, pp. 49-68, DOI: 10.3354/meps039049.

Genin, A. 2004. Bio-physical coupling in the formation of zooplankton and fish aggregations over abrupt topographies. *Journal of Marine Systems*, vol. 50, no. 1-2, pp. 3-20, DOI: 10.1016/j.jmarsys.2003.10.008.

Gersbach, G. H., Pattiaratchi, C. B., Ivey, G. N. & Cresswell, G. R. 1999. Upwelling on the southwest coast of Australia—source of the Capes Current? *Continental Shelf Research*, vol.19, no. 3, pp. 363-400, DOI: 10.1016/S0278-4343(98)00088-0.

Gilly, W., Markaida, U., Baxter, C., Block, B., Boustany, A., Zeidberg, L., Reisenbichler, K., Robison, B., Bazzino, G. & Salinas, C. 2006. Vertical and horizontal migrations by the jumbo squid *Dosidicus gigas* revealed by electronic tagging. *Marine Ecology Progress Series*, vol. 324, pp. 1-17, DOI: 10.3354/meps324001.

Gordon, R. & Marshall, N. 1976. Submarine canyons: Internal wave traps? *Geophysical Research Letters*, vol. 3, no. 10, pp. 622-624, DOI: 10.1029/GL003i010p00622.

Greene, C., Wiebe, P., Burczynski, J. & Youngbluth, M. 1988. Acoustical detection of high-density krill demersal layers in the submarine canyons off Georges Bank. *Science*, vol. 241, no. 4863, pp. 359-361, DOI: 10.1126/science.241.4863.359.

Haidvogel, D. B., Arango, H. G., Hedstrom, K., Beckmann, A., Malanotte-Rizzoli, P. & Shchepetkin, A. F. 2000. Model evaluation experiments in the North Atlantic Basin: simulations in nonlinear terrain-following coordinates. *Dynamics of Atmospheres and Oceans*, vol. 32, no. 3-4, pp. 239-281, DOI: 10.1016/S0377-0265(00)00049-X.

Hales, B., Karp-Boss, L., Perlin, A. & Wheeler, P. A. 2006. Oxygen production and carbon sequestration in an upwelling coastal margin. *Global Biogeochemical Cycles*, vol. 20, no. 3, pp 1-15, DOI: 10.1029/2005GB002517.

Haney, R.L., 1991. On the pressure gradient force over steep topography in sigma coordinate ocean models. *Journal of physical Oceanography*, vol. 21, no.4, pp.610-619, DOI: 10.1175/1520-0485(1991)021<0610:OTPGFO>2.0.CO;2

Hanson, C. E., Pattiaratchi, C. & Waite, A. 2005. Sporadic upwelling on a downwelling coast: phytoplankton responses to spatially variable nutrient dynamics off the Gascoyne region of Western Australia. *Continental Shelf Research*, Vol. 25, no. 12-13, pp. 1561-1582, DOI: 10.1016/j.csr.2005.04.003.

- Herzfeld, M. 1997. The annual cycle of sea surface temperature in the Great Australian Bight. *Progress in Oceanography*, vol. 39, no. 1, pp. 1-27, DOI: 10.1016/S0079-6611(97)00010-4.
- Herzfeld, M. & Tomczak, M. 1997. Numerical modelling of sea surface temperature and circulation in the Great Australian Bight. *Progress in Oceanography*, vol. 39, no. 1, pp. 29-78, DOI: 10.1016/S0079-6611(97)00011-6.
- Hickey, B., Baker, E. and Kachel, N., 1986. Suspended particle movement in and around Quinault submarine canyon. *Marine Geology*, vol. 71, no. 1-2, pp.35-83, DOI: 10.1016/0025-3227(86)90032-0
- Hickey, B. M. 1997. The response of a steep-sided, narrow canyon to time-variable wind forcing. *Journal of Physical Oceanography*, vol. 27, no. 5, pp. 697-726, DOI: 10.1175/1520-0485(1997)027<0697:TROASS>2.0.CO;2.
- Hill, R. & Johnson, J. 1974. A theory of upwelling over the shelf break. *Journal of Physical Oceanography*, vol. 4, no. 1, pp. 19-26, DOI: 10.1175/1520-0485(1974)004<0019:ATOUIOT>2.0.CO;2.
- Hovland, M. & Riggs, D. The Bremer Canyon 'ocean animal hotspot'. GIMS12, 2012 Taiwan, URL:  
[https://www.researchgate.net/publication/267949246\\_The\\_Bremer\\_Canyon\\_'ocean\\_animal\\_hotspot'\\_-seepage-induced\\_congregation](https://www.researchgate.net/publication/267949246_The_Bremer_Canyon_'ocean_animal_hotspot'_-seepage-induced_congregation)
- Huang, Z., Nichol, S. L., Harris, P. T. & Caley, M. J. 2014. Classification of submarine canyons of the Australian continental margin. *Marine Geology*, vol. 357, no. 1, pp. 362-383, DOI: 10.1016/j.margeo.2014.07.007.
- Huthnance, J. 1981. Waves and currents near the continental shelf edge. *Progress in Oceanography*, vol. 10, no. 4, pp. 193-226, DOI: 10.1016/0079-6611(81)90004-5.
- James, N. P., Bone, Y., Collins, L. B. & Kyser, T. K. 2001. Surficial sediments of the Great Australian Bight: facies dynamics and oceanography on a vast cool-water carbonate shelf. *Journal of Sedimentary Research*, vol. 71, no. 4, pp. 549-567, DOI: 10.1306/102000710549.
- Johannes, R., Pearce, A., Wiebe, W., Crossland, C., Rimmer, D., Smith, D. & Manning, C. 1994. Nutrient characteristics of well-mixed coastal waters off Perth, Western Australia. *Estuarine, Coastal and Shelf Science*, vol. 39, no. 3, pp. 273-285, DOI: 10.1006/ecss.1994.1064.
- Jordi, A., Orfila, A., Basterretxea, G. and Tintoré, J., 2005. Shelf-slope exchanges by frontal variability in a steep submarine canyon. *Progress in Oceanography*, vol. 66, no. 2-4, pp.120-141, DOI: 10.1016/j.pocean.2004.07.009

- Kämpf, J., Doubell, M., Griffin, D., Matthews, R. L. & Ward, T. M. 2004. Evidence of a large seasonal coastal upwelling system along the southern shelf of Australia. *Geophysical Research Letters*, vol. 31, no. 9, pp. 1-4, DOI: 10.1029/2003GL019221.
- Kämpf, J., 2005. Cascading-driven upwelling in submarine canyons at high latitudes. *Journal of Geophysical Research: Oceans*, vol. 110, no. C2, pp. 1-11, DOI: 10.1029/2004JC002554.
- Kämpf, J. 2006. Transient wind-driven upwelling in a submarine canyon: A process-oriented modeling study. *Journal of Geophysical Research: Oceans*, vol. 111, no. C11, pp 1-12, DOI: 10.1029/2006JC003497.
- Kämpf, J. 2007. On the magnitude of upwelling fluxes in shelf-break canyons. *Continental Shelf Research*, vol. 27, no. 17, pp. 2211-2223, DOI: 10.1016/j.csr.2007.05.010.
- Kämpf, J. 2009. On the interaction of time-variable flows with a shelfbreak canyon. *Journal of Physical Oceanography*, vol. 39, no. 1, pp. 248-260, DOI: 10.1175/2008JPO3753.1.
- Kämpf, J. 2010. On preconditioning of coastal upwelling in the eastern Great Australian Bight. *Journal of Geophysical Research: Oceans*, vol. 115, no. C12, pp. 1-11, DOI: 10.1029/2010JC006294.
- Kämpf, J. 2012. Lee effects of localized upwelling in a shelf-break canyon. *Continental Shelf Research*, vol. 42, no. 1, pp. 78-88, DOI: 10.1016/j.csr.2012.05.005.
- Kämpf, J. & Chapman, P. 2016. *Upwelling Systems of the World*, Springer.
- Kämpf, J. & Kavi, A. 2017. On the “hidden” phytoplankton blooms on Australia's southern shelves. *Geophysical Research Letters*, vol. 44, no. 3, pp. 1466-1473, DOI: 10.1002/2016GL072096.
- Kämpf, J. 2018. On the Dynamics of Canyon–Flow Interactions. *Journal of Marine Science and Engineering*, vol. 6, no. 4, pp 129-143, DOI: 10.3390/jmse6040129.
- Kinsella, E. D., Hay, A. E. & Denner, W. W. 1987. Wind and topographic effects on the Labrador Current at Carson Canyon. *Journal of Geophysical Research: Oceans*, vol. 92, no C10, pp. 10853-10869, DOI: 10.1029/JC092iC10p10853.
- Klinck, J. M. (1988). The influence of a narrow transverse canyon on initially geostrophic flow. *Journal of Geophysical Research*, 93(C1), 509. doi:10.1029/jc093ic01p00509
- Klinck, J. M. 1996. Circulation near submarine canyons: A modeling study. *Journal of Geophysical Research: Oceans*, vol. 101, no. C1, pp. 1211-1223, DOI: 10.1029/95JC02901.

- Khorrami, Z. and Banihashemi, M.A., 2019. Improving multi-block sigma-coordinate for 3D simulation of sediment transport and steep slope bed evolution. *Applied Mathematical Modelling*, vol. 67, no. 1, pp.378-398, DOI: 10.1016/j.apm.2018.10.02
- Koslow, J. A. & Ota, A. 1981. The Ecology of Vertical Migration in Three Common Zooplankters in the La Jolla Bight, April—August 1967. *Biological Oceanography*, vol. 1, no. 2, pp. 107-134, DOI: 10.1080/01965581.1981.10749435.
- Koslow, J. A., Pesant, S., Feng, M., Pearce, A., Fearn, P., Moore, T., Matear, R. & Waite, A. 2008. The effect of the Leeuwin Current on phytoplankton biomass and production off Southwestern Australia. *Journal of Geophysical Research: Oceans*, vol. 113, no. C7, pp. 1-19, DOI: 10.1029/2007JC004102.
- Kremer, P. & Kremer, J. N. 1988. Energetic and behavioral implications of pulsed food availability for zooplankton. *Bulletin of Marine Science*, vol. 43, no. 3, pp. 797-809, URL: <https://www.ingentaconnect.com/content/umrsmas/bullmar/1988/00000043/00000003/art00036#expand/collapse>.
- Lampert, W. 1989. The adaptive significance of diel vertical migration of zooplankton. *Functional Ecology*, vol. 3, no. 1, pp. 21-27, DOI: 10.2307/2389671.
- Legeckis, R. & Cresswell, G. 1981. Satellite observations of sea-surface temperature fronts off the coast of western and southern Australia. *Deep Sea Research Part A. Oceanographic Research Papers*, vol. 28, no. 3, pp. 297-306, DOI: 10.1016/0198-0149(81)90069-8.
- Legendre, L. & Rivkin, R. B. 2002. Fluxes of carbon in the upper ocean: regulation by food-web control nodes. *Marine Ecology Progress Series*, vol. 242, pp. 95-109, DOI: 10.3354/meps242095.
- Lett, C., Roy, C., Levasseur, A., Van Der Lingen, C. D. & Mullon, C. 2006. Simulation and quantification of enrichment and retention processes in the southern Benguela upwelling ecosystem. *Fisheries Oceanography*, vol. 15, no. 5, pp. 363-372, DOI: 10.1111/j.1365-2419.2005.00392.x.
- Lorenzen, C. J. 1972. Extinction of light in the ocean by phytoplankton. *ICES Journal of Marine Science*, vol. 34, no. 2, pp. 262-267, DOI: 10.1093/icesjms/34.2.262.
- Luyten, P. 1999. COHERENS—Dissemination and exploitation of a coupled hydrodynamical-ecological model for regional and shelf seas. MAS3-CT97-0088. Final Report. MUMM Internal Report, Management Unit of the Mathematical Models., URL: [https://uol.de/f/5/inst/icbm/ag/physoz/download/from\\_email/COHERENS/print/userguide.pdf](https://uol.de/f/5/inst/icbm/ag/physoz/download/from_email/COHERENS/print/userguide.pdf)

Macisaac, J., Dugdale, R., Barber, R., Blasco, D. & Packard, T. 1985. Primary production cycle in an upwelling center. *Deep Sea Research Part A. Oceanographic Research Papers*, vol. 32, no. 5, pp. 503-529, DOI: 10.1016/0198-0149(85)90042-1.

Macleod, C. D., Santos, M. & Pierce, G. J. 2003. Review of data on diets of beaked whales: evidence of niche separation and geographic segregation. *Journal of the Marine Biological Association of the United Kingdom*, vol. 83, no. 3, pp. 651-665, DOI: 10.1017/S0025315403007616.

Macquart-Moulin, C. & Patrìti, G. 1996. Accumulation of migratory micronekton crustaceans over the upper slope and submarine canyons of the northwestern Mediterranean. *Deep Sea Research Part I: Oceanographic Research Papers*, vol. 43, no. 5, pp. 579-601, DOI: 10.1016/0967-0637(96)00039-8.

Martin, J. H., Knauer, G. A., Karl, D. M. & Broenkow, W. W. 1987. VERTEX: carbon cycling in the northeast Pacific. *Deep Sea Research Part A. Oceanographic Research Papers*, vol. 34, no. 2, pp. 267-285. URL: [https://www.whoi.edu/cms/files/MartinKnauerKarl\\_CarbonVertex\\_DSR1987\\_52929.pdf](https://www.whoi.edu/cms/files/MartinKnauerKarl_CarbonVertex_DSR1987_52929.pdf)

Martell, C. & Allen, J. 1979. The generation of continental shelf waves by alongshore variations in bottom topography. *Journal of Physical Oceanography*, vol. 9, no. 4, pp. 696-711, DOI: 10.1175/1520-0485(1979)009<0696:TGOCSW>2.0.CO;2

Mason, E., Colas, F. & Pelegrí, J. L. 2012. A Lagrangian study tracing water parcel origins in the Canary Upwelling System. *Scientia Marina*, vol. 76, pp. 79-94, DOI: 10.3989/scimar.03608.18D.

Mccartney, M. S. & Donohue, K. A. 2007. A deep cyclonic gyre in the Australian–Antarctic Basin. *Progress in Oceanography*, vol. 75, no. 4, pp. 675-750, DOI: 10.1016/j.pocean.2007.02.008.

Mcclatchie, S., Middleton, J. F. & Ward, T. M. 2006. Water mass analysis and alongshore variation in upwelling intensity in the eastern Great Australian Bight. *Journal of Geophysical Research: Oceans*, vol. 111, no. 4, pp. 675-750, DOI: 10.1016/j.pocean.2007.02.008.

Mccreary, J. P., Shetye, S. R. & Kundu, P. K. 1986. Thermohaline forcing of eastern boundary currents: With application to the circulation off the west coast of Australia. *Journal of Marine Research*, vol. 44, no. 1, pp. 71-92, DOI: 10.1357/002224086788460184.

Mcdonagh, E. L., Bryden, H. L., King, B. A. & Sanders, R. J. 2008. The circulation of the Indian Ocean at 32°S. *Progress in Oceanography*, vol 79, no. 1, pp. 20-36, DOI: 10.1016/j.pocean.2008.07.001.

Meeuwig, J. & Turner, J. 2017. Bremer Canyon Progress Report Emerging Priorities Project EP2 – Spatial distribution of marine wildlife in the Bremer Bay region. Marine Biodiversity Hub, URL: [https://www.nespmarine.edu.au/system/files/Meeuwig%20et%20al%20Bremer%20Canyon%20Progress%20Report\\_Milestone%204%20FINAL\\_30Jun2017.pdf](https://www.nespmarine.edu.au/system/files/Meeuwig%20et%20al%20Bremer%20Canyon%20Progress%20Report_Milestone%204%20FINAL_30Jun2017.pdf)

Meeuwig, J., Turner, J. & Bouchet, P. 2016. Bremer Canyon Science Report. NESP Marine Biodiversity Hub Workshop held, URL: [https://www.researchgate.net/profile/Phil\\_Bouchet/publication/321208679\\_Bremer\\_Canyon\\_Science\\_Workshop\\_Report\\_-\\_NESP\\_Marine\\_Biodiversity\\_Hub\\_Emerging\\_Priorities\\_Project/links/5a14cdf40f7e9b925cd51bf1/Bremer-Canyon-Science-Workshop-Report-NESP-Marine-Biodiversity-Hub-Emerging-Priorities-Project.pdf](https://www.researchgate.net/profile/Phil_Bouchet/publication/321208679_Bremer_Canyon_Science_Workshop_Report_-_NESP_Marine_Biodiversity_Hub_Emerging_Priorities_Project/links/5a14cdf40f7e9b925cd51bf1/Bremer-Canyon-Science-Workshop-Report-NESP-Marine-Biodiversity-Hub-Emerging-Priorities-Project.pdf).

Middleton, J. F. & Bye, J. A. 2007. A review of the shelf-slope circulation along Australia's southern shelves: Cape Leeuwin to Portland. *Progress in Oceanography*, vol. 75, no. 1, pp. 1-41, DOI: 10.1016/j.pocean.2007.07.001.

Middleton, J. F. & Cirano, M. 2002. A northern boundary current along Australia's southern shelves: The Flinders Current. *Journal of Geophysical Research: Oceans*, vol. 107, no. C9, pp. 12-1-12-11, DOI: 10.1029/2000JC000701.

Middleton, J. F. & Platov, G. 2003. The Mean Summertime Circulation along Australia's Southern Shelves: A Numerical Study. *Journal of Physical Oceanography*, vol. 33, no. 11, pp. 2270-2287, DOI: 10.1175/1520-0485(2003)033<2270:TMSCAA>2.0.CO;2.

Mitchell, J., Holdgate, G., Wallace, M. & Gallagher, S. 2007. Marine geology of the Quaternary Bass Canyon system, southeast Australia: A cool-water carbonate system. *Marine geology*, vol. 237, no. 1-2, pp. 71-96, DOI: 10.1016/j.margeo.2006.10.037.

Mirshak, R. and Allen, S.E., 2005. Spin-up and the effects of a submarine canyon: Applications to upwelling in Astoria Canyon. *Journal of Geophysical Research: Oceans*, vol. 110, no. C2, pp. 1-14, DOI: 10.1029/2004JC002578.

Mondello, N. 2017. Physical oceanography off the South Coast of Western Australia. Murdoch University, URL: <https://www.semanticscholar.org/paper/Physical-oceanography-off-the-South-Coast-of-Mondello/364a9f9991cc8e2c68583be8898037b4d3f17fd6>.

Moors-Murphy, H. B. 2014. Submarine canyons as important habitat for cetaceans, with special reference to the Gully: A review. *Deep Sea Research Part II: Topical Studies in Oceanography*, vol. 104, pp. 6-19, DOI: 10.1016/j.dsr2.2013.12.016.

Morrice, M. G. 2004. Killer whales (*Orcinus orca*) in Australian territorial waters. Technical Paper. Deakin University, Victoria. Australia, URL: <http://citeseerx.ist.psu.edu/viewdoc/download?doi=10.1.1.597.2083&rep=rep1&type=pdf>.

Morrow, R. & Birol, F. 1998. Variability in the southeast Indian Ocean from altimetry: Forcing mechanisms for the Leeuwin Current. *Journal of Geophysical Research: Oceans*, vol. 103, no. C9, pp. 18529-18544, DOI: 10.1029/98JC00783.

Moulins, A., Rosso, M., Nani, B. & Würtz, M. 2007. Aspects of the distribution of Cuvier's beaked whale (*Ziphius cavirostris*) in relation to topographic features in the Pelagos Sanctuary (north-western Mediterranean Sea). *Journal of the Marine Biological Association of the United Kingdom*, vol 87, no. 1, pp. 177-186, DOI: 10.1017/S0025315407055002.

Navon, I. M. 1979. Finite-element simulation of the shallow-water equations model on a limited-area domain. *Applied Mathematical Modelling*, vol. 3, no. 5, pp. 337-348, DOI: 10.1016/S0307-904X(79)80040-2.

Nichol, L. M. & Shackleton, D. M. 1996. Seasonal movements and foraging behaviour of northern resident killer whales (*Orcinus orca*) in relation to the inshore distribution of salmon (*Oncorhynchus* spp.) in British Columbia. *Canadian Journal of Zoology*, vol. 74, no. 6, pp. 983-991, DOI: 10.1139/z96-111.

Nieblas, A.-E., Sloyan, B. M., Hobday, A. J., Coleman, R. & Richardsone, A. J. 2009. Variability of biological production in low wind-forced regional upwelling systems: A case study off southeastern Australia. *Limnology and Oceanography*, vol. 54, no. 5, pp. 1548-1558, DOI: 10.4319/lo.2009.54.5.1548.

Olesiuk, P., Bigg, M. & Ellis, G. 1990. Life history and population dynamics of resident killer whales (*Orcinus orca*) in the coastal waters of British Columbia and Washington State. Report of the International Whaling Commission, *Special*, vol. 12, pp. 209-43, ISBN: 0 906975 23

9. Pariwono, J., Bye, J. & Lennon, G. 1986. Long-period variations of sea-level in Australasia. *Geophysical Journal International*, vol. 87, no. 1, pp. 43-54, DOI: 10.1111/j.1365-246X.1986.tb04545.x.

Parsons, T., Stronach, J., Borstad, G., Louttit, G. & Perry, R. 1981. Biological fronts in the Strait of Georgia, British Columbia, and their relation to recent measurements of primary productivity. *Mar. Ecol. Prog. Ser.*, vol. 6, pp. 237-242, URL: <http://www.int-res.com/articles/meps/6/m006p237.pdf>.

Pattiaratchi, C. 2006. Surface and sub-surface circulation and water masses off Western Australia. *Bulletin of the Australian meteorological and Oceanographic Society*, vol. 19, pp. 95-

104. URL: [https://www.researchgate.net/publication/229042164\\_Surface\\_and\\_sub-surface\\_circulation\\_and\\_water\\_masses\\_off\\_Western\\_Australia](https://www.researchgate.net/publication/229042164_Surface_and_sub-surface_circulation_and_water_masses_off_Western_Australia)

Pattiaratchi, C. 2007. Understanding areas of high productivity within the South-west Marine Region. Report for the National Oceans Office. URL: [https://www.researchgate.net/profile/Charitha\\_Pattiaratchi/publication/235223453\\_Understanding\\_areas\\_of\\_high\\_productivity\\_within\\_the\\_south-west\\_marine\\_region\\_Report\\_prepared\\_for\\_the\\_National\\_Oceans\\_Office/links/0c96051fbc8ebccc36000000.pdf](https://www.researchgate.net/profile/Charitha_Pattiaratchi/publication/235223453_Understanding_areas_of_high_productivity_within_the_south-west_marine_region_Report_prepared_for_the_National_Oceans_Office/links/0c96051fbc8ebccc36000000.pdf)

Pattiaratchi, C. 2017. Bremer Bay Seaglider deployment 11 March – 13 April 2017. Pattiaratchi, C. & Woo, M. 2009. The mean state of the Leeuwin current system between North West Cape and Cape Leeuwin. *Journal of the Royal Society of Western Australia*, vol. 92, pp. 221-241, DOI: [researchgate.net/profile/Charitha\\_Pattiaratchi/publication/235223480\\_The\\_mean\\_state\\_of\\_the\\_Leeuwin\\_Current\\_system\\_between\\_North\\_West\\_Cape\\_and\\_Cape\\_Leeuwin/links/545741350cf2bccc490f5ab1/The-mean-state-of-the-Leeuwin-Current-system-between-North-West-Cape-and-Cape-Leeuwin.pdf](https://www.researchgate.net/profile/Charitha_Pattiaratchi/publication/235223480_The_mean_state_of_the_Leeuwin_Current_system_between_North_West_Cape_and_Cape_Leeuwin/links/545741350cf2bccc490f5ab1/The-mean-state-of-the-Leeuwin-Current-system-between-North-West-Cape-and-Cape-Leeuwin.pdf).

Paull, C. K., Mitts, P., Ussler Iii, W., Keaten, R. & Greene, H. G. 2005. Trail of sand in upper Monterey Canyon: offshore California. *Geological Society of America Bulletin*, vol. 117, no. 9-10, pp. 1134-1145, DOI: 10.1130/B25390.1.

Pearce, A. & Pattiaratchi, C. 1999. The Capes Current: a summer countercurrent flowing past Cape Leeuwin and Cape Naturaliste, Western Australia. *Continental Shelf Research*, vol. 19, no. 3, pp. 401-420, DOI: 10.1016/S0278-4343(98)00089-2.

Pearce, A. & Phillips, B. 1988. ENSO events, the Leeuwin Current, and larval recruitment of the western rock lobster. *ICES Journal of Marine Science*, vol. 45, no. 1, pp.13-21, DOI: 10.1093/icesjms/45.1.13.

Pedlosky, J. 2013. Geophysical fluid dynamics, Springer Science & Business Media, ISBN: 978-1-4612-4650-3.

Pérenne, N., Lavelle, J.W., Smith IV, D.C. and Boyer, D.L., 2001. Impulsively started flow in a submarine canyon: Comparison of results from laboratory and numerical models. *Journal of Atmospheric and Oceanic Technology*, 18(10), pp.1698-1718, DOI: 10.1175/1520-0426(2001)018<1699:ISFIAS>2.0.CO;2

Pond, S. & Pickard, G. L. 1983. Introductory dynamical oceanography, Elsevier, ISBN: 13:978 0 7506 2496 1.

- Pujol, M.-I., Faugère, Y., Taburet, G., Dupuy, S., Pelloquin, C., Ablain, M. & Picot, N. 2016. Duacs Dt2014: the new multi-mission altimeter data set reprocessed over 20 years. *Ocean Science*, vol. 12, pp. 1067-1090, DOI: 10.5194/os-12-1067-2016.
- Pujol, M. 2017. Sea Level TAC-DUACS products, URL: <http://apdrc.soest.hawaii.edu/doc/CMEMS-SL-QUID-008-032-051.pdf>.
- Rennie, S., Hanson, C., Mccauley, R., Pattiaratchi, C., Burton, C., Bannister, J., Jenner, C. & Jenner, M.-N. 2009a. Physical properties and processes in the Perth Canyon, Western Australia: Links to water column production and seasonal pygmy blue whale abundance. *Journal of Marine Systems*, vol. 77, no. 1-2, pp. 21-44, DOI: 10.1016/j.jmarsys.2008.11.008.
- Rennie, S. J., Pattiaratchi, C. B. & Mccauley, R. D. 2009b. Numerical simulation of the circulation within the Perth Submarine Canyon, Western Australia. *Continental Shelf Research*, vol. 29, no. 16, pp. 2020-2036, DOI: 10.1016/j.csr.2009.04.010.
- Rennie, S. J., Pattiaratchi, C. P. & Mccauley, R. D. 2007. Eddy formation through the interaction between the Leeuwin Current, Leeuwin Undercurrent and topography. *Deep Sea Research Part II: Topical Studies in Oceanography*, vol. 54, no. 8-10, pp. 818-836, DOI: 10.1016/j.dsr2.2007.02.005.
- Ridgway, K. & Condie, S. 2004. The 5500-km-long boundary flow off western and southern Australia. *Journal of Geophysical Research: Oceans*, vol. 109, no. C4, pp. 1-18, DOI: 10.1029/2003JC001921.
- Ridgway, K. & Dunn, J. 2007. Observational evidence for a Southern Hemisphere oceanic supergyre. *Geophysical Research Letters*, vol. 34, no. 13, pp. 1-5, DOI: 10.1029/2007GL030392.
- Rivas, D. & Samelson, R. 2011. A numerical modeling study of the upwelling source waters along the Oregon coast during 2005. *Journal of Physical Oceanography*, vol. 41, no. 1, pp. 88-112, DOI: 10.1175/2010JPO4327.1.
- Rochford, D. 1986. Seasonal changes in the distribution of Leeuwin Current waters of Southern Australia. *Marine and Freshwater Research*, vol. 37, no. 1, pp. 1-10, DOI: 10.1071/MF9860001.
- Rossby, C. G. 1939. Relation between variations in the intensity of the zonal circulation of the atmosphere and the displacements of the semi-permanent centers of action. *J. mar. Res.*, vol. 2, pp. 38-55, URL: [https://peabody.yale.edu/sites/default/files/documents/scientific-publications/jmr02-01-06-CG\\_ROSSBYetal.pdf](https://peabody.yale.edu/sites/default/files/documents/scientific-publications/jmr02-01-06-CG_ROSSBYetal.pdf)

Saldías, G.S. and Allen, S.E., 2020. The Influence of a Submarine Canyon on the Circulation and Cross-Shore Exchanges around an Upwelling Front. *Journal of Physical Oceanography*, vol. 50, no. 6, pp.1677-1698, DOI: 10.1175/JPO-D-19-0130.1

Saulitis, E., Matkin, C., Barrett-Lennard, L., Heise, K. & Ellis, G. 2000. Foraging strategies of sympatric killer whale (*Orcinus orca*) populations in Prince William Sound, Alaska. *Marine mammal science*, vol. 16, no. 1, pp. 94-109, DOI: 10.1111/j.1748-7692.2000.tb00906.x.

Scharffenberg, M. G. & Stammer, D. 2010. Seasonal variations of the large-scale geostrophic flow field and eddy kinetic energy inferred from the TOPEX/Poseidon and Jason-1 tandem mission data. *Journal of Geophysical Research: Oceans*, vol. 115, no. C2, pp. 1-29, DOI: 10.1029/2008JC005242.

Seuront, L., Leterme, S.C., Middleton, J., Byrne, S., James, C., Luick, J., Nedoncelle, K., Paterson, J., Teixeira, C. and van Dongen-Vogels, V., 2010. Biophysical couplings in South Australian shelf waters under conditions of summer upwelling and winter downwelling: results from the Southern Australia Integrated Marine Observing System (SAIMOS). *Proceedings of the "OceanObs"*, vol. 9, pp. 27-31, URL: <http://www.oceanobs09.net/proceedings/ac/FCXNL-09A02-1656269-1-ac2a31.pdf>.

She, J. and Klinck, J.M., 2000. Flow near submarine canyons driven by constant winds. *Journal of Geophysical Research: Oceans*, Vol. 105, no. C12, pp.28671-28694, DOI: 10.1029/2000JC900126

Shchepetkin, A.F. and McWilliams, J.C., 2005. The regional oceanic modeling system (ROMS): a split-explicit, free-surface, topography-following-coordinate oceanic model. *Ocean modelling*, vol. 9, no. 4, pp. 347-404, DOI: 10.1016/j.ocemod.2004.08.002

Shepard, F. P., Marshall, N. F. & McLoughlin, P. A. 1974. " Internal Waves" Advancing along Submarine Canyons. *Science*, vol. 183, no. 4121, pp. 195-198, DOI: 10.1126/science.183.4121.195.

Smith, R. L., Huyer, A., Godfrey, J. S. & Church, J. A. 1991. The Leeuwin current off western Australia, 1986–1987. *Journal of Physical Oceanography*, vol. 21, no. 2, pp. 323-345, DOI: 10.1175/1520-0485(1991)021<0323:TLCOWA>2.0.CO;2.

Spurgin, J.M. and Allen, S.E., 2014. Flow dynamics around downwelling submarine canyons. *Ocean Science*, vol. 10, no. 5, pp.799-819, DOI: 10.5194/os-10-799-2014

Stefanescu, C., Nin-Morales, B. & Massuti, E. 1994. Fish assemblages on the slope in the Catalan Sea (Western Mediterranean): influence of a submarine canyon. *Journal of the Marine Biological Association of the United Kingdom*, vol. 74, no. 3, pp. 499-512, DOI: 10.1017/S0025315400047627.

Tamsitt, V., Talley, L. & Mazloff, M. 2019. A Deep Eastern Boundary Current carrying Indian Deep Water south of Australia. *Journal of Geophysical Research: Oceans*, vol. 124, no. 3, pp. 2218-2238, DOI: 10.1029/2018JC014569.

Taylor, J. & Pearce, A. 1999. Ningaloo Reef currents: implications for coral spawn dispersal, zooplankton and whale shark abundance. *Journal of the Royal Society of Western Australia*, vol. 82, pp. 57-65, URL: [https://www.rswa.org.au/publications/Journal/82\(2\)/82\(2\)taylor.pdf](https://www.rswa.org.au/publications/Journal/82(2)/82(2)taylor.pdf).

Totterdell, J. 2014. Western Australian orca research: summary update (June 2014). *Marine Information and Research Group*, [www.mirg.org.au](http://www.mirg.org.au).

Tourism Western Australia, 2018. *Economic Contribution Of Tourism To Western Australia'S Tourism Regions 2016-17*. URL: [https://www.tourism.wa.gov.au/Publications%20Library/Research%20and%20reports/Economic%20Contribution%20of%20Tourism%20to%20WA%20s%20Tourism%20Regions%202016-17%20\(RTSA%202016-17\).pdf](https://www.tourism.wa.gov.au/Publications%20Library/Research%20and%20reports/Economic%20Contribution%20of%20Tourism%20to%20WA%20s%20Tourism%20Regions%202016-17%20(RTSA%202016-17).pdf)

Vetter, E. & Dayton, P. 1998. Macrofaunal communities within and adjacent to a detritus-rich submarine canyon system. *Deep Sea Research Part II: Topical Studies in Oceanography*, vol. 45, no. 1, pp. 25-54, DOI: 10.1016/S0967-0645(97)00048-9.

Vetter, E. & Dayton, P. 1999. Organic enrichment by macrophyte detritus, and abundance patterns of megafaunal populations in submarine canyons. *Marine Ecology Progress Series*, vol. 186, pp. 137-148, DOI: 10.3354/meps186137.

Von Der Borch, C. 1968. Southern Australian submarine canyons: their distribution and ages. *Marine Geology*, vol. 6, no. 4, pp. 267-279, DOI: 10.1016/0025-3227(68)90019-4.

Wellard, R., Lightbody, K., Fouda, L., Blewitt, M., Riggs, D. & Erbe, C. 2016. Killer whale (*Orcinus orca*) predation on beaked whales (*Mesoplodon* spp.) in the Bremer Sub-Basin, Western Australia. *PloS one*, vol. 11, no. 12, pp. 1-15, DOI: 10.1371/journal.pone.0166670.

Weller, E., Holliday, D., Feng, M., Beckley, L. and Thompson, P., 2011. A continental shelf scale examination of the Leeuwin Current off Western Australia during the austral autumn–winter. *Continental Shelf Research*, vol. 31, no. 17, pp.1858-1868, DOI: 10.1016/j.csr.2011.08.008.

Wijeratne, S., Pattiaratchi, C. and Proctor, R., 2018. Estimates of surface and subsurface boundary current transport around Australia. *Journal of Geophysical Research: Oceans*, vol. 123, no. 5, pp.3444-3466, DOI: 10.1029/2017JC013221.

Wilkerson, F. P., Lassiter, A. M., Dugdale, R. C., Marchi, A. & Hogue, V. E. 2006. The phytoplankton bloom response to wind events and upwelled nutrients during the CoOP WEST study. *Deep Sea Research Part II: Topical Studies in Oceanography*, vol. 53, no. 26, pp. 3023-3048, DOI: 10.1016/j.dsr2.2006.07.007.

Woo, L. M. 2005. Summer circulation and water masses along the West Australian coast. University of Western Australia, URL: <https://research-repository.uwa.edu.au/en/publications/summer-circulation-and-water-masses-along-the-west-australian-coa>.

Woo, M., Pattiaratchi, C. & Schroeder, W. 2006. Dynamics of the Ningaloo current off point cloates, *Western Australia. Marine and Freshwater Research*, vol. 57, no. 3, pp. 291-301, DOI: 10.1071/MF05106.

Woo, M. & Pattiaratchi, C. B. How the Capes Current ends: An investigation of a west Australian coastal current using an autonomous ocean glider. *Proceedings of the 15th Physics of Estuaries and Coastal Seas (PECS) Conference*, 2010, pp.14-17, URL: [https://www.researchgate.net/profile/Charitha\\_Pattiaratchi/publication/267695440\\_How\\_the\\_Capes\\_current\\_ends\\_an\\_investigation\\_of\\_a\\_west\\_Australian\\_coastal\\_current\\_using\\_an\\_autonomous\\_ocean\\_glider/links/5458465e0cf26d5090ab60d2/How-the-Capes-current-ends-an-investigation-of-a-west-Australian-coastal-current-using-an-autonomous-ocean-glider.pdf](https://www.researchgate.net/profile/Charitha_Pattiaratchi/publication/267695440_How_the_Capes_current_ends_an_investigation_of_a_west_Australian_coastal_current_using_an_autonomous_ocean_glider/links/5458465e0cf26d5090ab60d2/How-the-Capes-current-ends-an-investigation-of-a-west-Australian-coastal-current-using-an-autonomous-ocean-glider.pdf).

Woo, M. 2019. Ocean Gliders delayed mode QA/QC best practice manual Version 2.0, URL: [https://repository.oceanbestpractices.org/bitstream/handle/11329/1030/Delayed\\_Mode\\_QAQC\\_Best\\_Practice\\_Manual\\_OceanGliders\\_v2.0.pdf?sequence=1&isAllowed=y](https://repository.oceanbestpractices.org/bitstream/handle/11329/1030/Delayed_Mode_QAQC_Best_Practice_Manual_OceanGliders_v2.0.pdf?sequence=1&isAllowed=y).

Zaret, T. M. & Suffern, J. S. 1976. Vertical migration in zooplankton as a predator avoidance mechanism 1. *Limnology and oceanography*, vol. 21, no. 6, pp. 804-813, DOI: 10.4319/lo.1976.21.6.0804.

## APPENDICES

Table 7.1: The percentage of particles which did not leave the shelf break model domain within the sixty-day run time.

Experiment	Particles which did not exit the model after 60 days (%)	Notes
SB 1	4.46	N/A
SB 2	0	N/A
SB 3	23.26	All particles released > 500 m were trapped
SB 4	0	N/A
SB 5	0.96	N/A
SB 6	4.46	Same as SB1

Table 7.2: The percentage of particles which did not leave the deeper upwelling model domain within the sixty-day run time.

Experiment	Trapped Particles	Notes
DC1	0	N/A
DC2	15.28	N/A
DC3	0	N/A
DC4	0	N/A
DC5	0	N/A
DC6	0.14	N/A